DISSERTATION

SUPER-RESOLUTION IMAGING REVEALS MECHANISMS OF GLUTAMATE TRANSPORTER LOCALIZATION NEAR NEURON-ASTROCYTE CONTACTS

Submitted by

Ashley N. Leek

Department of Biomedical Sciences

In partial fulfillment of the requirements

For the Degree of Doctor of Philosophy

Colorado State University

Fort Collins, Colorado

Summer 2021

Doctoral Committee:

Advisor: Michael M. Tamkun

Shane T. Hentges
Ronald B. Tjalkens
Susan Tsunoda

ABSTRACT

SUPER-RESOLUTION IMAGING REVEALS MECHANISMS OF GLUTAMATE TRANSPORTER LOCALIZATION NEAR NEURON-ASTROCYTE CONTACTS

Astrocytes contact neurons at several locations, including somatic clusters of Kv2.1 potassium channels and synapses across the brain. A primary function of astrocytes at these locations is to limit the action of extracellular glutamate. Astrocytic glutamate transporters, such as Glt1, ensure the fidelity of glutamic neurotransmission by spatially and temporally limiting glutamate signals. Additionally, they act to limit glutamate-induced hyperexcitability by preventing the spread of glutamate to extrasynaptic receptors. The role of Glt1 in limiting neuronal hyperactivity relies heavily on the localization and diffusion of the transporter in the membrane, however, little is known about the mechanisms governing these properties. The work presented in this dissertation examines the mechanisms of Glt1 localization near Kv2.1-mediated neuron-astrocyte contact sites.

To that end, in Chapter 2, we used super-resolution imaging to analyze the localization of two splice forms of Glt1, Glt1a and Glt1b. In cultures of primary astrocytes, we find that Glt1a, but not Glt1b, is specifically localized over cortical actin filaments. We go on to discover that this localization is dependent on the Glt1a C-terminus, where Glt1a and Glt1b differ, as exogenous expression of the Glt1a C-terminus was able to prevent localization of Glt1a to cortical actin filaments. In the somatosensory cortex, astrocyte Glt1 forms net-like structures around neuronal Kv2.1 clusters, however the cause of this Glt1 localization pattern is unknown. In Chapter 3, using super-resolution imaging of mixed cultures of astrocytes and neurons, we replicate findings of astrocyte Glt1 in a net-like localization around neuronal Kv2.1 clusters. We discover that both astrocyte actin and

ER were excluded from the region across from neuronal Kv2.1 clusters. The actin-Glt1a relationship discussed in Chapter 2 is likely responsible for the net-like appearance of Glt1, as astrocytic Glt1 and actin colocalize in nets around Kv2.1 clusters at points of neuron-astrocyte contact. Neuronal control over the astrocyte cytoskeleton appears central to this Glt1a localization, although the mechanism of this control is still unknown. Together, these data describe a novel interaction between the Glt1a C-terminus and cortical actin filaments, which localizes Glt1 near neuronal structures involved in detecting ischemic insult.

Although the mechanism of neuronal control over the astrocyte cytoskeleton remains a mystery, presumably cell-cell contact has a major influence. Contacts between neurons and astrocytes at Kv2.1 clusters could be mediated by the Kv2.1 β-subunit, AMIGO, which acts a cell adhesion molecule. Only one member of the AMIGO family of proteins is known to be an auxiliary β-subunit for Kv2 channels and to modulate Kv2.1 electrical activity. However, the AMIGO family has two additional members of $\sim$50% similarity that have not yet been characterized as Kv2 β-subunits. In Chapter 4, we show that the surface trafficking and localization of all three AMIGOs are controlled by their interaction with both Kv2.1 and Kv2.2 channels. Additionally, assembly of each AMIGO with either Kv2 alters important electrophysiological properties of these channels. The co-regulatory effects of Kv2s and AMIGOs likely fine-tune both electrical and cell adhesion properties of the neurons in which they are expressed.

Altogether, the work presented in this dissertation further defines the composition of Kv2.1-induced neuron-astrocyte contact sites, representing the first significant addition to this field in more than a decade.

ACKNOWLEDGEMENTS

So many people formed the network that supported me throughout the creation of this dissertation: my family, my friends, my lab-mates, and several mentors. Truly, this would not have been possible without your unwavering belief that I could actually do this thing.

To my family—I could not ask for a better support system. Thanks for all the video calls, visits, vacations, and burnt ends. Thanks for always asking how my research was going even if you didn't understand a word of what I said. It means the world to me that you bothered to ask in the first place. I am so looking forward to seeing you all again soon.

Mike—thanks for taking a chance on me and my crazy passion for astrocytes. Despite that the project was difficult and tangential to the work in the lab, you still let me pursue it, and I don't think I'll ever quite be able to thank you enough for that gift. Although it was mentally taxing, I truly think it made me a better scientist. Thanks for allowing me to be creative at every opportunity and letting me explore the bounds of my project. Also—thank you for all of the doomsday-esque political conversations we've had over the years. There were far too many, but those conversations with you and Ben added some light to dark times. To my committee—thank you all for prompt email responses, your perspective, and much-needed pushes in the right direction.

To my lab-mates—I don't even know what to say, really. You are the best of friends and my chosen family. It has been a daily pleasure working alongside all of you in the Tamkun lab. Emily—you have been the best lab-sibling, roommate, and friend a woman could ask for. I feel endlessly lucky that you emailed me the summer before our first year asking to be roommates. Thank you for sharing this journey with me. All of the triumphs and tribulations would not have been nearly as enjoyable or as endurable without your support. I'll miss seeing you every day, but I hope we will

always be able to catch up over some Maverick Margs^{TM}. Laura—you are a marvelous scientist, a wonderful mother, and an even more incredible friend. I'll never be able to adequately thank you for all of the science and life advice you've given me all these years. Whether over "coffee", a drink, Hot Chicken, a board game, or a neighborhood walk, you've always been there, and I am forever grateful. I look up to you so much and I look forward to many more years of friendship. Ben—thanks for the laughs, the board games, the crossword puzzles, and the solving science. Although the world was on fire, it was always fun to talk with you about the insanity that was the news. I hope you will always remember that I am forever Galactic Overlord and that Xevi is a traitor. Liz—you truly personify my ideal scientist. You are unceasingly persistent, curious, and creative. Thanks for showing me the ropes and paving the way for creative women in the Tamkun lab. Thank you all for everything.

Dr. Roberts—thank you for instilling in me a love for research. My time in the lab at Trinity was foundational and formative. I would not be here now without you. Doc Martens and Ms. Stites—you'll likely never see this, but I would not have fallen in love with neuroscience without your classes that inspired questions and curiosity.

Finally, Joshua—you are my most steadfast and substantial supporter. You grounded me when my anxiety was taking over and you lifted me up when the many failures of research brought me down. Thank you for the morning coffee, the delicious dinners, the backpacking getaways, and the genuine interest in my research. I never thought I would be so lucky to have someone that cares so much for my mental and physical well-being. I love you and I am so excited to write the next chapter with you.

DEDICATION

To the artist-scientists that came before me and to all the teachers that inspired curiosity.

TABLE OF CONTENTS

LIST OF FIGURES

Chapter 1

Introduction

1.1 A historical perspective: initial observations of the nervous system

Perhaps the greatest advances in the understanding of brain structure can be attributed to Nobel laureates, Camillo Golgi and Santiago Ramòn y Cajal. Golgi vastly improved cellular staining by using methods to label random neurons and glial cells. Golgi's *reazione nera* (black reaction) stained whole cells, including small processes distant from the cell body, which allowed neurons and glia to be observed in greater detail than ever before (Figure 1.1A). Using the silver-chromate technique, Golgi published images of axons that traveled great distances, the entirety of a neuron's dendritic tree, and short protrusions along the dendritic fibers, which would later be identified as dendritic spines. In other publications, Golgi also described glial cells in the white and grey matter, as well as the interaction of star-shaped cells with vasculature. Because of this interaction, Golgi predicted that glia may carry nutrients from capillaries to neurons [1].

Two years after Golgi's seminal publications using his silver-chromate technique (1883-1886), Cajal published his first study of the cerebellar structure of birds (Figure 1.1B). In this work, he introduced improvements on Golgi's stain and provided the evidence to suggest neurons were discrete cells, and not joined in continuity to form a reticulum as was the prevailing theory at the time [1]. Incredibly, in this work, he also presented detailed drawings of dendritic spines, which he is credited for naming, and suggested that these spines were locations where axons from adjacent cells made contact for communication. Even though Cajal only observed static cells in fixed tissue, his brilliance was evident in his ability to envision these tissues as living and dynamic [2]. For instance, he imagined that the connections between axons and dendrites of adjacent cells

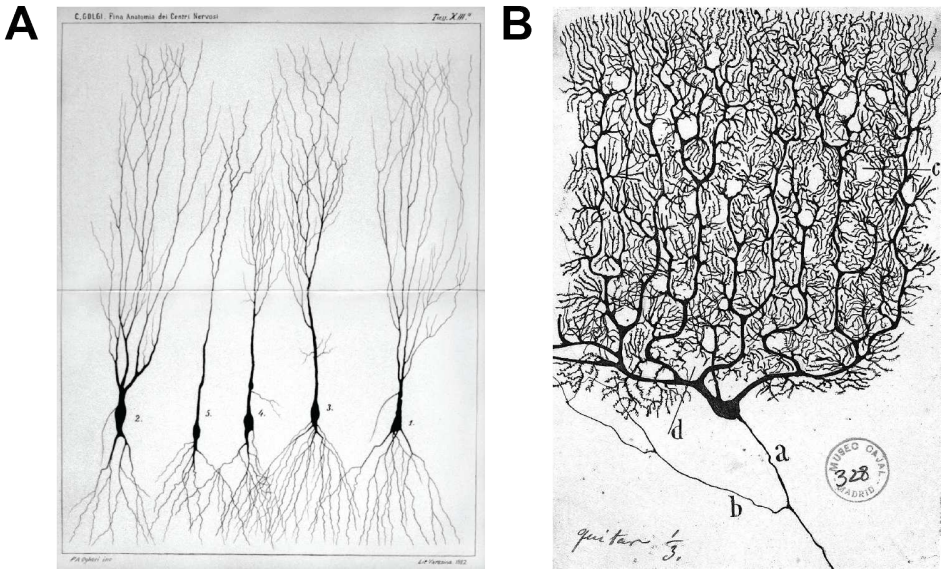

Figure 1.1: Neurons visualized with the Golgi technique. **A)** Golgi's depiction of neurons in the hippocampus which have been impregnated with silver chromate (Golgi 1885). **B)** A Purkinje neuron of the cerebellum as drawn by Ramòn y Cajal (1888).

were dynamically regulated —that these contacts could be strengthened, weakened, and created anew.

While Cajal's contribution to our understanding of neurons is undeniable, he also provided significant studies of glia, which particularly focused on the interactions of glia with neurons. Cajal experimented with several staining methods, ultimately discovering the best techniques to study various glial cells, which, even then, were understood to be highly heterogeneous [3]. Using these methods, Cajal observed several novel qualities of astrocytes. In the dentate gyrus, Cajal observed dividing astrocytes (Figure 1.2 "B"), lending support to the idea that astrocytes remained capable of mitosis, unlike neurons. In these preparations, Cajal also observed astrocytic endfeet in contact with blood vessels (Figure 1.2 "F") and large pyramidal neurons surrounded by astrocytes (Figure 1.2 "C" and "D"). Similar to his thoughts on neuronal dynamics, Cajal thought glial dynamics could affect both blood flow via connections to blood vessels and synaptic communication via astrocytic processes that invaded and retreated from the synaptic cleft [2]. These hypotheses were far ahead of their time, as astrocytes have only recently been

appreciated for their role in controlling blood flow to support metabolic demand and modulating synaptic communication.

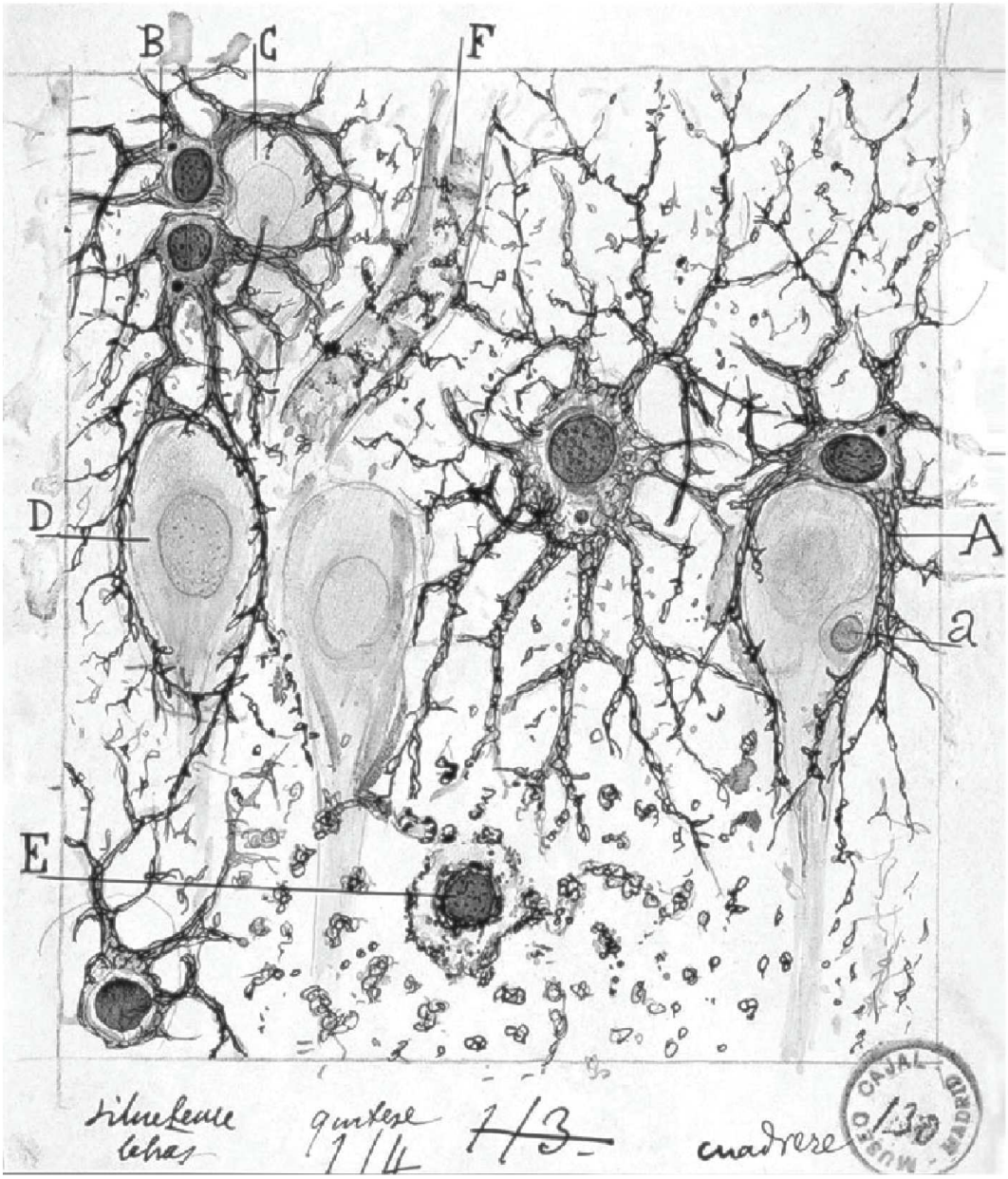

Figure 1.2: Neuron-astrocyte contacts were described early on by Ramon y Cajal. Pyramidal neurons and astrocytes of the *stratum pyrimidale* in the hippocampus. (A) Mature astrocyte, (B) dividing astrocytes, (C)(D) pyramidal neurons, (E) dying astrocyte, (F) blood vessel in contact with astrocyte endfeet, (Cajal 1913).

1.2 Astrocytes

Although studies of glia began well over a century ago, it was not until recently that we understood that glia and neurons exist in roughly equal numbers across the nervous system [4]. Glia encompass numerous cell types with specific functions, of which astrocytes, oligodendrocytes, and microglia seem to garner the majority of research attention. Astrocytes account for approximately 10-20% of total cells in the rodent brain [5], while actual percentages in individual brain regions vary. Astrocytes or astrocyte-like glia are present in the nervous systems of species ranging from roundworms, like *C. elegans*, to arthropods, such as *D. melanogaster*, through higher mammals [6]. An increase in astrocyte density increases with nervous system complexity, such that the glia-neuron ratio in invertebrates is $\sim$0.1 and $\sim$1.5 in humans [6]. Throughout species, astrocytes are considered important for homeostatic functions, including ionic homeostasis, volume regulation, neurotransmitter uptake, and metabolic support [6].

1.2.1 Morphology

Morphologically, astrocytes can be subdivided into two major populations: fibrous astrocytes of the white matter and protoplasmic astrocytes of the grey matter. Fibrous astrocytes have long processes that orient parallel to axon bundles, making contact at nodes of Ranvier and blood vessels with perivascular endfeet [7]. In contrast, protoplasmic astrocytes have a small soma that gives rise to approximately 5-10 primary processes, each of which is highly branched to form a dense arbor [8]. These astrocytes cover a large volume —approximately 20,000-80,000 μm^3, of which small arborizations account for around 85% of the total volume [8–11]. Adjacent protoplasmic astrocytes occupy entirely separate domains (Figure 1.3A) with overlap as little as 5% at the boundaries [8, 12–14]. Essentially, protoplasmic astrocytes tile the brain (Figure 1.3B & C), occupying distinct territories where they can individually respond to local neuronal demands.

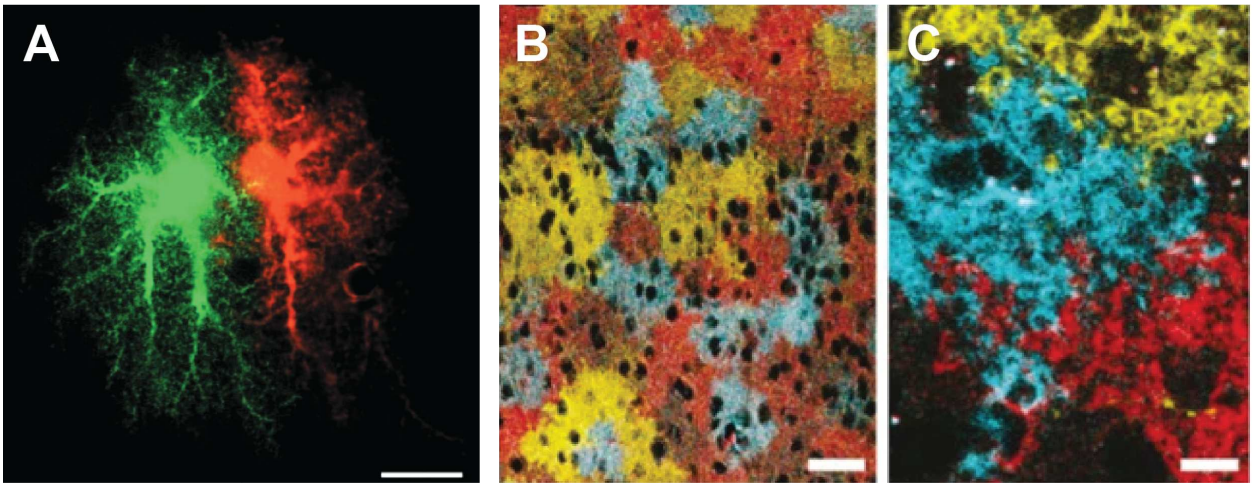

Figure 1.3: Adjacent protoplasmic astrocytes occupy distinct domains. A) Astrocytes filled with different fluorescent dyes reveal complex arborizations, which do not overlap between adjacent astrocytes. Adapted from [8]. Use of Brainbow to differentially express multiple fluorescent proteins in each cell reveals astrocytes tile the cortex (**B)** and colliculus (**C)**. Adapted from [13].

1.2.2 Astrocyte Functions

It is now known that astrocytes are a rather heterogeneous population. Protoplasmic astrocytes differ across the brain, with morphologically and functionally heterogenous astrocytes capable of occupying the same anatomical region [15–17]. Astrocytes in different regions of the brain may execute different functions tailored to the needs of that area [18]. Also, the contacts formed by peripheral astrocyte processes directly inform their function. However, all astrocytes are essential in maintaining homeostasis and providing crucial support to neurons to sustain neurotransmission [6]. By directly contacting blood vessels throughout the brain, astrocytes form a part of the blood brain barrier [19, 20], remove byproducts of metabolic processes [21], regulate local blood flow based on neuronal activity [22–24], and supply neurons with energy substrates, such as lactate [25–28]. Astrocytes also maintain homeostasis of the interstitial space by regulating pH and water content, and crucially, transporting ions and neurotransmitters [3,29–31]. Particularly, ionostasis and neurotransmitter uptake are vital in sustaining neuronal function, as high extracellular concentrations of K^+ and glutamate can lead to

neuronal hyperexcitability [32, 33]. Importantly, adjacent astrocytes are connected via gap junctions, allowing adequate buffering of K^+ and glutamate [34, 35].

In addition to homeostatic functions, it has recently been accepted that astrocytes are active contributors to synaptic communication [36, 37]. In response to neurotransmission, astrocytes release internal stores of Ca^{2+}, which can propagate throughout the cell and even into adjacent astrocytes through gap junctions [38–41]. This Ca^{2+} wave can cause the release of chemical transmitters, like glutamate and ATP, in response to neuronal activity through a process called gliotransmission [10, 36, 42]. Because astrocytes lack an active zone where vesicles accumulate, gliotransmission is thought to occur more diffusely and over a longer time scale. Nonetheless, gliotransmission is postulated to integrate activity from local networks of neurons [6, 36], synchronize local activity [43–47], and modulate synaptic activity [43–46, 48–51, 51–53].

1.3 Glutamate Homeostasis

Arguably, the most important function of astrocytes is to restrain excitatory transmission via the rapid uptake and buffering of synaptic glutamate signals. High extracellular glutamate concentrations are detrimental to neuronal health by inducing excitotoxicity and subsequent cell death [54]. To achieve efficient glutamate clearance from the extracellular space, astrocytes express high levels of Na^+-dependent glutamate transporters, which can maintain extracellular glutamate concentrations at or below 100 nM [55, 56].

1.3.1 Glutamate Transporters

In mammals, five genes encode Na^+-dependent glutamate transporters, which are part of the excitatory amino acid transporter (EAAT) family [57]. Each of these transporters is a homomeric trimer, and are designated EAAT1/GLAST, EAAT2/Glt1,

EAAT3/EAAC1, EAAT4, and EAAT5. To transport glutamate against a steep concentration gradient, EAATs co-transport 3 Na^+, 1 H^+, and 1 K^+ [58–60], and thus, transport is often coupled to the Na^+/K^+ ATPase to maintain ideal ionic concentration gradients for glutamate uptake [61,62]. Therefore, the transport of one molecule of glutamate expends one molecule of ATP [63]. Astrocytes are particularly suited for glutamate uptake because they maintain a stable negative membrane potential ($\sim$-80 mV [64]), Na^+ and K^+ gradients, and ATP supply [65–68].

Of the five subtypes, EAAT1/GLAST, and EAAT2/Glt1 are primarily expressed in astrocytes and are approximately 65% homologous at the amino acid level [69,70]. GLAST is highly expressed in the cerebellum, while Glt1 is highly expressed throughout the brain, but particularly abundant in the hippocampus [71–75]. The other glutamate transporters are expressed in neurons in specific brain regions; EAAT3 is expressed throughout the central nervous system (CNS) in both excitatory and inhibitory neurons [71,76–79], EAAT4 is expressed in cerebellar Purkinje neurons [75,80–85], and EAAT5 is expressed in retinal bipolar cells [86–89].

It appears astrocyte-expressed glutamate transporters are responsible for the majority of glutamate uptake. For GLAST, Glt1, and EAAC1, a single molecule of glutamate is transported in 10-50 ms [90]. Interestingly, evidence suggests EAAT4 and EAAT5 are very slow transporters (300+ ms per molecule) and have a large chloride conductance, thus operating more as inhibitory glutamate receptors rather than transporters [81,88,90–93]. However, all EAATs transport glutamate at a relatively slow rate compared to the lifetime of glutamate in the synaptic cleft (1.2 ms), indicating that both glutamate buffering and transport are important in the termination of glutamate signals [94].

1.3.2 The metabolic fate of glutamate

The majority (85%) of glutamate transported by astrocytic EAATs is converted into non-toxic glutamine [95]. Glutamate is converted into glutamine by glutamine synthetase (GS), which is exclusively expressed in astrocytes [96,97] and requires glutamate, ammonia, and ATP. Conversion to glutamine provides a stronger concentration gradient for more efficient uptake [98–103]. Impairment of GS increases NMDA receptor currents in cortical neurons, decreases glutamate uptake, and increases glutamate lifetime at the synaptic cleft [104]. Notably, since only astrocytes can synthesize glutamate from glucose *de novo*, neurons rely entirely on glutamine supplied by astrocytes to resupply glutamate for neurotransmission [102, 105]. After astrocytes convert glutamate to glutamine, it is shuttled to neurons via Na^+-dependent glutamine transporters (SNATs), whose activity is connected to the Na^+ flux of glutamate transporters [106, 107]. This process of glutamate uptake to glutamine synthesis and shuttling is called the glutamate-glutamine cycle.

The remaining 15% of transported glutamate is oxidized for energy production by the TCA cycle [95]. Theoretically, 24-27 ATP molecules can be produced from a single molecule of glutamate [63]. Since the transport of glutamate and conversion into glutamine require the expenditure of 1 ATP molecule each, this metabolic process is extremely important to sustain the glutamate-glutamine cycle. Interestingly, previous studies co-immunopurified mitochondrial proteins with Glt1 [108] and noted some colocalization between Glt1 and mitochondria in astrocyte processes [108, 109]. Transporters localized near mitochondria may be particularly suited to provide glutamate for the TCA cycle, although this hypothesis remains to be tested.

1.4 Glt1 Transporters

Glt1 is the most highly expressed glutamate transporter in the brain (4-6 fold greater than GLAST) and represents approximately 1% of total brain protein [110, 111]. Glt1 transporters are responsible for approximately 90% of total glutamate uptake [85], and thus their proper function is imperative for normal glutamate signaling.

1.4.1 Importance of Glt1

Glt1 knockout (KO) mice experience early-onset spontaneous seizures within 2 weeks and premature death within 12 weeks after birth [85], indicating Glt1 is vital for nervous system function. Unsurprisingly, Glt1 KO increases extracellular glutamate concentrations [85, 112, 113] and neuronal excitotoxicity [114]. Deletion of Glt1 also impairs the induction of long-term potentiation (LTP), suggesting synaptic strengthening relies on an appropriate level of glutamate at the synapse [115]. Correspondingly, overexpression of Glt1 impairs long-term depression (LTD; [116]). Mice with conditional Glt1 KO in astrocytes alone showed similar deficits to the global KOs and an 80% decrease in total glutamate uptake [117]. Mice with conditional KOs in neurons alone did not show behavioral deficits but did have lower glutamate content in synaptosomes [117]. Comparatively, GLAST KO mice develop normally and only show motor hyperactivity and minor deficits in motor coordination tasks [118, 119]. Altogether, these data indicate astrocytic Glt1 is the major contributor to glutamate uptake in the CNS, and the expression of other glutamate transporters does not compensate for its absence.

1.4.2 Glt1 is expressed throughout the CNS

Glt1 exists in 3 different splice variants, Glt1a, Glt1b, and Glt1c, which account for roughly 90%, 6%, and 1% of total hippocampal Glt1 protein, respectively [120]. Differences between each splice variant primarily occur at the distal C-terminus (Figure 1.4,

purple), which does not preclude heteromeric assembly [121,122]. Currently, no particular differences in regional expression of the splice variants have been observed, suggesting to some that their utility arises from differential regulation [120]. Interestingly, the final 11 amino acids (AA) of Glt1b confer PDZ domain interaction, such as with PSD-95, PICK1, and DLG1 [123–125]. The distal C-terminus AAs in Glt1a and Glt1c have not yet been attributed to any particular function.

Glt1 is expressed throughout the CNS, with the highest density in the hippocampus, and lowest in the cerebellum and retina, where GLAST predominates [111, 126]. In the hippocampus, most Glt1 is expressed in astrocytes, although approximately 5-10% is expressed in axon terminals [127–129], where it is believed to provide an immediate pool of glutamate to refill synaptic vesicles [117]. In general, Glt1 expression positively correlates with neuronal activity *in vitro* [130–132], with glutamate transport driving NfκB-mediated Glt1 gene upregulation [133]. Furthermore, neuronal input is likely required for any Glt1 expression, as monocultures of cortical astrocytes express little to no Glt1 [134]. Changes in Glt1 expression are present in many neurological diseases, including amyotrophic lateral sclerosis (ALS), schizophrenia, and ischemia (for

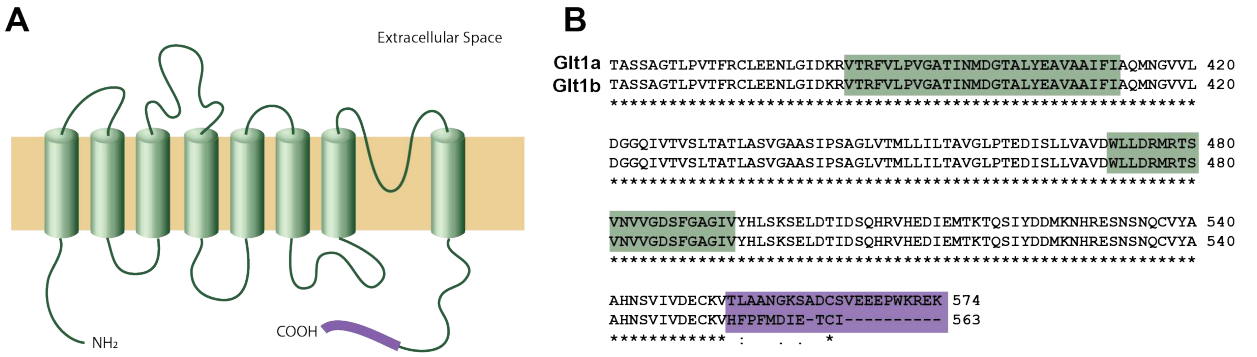

Figure 1.4: Glt1 splice variants differ in their distal C-termini. A) Model of a single Glt1 subunit, with 8 transmembrane domains (green) passing the plasma membrane (yellow). The distal C-terminus of each subunit differs between splice variants, Glt1a and Glt1b (purple). **B)** Amino acid alignment of Glt1a and Glt1b from AA 361 to the end, with transmembrane domains highlighted in green and non-conserved amino acids highlighted in purple.

review [135,136]), which may in some cases be mediated by alterations in NfκB signaling [137].

1.4.3 Glt1 forms nanoclusters in the plasma membrane

In the hippocampus, Glt1 density is extremely high at 8,500 transporters/μm^2 [111]. The majority is localized to the plasma membrane, where transporters are often located in small ($\sim$200 nm) diameter nanoclusters (Figure 1.5A) [130,138,139]. These nanoclusters are frequently localized to the tips of fine astrocyte processes, although they are found across the cell surface [130,140]. Previous studies have determined these nanocluster aggregates reside in cholesterol-rich lipid raft domains, as cholesterol removal resulted in the dissolution of nanoclusters [138,141,142]. Interestingly, cholesterol removal also decreased overall transporter activity by approximately 30%, implying the formation of nanoclusters may be functionally relevant for glutamate transport [138]. One study by Butchbach et al. (2004) showed rapid internalization of Glt1 after cholesterol disruption, which suggested that these nanoclusters might be in the early stages of endocytosis [141]. However, freeze-fracture electron microscopy found these nanoclusters were not associated with membrane invaginations [138], and thus perhaps localization to nanoclusters enhances the stability of Glt1 at the membrane.

Interestingly, neuronal activity seems to govern the localization of Glt1 nanoclusters. Neuronal activity induced by the GABA$_A$ receptor antagonist, gabazine, increased Glt1 nanocluster diameter by 49% and decreased Glt1 nanocluster distance to synapses [130]. Conversely, blocking neuronal activity with tetrodotoxin (TTX) reduced nanocluster size and increased synaptic distance [130]. Recent evidence suggests glutamate increases the surface diffusion of Glt1 molecules on the astrocyte membrane (Figure 1.5C) [140,143]. Interestingly, under resting conditions, Glt1 molecules also showed

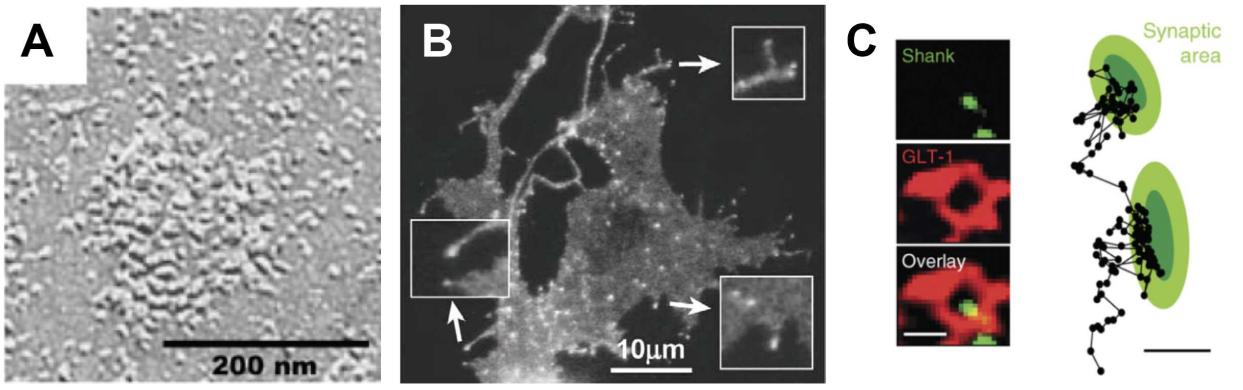

Figure 1.5: Glt1 nanoclusters localize to process tips and near synapses. A) Freeze-fracture electron microscopy of exogenous Glt1 expressed in BHK cells reveals nanoclusters on the plasma membrane of approximately 200 nm. [138] **B)** Nanoclusters of Glt1 localize to the tips of fine processes. [130] **C)** Static Glt1 (red) localizes near synapses (green, left panel), while mobile Glt1 slows its movement near synapses (right panel). [140]

slower diffusion near synapses, suggesting the existence of some mechanism to selectively trap Glt1 in the vicinity of synapses.

1.5 Astrocytes contact neurons at specialized locations

1.5.1 Astrocytes ensheath synapses

A single astrocyte contacts between 20,000 to 100,000 synapses in rodents and up to two million synapses in humans [144]. Across the brain, synaptic clefts are often associated with thin astrocyte protrusions called perisynaptic astrocyte processes (PAPs) in a structure now referred to as a tripartite synapse (Figure 1.6). PAPs have an extremely small diameter ($\sim$50 nm; [145]) and a large surface-to-volume ratio. These qualities render PAPs difficult to study using conventional light microscopy, to record electrophysiogically, and to isolate biochemically. Thus, most of our knowledge comes from electron microscopic (EM) studies of fixed tissue.

PAPs identified in EM studies seem to be remarkably devoid of mitochondria, microtubules, or ER membranes [146, 147]. However, these processes do contain glycogen

granules, ribosomes for local translation, and actin cytoskeleton [146,148–151]. Immunolabeling shows localization of actin-binding proteins [149,152], cell adhesion molecules [153], and proteins involved in the glutamate-glutamine cycle, including Glt1 [73,111, 148,154]. These data suggest the primary functions of PAPs are to buffer glutamate at synaptic adhesions.

The number of synapses associated with a PAP varies depending on the brain region. For instance, PAPs are localized adjacent to approximately 64-90% of synapses in the hippocampus (Figure 1.6) [155,156], 29-56% of synapses in the rat neocortex, and 90% of synapses in the mouse somatosensory cortex [146]. One PAP covers roughly 57% of each CA1 hippocampal synapse [156], which mostly form contacts at post-synaptic elements [157]. In contrast, PAPs almost entirely ensheath CA3 synapses [158], indicating there is large heterogeneity even within the same brain region. Interestingly, spines associated with PAPs tend to be larger [155,159,160], and the size of the astrocyte contact positively correlates with the surface area and complexity of the post-synaptic density

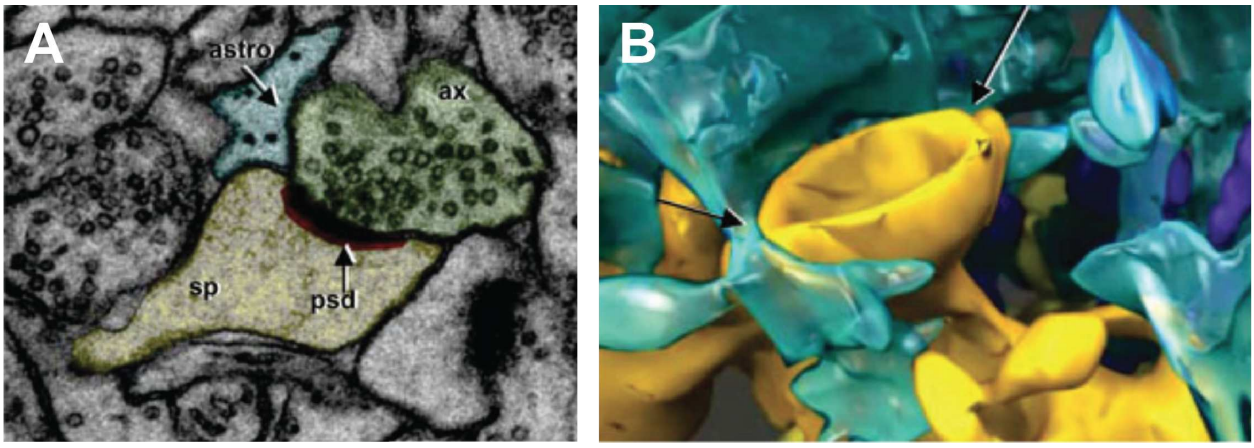

Figure 1.6: Astrocytes ensheath synapses. A) An EM micrograph depicting a synapse in the CA1 region of the hippocampus of an adult rat. In this example, an astrocyte (blue) contacts the axon-spine interface between an axon terminal (green) and a dendritic spine head (yellow). **B)** 3D reconstruction of serial EM data gathered from rat CA1 hippocampus. In this example, an astrocyte (blue) contacts 50% of a dendritic spine head (yellow). Adapted from: [155]

(PSD; [132,155]). These data suggest the astrocyte contact area is dynamically regulated in congruence with synaptic strength or activity.

In support of this notion, many recent studies have shown astrocytes undergo a remarkable amount of morphological changes in response to stimuli that increase neuronal activity. Environmental stimulation, including exercise and enrichment, increased arborization of astrocytes in the hippocampus, outgrowth of PAPs, and increased synaptic coverage [161–164]. Induction of long-term potentiation (LTP) also increased astrocyte coverage of both pre- and post-synaptic elements [160]. However, astrocyte contact with synapses appeared to decrease with sustained hyperactivity, as evidenced by a decrease in the number of synapses associated with astrocytes in cases of severe epilepsy [159].

In cultured astrocytes, glutamate exposure increased filopodia formation [165], which bear resemblance to PAPs. Structural changes in PAPs appear to require mGluR-activated Ca^{2+} signaling and actin cytoskeleton remodeling via the ERM protein, ezrin [152]. Inhibition of astrocyte Ca^{2+} signaling reduced the number of synapses in contact with astrocytes [166], suggesting a regular astrocyte Ca^{2+} response to synaptic activity is necessary to maintain tripartite synapse integrity.

Limiting the lifetime of glutamate at the synaptic cleft is highly dependent on astrocyte coverage of the synapse. While astrocyte coverage of cerebellar synapses is nearly complete, CA1 hippocampal synapses are believed to be incompletely covered [156]. Therefore, incomplete coverage allows for incomplete buffering of glutamate. This suggests a role for glutamate spill-over in the hippocampus, which allows diffusion to and activation of nearby synapses. Glutamate spill-over could be tightly controlled by the expression, localization, and function of Glt1 transporters near synapses, as well as, astrocyte coverage of the synapse, which is highly dynamic [146,152,163,167]. Interestingly, in the CA1 region of the hippocampus, astrocyte coverage of synapses seems to correlate

with synaptic size, such that larger synapses are less completely contacted by astrocytes, and thus more capable of contributing to and responding to glutamate spill-over [168]. Therefore, the amount of astrocyte contact with a synapse is capable of directly affecting glutamatergic communication at its immediate location and nearby synapses.

1.5.2 Glt1 shapes synaptic transmission

Given its abundance and widespread expression [110, 111], Glt1 is thought to provide the major mechanism for glutamate uptake at synapses [3,169,170]. To affect synaptic transmission, Glt1 must be localized near synapses. Indeed, Glt1 nanoclusters have been localized at the tips of fine processes and near synapses in PAPs (Figure 1.5B & C) *in vitro* and *in vivo* [130, 134, 139, 171, 172]. Additionally, numerous studies suggest glutamate transporter activity directly shapes glutamatergic transmission by limiting the lifetime of glutamate in the synaptic cleft [140, 173–178]. This is accomplished via several mechanisms, including glutamate transport, glutamate buffering via binding, and concentrating transporters near synapses. Glt1 transporters are capable of handling synaptic glutamate even in the case of high-frequency stimulation [179], indicating Glt1 transporters influence the lifetime of glutamate in the synaptic cleft regardless of activity conditions. One study found Glt1 distance from synapses decreased following neuronal stimulation, while distance increased following neuronal silencing [130], showing that Glt1 localization, and thus, its ability to shape synaptic signaling, is dynamically regulated by neuronal activity.

Although Glt1 is capable of handling large glutamate concentrations, it takes approximately 11-70 ms to complete the transport cycle of one molecule of glutamate [180–182], which is relatively long compared to the lifetime of glutamate in the synaptic cleft ($\sim$1.2 ms, [94]). To efficiently clear glutamate despite slow transport kinetics, Glt1 transporters initially act to buffer glutamate. Upon glutamate release at synap-

tic terminals, approximately 80% immediately diffuses out of the cleft, which is then bound and buffered by glutamate transporters [182]. Inexplicably, when glutamate binds to Glt1, lateral diffusion of Glt1 in the astrocyte plasma membrane increases (Figure 1.6C), effectively replacing bound transporters with unbound, naive transporters at the synapse [140,143]. In addition to observations of Glt1 localized near synapses, recent studies of Glt1 transporter dynamics in live cells show Glt1 lateral diffusion decreases in the astrocyte membrane facing synapses [140,143]. By cross-linking Glt1 transporters to prevent their lateral diffusion out of the perisynaptic astrocyte membrane but retain their transport function, Murphy-Royal et al. showed that glutamate buffering via lateral diffusion actively shapes the timecourse of excitatory post-synaptic currents (EPSCs) [140].

Altogether, these data indicate lateral transporter diffusion and transport itself are crucial to spatially and temporally limit glutamatergic signaling, both of which are dependent on the proper localization of Glt1 transporters. While we have known for some time that Glt1 is important for synaptic function, we know very little about the mechanisms of localizing Glt1 to PAPs, and thus synapses. Chapter 2 describes one possible mechanism.

1.5.3 Astrocytes contact neurons at clusters of Kv2.1 channels

In addition to forming contacts at synapses, astrocytes also contact the neuronal soma at surface clusters of the voltage-gated potassium channel, Kv2.1. Electron microscopy studies of rat brains show large diameter ($\sim$0.5 μm) clusters of immunogold labeled Kv2.1 channels on the plasma membrane of neuronal somas and proximal dendrites (Figure 1.7) [183]. Kv2.1 clusters were frequently in direct contact with thin astrocyte processes (<200 nm, blue) and with a sub-surface cistern (SSC) of endoplasmic reticulum (ER) membrane (red). Interestingly, Kv2.1 clusters facing astrocytes were more than twice as dense as those not facing astrocytes. Additionally, the clusters associated

with SSCs of ER membrane were nearly always in apposition to an astrocyte, perhaps implying ER Ca^{2+} signaling is important at these contacts.

These researchers also noted that Kv2.1 immunograins could be observed directly adjacent to post-synaptic densities. Kv2.1 immunograins were fairly common ($\sim$53%) at symmetric synapses, while they were more rarely observed at asymmetric synapses. Interestingly, at some of these synapses, astrocyte processes were in close contact with the Kv2.1 immunograins, possibly implicating the Kv2.1-astrocyte contact in the formation of tripartite synapses. In EM micrographs at the soma, the thin astrocyte processes apposed to Kv2.1 clusters bear a resemblance to PAPs in that they seem to lack organelles (Figure 1.7). Perhaps these two locations where astrocytes contact neurons are regulated by similar mechanisms.

Although we have known of the existence of this neuron-astrocyte contact for some time, very little is known about its function or structure. Perhaps the only known structural characteristic of these contacts is that astrocytic Glt1 localizes in nets around Kv2.1 clusters in the somatosensory cortex [184] (Figure 1.7B). Functionally, we know that proper Glt1 transport is necessary to maintain Kv2.1 cluster integrity [184, 185], as inhibition of Glt1 glutamate transport causes Kv2.1 cluster disintegration, the mechanism of which will be discussed at length in Section 1.7.2. A major aim of this dissertation was to further define the components at this neuron-astrocyte contact, which is presented in Chapter 3.

Recently, Cserép et al. found that over 90% of microglia-neuron contacts also occur at Kv2.1 clusters [186]. Immunofluorescence revealed that microglia membranes adjacent to Kv2.1 clusters were enriched in purinergic P2Y12 receptors, for which ATP is the primary ligand. These authors found that microglial contacts occurred most often near Kv2.1 clusters that were localized near active mitochondria, indicating purinergic

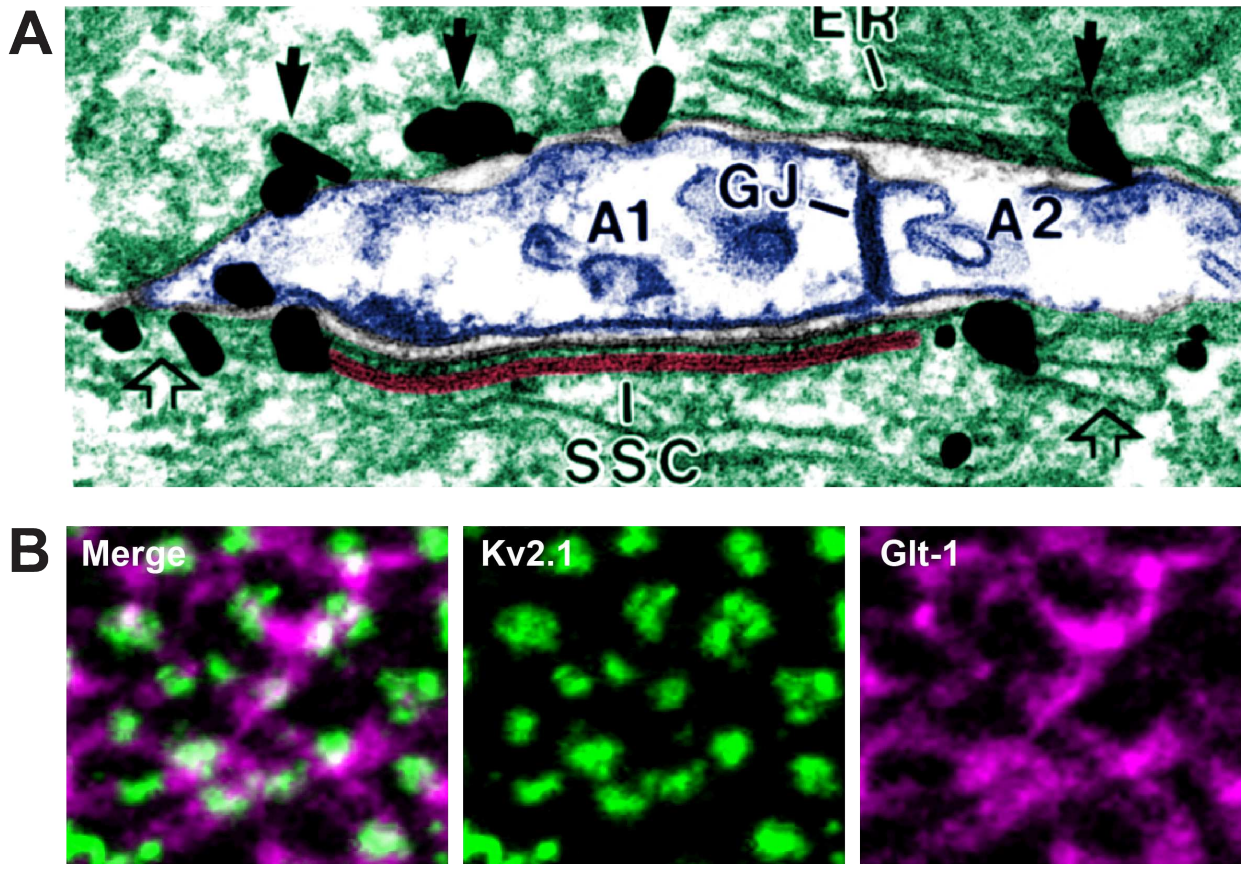

Figure 1.7: Astrocytes contact neurons at clusters of Kv2.1 channels. A) An EM micrograph depicting immunogold labeling of a cluster of Kv2.1 potassium channels (black grains) in the CA1 region of the hippocampus. In this example, two astrocyte processes (blue) contact adjacent neurons (green) at Kv2.1 clusters. A sub-surface cistern (SS**C)** of ER membrane lies directly beneath the Kv2.1 cluster (red). Lack of continuous immunogold labeling is likely due to incomplete antibody access. Adapted from: [183] **B)** Immunolabeled Glt1 (magenta) forms net-like structures around neuronal Kv2.1 clusters (green) in the somatosensory cortex of rats. Adapted from: [184]

signaling at Kv2.1 clusters is important for microglial monitoring of neurons. Altogether this work suggested Kv2.1 clusters may be specialized glia-neuron contact sites that are capable of communicating neuronal health and activity to glia. Given the abundance of astrocyte-neuron contacts at Kv2.1 clusters, it will be interesting to discover additional methods of neuron-to-glia communication that occur at these specialized junctions.

1.6 Kv2 Potassium Channels

The Kv2 family of voltage-gated potassium channels consists of two members, Kv2.1 and Kv2.2. Kv2.1 and Kv2.2 sequences are well conserved throughout the N-terminus (86%) and the six transmembrane domains (95%), which compose the majority of the channel structure [187]. Although both channels have large intracellular C-terminal domains, this sequence is less conserved (63%) [187]. Kv2 channels are possibly the most broadly expressed K^+ channel in mammalian tissue, as they are expressed on the plasma membrane in diverse excitable cell types, including in spinal α-motoneurons [188], cortical neurons [183, 189], hippocampal neurons [183], Purkinje and granule cerebellar neurons [190], olfactory granule neurons [191], retinal bipolar cells [192], cardiac myocytes [193], vascular and gastrointestinal smooth muscle [194,195], and pancreatic beta cells [196–200]. Immunolocalization and mRNA expression studies revealed overlapping but distinct patterns of Kv2.1 and Kv2.2 in the brain, with neurons primarily choosing to express one isoform over the other [189,190].

1.6.1 Kv2 Conductance

Classically, voltage-gated potassium channels are regulators of excitability in cells, like neurons. Delayed-rectifier voltage-gated potassium channels are activated during the later phase of the action potential, opening to conduct potassium current out of the excitable cell to repolarize the membrane potential back to its resting state. Characteristic of delayed-rectifiers, Kv2 channels are slow to inactivate and have a high activation threshold [201]. Kv2 channels are the major delayed-rectifiers in the brain, comprising approximately 80% of total delayed-rectifier current in hippocampal and cortical neurons [202]. Importantly, Kv2.1 modifies the action potential waveform and duration to enable high-frequency firing (1 Hz) in neurons [203–208]. When Kv2.1 is absent, neuronal action potentials fail to repolarize, which prevents Nav channels from exiting the inactivation

state, and subsequently, high-frequency firing terminates due to an inability to open Nav channels.

Interestingly, our lab has found the majority of Kv2 channels are electrically non-conducting. Cell-attached patch-clamp directly on a Kv2.1 cluster results in single-channel current recordings [209]. In a follow-up study, individual fluorescent Kv2.1 channels were counted and used to calculate overall expression while simultaneously recording currents from conducting channels. This study revealed that less than 30% of endogenous Kv2.1 channels were conducting in neurons, while only 4% were conducting when heterologously expressed in HEK cells at the highest expression density [210]. Recently, this work was expanded to show that Kv2.2 also has a non-conducting state [see Maverick, 2020 dissertation]. Due to the high levels of Kv2 expression, a non-conducting state is necessary to prevent electrical silencing of excitable cells. Altogether, these data suggest the majority of surface Kv2 channels are not conducting, and consequently, play additional important structural roles.

1.6.2 Kv2 Clustering

Interestingly, on a subcellular level Kv2 channels display a clustered localization on the plasma membrane of neurons *in vivo*, in neuronal culture, and HEK cells [211], where a few hundred channels occupy patches of approximately 0.5-1 μm^2 [212]. Early studies suggested Kv2.1 and Kv2.2 occupied distinct subcellular compartments, however, Kv2.2 was mislocalized due to the initial cloning of a truncated version of Kv2.2 [213]. Many early studies compared Kv2.1 to the truncated Kv2.2, and thus it was concluded that these two channels did not heteromerize, as they occupied separate locations [205]. It is now believed that, in neurons, both channels form clusters in the soma, proximal dendrites and, axon initial segment (AIS), and at least some of these channels are heteromers [183, 211, 213, 214].

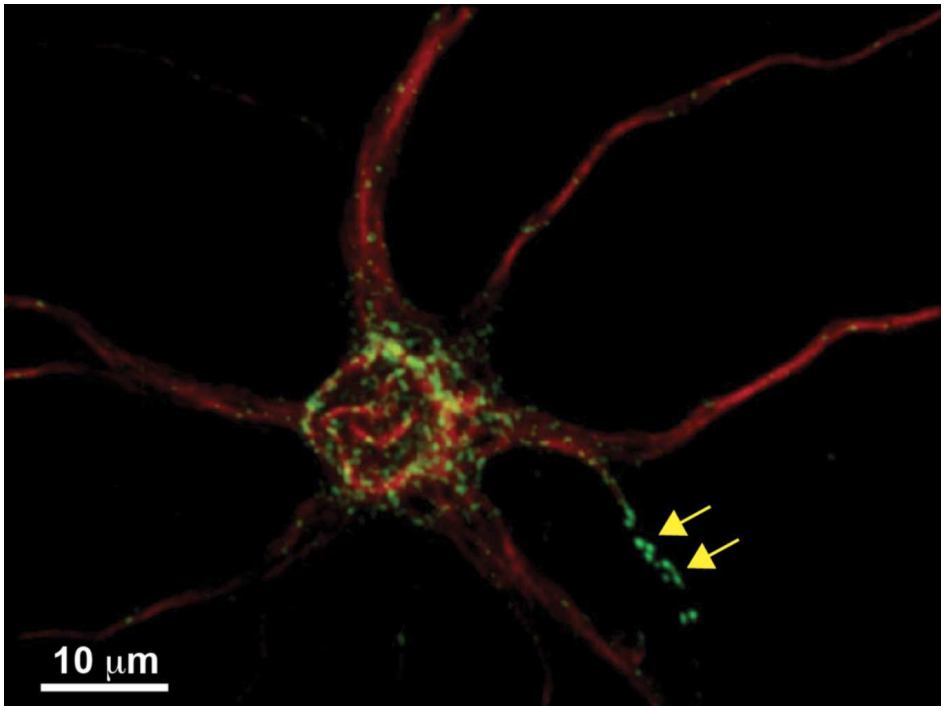

Figure 1.8: Kv2.1 channels form micron-sized clusters on the plasma membrane of neurons. Immunofluorescence image of a cultured hippocampal neuron transfected with GFP-Kv2.1 (green) and labeled with an antibody directed against MAP2 (red). Clusters localize to the soma, proximal dendrites, and the axon initial segment (yellow arrows). Scale bar is 10 μm. Adapted from: [215]

Mechanism of cluster formation

Kv2 clustering is dependent upon the phosphorylation of amino acid residues in the long C-terminus. Using truncation mutants, the Trimmer group discovered a region in the C-terminus of Kv2.1 which is required for clustering and which is heavily phosphorylated [212, 216]. A mutant Kv2.1, missing the last 318 amino acids, presented an entirely diffuse localization on the plasma membrane, while a mutant lacking the last 187 amino acids still conferred clustering. Therefore, the domain responsible for the clustered localization must exist in the C-terminus between amino acids 535-666. Further truncation studies discovered only 26 amino acids (AA 573-609) within this domain were necessary for clustering, denoted the proximal restriction and clustering domain (PRC), and point mutations showed three serines and one phenylalanine were critical [217].

Based on the fact that three serines are required for clustering, the post-translational modification was postulated to be caused by phosphorylation.

Recent work undertaken by our lab found that the PRC represents a non-canonical FFAT (two phenylalanines in an acidic tract) motif, which confers interaction with VAP proteins of the endoplasmic reticulum [218]. Knockdown of VAP expression with siRNA significantly reduced clustering of Kv2.1 channels on the surface of HEK-293 cells. In addition, expression of a VAP mutant, which cannot bind FFAT motifs, significantly decreased interaction with Kv2.1, as measured by Förster resonance energy transfer (FRET) [Appendix A]. Johnson et al. further narrowed the PRC domain to just 14 amino acids which are necessary for VAP interaction. Appending these amino acids to the intracellular domain of CD4, a single transmembrane domain protein, conferred clustering on the plasma membrane surface and colocalization with ER-localized VAP proteins. Interestingly, these 14 amino acids contain five serine residues, which are among those previously identified [217]. Indeed, these data explained published observations of colocalization between Kv2 clusters and ER membranes and proteins [183,210,219,220].

1.6.3 Endoplasmic Reticulum/Plasma Membrane Junctions

Clusters of Kv2 channels represent endoplasmic reticulum (ER) plasma membrane (PM) junctions, where the ER and PM come into very close contact (5-8 nm [183]). Recent studies estimate ER/PM junctions make up approximately 12% of the neuronal surface *in vivo* [221]. As such, this organelle may be critically involved in several cellular processes, including regulating Ca^{2+} homeostasis, post-translational modification, lipid exchange, and protein trafficking (for review [222,223]).

Kv2 clusters as trafficking hubs

Several studies have implicated Kv2 clusters in exocytosis. A Kv2.1 interaction with syntaxin mediates dense-core vesicle release from neuroendocrine cells, which is not reliant on K^+ flux [224, 225]. Following this work, our lab found that approximately 85% of plasma membrane insertions of both Kv2.1 and Kv1.4 occurred at the perimeter of Kv2.1 clusters [215]. In a subsequent study, we found that 82% of transferrin receptor exocytosis also occurred at the perimeter of even small ER/PM junctions lacking Kv2.1 channels, indicating that this preference for exocytosis is not limited to Kv channels [210]. Recent studies in pancreatic β-cells show insulin granule exocytosis also occurs at the perimeter of Kv2.1-induced ER/PM junctions [197, 198]. These are probably just a few examples of the exocytosed molecules that occur at Kv2 clusters. Given the association of Kv2 clusters with glia, perhaps some of these vesicles contain signaling molecules to communicate with glia, as suggested with ATP and microglia [186]. Beyond normal surface trafficking functions, the Kv2.1-syntaxin interaction is now understood to mediate increased surface expression of newly synthesized and conducting Kv2.1 channels that initiate apoptotic K^+ efflux. This is discussed more in Section 1.7.

1.6.4 AMIGO1 as a Kv2 β-subunit

In addition to interacting with VAP, Kv2.1 interacts directly with AMIGO1 (amphoterin-induced gene and ORF), which possesses an extracellular domain that acts as a cell-adhesion molecule (CAM) [226, 227]. AMIGO1 colocalizes with both Kv2.1 and Kv2.2 throughout the brain in many different mammalian species (Figure 1.9A [228]). Interaction with AMIGO1 modifies the voltage-dependence of activation of Kv2.1 [226], such that the midpoint of activation is $\sim$10 mV shifted in the hyperpolarizing direction.

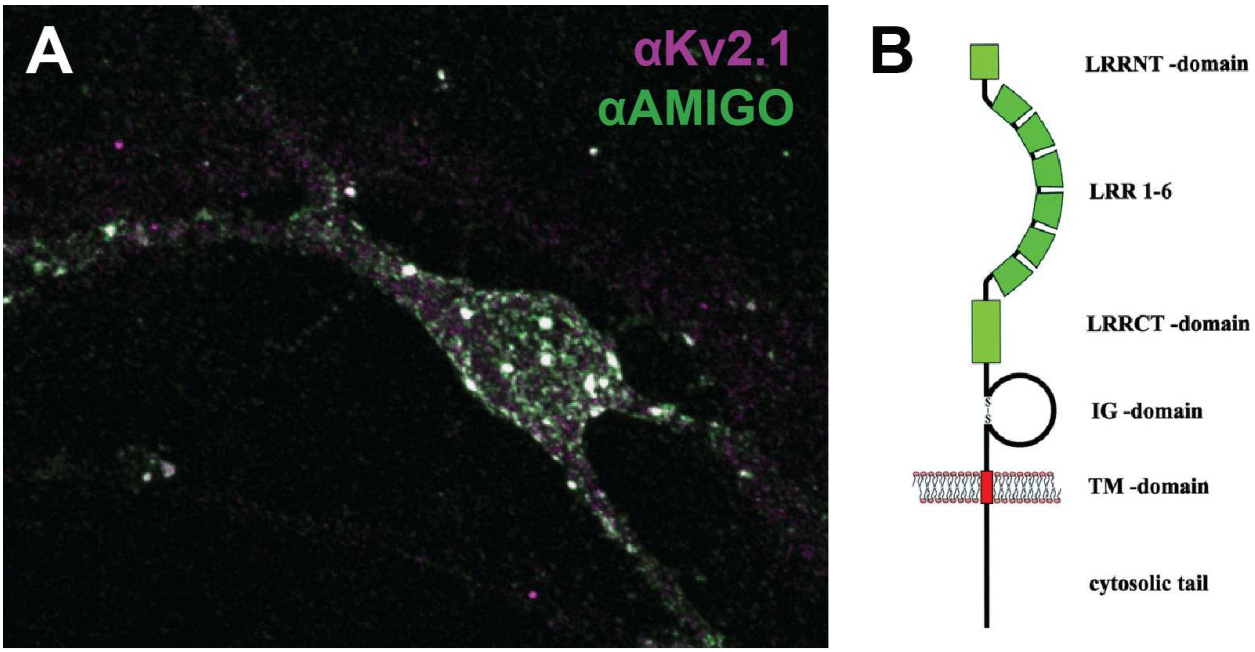

Figure 1.9: AMIGO1 colocalizes with Kv2.1 clusters in hippocampal neurons. A) Immunofluorescence image of a cultured hippocampal neuron labeled with an anti-Kv2.1 antibody (magenta) and an antibody directed against AMIGO1 (green), where white pixels indicate co-localization. **B)** Model of AMIGO1 protein. AMIGO1 has a large extracellular N-terminus, containing leucine-rich repeats and an immunoglobulin-like domain, which are responsible for adhesion. B Adapted from: [227]

AMIGO1 is homogeneously distributed throughout the cell membrane when Kv2 subunits are absent [228]. However, when Kv2 channels are expressed as well, AMIGO1 redistributes to Kv2 surface clusters, which still form ER/PM junctions [228]. Due to this redistribution, concentrations of cell-adhesion molecules exist at points across the membrane, which could facilitate cell-cell interactions, such as the neuron-glia contacts described above. Additionally, since ER/PM junctions exist at each of these surface clusters of Kv2 and AMIGO1, this junction may be especially apt for ER Ca^{2+} signaling and exocytic communication.

The AMIGO Family

The AMIGO family consists of 3 members (AMIGO1, 2, and 3), which are about 48% similar at the amino acid level [226]. AMIGOs are single-pass transmembrane proteins,

with short intracellular C-termini and extensive N-termini with 6 leucine-rich repeat (LRR) domains and an immunoglobulin-like domain (Figure 1.9B, [227,229]). Each member of the AMIGO family is capable of homophilic and heterophilic interactions within the family [227], as evidenced by immunoprecipitations and bead aggregation assays. AMIGOs are not known to participate in adhesion with any other type of CAM, however, many CAM families also contain leucine-rich repeat domains [230], and as such, it remains possible that their interactions extend beyond the immediate family. AMIGO1 is the most highly expressed in the brain, while the other two are more widespread in tissue distribution, although still enriched in the brain [227]. Although AMIGO2 and AMIGO3 were discovered at the same time as AMIGO1, no published studies have yet examined the relationship of these two proteins with Kv2 channels (see Chapter 4).

Known Functions of the AMIGO Family

The AMIGO family has been implicated in several cell biological processes, including developmental neurite outgrowth and guidance, cell survival, and adult axon growth inhibition [227,231–233]. AMIGO1 is involved in neurite outgrowth of neurons in culture and axon tract development in Zebrafish [227,234]. Culture dishes coated with AMIGO1 ectodomain increased neurite outgrowth by greater than 12 fold after 24 hours of culture [227]. Interestingly, AMIGO2 has been implicated in enhanced growth and survival in a variety of cell types, including cerebellar granule neurons [235], vascular endothelial cells [236], gastric adenocarcinoma cells [237], and melanoma cells [238]. This increase in cell viability may be due to an interaction between AMIGO2 and PDK1, a kinase that activates Akt in cell survival pathways [239]. Emerging evidence suggests AMIGO2 is particularly relevant for metastatic cancers, perhaps acting dually to enhance migration via cell adhesion and increase cell viability via the Akt pathway [237,238,240,241]. Park et al. uncovered the domain responsible for PDK1 interaction, and thus the effects on cell survival, using a combination of protein domain identification databases and exoge-

nous expression of C-terminal fragments [239]. Remarkably, the domain they identified is quite well conserved (∼73%) within the AMIGO family, suggesting AMIGO1 and AMIGO3 could have similar effects on cell survival, although this remains to be tested. While AMIGO cell adhesion has not yet been implicated in any cell-cell contacts *in vivo*, it is tempting to speculate that AMIGO adhesion is involved in the formation of glia-neuron contacts at Kv2.1 clusters.

1.7 Ischemia and Glutamate Excitotoxicity

Both astrocytic Glt1 and neuronal Kv2.1 clusters are critical in the response to metabolic insults that give rise to neuronal excitotoxicity. Pathophysiological levels of extracellular glutamate trigger cell death by over-activating neurons, leading to ionic rundown, ATP depletion, and high intracellular Ca^{2+}. These hallmarks of glutamate excitotoxicity are a result of dysfunction of glutamate homeostasis in both neurons and astrocytes [54, 242–244], and ultimately this dysfunction culminates in cell death. Glutamate excitotoxicity arises following several brain diseases, including traumatic brain injury, as a part of neurodegenerative disease, or following an ischemic attack [54]. Since it is easily modeled, most of the following discussion will be related to ischemic stroke.

Ischemic stroke occurs as a result of blood vessel occlusion, such that blood flow is diminished or blocked to the brain, leading to a deficit of glucose and oxygen. Lack of these energy substrates prevents the production of ATP via oxidative phosphorylation, and thus eventually leads to dysfunction of cellular processes that rely on ATP [242]. In ischemic stroke, tissue can be categorized into two zones of severity. The cells nearest the occlusion are part of the core, while cells surrounding the core are part of the penumbra. Cells in the core experience the greatest deficit in energy supply and within minutes suffer from irreversible cell death [245]. Cells in the penumbra also suffer from reduced energy supply, although to a lesser extent. As such, these cells do not die im-

mediately after stroke, but instead, experience spreading depolarizations and glutamate dyshomeostasis.

1.7.1 Astrocyte Response to Insult

Glutamate Transporter Function

As described in detail above, astrocyte glutamate transporters are the primary means by which glutamate is removed from the extracellular space to limit synaptic glutamate signaling [110, 243]. Glutamate uptake relies on ionic gradients of Na^+, K^+, and H^+ to transport glutamate against a steep concentration gradient, with the driving force of Na^+ and the negative membrane potential providing most of the energy required for uptake [245]. These ionic gradients are primarily maintained by the Na^+/K^+ ATPase, which catalyzes ATP to import two K^+ ions and export three Na^+ ions. During metabolic stress when the ATP supply is diminished, the Na^+/K^+ ATPase becomes non-functional, leading to depolarization of the membrane potential, the collapse of ionic gradients, and subsequent increases in extracellular glutamate concentration [242]. Similarly, glutamine synthetase (GS) relies on ATP, and therefore decreases in ATP supply increase intracellular glutamate concentrations, resulting in decreased uptake by glutamate transporters [104]. As such, this leads to an accumulation of extracellular glutamate, which prolongs the activation of synaptic and extrasynaptic glutamate receptors. Indeed, dysfunction of astrocytic glutamate transporters results in extracellular glutamate concentrations up to 1 μM [246], compared to the physiological concentration of 20-60 nM [56, 114, 247]. Altogether, the literature suggests Glt1 function can be disrupted at multiple levels during ischemic events.

Glutamate Transporter Expression

In addition to changes in functionality, glutamate transporter expression is altered following ischemic insult. Although a few studies have found contradictory results, the main consensus is that transporter expression is upregulated in the early phase of an ischemic event and decreased in the later phase [248–250]. Glutamate transporter expression also appears to scale with insult severity, as ischemic preconditioning upregulated the expression of Glt1a in the hippocampus, while severe ischemia induced a downregulation of Glt1a expression [249]. Several studies employing ischemic preconditioning paradigms have observed an increase in Glt1 expression, which abrogated cell death following an ischemic event [249, 251, 252]. Additionally, blocking the function of Glt1 receptors using dihydrokainic acid (DHK) prevented the protection provided by ischemic preconditioning [253], indicating that the upregulation of Glt1 expression is majorly responsible for neuroprotection following ischemic preconditioning.

Astrocytic Glutamate Release

In addition to decreases in glutamate uptake, the collapse of transmembrane ionic gradients, and depolarization of the membrane, increased intracellular glutamate concentrations can cause glutamate transporters to run in reverse [97,254]. The result of this is an even larger accumulation of extracellular glutamate. Increased intracellular Na^+ concentrations that occur due to Na^+/K^+ ATPase dysfunction lead to accumulation of intracellular Ca^{2+} via reversal of the Na^+/Ca^{2+} exchanger [255]. Recent evidence suggests that glutamate-containing vesicles can be exocytosed via a Ca^{2+} dependent mechanism in astrocytes [256], ultimately leading to additional extracellular glutamate. Furthermore, high extracellular K^+ leads to depolarization of both astrocytes and neurons, decreasing the driving force for glutamate uptake and exacerbating neuronal excitabil-

ity [97]. Together these data suggest that astrocytes can actively contribute to the rise in extracellular glutamate concentration, independent of impaired glutamate uptake.

1.7.2 Neuronal Response to Insult

Studies over the last 25 years implicate the localization and function of Kv2.1 in the ischemic and excitotoxic response. The neuronal response to insult seems to be divided into an early neuroprotective response, where the localization and activation of Kv2.1 are altered, and a secondary apoptotic response, where Kv2.1 surface expression and K^+ conductance are upregulated.

Kv2 clustering is sensitive to insult

Clustering of Kv2.1 is controlled by neuronal activity and pathophysiological events, such as ischemia [184,257–259]. For instance, Kv2.1 clusters in α-motoneurons are sensitive to extended stimulation, indicating clustering is regulated by neuronal activity [260]. Furthermore, under conditions of experimental ischemia and hyperexcitability, Kv2.1

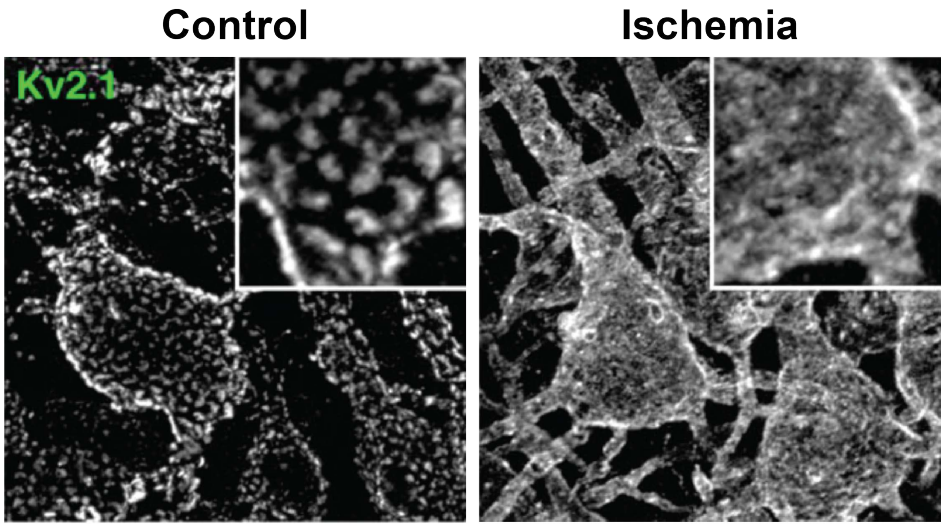

Figure 1.10: Kv2.1 clusters disintegrate following ischemic insult. Immunolabeled Kv2.1 channels in neurons of the somatosensory cortex in control (left) and ischemic (right) brains. The right image shows Kv2.1 channels are diffusely localized across the neuronal membrane after ischemic insult. Adapted from: [184]

channels disperse from their clustered state, and the voltage-dependence of activation shifts leftward by 35 mV, thus activating the channels at lower voltages and dampening neuronal excitability [257,261,262].

Kv2.1 cluster dispersion occurs rapidly after insult, on the order of minutes, and recovers over 15 minutes following reperfusion or washout in studies using experimental hypoxia and ischemia [257]. Interfering with Kv2.1 clustering via competitive interference of VAP interaction by a membrane permeable TAT peptide fused to the Kv2.2 C-terminus is neuroprotective *in vitro* and *in vivo* [263]. Mice that underwent medial cerebral artery occlusion (MCAo) and were subsequently treated with the TAT peptide that disperses Kv2.1 clusters showed decreased infarct volume after 24 hours [263]. Given these data, Kv2.1 declustering is likely neuroprotective in the early phases of the ischemic response.

The mechanism of declustering and the shift in voltage dependence both rely on altering the phosphorylation of the channel. Under conditions of high extracellular glutamate, extrasynaptic NMDA receptors are activated, leading to an influx of Ca^{2+}. Kv2.1 clusters and ER/PM junctions disintegrate due to Ca^{2+} dependent dephosphorylation of the channel's C-terminus by calcineurin (Figure 1.10) [261]. In this study, Misonou and colleagues also found the hyperpolarizing shift in Kv2.1 activation occurs as a result of graded dephosphorylation of multiple residues unrelated to the clustering motif. In summary, the early neuroprotective response to insult is due to a combination of dampening neuronal excitability and declustering of Kv2.1 channels.

Kv2.1 activity is essential for apoptosis

A characteristic of ischemia is delayed cell death in the penumbra surrounding the core. While necrotic cell death is the primary mechanism in the core, apoptotic cell death occurs in the penumbra in the days following insult. Increased K^+ efflux is essential

to the initiation of the apoptotic cascade, as it allows for the functioning of apoptotic enzymes, such as caspase-3 [259]. Enhanced K^+ efflux is thought to primarily occur through voltage-gated potassium channels, as a widespread antagonist of the Kv family, TEA, is neuroprotective in models of ischemia [264].

Subsequent studies found Kv2.1 is the primary contributor to apoptotic K^+ efflux. Pal and colleagues found that the expression of a dominant-negative Kv2.1 subunit completely abolished the apoptotic potassium current, which was neuroprotective [265]. Exogenous expression of Kv2.1 in CHO cells rendered them more susceptible to an apoptotic stimulus [265]. Follow-up studies by the Aizenman lab have found the increase in Kv2.1 potassium current is due to the insertion of newly synthesized channels [266]. As such, the syntaxin-binding domain in the C-terminus of Kv2.1 is required for increased surface expression, and thus, the apoptotic K^+ surge [267]. Insertion of new Kv2.1 channels primarily occurs at the edge of existing Kv2.1 clusters [215]. By dispersing clusters with the TAT peptide described above, neurons were protected by preventing the apoptotic K^+ current [263]. This suggests that reformation of Kv2.1 clusters after the initial neuroprotective dispersion is required for new insertion of Kv2.1 channels, and thus apoptosis. Therefore, the response of Kv2.1 is both neuroprotective and neuro-damaging depending on the time after insult.

1.7.3 Kv2.1-Astrocyte Contacts are at the Nexus of the Ischemic Response

The evidence outlined above provides a solid foundation for understanding Kv2.1-astrocyte contacts in the context of ischemic insult. Altogether, the localization of Glt1 in nets around neuronal Kv2.1 clusters [184] could be considered the first checkpoint in detecting pathophysiological levels of extracellular glutamate, at concentrations above the maximum capacity of astrocyte transporters. Indeed, in studies where Glt1 glutamate transport was pharmacologically blocked by DHK, Kv2.1 channels were largely dephos-

phorylated, suggesting Glt1 dysfunction can lead to dispersal of Kv2.1 clusters [184,185]. Additionally, impairment of astrocyte metabolism by fluorocitrate was sufficient to induce Kv2.1 dephosphorylation, and presumable cluster disintegration [184], thus initiating the neuronal ischemic response. The concentration of Glt1 transporters around Kv2.1 clusters could act to locally limit levels of ambient glutamate, ensuring that Kv2.1 cluster dispersal events only occur in cases where a rapid neuroprotective response is necessary.

1.8 Overview of this Dissertation

While the importance of Glt1 and Kv2.1 in the response to insult is, at this point, undeniable, we still know very little about the structure and function of astrocyte-Kv2.1

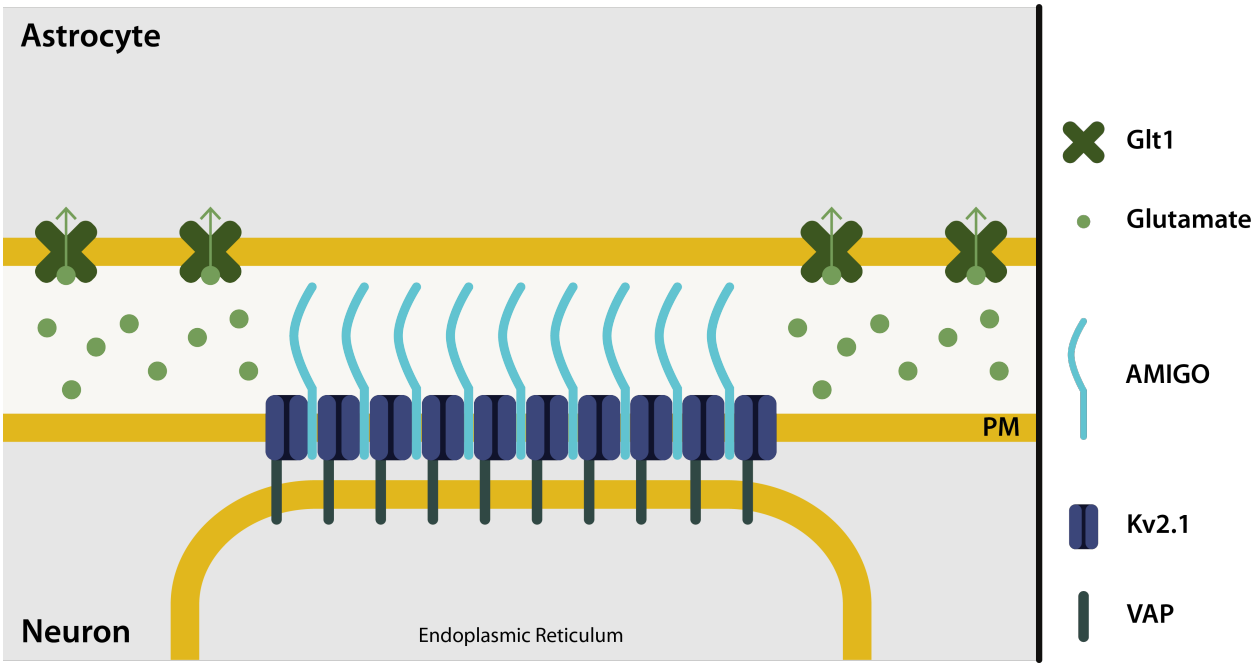

Figure 1.11: Current model of neuron-astrocyte contact at Kv2.1 clusters. Kv2.1 channels (dark blue) form micron-sized clusters on the plasma membrane surface of neurons. Kv2.1 clusters are formed by an interaction with the ER membrane protein VAP (grey). Kv2.1 has an auxiliary subunit, called AMIGO (light blue), which acts as a cell adhesion molecule. Astrocytes contact neurons at these clusters of Kv2.1 and astrocyte glutamate transporter, Glt1 (dark green), forms nets around these neuronal Kv2.1 clusters.

contacts under physiological conditions (Figure 1.11). My dissertation aims to further define the components that make up these remarkable cell junctions, so that future studies could unmask their physiological functions.

Chapter 2 describes a novel interaction between Glt1 and cortical actin filaments at the astrocyte membrane. We found that this interaction alters the localization of Glt1a on the membrane, which relies on the terminal amino acids of the Glt1a C-terminus. Significantly, this protein interaction could position Glt1 transporters both near synapses and somatic Kv2.1 clusters, which is the subject of Chapter 3.

Chapter 3 presents experiments designed to further define the relationship of Glt1 to neuronal structures. The first part of the chapter details the localization and diffusion of astrocytic Glt1 around neuronal Kv2.1 clusters on the soma, which appears to rely on an interaction with actin. The second half of the chapter looks at the relationship of Kv2.1 and AMIGO to synapses, and whether that relationship correlates with astrocyte presence at synaptic structures.

Chapter 4 seeks to further characterize the interaction between Kv2 channels and AMIGO family auxiliary subunits. In this chapter, we propose that all three members of the AMIGO family act as auxiliary subunits for the Kv2 family, impacting the function of Kv2 channels, as well as, the composition of neuronal ER/PM junctions. In the context of neuron-astrocyte contacts, it is important to understand the cell adhesion molecule components of these Kv2.1 clusters, as they could assign particular properties to the cell junction.

Chapter 5 summarizes the results presented in Chapters 2-4 of this dissertation. It places these results in the context of the current literature and supplies an updated model of this cell junction. Finally, it proposes ideas for potential lines of research to further interrogate neuron-astrocyte contacts.

Appendix A presents Förster resonance energy transfer (FRET) results showing the direct interaction of Kv2.1 channels and the ER-resident protein, VAP. These data were originally published in [218], which marks the identification of VAP interaction as the mechanism of Kv2.1 cluster formation and Kv2.1-induced ER/PM junctions.

Appendix B depicts maps of DNA plasmids that were generated to perform the experiments in this dissertation.

Chapter 2

Glt1a C-terminal interaction with actin cytoskeleton determines size and location of Glt1a nanoclusters

2.1 Summary

Astrocytic glutamate transporters, such as Glt1, ensure the fidelity of glutamic neurotransmission by spatially and temporally limiting glutamate signals. The role of Glt1 in limiting neuronal hyperactivity relies heavily on the localization and diffusion of the transporter in the membrane, however, little is known about the mechanisms governing these properties. Here, we used high-resolution imaging to show that two isoforms of Glt1, Glt1a and Glt1b, form nanoclusters on the surface of HEK-293 cells and astrocytes. Using super-resolution imaging, we found the concentration of Glt1a, but not Glt1b, nanoclusters adjacent to cortical actin filaments, which was maintained even after the addition of glutamate. Glt1a nanocluster concentration near actin filaments could be prevented by the expression of a cytosolic Glt1a C-terminus, suggesting that the distal C-terminus of Glt1a is likely responsible for interaction with a component of the cytoskeleton. Overall, these data describe a novel interaction between the Glt1a C-terminal tail and cortical actin filaments, which localizes Glt1 in nanoclusters at the astrocyte plasma membrane.

2.1.1 Hypotheses to be tested —

1. Glt1 nanoclusters exist on the plasma membrane surface of cultured astrocytes.
2. Surface Glt1 nanoclusters colocalize with cortical actin.
3. Glt1 collisions with cortical actin will alter the membrane diffusion of Glt1.
4. The C-terminus of Glt1a regulates actin-mediated localization and diffusion.

2.2 Introduction

Glutamate is the most abundant excitatory neurotransmitter in the central nervous system, and therefore, it is imperative to maintain a low extracellular glutamate concentration to enhance the spatial and temporal resolution of glutamatergic signaling. Excessive extracellular glutamate results in neuronal hyperactivity and subsequent neuronal death due to the rundown of ionic gradients and toxic levels of intracellular Ca^{2+} (for review, [54]). To achieve efficient glutamate clearance against a steep electrochemical gradient, astrocytes couple glutamate uptake to the ionic movement of Na^+, K^+, and H^+ using abundantly expressed glutamate transporters, such as Glt1 and GLAST [75].

It is estimated that Glt1 is responsible for approximately 90% of total glutamate uptake [85, 268] and together, glutamate transporters represent $\sim$1% of total brain protein [111]. Glt1 is dense in the hippocampal astrocyte membrane, with an average of approximately 8500 molecules/μm^2 across the entire membrane [111], and localizes near synapses in peri-synaptic astrocyte membranes [73, 110]. Perhaps one reason for their abundance is the relatively slow transport cycle of 11 to 70 ms per molecule of glutamate [180, 181, 269], which is long compared to the lifetime of glutamate in the synaptic cleft ($\sim$1.2 ms, [94]). The high abundance of Glt1 also limits glutamate spill-over into other synaptic clefts, preventing excitation at inactive synapses [270].

In addition to localization, the mobility of active Glt1 transporters in the membrane is important in shaping glutamate neurotransmission in the hippocampus [140]. Unbound transporters are relatively immobile, especially near synapses, but when glutamate is bound, transporter diffusion increases, thus allowing transporters to diffuse away from high concentrations of glutamate [140, 143]. This mobility change is effectively responsible for replacing glutamate-bound transporters with unbound transporters, conceivably to overcome the slow transport. Given the importance of Glt1 in regulating

synaptic glutamate signals, it is vital to understand the mechanisms governing the localization and diffusion of these transporters.

Membrane protein localization and diffusion are governed by several factors, including interactions with other proteins, corralling by or anchoring to the actin cytoskeleton, and interactions with organelles that come into close contact with the plasma membrane [271–274]. Glt1 can be expressed as 3 different splice variants, Glt1a, Glt1b, and Glt1c [275–277]. Averages calculated from multiple publications reveal that Glt1a accounts for approximately 90% of the total Glt1 population in the hippocampus, while Glt1b and Glt1c make up 6% and 1%, respectively [120]. Glt1a and Glt1b differ in the last 11-22 amino acids of the distal C-terminus [120], which is known to give Glt1b the ability to bind PDZ domain proteins, such as PSD-95 [123]. However, at this time, no function has been attributed to the unique amino acids in Glt1a. A wide variety of proteins have been identified as Glt1 interactors, including cytoskeleton-associated proteins Ajuba [278] and Sept2-associated BORG4 [279], PDZ proteins PICK1 [124] and MAGI1 [280], the Na^+/K^+ ATPase α-subunit [108], and various mitochondrial proteins [108]. Any one of these interactors could reasonably contribute to the immobilization of Glt1 molecules on the membrane.

The present study aimed to determine factors governing Glt1 localization and diffusion. The results of this work show extensive colocalization of large Glt1a, but not Glt1b, nanoclusters with actin in close contact with the plasma membrane (PM). Expression of a soluble Glt1a C-terminus interfered with localization on actin filaments, suggesting a Glt1a specific C-terminus interaction is primarily responsible for actin localization. Single-particle tracking of Glt1a showed that diffusion was decreased near actin, which was also eliminated by co-expression of the C-terminus. While glutamate increased overall Glt1a diffusion, it did not alter the colocalization of nanoclusters with actin, suggesting that glutamate primarily affects the diffusion of free transporters. To-

gether, these data describe a novel interaction between Glt1a glutamate transporters and the cortical actin cytoskeleton, which is unaffected by glutamate.

2.3 Materials and Methods

2.3.1 DNA Constructs

For specific expression of proteins in astrocytes or neurons, the gfaABC1D and SYN promoters were used, respectively. GFP-Glt1a-V5 and GFP-Glt1b-V5 were generous gifts from Josef Kittler (University College London). Ruby2-Glt1a-V5 was made by digestion of mRuby2-C1 and GFP-Glt1a-V5 with NheI and XhoI, with Ruby2 then ligated in place of GFP. GFP-Actin was obtained from Takara Bio. To create the gfaABC1D>Ruby2-Glt1a-CT construct, expressing only the Glt1a C-terminal 81 amino acids, PCR was used to generate a fragment flanked by BspEI and BamHI restriction sites (Primers: 5 GCTTACTCCGGATATCACCTTTCCAAGTCC 3 and 5 AGTCCGGGATCCTTATTTTTCACGTTTCCAAGG 3). This fragment was then digested with BspEI and BamHI and ligated into the gfaABC1D>Ruby2-Glt1a-V5 cut with the same enzymes to create a Ruby2-tagged Glt1a C-terminus. Maps of DNA constructs generated for use in this body of work are presented in Appendix B.

2.3.2 Cell Culture, Transfection, and Labeling

Hippocampal mixed cultures of neurons and astrocytes were isolated from E18 rat brains. Pregnant rats were deeply anesthetized with isoflurane, as outlined in a protocol approved by the Institutional Animal Care and Use Committee of Colorado State University (protocol ID: 15-6130A). Embryos of both sexes were used to generate cultures, and thus the cells are a mixed population of male and female origins. Hippocampi were dissociated and cultured as previously described for neurons [281, 282]. Cultures were plated on glass-bottom 35mm with No.1.5 coverslips (MatTek, Ashland,

MA) dishes coated with poly-L lysine (Sigma-Aldrich, St. Louis, MO) in borate buffer, and plated in a plating medium composed of 5% FBS, Neurobasal (Gibco/Thermo Fisher Scientific, Waltham, MA), B27 Plus Supplement (Gibco/Thermo Fisher Scientific, Waltham, MA), Penicillin/Streptomycin (Cellgro/Mediatech, Manassas, VA), and GlutaMAX (Gibco/Thermo Fisher Scientific). After 24 hours in the plating medium, the media was replaced with a maintenance medium which was identical to the plating medium without FBS.

At DIV7, cultures were transfected using DNA, Lipofectamine 2000 (Invitrogen, Life Technologies, Grand Island, NY), and OptiMEM for experiments the following day. The following amounts of DNA were transfected per dish: gfaABC1D>Ruby2-Glt1a-V5 (0.5 μg), gfaABC1D>Glt1a-V5 (0.5 μg), gfaABC1D>Glt1b-V5 (0.5 μg), gfaABC1D>Ruby2-Glt1aCT (1 μg), GFP-Actin (0.2 μg). After 24 hours, the cultures were transferred to imaging saline (126 mM NaCl, 4.7 mM KCl, 2.5 $CaCl_2$, 0.6 mM $MgSO_4$, 0.15 mM NaH_2PO_4, 0.1 mM ascorbic acid, 8 mM glucose, and 20 mM Hepes, pH 7.4, 300 mOsm) containing 1:1000 αV5-CF640 (Biotium, Hayward, CA) for 3 minutes at 37 C. The cultures were washed 2 times with imaging saline and then transferred to the TIRF microscope (described below) for experimentation.

HEK-293 cells were maintained in 10 cm dishes (CellTreat 229620, Pepperell, MA) at 37 C under 5% CO2 in DMEM (Corning10-013-CV, Corning, NY) supplemented with 10% FBS. For transfections, cells were trypsinized and electroporated (BioRad GenePulse Xcell, Berkeley, CA) with 1 μg Ruby2-Glt1a-V5 or Ruby2-Glt1b-V5. Following transfection, cells were plated on Matrigel-coated glass-bottom 35mm with No.1.5 coverslips (MatTek, Ashland, MA) and imaged the following day.

2.3.3 Microscopy

Total internal reflection fluorescence (TIRF) microscopy was performed on a Nikon Eclipse Ti fluorescence microscope. Images were acquired with an Andor iXon (DU-897) camera and 100X Plan Apo TIRF, NA 1.49 objective lens. Diode lasers (405, 488, 561, 647 nm, 100 mW) were controlled with an acousto-optic tunable filter (AOTF) and excitation occurred with lasers at an incident angle of 63 degrees, allowing the evanescent wave to penetrate approximately 144 nm at a wavelength of 488 nm. Emitted light was collected through the proper bandpass filters. Movies were acquired at 20 Hz (50 ms exposure) for 2000 total frames with a beam splitter, such that emitted green and far-red could be imaged simultaneously. All imaging was performed at 37 C using a heated stage and objective heater.

2.3.4 Photobleaching steps

HEK-293 cells or DIV8 primary astrocytes expressing Ruby2-Glt1a-V5 or Ruby2-Glt1b-V5 were fixed using 4% paraformaldehyde and then washed using 1X PBS. Subsequently, these cells were tagged with a rabbit antibody conjugated with CF640 and directed against the V5 epitope (αV5-CF640 (Biotium)) at 1:1000 for 15 minutes. The fixed cells were then imaged on the TIRF microscope for 30,000 frames at 20 Hz and 30% power of a 100 mW 640 nm laser. Using ImageJ, local maxima were identified in the first frame of the movie and small circular ROIs were drawn around each point. The ROIs were then used to measure the fluorescence of that spot over the entire course of the movie. The results of these measurements were transferred to Microsoft Excel. Using a moving average of 50 frames, the smallest sustained drops in fluorescence, which indicate a single bleached molecule, were used to determine the number of fluorescent molecules in the initial nanocluster. According to specifications from Biotium, each αV5 antibody was conjugated with five CF640 molecules. Using this knowledge, we esti-

mated the total number of antibodies per nanocluster. Due to the difficulty in assessing antibody binding efficiency, we did not convert the number of antibodies to a number of transporters in each nanocluster.

2.3.5 Labeling and image acquisition

DIV8 rat hippocampal mixed cultures expressing Glt1a-V5 or Glt1b-V5 were labeled with 1:1000 αV5-CF640 in imaging saline for 3 minutes at 37 C. Due to the propensity of Glt1 to form nanoclusters, the acquired movies contain both immobile nanoclusters and mobile (presumably single) transporters. Astrocytes were identified by morphology in fluorescence and DIC. Astrocytes co-expressing organelle markers, Glt1a, Glt1b, and Glt1aCT (if necessary) were identified, and single frames were imaged. The beam splitter was then inserted, and 2000 frame movies were acquired before and after chemical intervention (100 μM glutamate). One mL of 200 μM glutamic acid in imaging saline was applied to the dish with 1 mL normal imaging saline on the microscope and allowed to bind to Glt1 for 3 minutes before acquiring +Glu movies.

For the processing of TIRF movies, individual channels were aligned using DIC images captured through the beam splitter. Due to the widespread coverage of astrocytes across the glass surface of the dish, multi-colored beads, conventionally used for aligning beam splitter images, could not be used. DIC images acquired through the beam splitter were aligned using the AutoAlign plugin in ImageJ. These alignment settings were then applied to the other channels.

2.3.6 Super-resolution radial fluctuations (SRRF)

To avoid limitations in lateral resolution due to Abbe's diffraction limit, we applied the super-resolution radial fluctuations (SRRF) approach to achieve less than 100 nm lateral resolution [283]. Other popular super-resolution methods, like PALM and STORM,

require repeated localizations of transiently emitting single fluorophores to reconstruct precise maps of fluorophore positions. SRRF is advantageous in many ways, including that data is acquired over a shorter time frame, on standard microscope setups, on live or fixed samples, and with various emitting fluorophore densities. SRRF relies on the principles of radiality and temporal correlation of a signal, where a fluorophore is most likely localized at points where spatial gradients converge and where these spatial gradients occur at multiple time points. SRRF was used for all images in this chapter with the exceptions of Figure 2.1 & Figure 2.2.

For images acquired on the TIRF microscope, 2000 continuous frames were acquired at 20 Hz on live culture samples. These videos were obtained through a beam splitter, which allowed the simultaneous collection of emissions from two different fluorophores. Subsequently, these videos were background subtracted and analyzed using the NanoJ-SRRF plugin for FIJI/ImageJ [284]. The SRRF algorithm was applied over 50 frames, and therefore final super-resolution frame rate was 1 frame every 2.5 s.

2.3.7 Single-particle tracking

Images containing Glt1 molecules were background subtracted and a gaussian filter of 0.7 SD was applied to each frame in ImageJ. The channel images containing actin underwent processing for SRRF analysis, such that 2000 frames were temporally correlated and averaged to 40 frames [283]. This sequence of images was converted to binary and was eventually used to determine nanocluster location. Individual Glt1 molecules were tracked using the U-track algorithm in MATLAB [285]. Subsequently, tracks were separated based on the spatial relationship to actin (on and off) using a custom MATLAB code into 'on' states when they are found to colocalize with actin and 'off' states otherwise. A 3-pixel barrier between the two regions was excluded, such that trajectories were certainly within each region. Trajectory segments in each state (on or off)

were discarded if they did not remain for at least 40 consecutive frames (2 seconds) in the same state. The trajectories in each region were then used to calculate individual time-averaged mean square displacements (MSD) using the equation,

$$\overline{r^2(\Delta t)} = \frac{1}{T-(\Delta t)} \int_0^{T-\Delta t} [r(t+\Delta t) - r(t)]^2 dt$$

where r(t) is the two-dimensional particle position at time t. The individual MSDs of all molecules were then averaged for total MSD using a custom MATLAB code. The diffusion coefficient (D) and localization error (σ) were calculated using the equation,

$$MSD(\Delta t) = 4D(\Delta t) + 4\sigma^2$$

where Δt is the lag time, for MSDs which displayed a linear relationship to time. For non-linear MSDs, the anomalous diffusion coefficient (K) and anomalous exponent (α) were calculated using the equation,

$$MSD(\Delta t) = K(\Delta t)^{\alpha} + 4\sigma^2$$

K represents the area explored by a molecule in a unit time, while α describes the deviations from Brownian motion, which may be due to obstructions or transient confinement [286]. α= 1 is indicative of Brownian motion, $1 < \alpha < 2$ is indicative of superdiffusivity, and $0 < \alpha < 1$ is indicative of subdiffusivity, which is commonly observed in biological samples [287]. It should also be noted that due to the inability to only label mobile transporters, MSDs presented in the results contain both mobile single transporters and immobile nanoclusters.

2.3.8 Nanocluster measurements

For nanocluster measurements, we used the same movies that were acquired for single-particle tracking analysis. By temporally averaging frames and background subtracting the fluorescence caused by diffusing transporters, we were able to isolate the fluorescent signal from immobile nanoclusters. Nanoclusters are smaller than the diffraction limit of conventional microscopy, and thus, location was determined by identifying the centroids of point-spread functions from 50 averaged frames of Glt1 movies. For the random pixel control, an equal number of XY coordinates were randomly generated in MATLAB. These XY coordinates were then compared to 50 averaged frames of actin images and determined to be on or off actin. For calculating distance to actin, the 50 averaged frames of actin were converted to a Euclidean distance map (EDM) in MATLAB [220]. Nanocluster centroids were then correlated to a distance from the nearest actin filament using the EDM.

2.3.9 Image Processing and Analysis

Image processing was done in ImageJ (v. 1.52). Analysis was completed in MATLAB (R2019A). Statistics and graphs were generated in GraphPad Prism 9. In cases where multiple groups were compared, one-way ANOVAs were used followed by post-hoc Sidak's tests to compare specific groups to one another, unless otherwise noted.

2.4 Results

2.4.1 Glt1 forms nanoclusters on the surface of HEK cells and astrocytes

Previous work using freeze-fracture electron microscopy suggested that Glt1 forms small clusters of approximately 200 nm in diameter when exogenously expressed in baby hamster kidney (BHK) cells [138]. To determine whether we could observe surface-

localized nanoclusters using fluorescence microscopy, we expressed GFP-Glt1a-V5 and GFP-Glt1b-V5 in primary astrocytes and HEK-293 cells and labeled the extracellular V5 epitope with an antibody conjugated to CF640 to specifically detect transporters on the cell surface. Transfected GFP-Glt1a and GFP-Glt1b localized predominantly to the astrocyte surface (Figure 2.1A-B) indicated by the ring of green fluorescence outlining the cell when looking at a z-slice through the center of the cell. To estimate nanocluster size, antibody labeling was performed after fixation to ensure that nanoclustering was not enhanced by the bivalent nature of the antibody combined with multiple V5 epitopes per transporter. However, even in unfixed, live cells the V5 antibody did not appear to greatly alter the appearance of GFP-Glt1 on the surface, as seen by the similar size of Glt1 puncta in unlabeled Figure 2.1C and V5 antibody labeled Figure 2.1D.

Each functional Glt1 transporter is a trimer composed of three subunits. Each of these subunits has a single V5 epitope, which binds a single antibody, and therefore one transporter could have up to three antibodies attached. To estimate the number of antibodies bound to each nanocluster, we labeled the V5 epitope with an antibody conjugated to a known number of CF640 molecules. Subsequently, we photobleached the entire cell surface, such that we could resolve bleaching events of single CF640 fluorophores (similar to the approaches used by [288,289]). Using the magnitude of a single bleaching event and the number of CF640 molecules per antibody, the original number of antibodies bound to a nanocluster was estimated.

Both isoforms, Glt1a and Glt1b, formed nanoclusters on the surface of astrocytes (Figure 2.2A) and HEK cells (Figure 2.2C). A histogram detailing the incidence of antibodies per nanocluster reveals Glt1a nanoclusters showed a bimodal distribution, with peaks at 9-12 antibodies and 24-27 antibodies per nanocluster in astrocytes (Figure 2.2B, magenta bars). In contrast, most Glt1b nanoclusters contained only 6 antibodies (Figure 2.2B, green bars), however, this might be an underestimation of the true density of

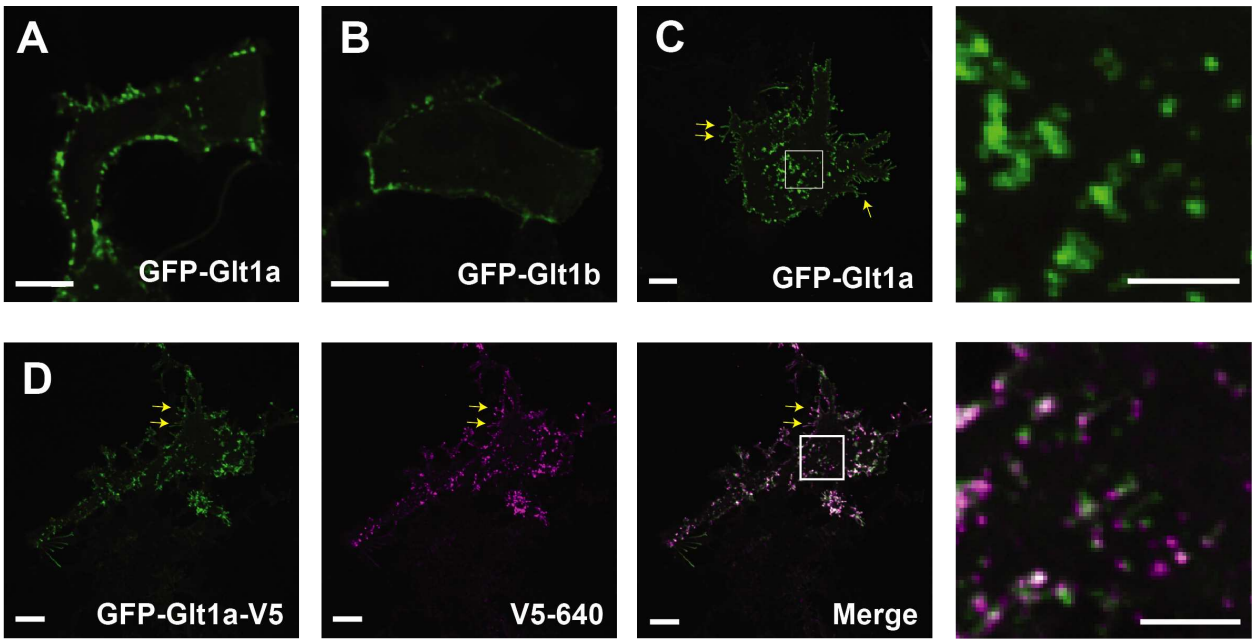

Figure 2.1: Majority of transfected Glt1 localized to plasma membrane in cultured astrocytes. Most transfected GFP-Glt1a **(A)** and GFP-Glt1b **(B)** are localized to the surface of a cultured astrocyte, as seen in these slices through the center of each cell. **C)** The basal surface of an astrocyte expressing GFP-Glt1a shows localization to filopodial process tips and in nanoclusters. Zoom (right) scale bar = 5 μm. **D)** An astrocyte expressing GFP-Glt1a-V5, which has been labeled with an antibody directed against V5 and conjugated to a CF640 molecule, also shows localization to filopodia process tips and nanoclusters on the basal surface. Notably, there do not appear to be more nanoclusters or larger nanoclusters in the cell labeled with the V5 antibody. Zoom (bottom right) scale bar = 5 μm. Each image depicts a single z-plane. Scale bars are 10 μm, unless otherwise noted. Yellow arrows point to filopodia.

Glt1 nanoclusters in astrocytes, due to high endogenous expression of Glt1. In HEK-293 cells, which lack endogenous Glt1 expression, we observed a peak for Glt1a at 12 antibodies per nanocluster (Figure 2.2D, magenta bars). In contrast, Glt1b showed a bi-modal distribution, with peaks at both 6 antibodies and 15 antibodies per nanocluster (Figure 2.2D, green bars). Due to the lack of endogenous expression of Glt1 in HEK-293 cells, these measures may be a more accurate estimate of nanocluster size. Notably, the population of Glt1a nanoclusters with more transporters was absent in the HEK-293 data set, perhaps suggesting astrocyte-specific expression of a Glt1a binding partner.

While Glt1a and Glt1b subunits have been shown to colocalize in astrocytes [122], these studies did not delineate between Glt1 transporters localized to the surface or in

internal stores. To determine whether Glt1a and Glt1b could occupy the same nanoclusters on the surface of astrocytes, GFP-Glt1a-V5 and Ruby2-Glt1b-V5 were expressed and labeled with the CF640 conjugated V5 antibody described above. Using the V5 sig-

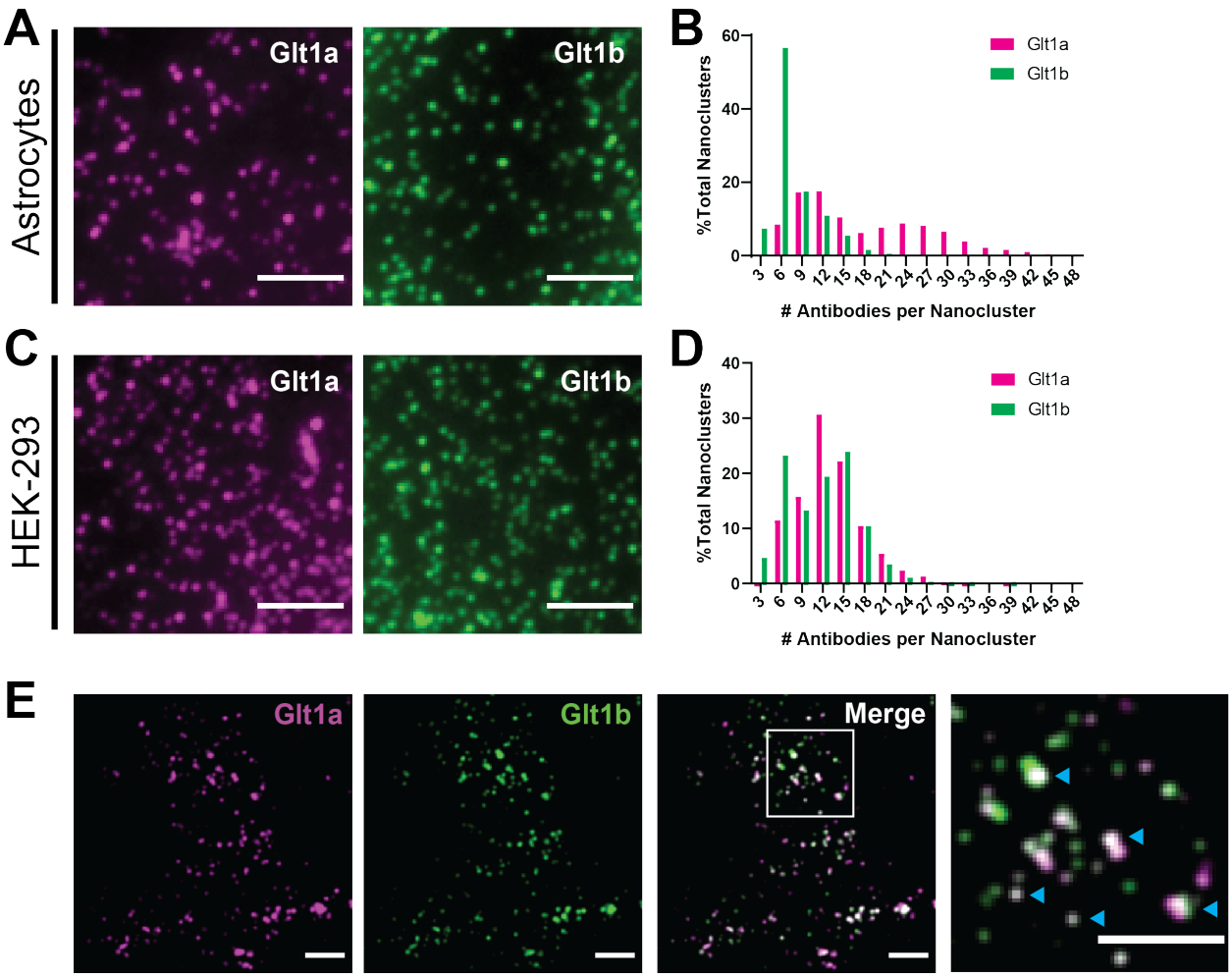

Figure 2.2: Glt1 forms nanoclusters on the surface of astrocytes and HEK cells. A) Representative images of nanoclusters of Glt1a (left, magenta) and Glt1b (right, green) in astrocytes. **B)** Distribution of Glt1a (magenta) or Glt1b (green) transporters per nanocluster in hippocampal astrocytes. Glt1a showed a bimodal distribution, with peaks at 9-12 antibodies and 24-27 antibodies per nanocluster. Glt1b favored smaller nanoclusters of 6 antibodies, however, this may be skewed by endogenous expression of Glt1a. **C)** Representative images of nanoclusters of Glt1a (left, magenta) and Glt1b (right, green) in HEK cells. **D)** Distribution of Glt1a (magenta) or Glt1b (green) antibodies per nanocluster in HEK cells. Glt1a favored nanoclusters of 12 antibodies, while Glt1b showed a bimodal distribution with peaks at both 6 and 15 antibodies per nanocluster. **E)** Astrocytes expressing GFP-Glt1a-V5 and Ruby2-Glt1b-V5 were labeled with a V5 antibody. The signal from the V5 was used to determine the fluorescence contribution of Glt1a and Glt1b to surface nanoclusters. These astrocytes displayed surface nanoclusters that contained both Glt1 isoforms (cyan carets in the zoom, right). Scale bars represent 5 μm in all panels.

nal, which should only represent transporters on the surface, we determined that GFP-Glt1a-V5 and Ruby2-Glt1b-V5 signals resided in the same surface nanoclusters (Figure 2.2E). Consistent with previous studies, Glt1a and Glt1b could presumably create heterotrimers and/or occupy the same nanoclusters, indicating that nanoclustering is independent of the distal C-terminus, where Glt1a and Glt1b differ. To our knowledge, this work is the first to attempt to quantify the number of Glt1 transporters in surface nanoclusters. Many previous studies have observed Glt1 nanoclusters, although, to our knowledge, only one group labeled Glt1 extracellularly [140], making it difficult to discern whether clusters were located on the plasma membrane or internally [130, 134, 138, 139, 143, 172, 279, 290–292].

2.4.2 Glt1a nanoclusters localize near cortical actin filaments in astrocytes

Membrane protein clustering is driven by several factors, including lipid-protein interactions [293, 294], protein-protein interactions between a membrane protein and organelle protein [218, 295], and cytoskeletal corralling [296–298]. Previous studies have used pharmacology and biochemical approaches to propose the cytoskeleton is involved in the regulation of glutamate transporters [139, 278, 279]. However, none of these studies have shown colocalization of Glt1 transporters with the actin cytoskeleton, although some have noted Glt1 localization in actin-rich filopodia [130, 139, 299]. We wanted to know whether the Glt1 nanoclusters shown in Figure 2.2 were associated with actin structures in close contact with the astrocyte plasma membrane. Using a combination of super-resolution radial fluctuations (SRRF) analysis and TIRF microscopy, we correlated the location of Glt1 nanoclusters with actin within 100 nm of the membrane. By using SRRF, we achieved less than 100 nm lateral resolution, which ensured a more precise localization of both nanoclusters and cortical actin filaments. Hippocampal astrocytes were transfected with Ruby2-Glt1a-V5 or Ruby2-Glt1b-V5 and GFP-Actin, and subsequently,

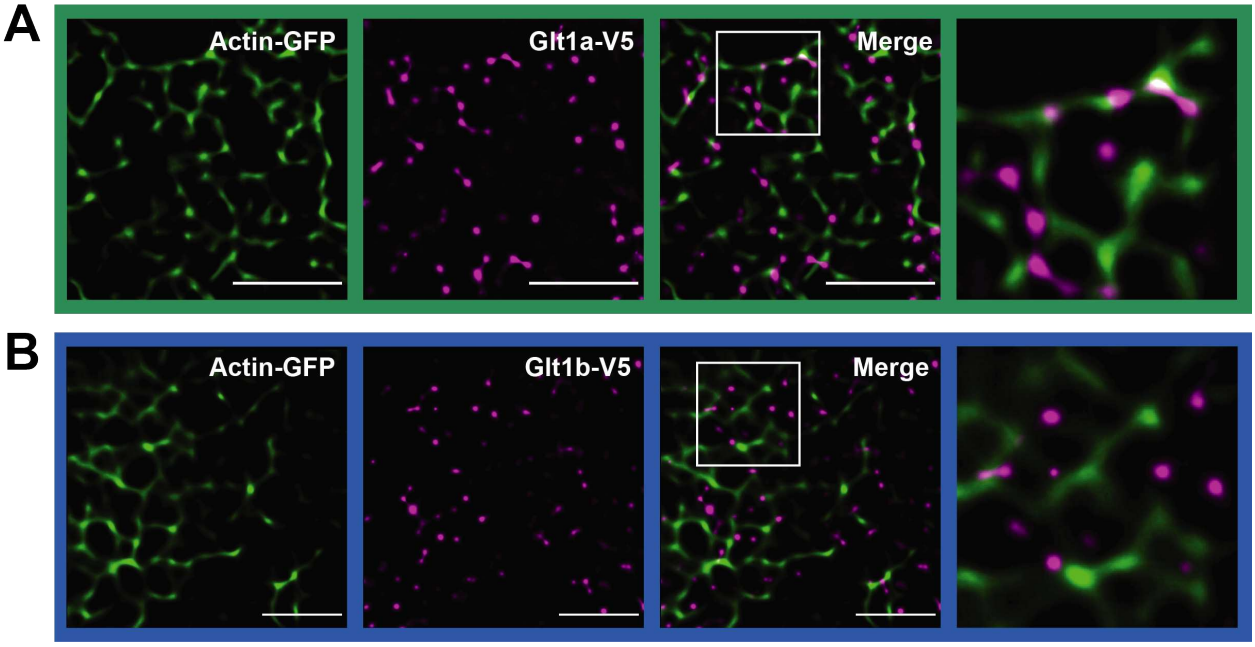

Figure 2.3: Glt1 transporters colocalize with actin near the surface of the astrocyte plasma membrane. Astrocytes co-expressing GFP-actin and Ruby2-Glt1a-V5 were labeled with a V5 antibody conjugated to CF640, imaged using TIRF microscopy, and subsequently, processed using SRRF to improve spatial resolution. **A)** Glt1a nanoclusters (magenta) colocalize with cortical actin filaments (green) in primary astrocyte cultures. **B)** Glt1b nanoclusters (magenta) rarely colocalize with cortical actin filaments (green) in primary astrocytes. Scale bars are 5 μm.

labeled with a V5 antibody conjugated to CF640 to tag transporters extracellularly before imaging.

Glt1a nanoclusters frequently colocalized with the actin cytoskeleton (Figure 2.3A), shown by the magenta nanoclusters often on top of or directly adjacent to actin filaments (green). In contrast, Glt1b nanoclusters were less likely to associate with actin filaments (Figure 2.3B). To quantitatively measure nanocluster concentration on cortical actin filaments, the fraction of Glt1 nanoclusters colocalized with actin filaments was compared to the fraction of the surface area covered by actin. In this comparison, a ratio of 1 indicates that nanoclusters are randomly distributed, while ratios greater than or less than 1 indicate concentration or exclusion from actin, respectively. Glt1a nanoclusters were significantly concentrated on actin (mean $\pm$ SEM = 1.56 $\pm$ 0.081), compared to a matched random pixel control (mean $\pm$ SEM = 0.98 $\pm$ 0.030, $p < 0.0001$, Figure 2.4A). Glt1b (mean

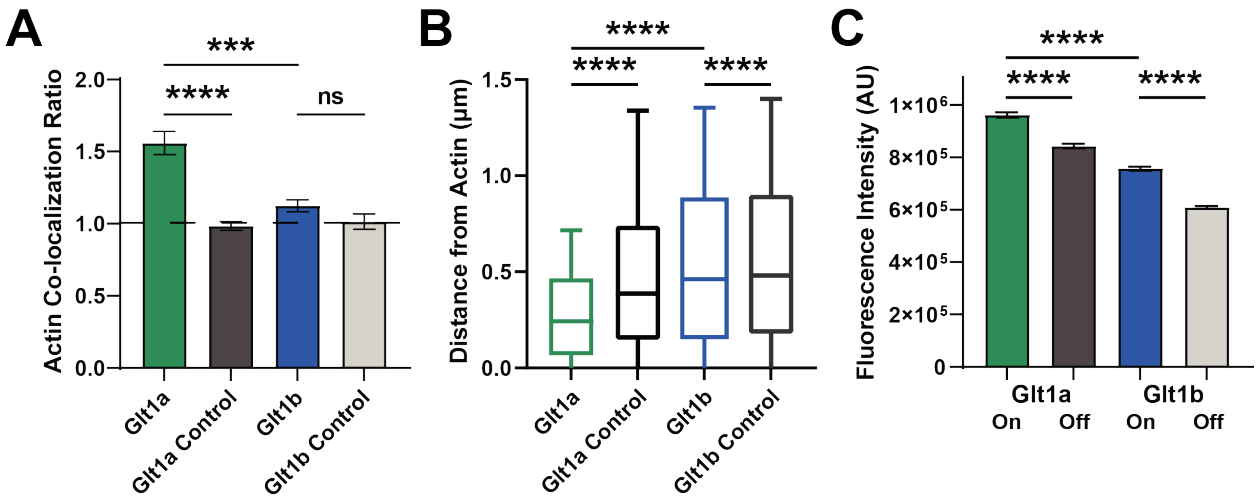

Figure 2.4: Glt1 nanoclusters are concentrated on actin. A) The ratio of % of total nanoclusters and % area covered by actin shows a concentration of Glt1a molecules on actin (green bar, N = 58 cells, mean ± SEM = 1.56 ± 0.081), compared to a matched random pixel control (dark grey bar, N = 58 cells, mean ± SEM = 0.98 ± 0.030, ANOVA F = 13.65, $p < 0.0001$). Glt1b (N = 17 cells, mean ± SEM = 1.12 ± 0.042) was not significantly concentrated on actin compared to a random pixel control (N = 17 cells, mean ± SEM = 1.02 ± 0.053, $p = 0.998$). Glt1a nanoclusters were also significantly concentrated on actin compared to Glt1b ($p < 0.001$). **B)** Distance of both Glt1a (green) and Glt1b (blue) nanoclusters from actin filaments. Glt1a nanoclusters (median = 0.308 μm, N = 622826 nanoclusters) were localized significantly closer to actin filaments than the random pixel control (median = 0.499 μm, N = 622826 nanoclusters, $p < 0.0001$). Glt1b nanoclusters (median = 0.544 μm, N = 158864 nanoclusters) were localized slightly closer to actin than the random pixel control (median = 0.562 μm, N = 158864 nanoclusters, $p < 0.0001$). Notably, Glt1a nanoclusters were localized significantly closer to actin filaments compared to Glt1b nanoclusters ($p < 0.0001$). Box plots represent the median and interquartile range. Bars represent the 10th - 90th percentile. **C)** Glt1a nanoclusters had significantly greater fluorescence intensity on actin (mean ± SEM = 7.66E5 ± 2.98E3 arbitrary units (AU), 57 cells, N = 34774 nanoclusters) than off actin (mean ± SEM = 6.05E5 ± 9.36E2 AU, 57 cells, N = 219464 nanoclusters, $p < 0.0001$). Glt1b nanoclusters were also significantly different in fluorescence intensity on actin (mean ± SEM = 5.81E5 ± 3.41E3 AU, 17 cells, N = 13365 nanoclusters) versus off actin (mean ± SEM = 4.40E5 ± 8.92E2 AU, 17 cells, N = 99045 nanoclusters, $p < 0.0001$). In addition, Glt1a nanoclusters also had significantly larger fluorescence intensity than Glt1b nanoclusters ($p < 0.0001$).

± SEM = 1.12 ± 0.042) was not significantly concentrated on actin compared to a random pixel control (mean ± SEM = 1.02 ± 0.053, $p = 0.998$). These data suggest that Glt1a nanoclusters are specifically concentrated along actin filaments, perhaps due to the amino acids in the distal C-terminus, which are different in Glt1a and Glt1b.

To further assess the spatial relationship between each Glt1 nanocluster and actin, we measured the distance of each nanocluster to the nearest actin filament. Glt1a nanoclusters were localized close to actin, with a median distance of 0.308 μm, compared to 0.499 μm for randomly generated pixels (Figure 2.4D, p<0.0001). Glt1b was also localized slightly closer to actin (median=0.544 μm) than the random pixel control (median=0.562 μm, p<0.0001, Figure 2.4D), which may be explained by the formation of heteromeric complexes with the endogenously expressed Glt1a.

To determine whether nanocluster size was correlated with localization, we measured the fluorescence intensity of Glt1 nanoclusters on actin filaments versus those off actin filaments. The fluorescence intensity in each nanocluster should scale with the number of transporters within each nanocluster, as was the case in Figure 2.2. Glt1a nanoclusters had significantly higher fluorescence intensity on actin than off actin (Figure 2.4B, $p < 0.0001$), and Glt1b nanoclusters had significantly lower fluorescence intensity than Glt1a nanoclusters ($p < 0.0001$). Although Glt1b nanoclusters were not concentrated on actin filaments, those nanoclusters that did colocalize with actin also had significantly higher fluorescence intensity than those off actin ($p < 0.0001$). These data suggest the two populations of Glt1a nanoclusters identified in Figure 2.2B represent nanoclusters localized to different compartments of the plasma membrane. Notably, the population of Glt1a nanoclusters with more transporters was absent in the HEK-293 data set, perhaps suggesting astrocyte-specific expression of the Glt1a actin-binding partner. Altogether, these data support a specific preference of the Glt1a isoform for localization near actin filaments.

2.4.3 Glt1a-Actin interaction is disrupted by cytosolic Glt1a C-terminus expression

Thus far, the observed colocalization between actin and Glt1 nanoclusters appears to be specific to the Glt1a isoform. Since Glt1a and Glt1b differ only in the distal

amino acids of the C-terminus, we wanted to know whether the expression of a cytosolic Glt1a C-terminus could interfere with Glt1a nanocluster localization on actin. A Ruby2-tagged Glt1a C-terminus (CT) was expressed in astrocytes, and the association of Glt1a nanoclusters with actin was assessed as described above. When co-expressed with the CT, Glt1a nanoclusters (magenta) appeared to colocalize less often with actin

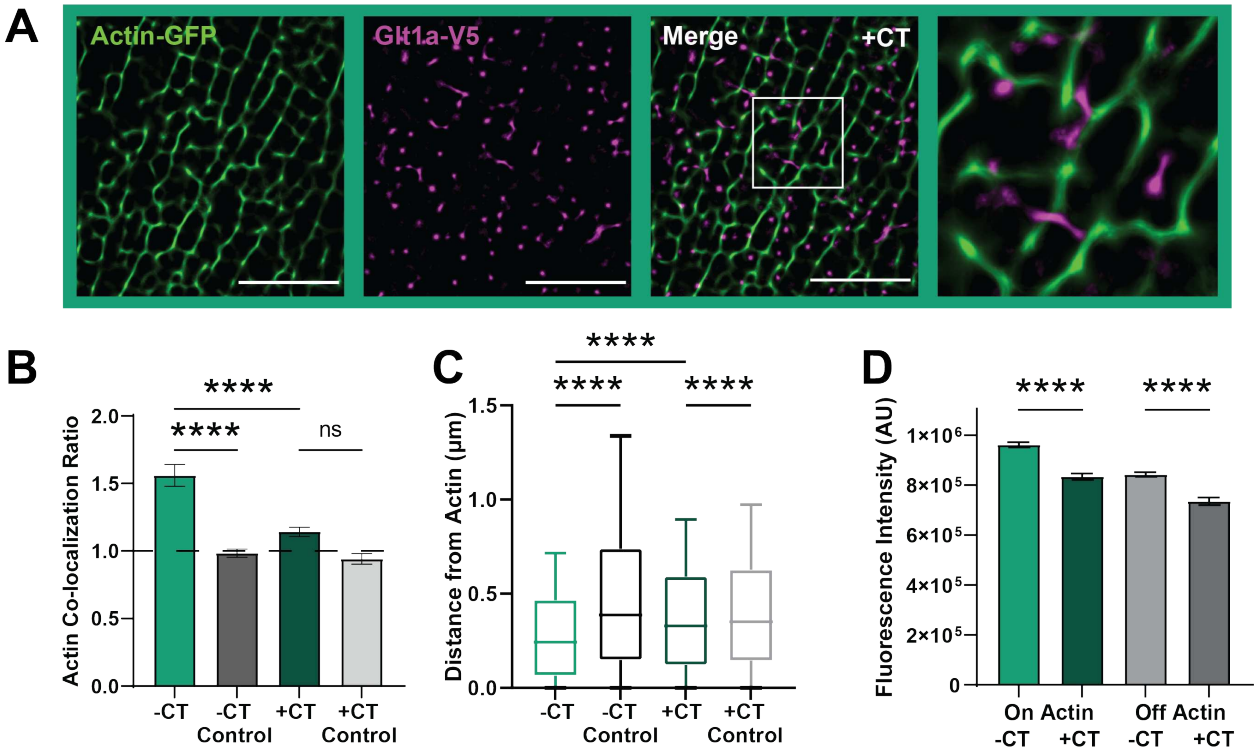

Figure 2.5: Glt1a-Actin interaction disrupted by cytosolic Glt1a C-terminus expression. Astrocytes co-expressing GFP-actin, Glt1a-V5, and Ruby2-Glt1a-CT were labeled with a V5 antibody conjugated to CF640, imaged using TIRF microscopy and subsequently, processed using SRRF to improve spatial resolution. **A)** Representative images of Glt1a-V5 nanoclusters (magenta) overlying Actin-GFP filaments (green) with a co-expressed cytosolic Glt1a C-terminus (+CT). **B)** A measure of concentration on actin shows a significant decrease in concentration on actin with co-expression of a competing Glt1a C-terminus (mean $\pm$ SEM = 1.14 $\pm$ 0.034, N = 28 cells, $p < 0.0001$). Glt1a +CT was not significantly concentrated on actin relative to a random pixel control (mean $\pm$ SEM = 0.94 $\pm$ 0.039, p = 0.38). **C)** Glt1a nanoclusters (median = 0.308 μm, N = 622826 nanoclusters) were localized further from actin filaments when co-expressed with the CT (median = 0.366 μm, N = 315362 nanoclusters, $p < 0.0001$). Box plots represent the median and interquartile range. Bars represent the 10th - 90th percentile. **D)** Co-expression of the cytosolic Glt1a CT significantly decreased nanocluster fluorescence intensity on actin (mean $\pm$ SEM = 5.71E5 $\pm$ 2.56E3 AU, 28 cells, N = 26307 nanoclusters, $p < 0.0001$) and off actin (mean $\pm$ SEM = 4.71E5 $\pm$ 7.49E2 AU, 28 cells, N = 193666 nanoclusters, $p < 0.0001$

filaments (green) compared to cells without the CT expressed (Figure 2.5A). Indeed, expression of the CT significantly reduced Glt1a nanocluster concentration on actin (Figure 2.5B, $p < 0.0001$), suggesting that the distal C-terminus of Glt1a is vital in localizing nanoclusters to actin filaments. In addition, distribution analysis showed that Glt1a nanocluster distance to actin filaments significantly increased with co-expression of the CT (median=0.366 μm, $p<0.0001$, Figure 2.5C).

Furthermore, Glt1a nanocluster fluorescence intensity on actin filaments was also significantly decreased by co-expression of the CT (Figure 2.5C, $p < 0.0001$). Interestingly, nanocluster fluorescence intensity off actin was also decreased by expression of the CT ($p < 0.0001$), suggesting that the C-terminus is important in regulating the number of transporters per nanocluster, regardless of actin localization. Together these data suggest that the Glt1a C-terminus is important in localizing nanoclusters near actin filaments and regulating the number of transporters per nanocluster.

2.4.4 Glt1a diffusion is altered by cytosolic Glt1a C-terminus expression

We next wanted to know whether the CT could alter Glt1a diffusion dynamics since Glt1 mobility is important for buffering glutamate [140, 143]. Since nanoclusters are largely immobile, a disruption of nanocluster integrity could increase the number of mobile transporters in the membrane. Our collected trajectories of Glt1a molecules included both freely diffusing single transporters and nanoclusters of multiple transporters. To determine whether actin localized molecules showed diffusion differences after CT expression, we separated trajectories according to their location relative to actin. Mean square displacements under normal conditions show that diffusion on and off actin (green and grey lines, respectively) are different, with Glt1a molecules off actin diffusing more than those on actin (Figure 2.6A and C, $p < 0.0005$). This result is consistent with the observation that immobile nanoclusters prefer to localize on actin. Expression

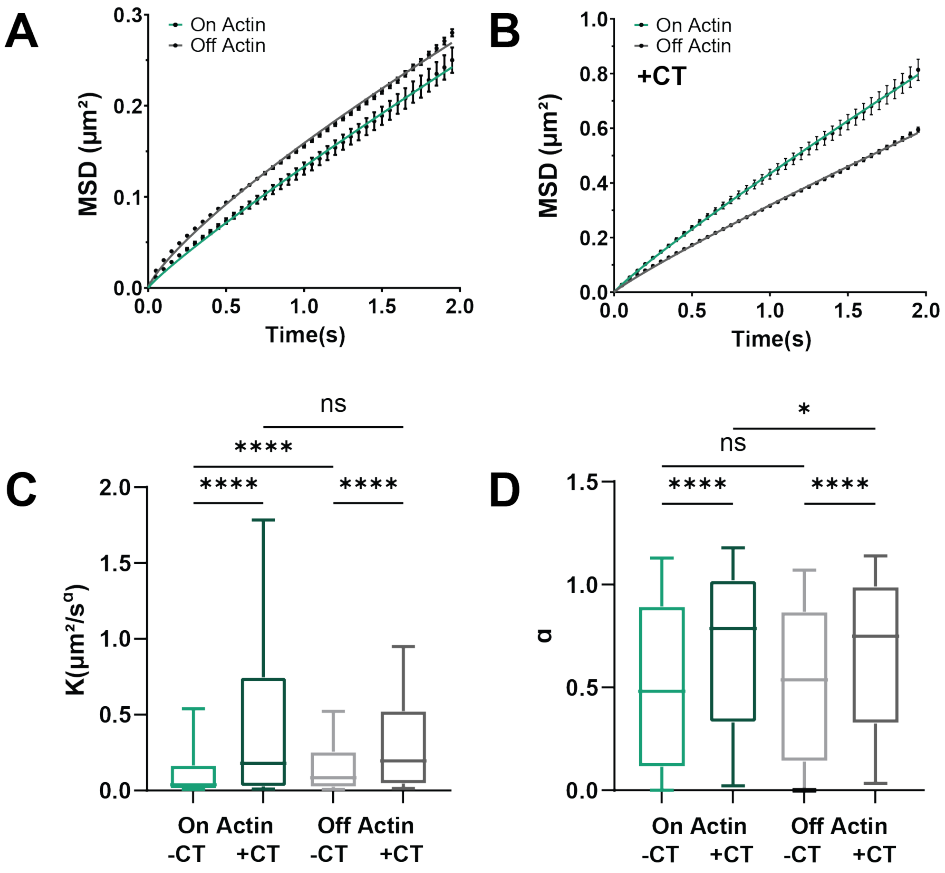

Figure 2.6: Glt1a diffusion increased by expression of cytosolic Glt1a-CT. Mean square displacements of diffusing Glt1a molecules on actin (green) and off actin (grey), in normal conditions (**A)** and with co-expression of cytosolic C-terminus (**B)**. Lines shown are fits of the data to Eqn 3 (A: On K = 0.133, α = 0.898, R^2 = 0.998; A: Off K = 0.159, α = 0.790, R^2 = 0.998; B: On K = 0.434, α = 0.909, R^2 = 0.999; B: Off K = 0.319, α = 0.904, R^2 = 0.999). **C)** Anomalous diffusion coefficients (K) of Glt1a molecules on actin (median = 0.0375, N = 3022 trajectories) is significantly slower than Glt1a molecules off actin (median = 0.0839, N = 18539 trajectories, $p < 0.0001$). Diffusion on actin significantly increases with co-expression of the Glt1a CT (median = 0.18, N = 1677 trajectories, $p < 0.0001$). Expression of the Glt1a CT also significantly increased the diffusion of Glt1a off actin (median = 0.196, N = 11443, $p < 0.0001$). **D)** The anomalous exponent (α) is similar in trajectories on and off actin (On: median = 0.482, N = 3022 trajectories; Off: median = 0.537, N = 18539 trajectories; p = 0.9877). The anomalous exponent increases with co-expression of the cytosolic C-terminus in both trajectories localized on actin (median = 0.787, N = 1677 trajectories, $p < 0.0001$) and off actin (median = 0.749, N = 11443, $p < 0.0001$). Box plots in C and D represent the median and interquartile range. Bars represent the 10th - 90th percentile.

of the CT increased the diffusion both on and off actin (Figure 2.6B). In the presence of the CT, the generalized diffusion coefficient (K) of Glt1a molecules on actin increased by a factor of 4.8 ($p<0.0001$), and off actin by a factor of 2.3 (Figure 2.6A-C). In addition, analysis of the anomalous exponent (α), which describes deviations from free diffusion,

revealed trajectories of Glt1a on actin filaments (mean ± SEM = 0.523 ± 0.00887) showed more subdiffusive motion compared to those measured in the presence of the CT (mean ± SEM = 0.694 ± 0.0112, p<0.0001, Figure 2.6D). Likewise, trajectories of Glt1a off actin filaments (mean ± SEM = 0.527 ± 0.00323) showed more confinement compared to those measured in the presence of the CT (mean ± SEM = 0.664 ± 0.00398, p<0.0001, Figure 2.6D). These data imply the C-terminus of Glt1a is important for limiting Glt1a diffusion both on actin and off actin, further suggesting the C-terminus is involved in more than just mediating the Glt1a-actin interaction. Furthermore, these data suggest that perturbations of immobile nanoclusters could increase the glutamate buffering capacity of Glt1 transporters.

2.4.5 Glutamate does not affect Glt1a nanoclustering

Previous studies of Glt1 diffusion found that 100 μM glutamate increased the average diffusion coefficient by ∼36% [140,143]. One possible explanation for this increase in the rate of diffusion is by releasing a pool of previously immobile transporters, such as by perturbing the nanoclusters described above. To ensure we could observe the increase in diffusion after adding glutamate, we used single-particle tracking and averaged the mean square displacements (MSDs) of the total population of Glt1 transporters. The average MSDs of the total population of Glt1a or Glt1b molecules changed after glutamate addition, such that each transporter explored a larger area of the membrane in a given amount of time (Figure 2.7A and B). This effectively increased the generalized diffusion coefficient (K) by 13% and 49% for Glt1a and Glt1b, respectively, (Figure 2.7C) and the anomalous exponent (α) by 7% and 19%, for Glt1a and Glt1b, respectively (Figure 2.7D), indicating a significant increase in mobility caused by glutamate and supporting previous observations [140,143].

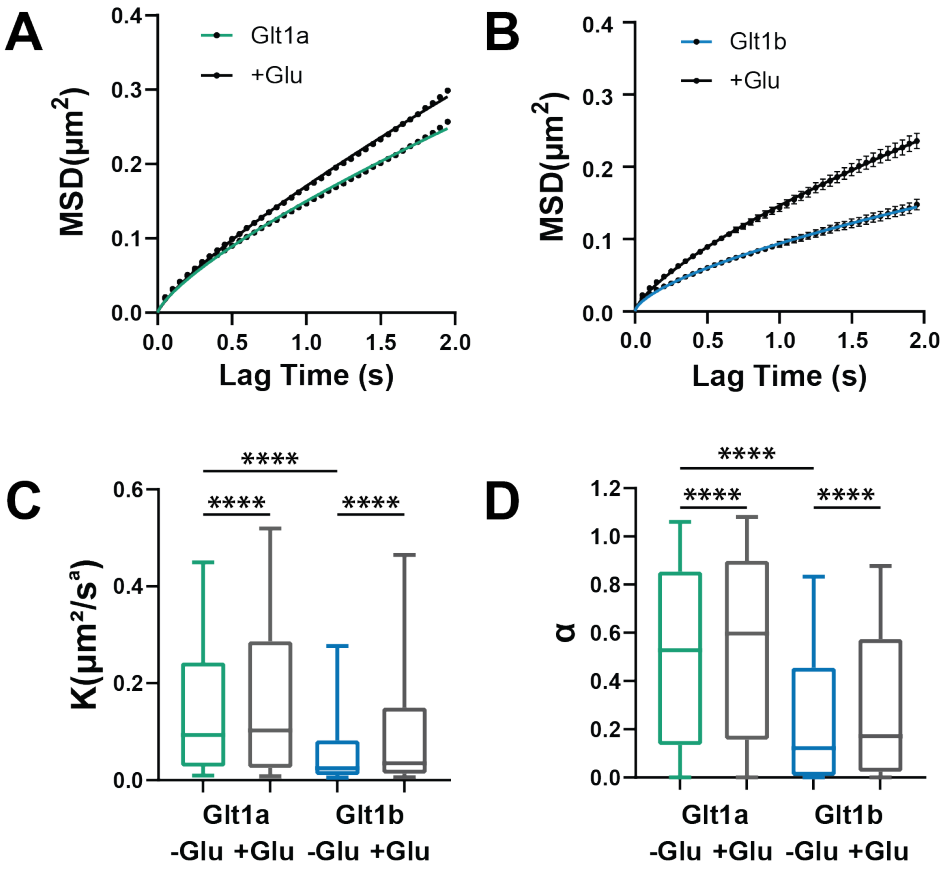

Figure 2.7: Glt1 diffusion increased by application of 100 μM glutamate. Mean square displacement (MS**D)** as a function of lag time (s) shows an increase in diffusion of Glt1a (**A)** and Glt1b (**B)** with 100 μM glutamate application. Lines shown are fits of the data to Eqn 3 (A: K = 0.150, α = 0.752, R^2 = 0.998; A: +Glu K = 0.170, α = 0.800, R^2 = 0.998; B: K = 0.0939, α = 0.645, R^2 = 0.999; B: +Glu K = 0.146 α = 0.714, R^2 = 0.999). **C)** The anomalous diffusion coefficient (K) of Glt1a (green, median = 0.093, N = 32432 trajectories) or Glt1b (blue, median = 0.025, N = 2821 trajectories) significantly increases with glutamate application (Glt1a +Glu: median = 0.103, N = 34540 trajectories, $p < 0.0001$; Glt1b +Glu: median = 0.035, N = 3133 trajectories, $p < 0.0001$). The anomalous diffusion coefficient for Glt1a was significantly higher than Glt1b ($p < 0.0001$). **D)** The anomalous exponent (α) of Glt1a (green, median = 0.528, N = 32432 trajectories) or Glt1b (blue, median = 0.121, N = 2821 trajectories) significantly increases with glutamate application (Glt1a +Glu: median = 0.596, N = 34540 trajectories, $p < 0.0001$; Glt1b +Glu: median = 0.171, N = 3133 trajectories, $p < 0.0001$). The anomalous exponent for Glt1a was significantly higher than Glt1b ($p < 0.0001$). Box plots represent the median and interquartile range. Bars in box plots represent the 10th - 90th percentile.

To test the possibility that Glt1 nanoclusters localized on actin release mobile transporters after glutamate addition, we measured nanocluster localization and intensity before and after applying 100 μM glutamate. Representative images of Glt1a nanoclusters in the same cell before and more than 3 minutes after 100 μM glutamate application are

shown in Figure 2.8A. Notably, Glt1a nanocluster localization on actin filaments does not appear to change after glutamate addition. Indeed, when nanocluster concentration on actin was quantified, adding glutamate did not significantly increase or decrease the density of Glt1a nanoclusters localized to actin regions (Figure 2.8B), indicating that nan-

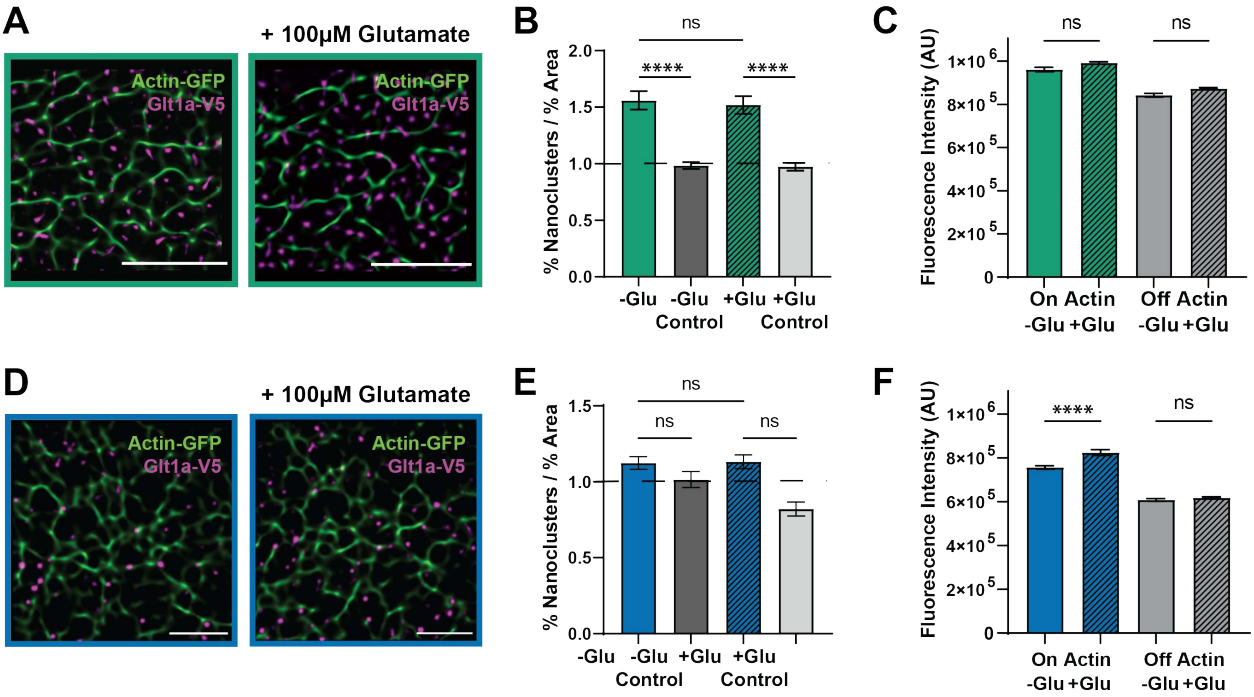

Figure 2.8: Glutamate does not affect Glt1a nanoclustering. A) Representative images of Glt1a nanoclusters (magenta) overlying actin (green) before and after the addition of 100 μM glutamate. **B)** Glt1a nanoclusters are concentrated to actin filaments even after the addition of 100 μM glutamate (mean $\pm$ SEM = 1.52 $\pm$ 0.079, N = 58 cells) versus a random pixel control (mean $\pm$ SEM = 0.97 $\pm$ 0.034, N = 58 cells, $p < 0.0001$). **C)** Glt1a nanocluster sum intensity on actin filaments (mean $\pm$ SEM = 9.61E5 $\pm$ 1.04E4, N = 43 cells, 34774 nanoclusters) does not change after addition of 100 μM glutamate (mean $\pm$ SEM = 9.91E5 $\pm$ 5.76E3, N = 27 cells, 34615 nanoclusters, $p = 0.239$). Glt1a nanoclusters localized off actin (mean $\pm$ SEM = 8.42E5 $\pm$ 8.43E3, N = 43 cells, 219464 nanoclusters) also do not change in size after glutamate application (mean $\pm$ SEM = 8.73E5 $\pm$ 4.58E3, N = 43 cells, 204549 nanoclusters, $p = 0.218$) **D)** Representative images of Glt1b nanoclusters (magenta) overlying actin (green) before and after addition of 100 μM glutamate.**E)** Glt1b nanoclusters are not concentrated to actin filaments even after addition of 100 μM glutamate (mean $\pm$ SEM = 1.13 $\pm$ 0.045, N = 17 cells) versus a random pixel control (mean $\pm$ SEM = 0.82 $\pm$ 0.046, N = 17 cells, $p < 0.0001$).**F)** Glt1b nanocluster sum intensity on actin filaments increases after addition of 100 μM glutamate (mean $\pm$ SEM = 8.14E5 $\pm$ 9.73E3, 17 cells, N = 13589 nanoclusters, $p < 0.0001$). However, Glt1b nanoclusters localized off of actin mean $\pm$ SEM = 6.13E5 $\pm$ 3.66E3, N = 17 cells, 99045 nanoclusters) do not change in density after glutamate application (mean $\pm$ SEM = 6.18E5 $\pm$ 4.09E3, N = 17 cells, 105676 nanoclusters, $p = 0.986$). Scale bars are 5 μm.

oclusters on actin do not disintegrate after glutamate addition to increase total diffusion. In addition, Glt1a nanocluster fluorescence intensity did not change following glutamate treatment, including nanoclusters located away from actin, suggesting that few, if any, individual transporters leave nanoclusters (Figure 2.8C). Similar to Glt1a, Glt1b nanocluster localization relative to actin did not appear to change after glutamate treatment (Figure 2.8D and E). However, Glt1b nanoclusters localized on actin significantly increased in fluorescence intensity after glutamate treatment (Figure 2.8F), suggesting glutamate binding might free additional Glt1b that subsequently become trapped in existing nanoclusters near actin.

Altogether, these data suggest that glutamate does not alter the localization or morphology of Glt1a nanoclusters, and thus Glt1a nanocluster disintegration is not likely linked to the increase in diffusion seen after glutamate treatment. Since nanoclusters off actin were also unaffected, it appears the effect of glutamate on diffusion primarily affects free transporters, although the underlying mechanism remains elusive.

2.5 Discussion

2.5.1 Summary

To maintain the fidelity of glutamate neurotransmission, astrocytes use highly expressed glutamate transporters, such as Glt1, to limit glutamate signals spatially and temporally [300,301]. Here, we described the localization of Glt1a nanoclusters on cortical actin filaments using a combination of high-resolution microscopy, bleach step analysis, and single-particle tracking. Our results indicate that Glt1a and Glt1b can both form nanoclusters in multiple cell types and both isoforms can occupy the same nanoclusters. However, these isoforms differed in their localization, with Glt1a nanoclusters colocalizing strongly with cortical actin filaments, while Glt1b nanoclusters did not. Both

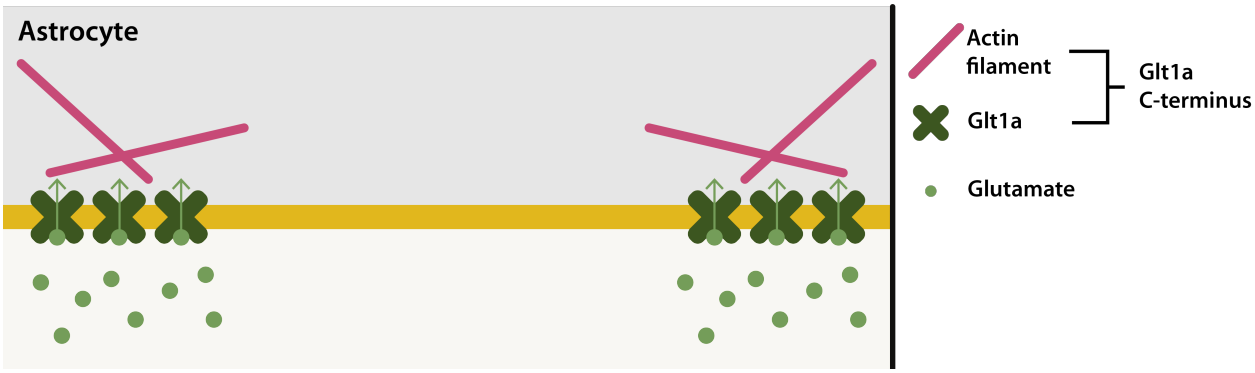

Figure 2.9: Model of astrocyte Glt1 nanoclusters. Astrocyte Glt1 transporters (green) are localized in nanoclusters at the surface of astrocytes, perhaps due to the interaction of the Glt1a C-terminus with a component of the actin cytoskeleton (magenta).

Glt1a and Glt1b nanoclusters had higher fluorescence intensity when localized on actin filaments, analogous to an increased number of transporters per nanocluster. Expression of a cytosolic Glt1a C-terminus protein disrupted the localization and fluorescence of Glt1a nanoclusters on actin filaments, indicating the C-terminus plays an important role in this interaction. Expression of the C-terminus also increased the overall diffusion of Glt1a transporters both on and off of actin filaments, suggesting the C-terminus plays a larger role in governing transporter diffusion. We also found that Glt1a nanocluster localization and fluorescence intensity on actin was undisturbed by glutamate application, indicating that glutamate binding or transport does not strongly affect the localization of Glt1a nanoclusters. However, Glt1b nanoclusters localized on actin displayed a significant increase in fluorescence intensity, indicating an increased number of transporters per nanocluster after glutamate application. Altogether, these data strongly suggest that the actin cytoskeleton plays a role in organizing Glt1 nanoclusters in the astrocyte plasma membrane. A model summarizing the results presented in this chapter is shown in Figure 2.9.

2.5.2 Nanoclustering is a conserved feature of both Glt1 splice forms

The data presented here suggest that 2 isoforms of Glt1, Glt1a and Glt1b, are capable of forming nanoclusters (Figure 2.2), which implies a shared mechanism initiates nanocluster formation, possibly via interaction with membrane cholesterol, as suggested previously [138,141,142]. Here, we used the number of antibodies per nanocluster as a proxy for the number of transporters localized in a nanocluster (Figure 2.2B & D). It is difficult to estimate the number of antibodies that could bind to individual transporters, which could be anywhere from 1-3 depending on steric hindrance. However, because Glt1a and Glt1b are similar in most of their sequence, we do not believe a different number of antibodies would bind to transporters containing either splice variant. Therefore, differences between Glt1a and Glt1b should remain, regardless of the number of antibodies bound to each transporter. We also found that only Glt1a nanoclusters are localized near actin, indicating cytoskeleton interaction both localizes Glt1a nanoclusters (Figure 2.3A & C) and increases the number of Glt1a transporters per nanocluster (Figure 2.3D). Together with Figure 1, these results indicate multiple mechanisms can regulate Glt1 nanocluster formation and stability.

2.5.3 Cortical actin is central to Glt1a nanocluster location

Our understanding of plasma membrane organization and architecture has evolved from the Singer-Nicholson fluid mosaic model, which postulated a homogeneous lipid bilayer embedded with freely diffusing proteins [302]. The current prevailing model is far more complex, with the plasma membrane consisting of heterogeneous patches of lipids and proteins, which are dynamically regulated [297,303–306]. Compartmentalization of the plasma membrane is thought to improve regulatory efficiency and provide specialized signaling domains [297]. Protein constituents of these domains are manipu-

lated by lipid composition and turnover, extracellular matrix contacts, and cytoskeletal encounters [298].

A fine mesh of cortical cytoskeleton filaments that lie just beneath the plasma membrane act as diffusion barriers [274, 307] and nanocluster nucleators [308, 309]. Cortical cytoskeleton filaments, composed of actin and septins, can simultaneously limit the lateral diffusion of membrane proteins and facilitate interactions between membrane proteins or lipids and cytoskeletal components to generate nanoclusters [298]. The work in this paper suggests this mechanism is relevant to glutamate transporters as well. However, Glt1a nanoclusters clearly do not directly bind cortical actin, for nanoclusters were often found adjacent to actin, as opposed to being entirely colocalized when using the SRRF super-resolution approach. Therefore, the Glt1a C-terminus may interact with an unknown protein that in turn associates with actin.

2.5.4 Looking towards the Glt1 interactome

Membrane protein localization and diffusion are governed by several factors, including interactions with other proteins, corralling by or anchoring to the actin cytoskeleton, and interactions with organelles that come into close contact with the plasma membrane [271–274]. Biochemical approaches have identified several proteins that could act as Glt1 interactors, including cytoskeleton-associated proteins Ajuba [278] and Sept2-associated BORG4 [279], PDZ proteins PICK1 [124] and MAGI1 [280], the Na^+/K^+ ATPase α-subunit [108], and various mitochondrial proteins [108]. Any one of these interactors could reasonably contribute to the immobilization of Glt1 molecules on the astrocytic surface, both near neuronal synapses and somatic Kv2.1 clusters. The present work suggests the primary mechanism of Glt1 immobilization is via an interaction with a cytoskeleton-associated protein (Figure 2.3). An Ajuba interaction is unlikely to explain the observations presented here because the N-terminus of Glt1 is thought to regulate

the interaction, which is identical between Glt1a and Glt1b. Also, our results in Figure 2.5 and Figure 2.6 implicate the Glt1a C-terminus in regulating the localization of nanoclusters to cortical actin filaments. The specific amino acid residues involved in the BORG4/Sept2 interaction with Glt1 have not yet been identified, and this partnership should be the focus of future investigations.

Interestingly, GLAST, another highly expressed glutamate transporter, interacts with Sept2 in Bergmann glia via the GLAST C-terminus [310]. More recent evidence suggests that this interaction is dependent on the septin effector, BORG4, and is crucial in localizing GLAST to perisynaptic astrocyte membranes [311]. Mislocalization of GLAST caused impairment in the time course of glutamate clearance, suggesting the perisynaptic localization of GLAST is imperative for proper glutamate signaling dynamics in the cerebellum. Together with the data presented in this work, this suggests cytoskeletal interaction may be a ubiquitous method of localizing glutamate transporters.

While the data presented here focus on localization near the actin cytoskeleton, the septin cytoskeleton is intimately connected and dependent upon the actin cytoskeleton (for review: [312]). We found Glt1a was localized on and adjacent to actin filaments (Figure 2.3), perhaps implicating the septin cytoskeleton in Glt1a localization. Septins colocalize prominently with certain features of actin filaments [312], most notably stress fibers and focal adhesions, which are necessary to maintain peripheral astrocyte processes and stabilize cell adhesions [313]. Multiple glutamate transporters, including Glt1, are localized to the tips of such processes [299], which might rely on a septin interaction.

2.5.5 Nanoclustering may impact transporter function

Nanoclustering is thought to be important in regulating several features of membrane protein function, such as concentrating ligand binding sites, improving signal transduction, and allowing allosteric cooperation [297]. Certainly, the concentration of

Glt1 transporters near synapses is vital in limiting glutamate neurotransmission. Interestingly, neuronal activity induced by gabazine increased Glt1 nanocluster diameter by 49% and decreased Glt1 nanocluster distance to synapses [130]. Although we did not observe increases in Glt1a nanocluster fluorescence intensity after glutamate addition, which should be comparable to nanocluster diameter, it is difficult to equate the neuronal activity elicited by gabazine and the concentration of glutamate used in this study. Furthermore, Glt1 transporters are rapidly internalized under conditions of high extracellular glutamate, such as in ischemia and traumatic brain injury [314]. Given the importance of actin in endocytosis [315], localizing Glt1 nanoclusters near actin filaments could be a mechanism to swiftly internalize glutamate-bound transporters unable to function due to ionic gradient perturbations in pathophysiological conditions [316]. Additionally, nanocluster disruption via cholesterol depletion decreased transport efficiency by $\sim$30%, suggesting that nanoclustering of Glt1 may be important for transporter function or membrane stability [138]. In another study, cholesterol disruption resulted in rapid internalization of Glt1 transporters, supporting the idea that nanoclustering enhances Glt1 surface stability [141]. Whether nanoclustering affects transport efficiency directly or by increasing Glt1 transporter stability in the membrane awaits future investigation.

Overall, these data indicate that the Glt1a C-terminus is important in determining the localization of Glt1a in the plasma membrane. Due to the slow transport cycle of Glt1, transporters must be localized at the right place at the right time. Understanding the mechanisms regulating Glt1a C-terminal interaction with the actin cytoskeleton, and thus transporter localization will be essential to identify new targets for mitigation of neuronal insults which lead to high ambient glutamate, such as ischemic stroke, traumatic brain injury, and epilepsy. Whether the Glt1a-actin interaction is necessary for localization near neuronal structures involved in sensing glutamate is explored in the next chapter.

Chapter 3

Astrocytic Glt1-actin interaction localizes glutamate transporters near neuronal structures involved in glutamate sensation

3.1 Summary

Astrocytes contact neurons at somatic clusters of Kv2.1 potassium channels and approximately 2/3 of synapses in the hippocampus. In the somatosensory cortex, astrocyte Glt1 forms net-like structures around neuronal Kv2.1 clusters, and pharmacological inhibition of Glt1 glutamate uptake causes Kv2.1 cluster disintegration. Therefore, we wanted to determine the cause of the Glt1 localization pattern surrounding neuronal Kv2.1 clusters. Using super-resolution imaging of mixed cultures of astrocytes and neurons, we replicate findings of astrocyte Glt1 in a net-like localization pattern around neuronal Kv2.1 clusters. By expressing organelle markers for actin, ER, and mitochondria specifically in astrocytes, we found that both actin and ER were excluded from the region across from neuronal Kv2.1 clusters. The actin-Glt1 relationship discussed in Chapter 2 is likely responsible for the net-like appearance of Glt1, as astrocytic Glt1 and actin colocalize in nets around Kv2.1 clusters at points of neuron-astrocyte contact. Neuronal control over the astrocyte cytoskeleton appears central to this Glt1a localization. Together with Chapter 2, these data describe a novel interaction between the Glt1a C-terminus and cortical actin filaments, which localizes Glt1 near neuronal structures involved in detecting ischemic insult. Since Glt1 is also localized near synapses, we go on to describe the localization of Kv2.1 and its auxiliary β-subunit AMIGO1 at mature postsynaptic compartments, where Glt1 was also commonly associated. These data suggest these two glutamate-sensing neuronal structures where Glt1 is localized may be formed and regulated by similar mechanisms.

3.1.1 Hypotheses to be tested —

1. Astrocyte Glt1 and actin will colocalize in nets surrounding neuronal Kv2.1 clusters.

2. Glt1 diffusion will be altered across from neuronal Kv2.1 clusters, similar to that seen at synapses.

3. Synapses will colocalize with Kv2.1, AMIGO1, and Glt1.

3.2 Introduction

The astrocyte-expressed glutamate transporter, Glt1, provides the major mechanism for glutamate uptake at synapses [3,169,170]. Glt1 concentration is especially high in peri-synaptic astrocyte processes (PAPs) [73,110], where it limits the time-course of glutamate transmission and limits spill over into other synaptic clefts, thereby preventing excitation at inactive synapses [270]. The distance of Glt1 to synapses is dynamically regulated by synaptic activity, such that Glt1 is localized closer to active synapses [130].

In addition to localization, the mobility of active Glt1 transporters in the membrane is important in shaping glutamate neurotransmission in the hippocampus [140]. Unbound transporters are relatively immobile, especially near synapses, but when glutamate is bound, transporter diffusion increases, thus allowing transporters to diffuse away from high concentrations of glutamate [140,143]. This mobility change is effectively responsible for replacing glutamate-bound transporters with unbound transporters, conceivably to overcome slow transport. Given the importance of Glt1 in regulating synaptic glutamate signals, it is vital to understand the mechanisms governing the localization and diffusion of these transporters.

The majority of published work on Glt1 localization has focused on localization adjacent to synapses [73, 110, 156], however, a smaller literature describes a functional and spatial relationship of astrocytic Glt1 transporters and clusters of Kv2.1 channels on the neuronal soma [184, 185]. Kv2.1 is a voltage-gated potassium channel that resides in micron-sized clusters on the soma, dendrites, and AIS of pyramidal neurons [191, 211, 214, 317, 318]. Clusters represent areas of the plasma membrane where hundreds of Kv2.1 channels interact with endoplasmic reticulum (ER) resident VAP proteins to bring the ER into close apposition with the plasma membrane (PM) [210, 218, 220, 295]. While not all functions of Kv2.1-induced ER/PM junctions are fully elucidated, these junctions are thought to be crucially involved in Ca^{2+} homeostasis, lipid transfer, and exocytosis [196,198,215,221,224,225,319–321]. ER/PM junctions make up approximately 12% of the total neuronal surface *in vivo* [221], indicating this organelle may be critically involved in several cellular processes.

In addition, Kv2.1 interacts directly with AMIGO1, which modifies the voltage-dependence of activation of Kv2.1 and possesses an extracellular domain that acts as a cell-adhesion molecule [226–228]. AMIGOs are single-pass transmembrane proteins, with short intracellular C-termini and extensive N-termini with 6 leucine-rich repeat (LRR) domains and an immunoglobulin-like domain [227, 229]. The AMIGO family consists of 3 members (AMIGO1, 2, and 3), which are about 48% similar at the amino acid level, and all are now known to capably interact with Kv2.1 to modify its function [226, 228] (see Chapter 4). AMIGO1 is the most highly expressed in the brain, while the other two are more widespread in tissue distribution, although still enriched in the brain [227].

Previous EM studies of Kv2.1 in the murine brain show Kv2.1 clusters are often apposed to astrocyte processes [183], although the mechanism of cell adhesion remains to be discovered. Subsequent investigations of this Kv2.1-astrocyte contact have

been limited to primarily functional studies, focusing on the relationship of Kv2.1 and the astrocyte-expressed glutamate transporter, Glt1. Pharmacological blockade of the astrocyte expressed Glt1 results in glutamate-induced declustering of Kv2.1 [184, 185], due to the dephosphorylation of the VAP interacting FFAT motif in the C-terminus of Kv2.1 [184, 218, 257, 261, 262, 322, 323]. Interestingly, Glt1 resides in net-like structures around Kv2.1 clusters in the somatosensory cortex, although the cause of localization is unknown [184].

This work aimed to determine the mechanism of astrocyte Glt1 exclusion from membrane across from neuronal Kv2.1 clusters. The work presented here shows astrocytic Glt1 localizes in net-like structures around neuronal Kv2.1/AMIGO clusters. In hippocampal mixed cultures of astrocytes and neurons, we find that both astrocytic actin and ER are excluded from the region directly across from Kv2.1/AMIGO1 clusters in neurons. Subsequently, we demonstrate that in hippocampal mixed cultures of astrocytes and neurons, astrocytic Glt1 and actin colocalize in net-like structures around neuronal clusters of Kv2.1. In contrast to published work on the diffusion of Glt1 near synapses [140], we show that astrocytic Glt1 mobility does not decrease across from neuronal Kv2.1 clusters, suggesting that the exclusion of actin, not Glt1, is responsible for the net-like localization. Because Glt1 is localized near both Kv2.1 and synapses, we also performed studies of Kv2.1 and AMIGO1 localization at synapses in mature hippocampal cultures. We discover Kv2.1 and AMIGO1 both localize to synaptic structures, which were often associated with astrocytic Glt1. To our knowledge, these studies are the first to describe Kv2.1 and AMIGO at synapses in culture. Altogether, these data further elucidate the mechanisms governing Glt1 localization, particularly near glutamate-sensitive neuronal structures [184, 185, 210, 322].

3.3 Materials and Methods

3.3.1 DNA Constructs

For specific expression of proteins in astrocytes or neurons, the gfaABC1D and SYN promoters were used, respectively. The gfaABC1D promoter was inserted via PCR-mediated addition of restriction sites, AseI and NheI, to the ends of the gfaABC1D promoter from pAAV.GfaABC1D.GluSnFr.SV40 (a gift from Baljit Khakh, Addgene plasmid 100889). gfaABC1D>Glt1a-V5 was generated by restriction digest of gfaABC1D>Ruby2-Glt1a-V5 with AgeI and BspEI to remove the Ruby2, followed by ligation. This construct was then sent to VectorBuilder (Chicago, IL), where it was cloned into an AAV vector and packaged into an AAV5 virus. gfaABC1D>Ruby2-Actin was generated by restriction digest of gfaABC1D>Ruby2-Glt1a-V5 and GFP-Actin with NheI and XhoI and subsequent ligation of the NheI-GFP-Actin-XhoI into the XhoI-gfaABC1D-NheI vector. AAV9: SYN>AMIGO-GFP was used to label the endogenous Kv2.1 clusters in neurons. This virus was also packaged by VectorBuilder. GFP-TOMM20-N-10 was a gift from Michael Davidson (Addgene plasmid 57158). For full maps of gfaABC1D>Ruby2-Actin, gfaABC1D>Ruby2-Tomm20, and gfaABC1D>dsRed-ER, and other plasmids, see Appendix B.

3.3.2 Cell Culture, Transfection, Infection and Labeling

See Section 2.3.2.

DIV7 cultures were infected with AAV for immunocytochemistry or live mixed cultures, which were performed on DIV14 or later. For live co-culture experiments, DIV7 cells were infected with AAV9:SYN>AMIGO-GFP (1×10^{10} genocopies) and AAV5: gfaABC1D> Glt1a-V5 (5×10^{9} genocopies). Subsequently, these cultures were transfected with gfa-ABC1D> Ruby2-Actin (0.5 μg), gfaABC1D> Ruby2-Tomm20 (0.5 μg),

gfaABC1D> dsRed-ER (0.5 μg), CMV> GFP-PSD-95 (0.5 μg), or CMV> vGluT1-mCherry (0.5 μg). On the day of imaging, cultures were washed 2 times with imaging saline and then either prepared for immunocytochemistry or were immediately transferred to the spinning disk confocal microscope (described below) for live experimentation.

3.3.3 Immunocytochemistry

DIV14 cells were washed once with imaging saline and then fixed in 4% paraformaldehyde in imaging saline for 10 minutes at 37 C. After washing, cells were incubated in 10% goat serum, 0.1% TritonX-100 in imaging saline for 15 minutes at room temperature. The solution was removed and replaced with 10% goat serum containing a combination of the following antibodies: 1:200 mouse αAMIGO1 (NeuroMab), 1:200 mouse αKv2.1 (NeuroMab), 1:1000 rabbit αEAAT2/Glt1 (Abcam), 1:1000 rabbit αSynapsin (Synaptic Systems). Cells were incubated in primary antibody solutions overnight at 4 C without agitation. The following day, cultures were washed 4 times with 1X PB2 + 0.2% Tween-20. Cultures were then incubated in secondary antibody solutions containing 10% goat serum and a combination of the following antibodies: 1:1000 goat α-mouse AlexaFluor488 (Thermo Fisher Scientific), 1:1000 goat α-mouse AlexaFluor647 (Thermo Fisher Scientific), 1:1000 goat α-rabbit AlexaFluor488 (Thermo Fisher Scientific), 1:1000 goat α-rabbit AlexaFluor647 (Thermo Fisher Scientific). After 45 minutes of incubation, the dishes were washed 4 times with 1X PB2 + 0.2% Tween-20, and then coverslips were mounted on top of cells with AquaPoly Mount and sealed with clear nail polish. Dishes were stored in the dark at 4 C until use.

3.3.4 Microscopy

Spinning disk confocal microscopy was performed on a Yokogawa (Musa-shino, JP) based CSUX1 system with an Olympus (Tokyo, JP) IX83 inverted stand, and coupled to an Andor (Abingdon, GB) laser launch containing 405, 488, 568, and 637 nm diode lasers,

100-150 mW each. Images were collected using two Andor iXon EMCCD cameras (DU-897), oriented perpendicularly, and 100X Plan Apo, 1.4 NA objective. To split the emitted fluorescence when imaging concurrently for single-particle tracking and fluorescence recovery after photobleaching, a dichroic mirror was used. This system is equipped with the ZDC constant focus system and a Tokai Hit chamber and objective heater. Images were collected using MetaMorph software (version 7.8.13.0).

3.3.5 Super-resolution radial fluctuations (SRRF)

See Section 2.3.6.

For images acquired on the spinning disk confocal microscope, 200 frames for each wavelength were acquired sequentially at each focal plane in fixed co-culture samples. Subsequently, these videos were background subtracted and analyzed using the NanoJ-SRRF plugin for FIJI/ImageJ [284]. The SRRF algorithm was applied over 200 frames, and therefore one super-resolution image represented each focal plane.

3.3.6 Single-particle tracking

DIV14 rat hippocampal mixed cultures infected with AAV9:SYN-AMIGO-GFP and AAV5:gfaABC1D-Glt1a-V5 were labeled with αV5-CF640 for 3 minutes in imaging saline and subsequently transferred to the spinning disk confocal microscope for imaging. The chamber was kept at 37 C for the entirety of imaging. Using a dual-camera system and a dichroic mirror, AMIGO and Glt1a were imaged simultaneously at 20 Hz for 2000 frames. Before imaging, a dish covered in TetraSpeck beads (Invitrogen) was imaged through both cameras to use for alignment purposes.

Images containing Glt1 molecules were background subtracted and a Gaussian filter with a standard deviation of 0.7 pixels was applied to each frame in ImageJ. The

channel images containing actin or AMIGO underwent processing for SRRF analysis, such that 2000 frames were temporally correlated and averaged to 40 frames [283]. This sequence of images was converted to binary. Individual Glt1 molecules were tracked using the U-track algorithm in MATLAB [285], as previously described [324, 325]. Subsequently, tracks were separated based on the spatial relationship to AMIGO (on and off) using a custom MATLAB code into on states when they are found to colocalize with AMIGO and off states otherwise. A 3-pixel barrier between the two regions was excluded, such that trajectories were identified within each region with a high degree of certainty. Trajectory segments in each state (on or off) were discarded if they did not remain for at least 20 consecutive frames (1 second) in the same state. The trajectories in each region were then used to calculate individual time-averaged mean square displacements (MSD) (see Section 2.3.7 for equations).

3.3.7 Fluorescence recovery after photobleaching (FRAP)

Astrocytes expressing gfaABC1D >Ruby2-Glt1a-V5 in contact with neurons expressing AAV9:SYN>AMIGO-GFP were imaged simultaneously using spinning disk confocal microscopy. Movies were acquired at 1 Hz for 500 seconds at the plane where the two cells came into the most contact. The first ten frames were collected to measure initial fluorescence. We then bleached the astrocyte surface with a high-intensity 561 nm laser, which ensured only the Glt1a was photobleached. Photobleaching resulted in approximately 80% loss of fluorescence after background subtraction and bleaching correction. A mask was created from the AMIGO-GFP signal and subsequently used to measure the recovery of Glt1a diffusion inside and outside of this region. Fluorescence measurements in each region were normalized to the average of the first 10 frames.

3.3.8 Image Processing and Analysis

Image processing was done in ImageJ (v. 1.52). Analysis was completed in MATLAB (R2019A). Statistics and graphs were generated in GraphPad Prism 9. In cases where multiple groups were compared, one-way ANOVAs were used followed by post-hoc Sidak's tests to compare specific groups to one another, unless otherwise noted.

3.4 Results

3.4.1 Glt1 localizes around astrocyte membrane across from neuronal Kv2.1 clusters

Previous work suggests that Glt1 transporters reside in net-like structures around neuronal Kv2.1 clusters in the somatosensory cortex [184]. To determine whether we could replicate these data *in vitro*, hippocampal mixed cultures of neurons and astrocytes were cultured for 14 days, and subsequently fixed and immunostained for Kv2.1 and Glt1. Because the original work utilized an enhanced resolution technique called structured illumination microscopy (SIM), we applied another super-resolution technique, SRRF, to observe the localization of Glt1 and Kv2.1. Focusing on the z-plane where neurons and astrocytes came into contact (Figure 3.1A), SRRF also revealed net-like localization of Glt1 around Kv2.1 clusters (Figure 3.1B). To determine the average relationship of astrocytic Glt1 and Kv2.1, every Kv2.1 cluster and the surrounding area were averaged (Figure 3.1C). Using this analysis, we found that Glt1 rarely colocalized with neuronal Kv2.1 (Figure 3.1C, third panel). A line-scan through the center of the averaged image shows lower Glt1 fluorescence (magenta) in the region across from Kv2.1 cluster peak fluorescence (green, line-scan, right). These data indicate the net-like localization, previously observed in the somatosensory cortex [184], can be replicated in DIV14 culture.

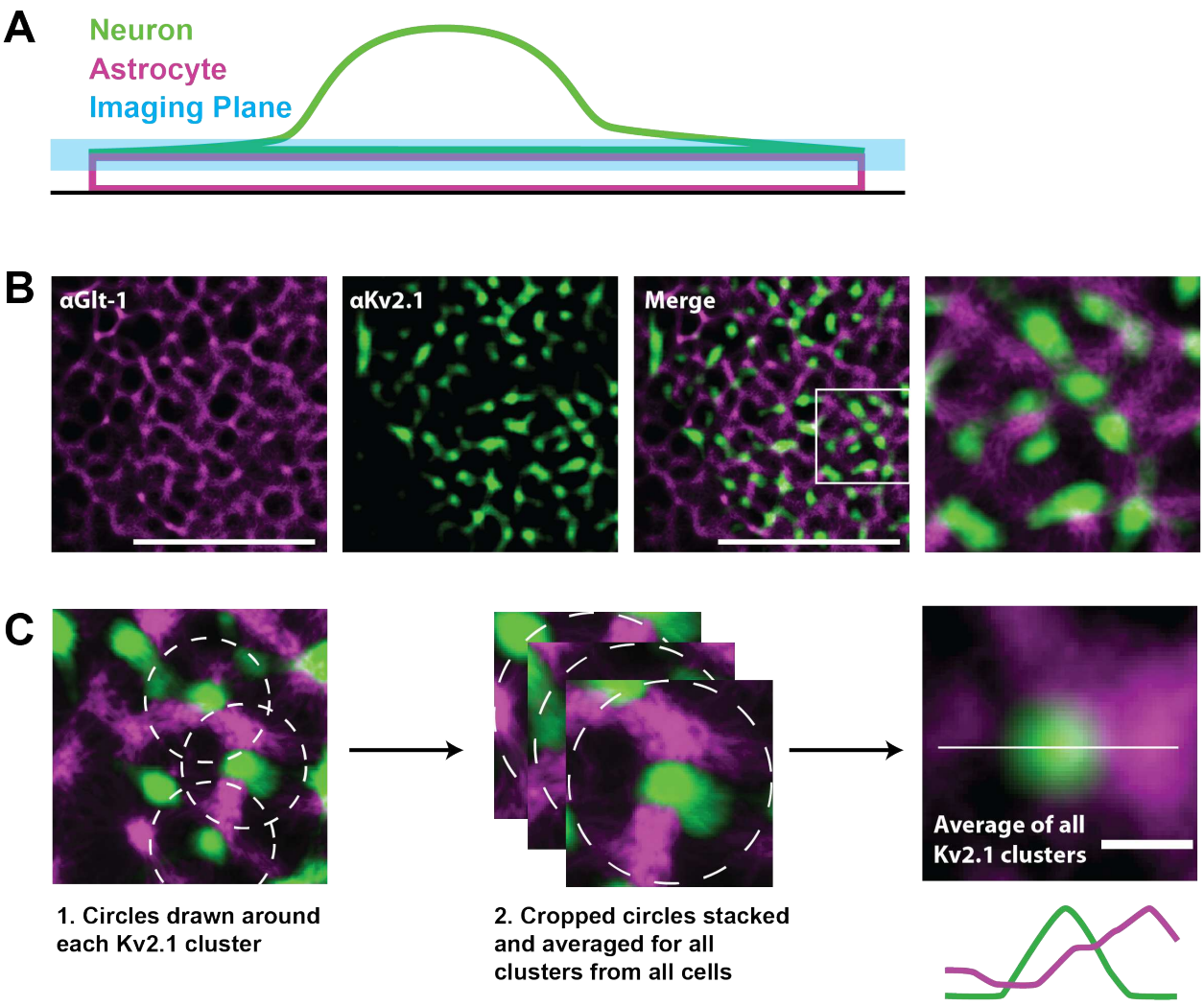

Figure 3.1: Astrocytic Glt1 forms nets around neuronal Kv2.1 clusters. A) Schematic diagram of the hippocampal co-culture system. Neurons sit directly on top of a sheet of astrocytes. For imaging, 200 frames were acquired at every z-plane for SRRF analysis. **B)** Representative images of the localization pattern of astrocytic Glt1 (magenta) around Kv2.1 in neurons (green) in DIV14 hippocampal mixed cultures. This image represents a single z-plane between a neuron and astrocyte. Scale bars = 5 μm. **C)** Every Kv2.1 cluster from every cell (N = 9 cells) was averaged to create the image on the right, showing Glt1 surrounds Kv2.1 clusters, with occasional colocalization. Scale bar = 0.5 μm.

3.4.2 Astrocytic actin and ER are excluded from the region across from Kv2.1 clusters in neighboring neurons

The experiments illustrated in Chapter 2 suggest actin plays a significant role in governing the localization of astrocyte Glt1. Therefore, we wanted to know whether

astrocyte actin would display a similar localization to Glt1 concerning neuronal Kv2.1 clusters. To this end, we expressed a Ruby2-Actin specifically in astrocytes using the gfaABC1D promoter. Simultaneously, we expressed a GFP-tagged AMIGO1 specifically in neurons using the SYN promoter. AMIGO1 is an auxiliary subunit of Kv2.1, which resides in the same clusters but does not increase their size [226]. The use of cell-specific promoters was essential to ensure the imaged actin was located in astrocytes. Using SRRF and focusing on the plane where the two cell types had the most contact, we found that astrocytic actin also displayed a net-like localization pattern around neuronal Kv2.1 clusters (Figure 3.2). Indeed, when every cluster was averaged, astrocytic actin mostly occupied the region directly around Kv2.1 clusters (Figure 3.2, right panel).

To determine whether this exclusion was unique to astrocyte actin, we performed similar experiments where dsRed-ER and Ruby2-TOMM20 were expressed specifically in astrocytes to mark the endoplasmic reticulum and mitochondria, respectively. Inter-

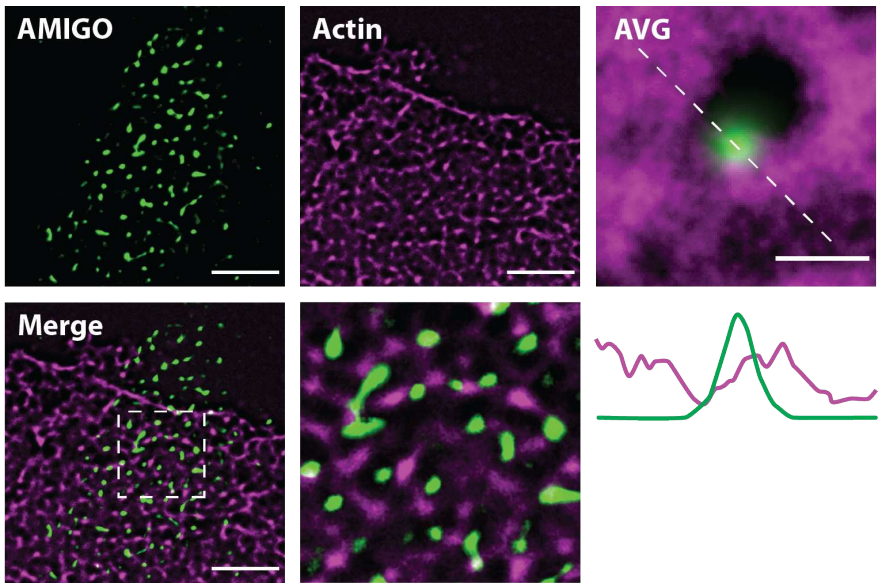

Figure 3.2: Astrocytic actin is localized in nets around neuronal Kv2.1 clusters. Representative images of astrocyte expressed Ruby2-actin (magenta) localizing in nets around neuronal AMIGO (green), which resides in Kv2.1 clusters. Every Kv2.1 cluster from every cell (N = 15 cell pairs) was averaged to create the image on the right, showing astrocytic actin surrounds Kv2.1 clusters, with rare colocalization. The scale bar in this image is 0.5 μm. A line-scan illustrates an actin (magenta) hole at the edge of the average cluster (green). Scale bars are 5 μm.

estingly, we found that astrocyte ER was also excluded from the region directly across from neuronal Kv2.1/AMIGO clusters (Figure 3.3). Averaging every cluster from every neuron revealed little to no colocalization between the ER and neuronal Kv2.1/AMIGO clusters. In contrast, astrocyte mitochondria displayed no particular localization pattern relative to neuronal Kv2.1/AMIGO clusters (Figure 3.4). Mitochondria were capable of overlapping with Kv2.1 clusters, but did not seem specifically localized across from clusters. When every cluster was averaged from every cell, mitochondria fluorescence overlaps quite well with the Kv2.1/AMIGO cluster signal, indicating mitochondria are not organized relative to neuronal Kv2.1 clusters. Altogether, these data suggest exclusion is not specific to actin, but that the localizations of other astrocyte organelles are also regulated by this neuron-astrocyte contact site.

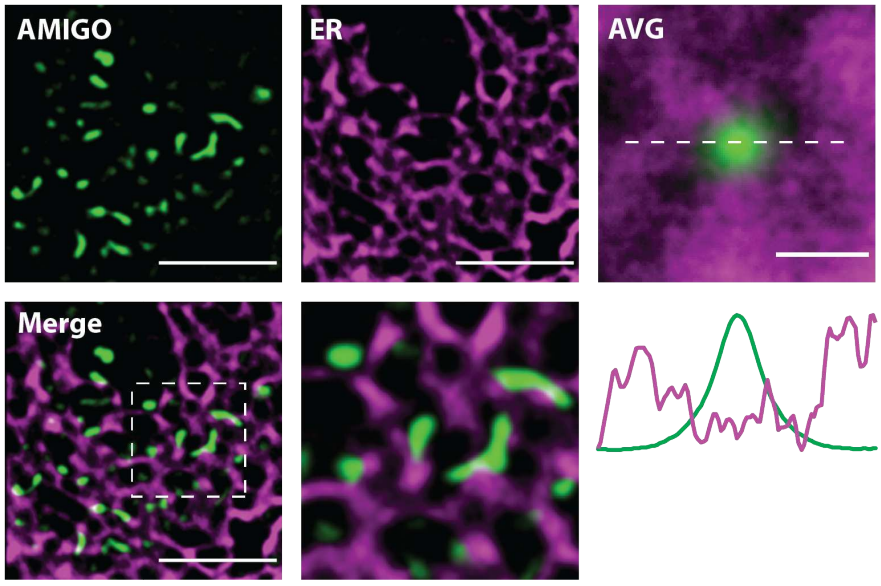

Figure 3.3: Astrocytic ER is excluded from the region across from neuronal Kv2.1 clusters. Representative images of astrocyte expressed Ruby2-ER (magenta) localizing in nets around neuronal AMIGO (green), which resides in Kv2.1 clusters. Every Kv2.1 cluster from every cell (N = 9 cell pairs) was averaged to create the image on the right, showing astrocytic ER surrounds Kv2.1 clusters, with rare colocalization. Scale bar in this image is 0.5 μm. A line-scan illustrates an ER (magenta) hole at the edge of the average cluster (green). Scale bars are 5 μm.

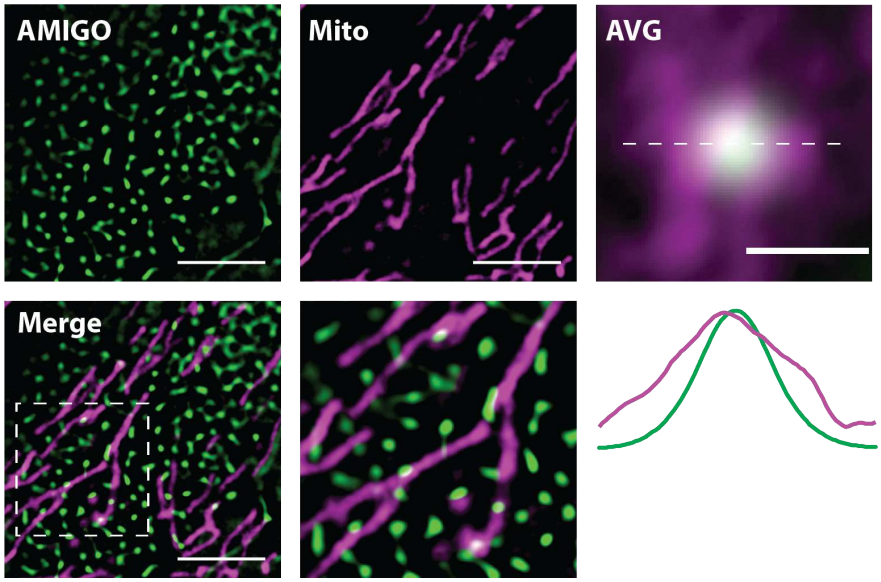

Figure 3.4: Astrocytic mitochondria show no distinct localization relative to neuronal Kv2.1 clusters. Representative images of astrocyte expressed Ruby2-mitochondria (magenta) relative to neuronal AMIGO (green), which resides in Kv2.1 clusters. Every Kv2.1 cluster from every cell (N = 24 cell pairs) was averaged to create the image on the right, showing astrocytic mitochondria can colocalize with Kv2.1 clusters. Scale bar in this image is 0.5 μm. A line-scan illustrates mitochondria (magenta) fluorescence overlaps with the average cluster (green). Scale bars are 5 μm.

3.4.3 Astrocytic actin colocalizes with Glt1 around neuronal Kv2.1 clusters

Since previous experiments in Chapter 2 and Figure 3.2 suggested actin might cause the localization of astrocyte Glt1 around neuronal Kv2.1 clusters, we wanted to know whether astrocyte actin would colocalize with Glt1 in nets around Kv2.1/AMIGO clusters. Using a combination of the above approaches, we discovered that astrocytic actin (yellow) and Glt1 (magenta) colocalize in the net surrounding neuronal Kv2.1/AMIGO clusters (cyan, Figure 3.5). These results strongly suggest the Glt1a-actin interaction is responsible for the localization pattern observed previously [184], and necessary for localization near neuronal structures involved in glutamate sensing.

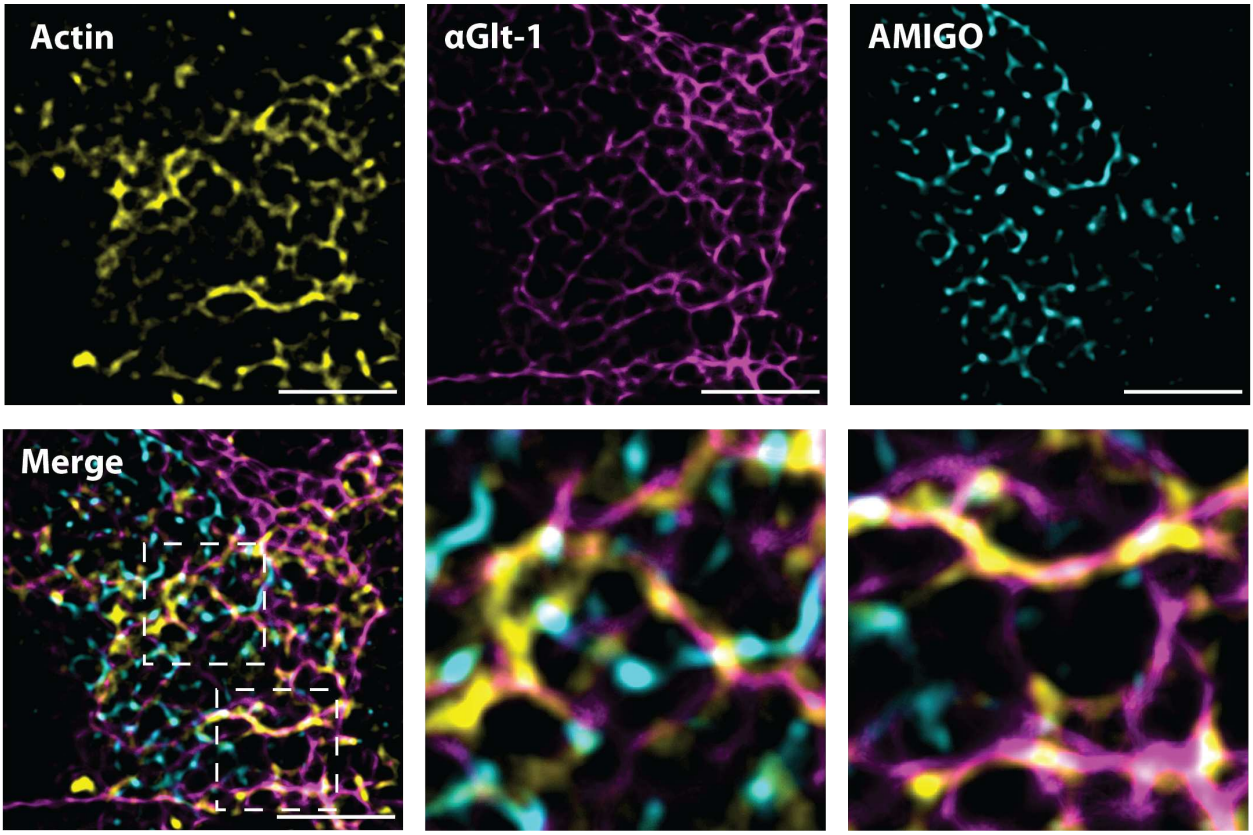

Figure 3.5: Astrocytic actin colocalizes with Glt1 in nets around neuronal Kv2.1 clusters. A) Representative images of astrocyte expressed Ruby2-actin (magenta) localizing in nets around neuronal AMIGO (green), which resides in Kv2.1 clusters. Every Kv2.1 cluster from every cell (N = 15 cell pairs) was averaged to create the image on the right, showing astrocytic actin surrounds Kv2.1 clusters, with rare colocalization. Scale bar in this image is 0.5 μm. A line-scan illustrates an actin (magenta) hole at the edge of the average cluster (green). **B)** Representative images showing astrocytic Ruby2-actin (yellow) and Glt1 (magenta) colocalize and together form nets around neuronal Kv2.1/AMIGO clusters (cyan). Zooms on the bottom row show overlapping Glt1 and actin, which rarely colocalize with Kv2.1/AMIGO clusters. Scale bars are 5 μm.

3.4.4 Astrocytic Glt1 displays unrestricted diffusion across from neuronal Kv2.1 clusters

Considering previous data suggesting Glt1 diffusion decreases in peri-synaptic astrocyte processes [140], we measured the diffusion of Glt1 in astrocytes near neuronal Kv2.1 clusters (Figure 3.6A-D). Using single-particle tracking of astrocyte expressed Glt1a-V5 while simultaneously imaging neuronal expressed GFP-AMIGO to mark Kv2.1 clusters, we found that Glt1a-V5 mean square displacement (MSD) decreased in the re-

gion of astrocyte membrane across from Kv2.1 clusters (On, blue line, Figure 3.6B). Indeed, the generalized diffusion coefficient (K) and anomalous exponent (α) significantly decreased across Kv2.1 clusters compared to Glt1a elsewhere in the astrocyte membrane (Figure 3.6C-D, $p<0.05$), indicating decreased mobility.

A sharp decrease in diffusion, and thus a concentration of molecules, within a specific region may indicate interaction with an underlying scaffold [324, 326]. However, we did not observe increased localization of Glt1 in the region across from Kv2.1 clusters in Figure 3.1. In addition, the possibility existed that the mass of the bound anti-V5 antibody could sterically hinder diffusion at the narrow junction between the neuronal Kv2.1 clusters and astrocyte membrane. Therefore, we used a complementary approach, fluorescence recovery after photobleaching (FRAP), to measure bulk diffusion in a region of the bleached membrane as illustrated in Figure 3.6E-F. Here we avoided the anti-V5 antibody labeling and relied on the Ruby2 fluorescence to detect Glt1a. We also avoided the SRRF analysis since time-dependent fluorescence recovery was being quantified. In contrast to the single-particle tracking approach, our FRAP data showed no differences in bulk diffusion between the astrocyte membrane either directly across from, or removed from, the neuronal Kv2.1 clusters (Figure 3.6F). These results suggest the decrease in diffusion observed with single-particle tracking is an artifact due to extracellular labeling. However, these contrasting data reveal that Glt1 transporters are not restricted from diffusing in the region across Kv2.1 clusters, suggesting that the concentration of Glt1 in nets around Kv2.1, as observed in the super-resolution images, is likely due to an effect of the neuronal-glial adhesion on astrocytic actin, not Glt1 itself. Overall, these data suggest Glt1 is localized in nets around neuronal Kv2.1 clusters, most likely due to exclusion of astrocytic actin in the region directly across from neuronal Kv2.1 clusters.

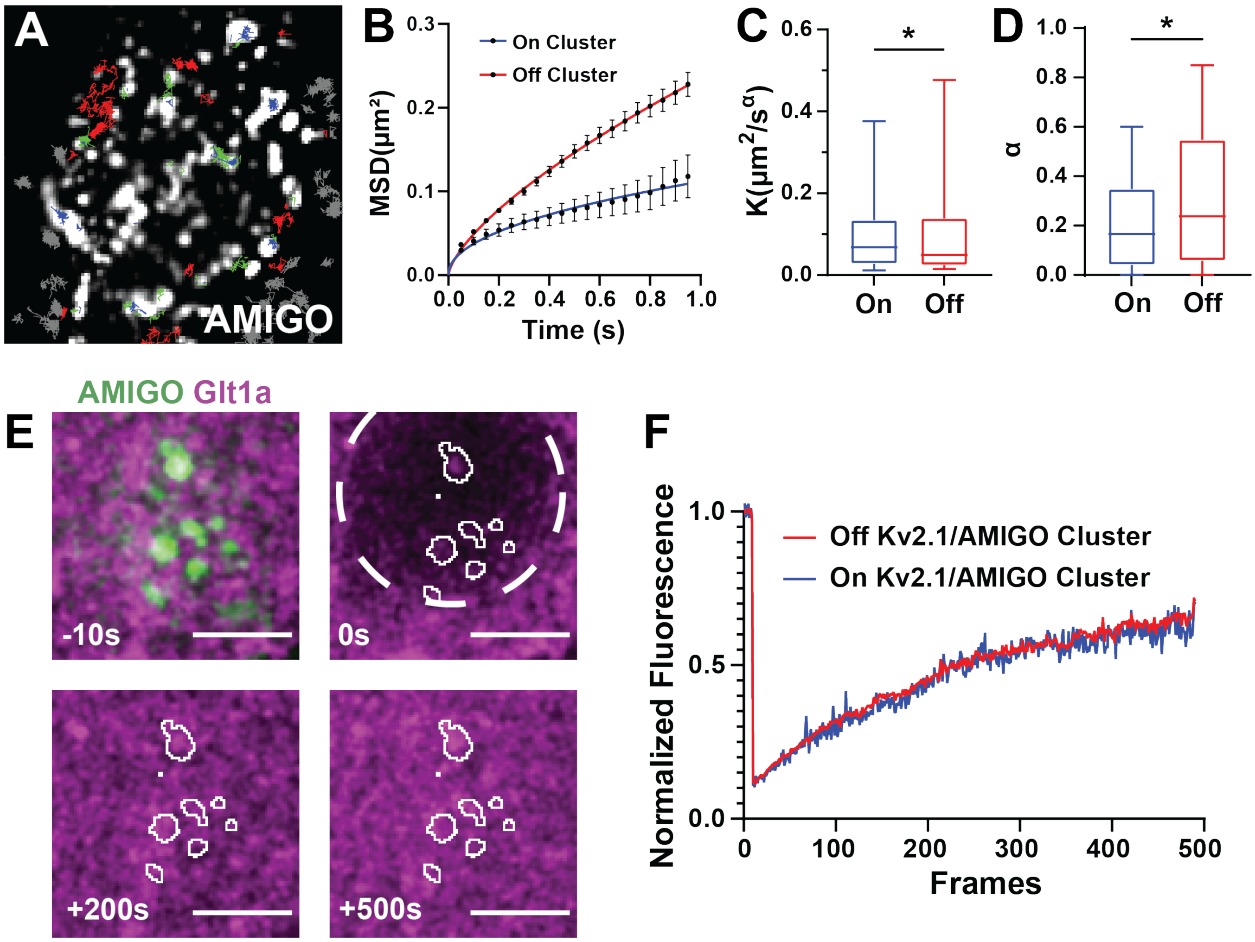

Figure 3.6: In contrast to single-particle tracking, FRAP shows no differences in astrocytic Glt1a diffusion on or off neuronal Kv2.1 clusters. A) Glt1a trajectories from an astrocyte overlayed on top of Kv2.1 clusters from the overlying neuron. Red and blue trajectories are off and on cluster areas, respectively. The green trajectories were thrown out from analysis as they were localized in the 3-pixel region between on and off. Grey trajectories represent Glt1 on the astrocyte surface, but not underneath a neuron, and as such these were not included in the analysis. **B)** Mean square displacement (MS**D)** of single astrocytic Glt1a transporters show decreased diffusion in membrane across from neuronal Kv2.1 clusters. Lines shown are fits of the data to Eqn 3 (On K = 0.112, α = 0.476, R^2 = 0.975; Off K = 0.235, α = 0.682, R^2 = 0.999). **C)** General diffusion coefficient (K) of astrocyte Glt1a is significantly different across from neuronal Kv2.1 clusters (On: N = 92 trajectories, mean ± SEM = 0.181 ± 0.0388; Off: N = 2362 trajectories, mean ± SEM = 0.161 ± 0.0100, $p < 0.05$). **D)** The anomalous exponent (α) of astrocyte Glt1a is significantly different across from neuronal Kv2.1 clusters (On: N = 92 trajectories, mean ± SEM = 0.217 ± 0.0326; Off: N = 2362 trajectories, mean ± SEM = 0.316 ± 0.00709, $p < 0.05$).**E)** Representative images of Ruby2-Glt1a (magenta) fluorescence recovery after photobleaching (FRAP). The Ruby2-Glt1a signal is underneath a population of neuronal Kv2.1 clusters (green), labeled with the auxiliary subunit GFP-AMIGO. Images show Glt1a fluorescence at different time points in a single 500-second movie. Scale bars = 5 μm. **F)** Normalized fluorescence shows no differences in fluorescence recovery of Glt1a molecules at Kv2.1 clusters versus off Kv2.1 clusters in average recoveries from 10 cell pairs. Time constants ($t^{1/2}$) were not noticeably different (On: $t^{1/2}$ = 239 ± 3.57 seconds, Off: $t^{1/2}$ = 242 ± 7.39 seconds).

3.4.5 Kv2.1 colocalizes with synaptic elements in culture

Astrocytes contact neurons at both somatic Kv2.1 clusters and synapses. At synaptic contacts, peri-synaptic astrocyte processes display a high concentration of Glt1 transporters and show activity-dependent structural plasticity, which is most likely dependent on actin regulation [152]. Given these similarities between the two neuron-astrocyte contact sites, we wanted to know whether astrocyte-synapse contacts may also be regulated by Kv2.1 clusters. Although most previous research has focused on the presence of Kv2.1 clusters on the somatic surface of neurons, a few reports in the literature suggest these clusters are also present at synapses [183,221], and in α-motoneurons, somatic Kv2.1 clusters represent sites of somatic cholinergic input [188]. Due to the high signal of clusters at the soma in fluorescence studies, and the fact that many studies have been performed in younger neuronal cultures, the signal of Kv2.1 clusters in neurites and synaptic elements may have gone unnoticed.

To determine whether we could observe Kv2.1 localization at synapses, mixed cultures of astrocytes and neurons were maintained for 3 weeks (DIV21), a time when synapses in culture have reached maturity [327]. At DIV7, cultures were transfected with GFP-PSD-95 to mark dendritic spines. Two weeks after transfection, these cultures were fixed and immunostained for Kv2.1. In mature cultures, we found that Kv2.1 clusters existed along neurites and colocalized with transfected PSD-95 (Figure 3.7A). Interestingly, we found some Kv2.1 appears to localize to spine heads where the PSD-95 signal was most prominent (Figure 3.7B), suggesting some role for Kv2.1 in post-synaptic function. When we fixed and immunostained cultures for both Kv2.1 and synapsin to mark presynaptic boutons, we found Kv2.1 and synapsin highly colocalize in neurites throughout the culture dish (Figure 3.7C). The synapsin antibody used in these studies recognizes synapsins IA, IB, IIA, and IIB, which exist at both excitatory and inhibitory synapses, and therefore, we cannot say at which type of synapses Kv2.1 localizes. Since we did

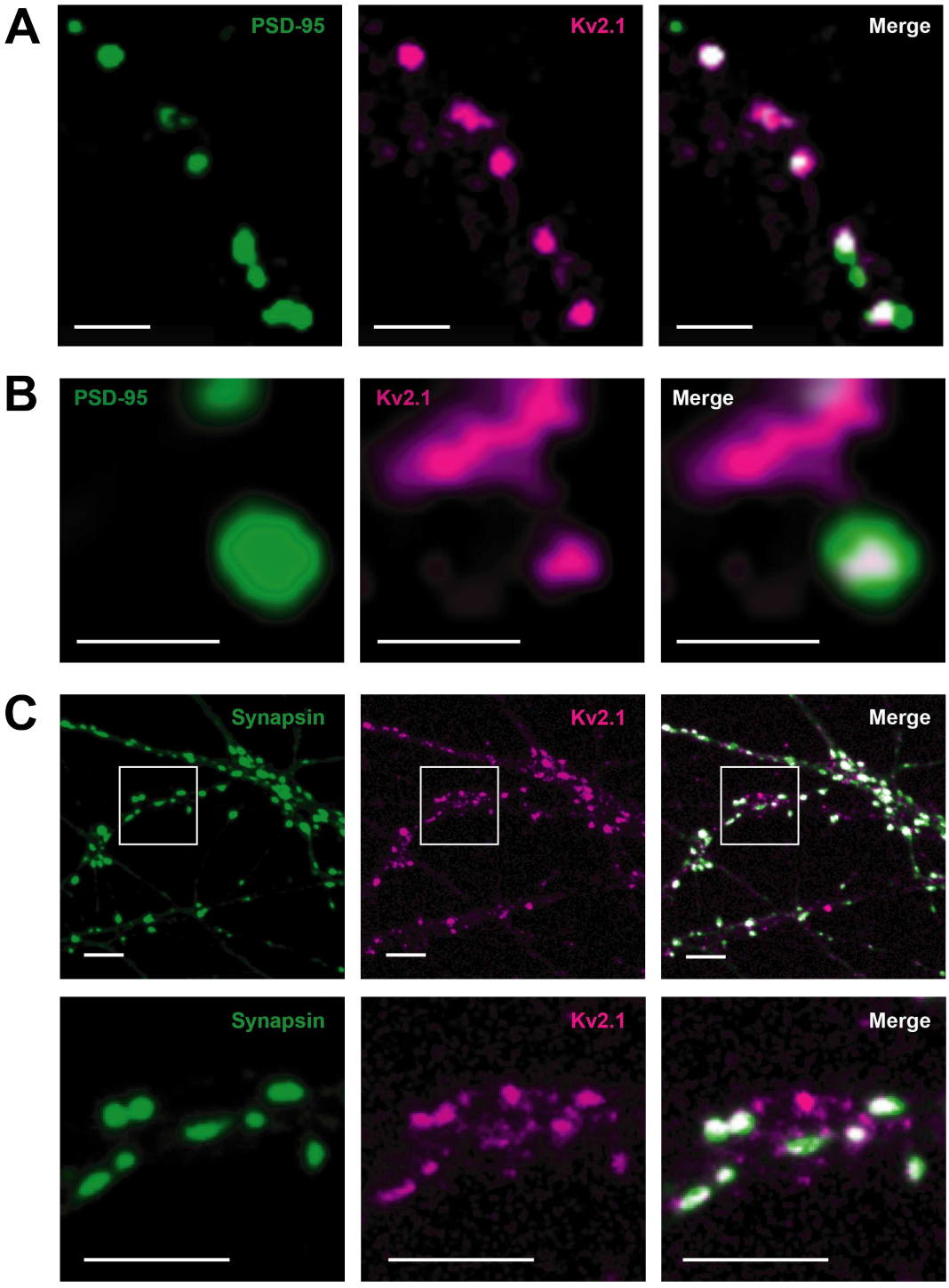

Figure 3.7: Kv2.1 colocalizes with PSD-95 in dendritic spine heads and synapsin in axonal varicosities in DIV21 neurons. A) Kv2.1 (magenta) colocalizes with transfected PSD-95 (green) in dendritic spine heads. Scale bars are 2 μm. **B)** Representative image of a single dendritic spine showing Kv2.1 puncta colocalized with PSD-95. Scale bars are 1 μm. **C)** Representative image of neurites immunolabeled for synapsin (green) and Kv2.1 (magenta). Synapsin highly colocalizes with Kv2.1. The bottom three images are zooms of the boxed area. Scale bars are 5 μm.

not employ super-resolution techniques, we cannot know whether Kv2.1 actually localizes to pre-synaptic compartments, post-synaptic compartments, or both, as all would appear similar in diffraction-limited images. However, together these data strongly suggest a role of Kv2.1 at synapses, and future studies will determine whether that role is structural (i.e. ER/PM junctions, glial adhesion) or functional.

3.4.6 AMIGO1 colocalizes with mature post-synaptic compartments in culture

AMIGO1 promotes neurite outgrowth and axonal fasciculation in neurons, presumably via homophilic cell adhesion activity [227,231,234]. To have this effect, AMIGO1 must be localized in neurites during development. Interestingly, each member of the AMIGO family was detected in both glial cells and neurons [231, 328], indicating that AMIGO family adhesions might mediate glia-neuron contact sites. Given that Kv2.1 clusters at the soma also contain AMIGO1 and our observations that Kv2.1 exists at synaptic structures, we next wanted to know whether AMIGO1 also colocalized with synaptic elements, where it could mediate tripartite synapse adhesion. Similar to the experiments conducted with Kv2.1, we fixed and immunostained DIV21 cultures for AMIGO1 and synapsin. Synapsin (green) and AMIGO1 (magenta) frequently colocalized in DIV21 hippocampal cultures (Figure 3.8A). Quantifying the nearest neighbor distances between synapsin and AMIGO1 fluorescence revealed that approximately 2/3 of synapsin puncta had AMIGO1 fluorescence within 100 nm of the synapsin centroid (Figure 3.8B). This suggests, at least in culture, that AMIGO1 is often associated with pre-synaptic axonal varicosities. Interestingly, AMIGO1 associated synapsin puncta were significantly more voluminous ($3\times$) than those more distant to AMIGO1 (Figure 3.8C). However, because this data was acquired using immunolocalization and without super-resolution, we cannot be sure that AMIGO1 and synapsin are localized to the same compartment of the tripartite synapse.

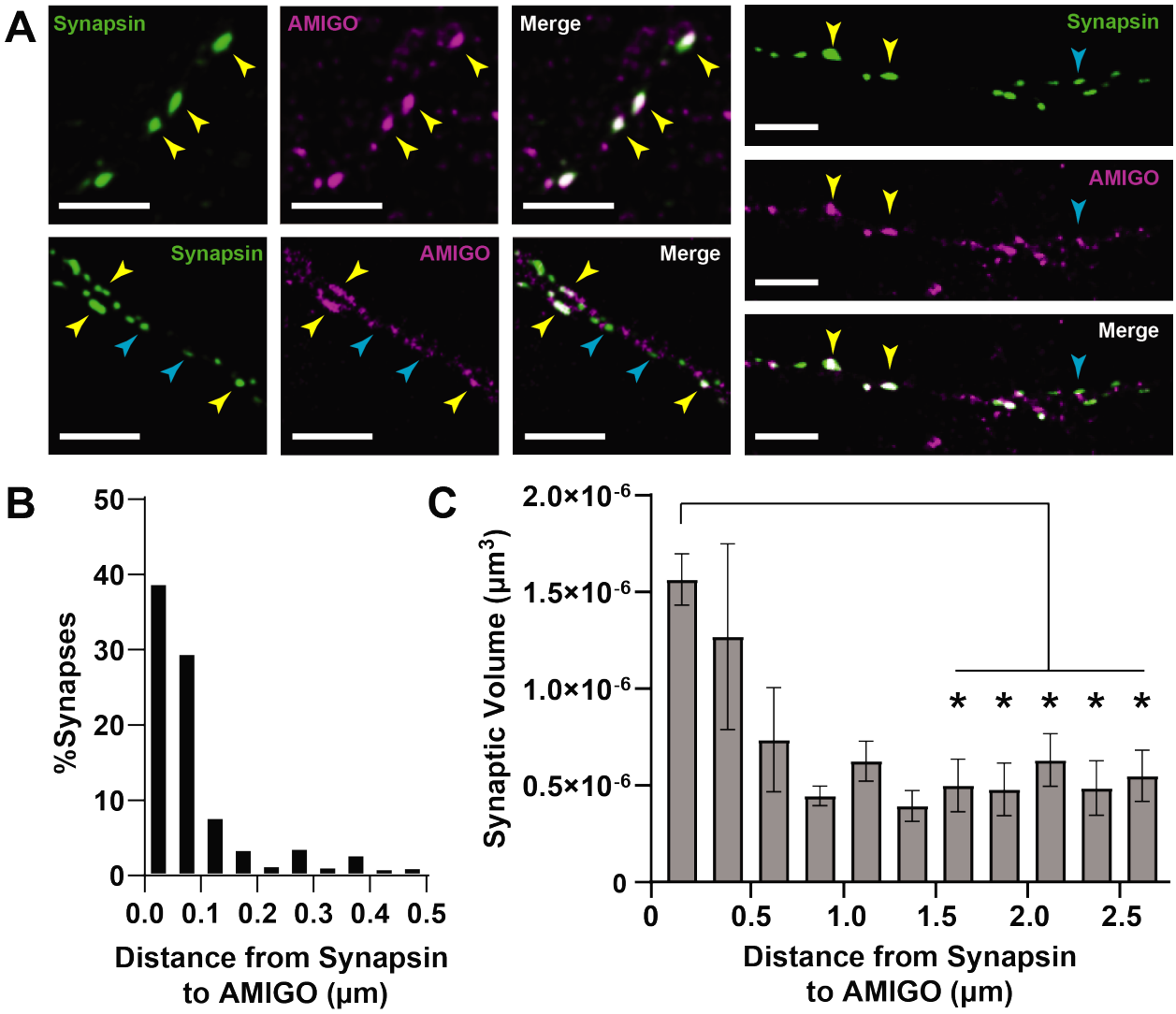

Figure 3.8: AMIGO1 colocalizes with high volume synapsin puncta in DIV21 hippocampal cultures. A) Three representative images of the colocalization of synapsin (green) with AMIGO1 (magenta). Large synapsin puncta co-localizing with AMIGO1 are indicated by the yellow arrows, while small synapsin puncta that do not colocalize with AMIGO1 are indicated by the cyan arrows. Scale bars are 5 μm. Each image represents a single z-plane. **B)** Approximately 2/3 of synapsin puncta were localized within 100 nm of AMIGO1. Histogram showing the percent of synapses at a certain distance from AMIGO1. Nearest neighbor distances were measured from synapsin puncta centers to the nearest edge of AMIGO1. **C)** Synapsin puncta closer to AMIGO1 are larger in volume. Synapsin volumes were binned and averaged according to their distance from AMIGO1, with bin widths of 0.25 μm. Synapsin puncta that were greater than 1.5 μm away from AMIGO1 had significantly lower volumes than synapsin nearest AMIGO1 ($p<0.05$). N = 6005 synapsin puncta.

While Kv2.1 is not expressed in neuronal culture until about DIV10-12, we have observed AMIGO1 expression as early as DIV4 (data not shown). The involvement of AMIGO1 in neurite outgrowth [227, 231] and our observations of early expression suggested that AMIGO1 may be an early resident of nascent synapses. To this end, we performed the above immunolocalization experiments at two early time points, DIV8 and DIV12, where Kv2.1 is just beginning to express and synapses are just beginning to form. At both of these time points, AMIGO1 did not appear to colocalize at all with synapsin puncta (Figure 3.9). These data suggest AMIGO1 is not localized to synapses during development but appears later on in synaptic maturity.

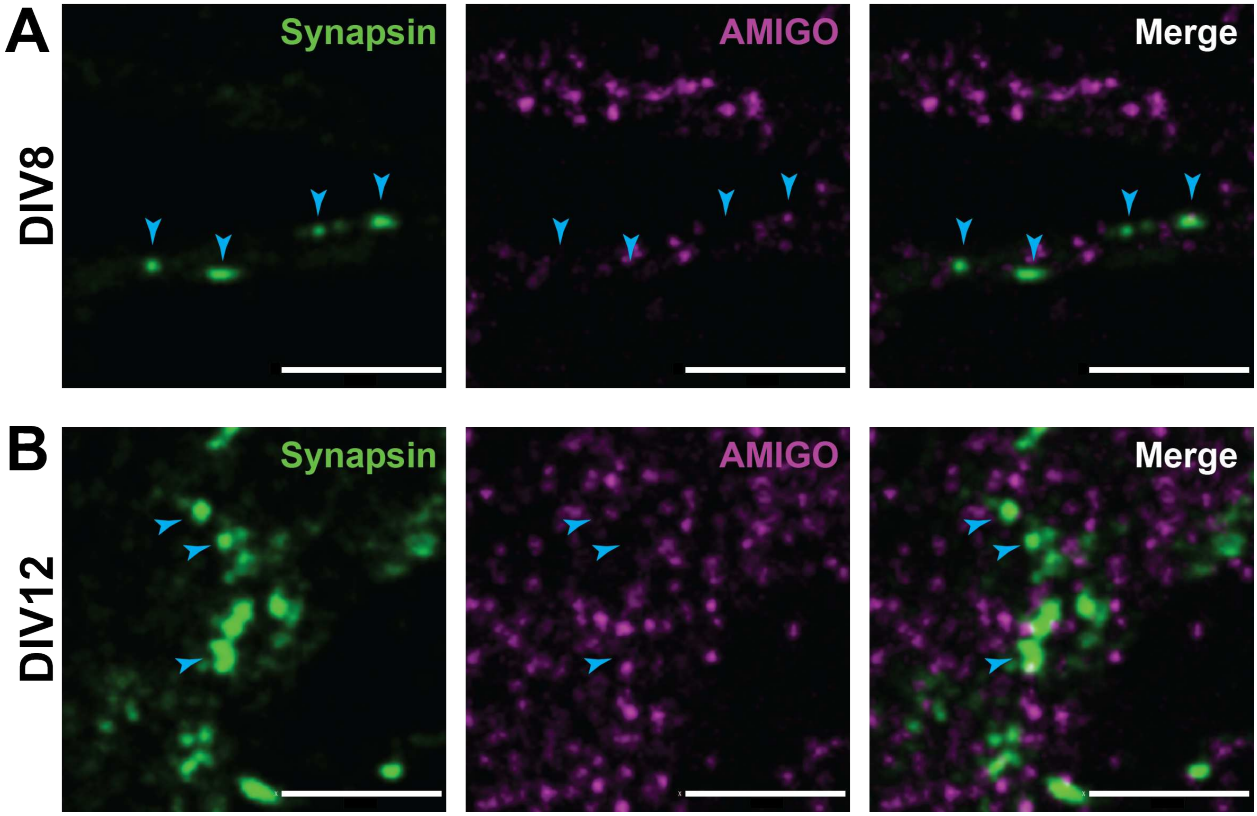

Figure 3.9: AMIGO1 is not localized to nascent synapses in DIV8 or DIV12. Representative images of synapsin (green) and AMIGO1 (magenta) immunolocalization in DIV8 (**A)** and DIV12 (**B)** hippocampal cultures. Cyan carets point to synapsin puncta, none of which colocalize well with AMIGO1. Scale bars are 5 μm. Each image represents a single z-plane.

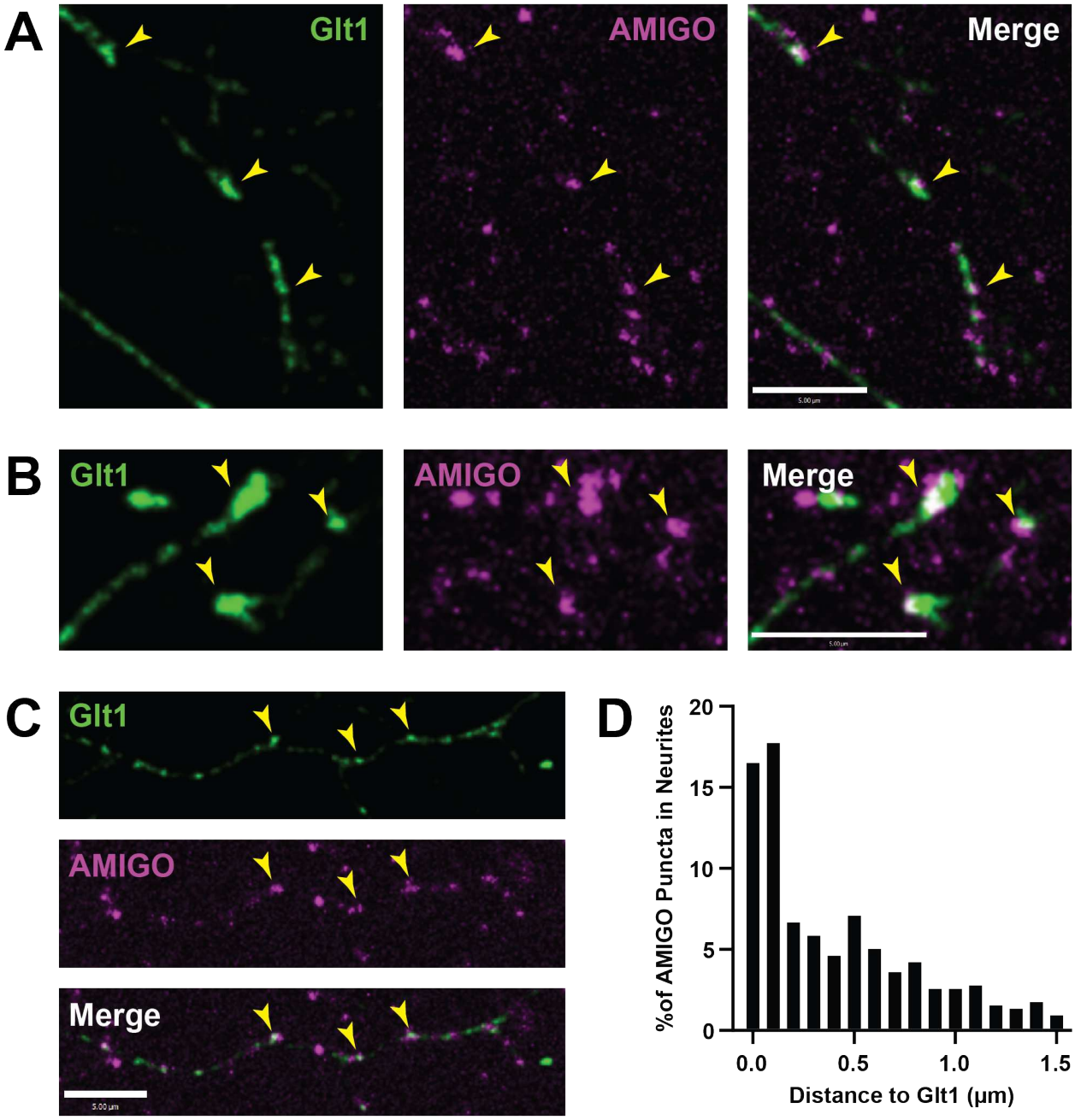

Figure 3.10: Glt1 is localized near AMIGO1 in DIV21 neurites. A-C) Representative images of Glt1 (green) and AMIGO1 (magenta) immunolocalization in DIV21 hippocampal mixed cultures. Yellow carets point to points of colocalization between AMIGO1 and Glt1. Scale bars are 5 μm. **D)** Histogram depicting the distance of the nearest Glt1 neighbor to AMIGO1 puncta in neurites.

3.4.7 Astrocyte Glt1 localizes near AMIGO in neurites

Approximately 2/3 of synapses in the hippocampus are associated with a perisynaptic astrocyte process [155, 156], and on average, these synapses are larger [155, 159]. Considering the observations that Kv2.1 and AMIGO1 colocalized with synapsin, AMIGO1-associated synapses were larger and that most, if not all, Kv2.1 clusters were associated with astrocyte processes [183], we next wanted to know whether Glt1 localizes near AMIGO1 in neurites. Therefore, we fixed and immunostained DIV21 mixed cultures of neurons and astrocytes for Glt1 and AMIGO1. Across the dish, we found AMIGO1 (magenta) puncta in neurites which often colocalized or localized near puncta of Glt1 (green) (Figure 3.10A-C, yellow carets). Indeed, when the shortest distance was measured from each AMIGO1 spot to the nearest Glt1 spot, we found approximately 1/3 of AMIGO1 in neurites had Glt1 within 100 nm (Figure 3.10D). In addition, more than half of AMIGO puncta showed Glt1 within 0.5 μm. Although most of the larger AMIGO puncta appeared to localize to neurites, we cannot discount that at least some of this AMIGO1 is localized to astrocytes, as western blots revealed expression in hippocampal astrocyte monocultures (data not shown). These data suggest at least some of AMIGO1 is localized to glutamatergic synapses, where glutamate transporters would be required. Altogether, these synaptic data are quite preliminary but provide additional evidence to support a role for Kv2.1 and AMIGO1 at synaptic structures, which may mediate astrocyte adhesion.

3.5 Discussion

Neuron-astrocyte adhesions occur at both tripartite synapses [329] and clusters of Kv2.1 channels [183]. The mechanism of Glt1 localization near these neuronal structures is unknown. However, considering the localization of Glt1 and the heavy involvement of actin in cell-cell contact [330,331], the Glt1a-actin interaction is likely crucial for this pat-

tern of localization near neuronal Kv2.1 clusters. Indeed, using astrocyte-neuron mixed cultures, we showed that astrocytic actin and endogenously expressed Glt1 colocalized in nets around neuronal Kv2.1 clusters (Figure 3.1, Figure 3.2, and Figure 3.5), which are themselves regulated by high extracellular glutamate. In addition, we found Kv2.1 and its β-subunit, AMIGO1, localize to both pre-synaptic and post-synaptic structures (Figure 3.7 & Figure 3.8). This observation could have important implications for synaptic structure and function, which without a doubt, will be the subject of future investigations. We also found that Glt1 and AMIGO1 frequently colocalize in neurites, perhaps suggesting Kv2.1/AMIGO1 clusters also mediate neuron-astrocyte contacts at synapses.

3.5.1 Kv2.1 clusters as points of neuron-astrocyte adhesion

Kv2.1 channels form micron-sized clusters on the membrane of central neurons, which represent sites of endoplasmic reticulum/plasma membrane junctions [183, 210, 218, 295]. These Kv2.1 clusters are localized adjacent to both astrocyte and microglia processes in the murine brain [183, 186], adhesion sites which might be regulated by the Kv2.1 auxiliary subunit, AMIGO1, a cell adhesion molecule [226, 227]. In the present study, we found that both astrocytic Glt1 and actin filaments were localized in nets around Kv2.1/AMIGO clusters in neurons (Figure 3.1, Figure 3.2, and Figure 3.5). Given the decreased diffusion of the extracellularly labeled Glt1a at Kv2.1/astrocyte contacts (see Figure 3.6A-D), it is likely this space is crowded with adhesion molecules. Although the adhesion molecules involved in Kv2.1-astrocyte contact are currently unknown, it seems that, like junctions in endothelial cells, this adhesion site is capable of regulating actin filaments. A working model of this adhesion site is depicted in Figure 3.11; however, the mechanism by which somatic Kv2.1 clusters regulate astrocytic actin is an open question.

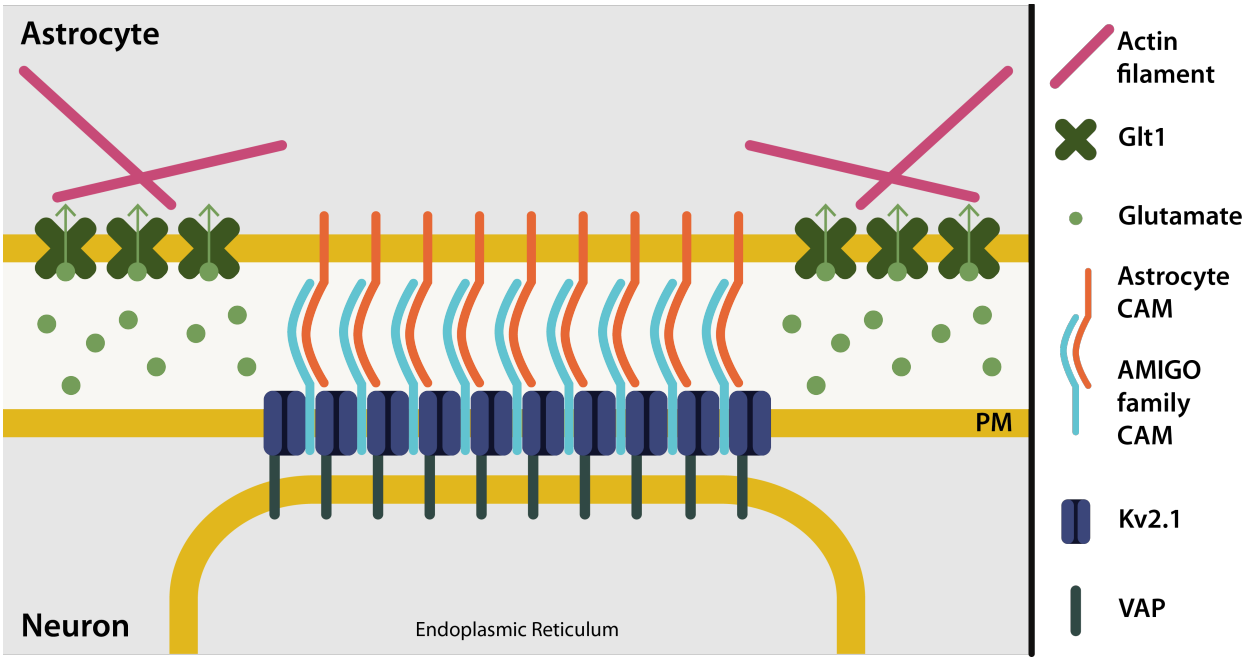

Figure 3.11: Model of neuron-astrocyte contact site at Kv2.1 clusters. Clusters of Kv2.1 channels (dark blue) in the neuronal plasma membrane (yellow) are sites where neurons and glia come together. Kv2.1 channels have an auxiliary subunit, AMIGO (light blue), which is a cell adhesion molecule (CAM). Presumably, an astrocyte cell adhesion molecule (orange) interacts with AMIGO to bring neurons and astrocytes together at this junction. Astrocyte Glt1 transporters (green) are localized in nets around neuronal Kv2.1 clusters, perhaps due to the interaction of Glt1a with actin (magenta). Kv2.1 clusters also form ER/PM junctions by interacting with the ER protein, VAP (grey).

3.5.2 The neuron/astrocyte junction and the response to ischemic insult

The localization of Glt1 in nets around neuronal Kv2.1 clusters ([184] and Figure 3.1) likely has a homeostatic role that can be overwhelmed under pathophysiological conditions. Ischemia, excitotoxicity, or pharmacological inhibition of Glt1 function cause a rapid dispersal of clustered Kv2.1 channels, leading to cortical ER retraction within the neuron [184, 185, 210] and increases in glial contact with the neuronal soma [186, 263]. Following ischemic insult, reduced astrocytic glutamate uptake activates extrasynaptic NMDA receptors, where the resulting Ca^{2+} influx induces calcineurin-dependent dephosphorylation within the Kv2.1 C-terminus [257]. Channel dephosphorylation breaks contact with the ER and results in declustering of Kv2.1. Perhaps actin-based concentra-

tion of astrocytic Glt1a nanoclusters adjacent to the neuronal Kv2.1 microclusters exists to ensure Kv2.1-mediated ER/PM junctions remain under normal levels of extracellular glutamate. Only when these transporters are dysfunctional following ischemic insult are the Kv2.1-induced ER/PM junctions lost. Whether astrocytic Glt1a localization is altered following declustering of the Kv2.1/AMIGO adhesion molecule complex is an area for future study. Altogether, these studies suggest the Kv2.1-astrocyte contact is an important sensor for neuronal insult.

3.5.3 Kv2.1 and AMIGO1 at synapses

While most studies of Kv2.1 have focused on the large (0.5-1 μm^2) clusters located on the somatic surface, a few studies have described Kv2.1 localization to synaptic elements. In a study of somatic Kv2.1 clusters on α-motoneurons, Muennich et al. found strong colocalization of somatic clusters with immunolabeled synaptophysin (axon terminals), vesicular acetylcholine transporter (vAChT, pre-synaptic), and m2 muscarinic acetylcholine receptors (post-synaptic) [188, 208]. Additionally, observations of Kv2.1 in the intact hippocampus revealed non-somatic localization of Kv2.1 immunograins to both symmetric and asymmetric synapses [183]. Kv2.1 immunogold labeling was observed flanking the post-synaptic density (PSD) in approximately half of all symmetric (inhibitory) synapses. Kv2.1 immunoreactivity was also seen surrounding the PSD of asymmetric (excitatory) synapses at a higher density, although, at a smaller percentage of total excitatory synapses. To our knowledge, the results presented in Figure 3.7 represent the first observations of Kv2.1 localization to synapses *in vitro* and by fluorescence in central neurons.

The ramifications of Kv2.1 synaptic localization could be structural or functional in nature. Recently, the inactivation of pre-synaptic Kv1 channels by Kvβ1 auxiliary subunits was found to be essential for synaptic facilitation induced by high-frequency

stimulation [332]. Perhaps synaptic Kv2.1 could also play a functional role, particularly given the effects of some AMIGO subunits on inactivation (see Chapter 4). Structurally, more than 90% of ER/PM junctions were associated with Kv2.1 [183]. One recent study, which performed electron microscopic 3D reconstruction of organelles in neurons, found 54% of dendritic spines had ER/PM junctions [221]. ER/PM junctions are critically involved in lipid homeostasis and Ca^{2+} signaling [333]. Given that Kv2.1 is present at more than 90% of ER/PM junctions and the fact that ER/PM junctions are present in more than half of dendritic spines, Kv2.1 localization to dendritic spines may have important implications for signaling processes that involve lipid metabolism and ER Ca^{2+} release, as is the case for several types of synaptic plasticity [334–336].

It has been previously suggested that AMIGOs might be involved in adhesion at synapses [329]. Several studies have implicated AMIGO adhesion in both axon and dendrite outgrowth [227,231,232,234], indicating AMIGO adhesion is important for neuronal development. However, the studies presented in Figure 3.9 suggest AMIGO1 is not present at synapses *in vitro* until a later time point. AMIGO1 is expressed in both astrocytes and neurons of the central nervous system [231], and patterning the AMIGO1 extracellular domain on culture dishes increases neurite outgrowth [227], suggesting that transcellular adhesion is critical for neurite development. To our knowledge, this is the first published observation of AMIGO1 synaptic localization (Figure 3.8). Given the likely involvement of AMIGO in neuron-glia adhesion, the role of AMIGO1 in mediating tripartite synapse adhesion should be investigated. In Figure 3.10, we noted that approximately 1/3 of AMIGO puncta in presumed neurites was associated with astrocytic Glt1. How does disrupting AMIGO adhesion affect Glt1 localization near synapses? Is the actin-Glt1 interaction important for localization to tripartite synapses? These and other questions await future investigation.

3.5.4 Conclusions

Overall, these data indicate that the Glt1-actin interaction is important in determining the localization of Glt1 near somatic Kv2.1 clusters involved in glutamate sensing. Disruption of Glt1 localization to somatic Kv2.1 clusters could exacerbate neuronal hyperexcitability, and diminish positive outcomes for severe insults. Understanding the mechanisms regulating transporter localization, particularly to actin filaments, will be essential to identify new targets for mitigation of neuronal insults which lead to high ambient glutamate, such as ischemic stroke, traumatic brain injury, and epilepsy. Furthermore, we provide additional evidence to suggest a role of Kv2.1 and AMIGO1 at synapses, which may mediate astrocyte adhesion at tripartite synapses, although this awaits further investigation.

In the next chapter, we further characterize the ability of the AMIGO family to act as β-subunits for Kv2 channels.

Chapter 4

Kv2 channel/AMIGO β-subunit interaction modulates both channel function and cell adhesion molecule surface trafficking

4.1 Summary

The Kv2 channels encode delayed rectifier currents in excitable cells that maintain membrane polarization under conditions of high excitability. They also form stable junctions between the endoplasmic reticulum and plasma membranes in many different cell types, creating membrane contact sites that mediate functions distinct from membrane excitability. Therefore, proteins that interact with Kv2 channels can alter conducting and/or non-conducting channel properties. One member of the AMIGO family of proteins is an auxiliary β-subunit for Kv2 channels and modulates Kv2.1 electrical activity. However, the AMIGO family has two additional members of $\sim$50% similarity that have not yet been fully characterized as Kv2 β-subunits. Previous data out of our lab showed that each of the three AMIGOs functionally modifies the voltage-dependence of activation, and AMIGO2 in particular decreases inactivation. In this work, we show that all three AMIGOs are redistributed to surface clusters of Kv2 channels upon coexpression in both HEK-293 cells and primary cultures of hippocampal neurons. Additionally, the surface trafficking of all three AMIGOs was improved by coassembly with Kv2 subunits, while the surface trafficking of Kv2 channels was unaffected. These data further support the idea that all three AMIGOs are β-subunits for Kv2 channels, and that coassembly of these two proteins increases the surface expression and concentration of cell adhesion molecules on the surface of cells in which they are expressed. Together with previously published data, this work suggests that each of the three AMIGOs act as function-modifying β-subunits of Kv2 channels.

4.1.1 Hypotheses to be tested —

1. Each of the three members of the AMIGO family will colocalize with Kv2.1 and Kv2.2 in clusters on the surface of transfected HEK cells and primary hippocampal neurons.

2. Co-expression of members of the AMIGO family with Kv2.1 or Kv2.2 will AMIGO trafficking to the cell surface.

4.2 Introduction

β-subunits of the voltage-gated potassium channel (Kv) superfamily are important regulators of nervous system function. Indeed, this diverse class of proteins can modulate almost every aspect of Kv channel physiology including subunit assembly, trafficking, protein stability, conduction, localization, and pharmacology [337–339]. For example, the classical Kv auxiliary subunits, Kvβ1, 2, and 3, are soluble proteins that interact with the cytoplasmic domains of Kv1 channels. They confer dramatic effects on channel gating, in some cases inducing fast inactivation in otherwise non-inactivating channels [340, 341]. Recently, AMIGO1 (amphotericin-induced gene and ORF 1) was identified as a β-subunit of Kv2.1 and Kv2.2 channels [226, 228]. This work showed that AMIGO1 assembles with both Kv2 isoforms in neurons and when co-expressed in HEK-293 cells and induces a hyperpolarizing shift in the voltage-dependence of Kv2.1. Furthermore, while trafficking and localization of Kv2.1 and Kv2.2 were unchanged by assembly with AMIGO1, both Kv2s increased the surface expression of AMIGO1 and redistributed it to large clusters which are characteristic of Kv2 channel localization.

The clustered pattern of Kv2s is due to a phosphorylation-regulated interaction with endoplasmic reticulum (ER) protein, VAP [218, 295]. Interaction between Kv2s and VAP brings the ER into close apposition with the PM, forming an increasingly appre-

ciated organelle, called the ER/PM junction [210, 218, 342]. In an electron microscopy (EM) study of rat brains, 90% of sub-surface cisterns of ER membrane were positive for Kv2.1 channels [183]. Another EM study that heterologously expressed Kv2.1 in HEK-293 cells found these Kv2.1 clusters were localized to the plasma membrane surface [210], which has also been observed via fluorescent labeling of surface channels in live cells [218, 220]. ER/PM junctions represent ∼12% of the total neuronal surface [221] and regulate many cellular processes, including endo- and exocytosis [196, 210, 215, 343], Ca^{2+} signaling and store refilling [195, 210, 320], and neuron-glia and neuron-neuron interactions [183, 186, 221]. The consequences of AMIGO localization to Kv2-induced ER/PM junctions for each of these functions are not well understood.

In addition to regulating cell function via ER/PM junction formation, Kv2 channels are important regulators of neuronal excitability. They underlie most of the delayed rectifier current in central neurons [202] and control neuronal excitability under conditions of high-frequency firing [204, 257, 262]. In the mouse hippocampus, Kv2 channel expression is higher in CA1 than CA2 and confers differences in the firing patterns of pyramidal neurons between these two areas [344]. Indeed, the entire complement of ion channel and auxiliary subunit expression in an individual neuron will determine its unique firing patterns.

While the assembly of Kv2 channels and AMIGO1 is well-documented [226, 228], little is known about the assembly of Kv2s with other members of the AMIGO family. The AMIGO family consists of 3 members (AMIGO1, AMIGO2, and AMIGO3), all of which are type-I single-pass transmembrane proteins [227]. All three AMIGOs have an extracellular domain, which contains six leucine-rich repeats and an immunoglobulin-like domain, that allows them to act as homophilic and heterophilic cell adhesion molecules [227, 229]. AMIGO1 is almost exclusively expressed in the brain, while AMIGO2 and AMIGO3 are more widespread, but also enriched in the brain [227]. Likewise,

AMIGOs 2 and 3 show widespread expression in tissues where AMIGO1 is low or absent [227]. Interestingly, Kv2 channels have perhaps the widest tissue distribution of any Kv channel, being expressed in cells as diverse as cortical, hippocampal, and spinal motor neurons [183,188,190,211,228], vascular smooth muscle cells [194,195], retinal ganglion cells [192], and pancreatic beta cells [196–200]. Therefore, the consequences of AMIGO family interactions with Kv2 channels have implications for cell function far beyond the nervous system.

Functionally, AMIGOs have been implicated in early axon guidance, growth, survival, and adult axon growth inhibition [227,231–233]. Interestingly, AMIGO2 has also been implicated in enhanced growth and survival in a variety of cells [235–238]. This increase in cell viability may be due to an interaction between AMIGO2 and PDK1, a kinase that activates Akt in cell survival pathways [239]. While the residues involved in Kv2.1-AMIGO1 interaction are unknown, electrophysiology studies with chimeras between AMIGO1 and NCAM (neuronal cell adhesion molecule) suggest that the AMIGO1 transmembrane domain is required for interaction with Kv2.1 [226]. The transmembrane domain of the AMIGO family is $\sim$48% conserved, supporting the possibility that the other AMIGO family members could also act as β-subunits for the Kv2 family.

In further support of this notion, other recent studies out of our lab show that both AMIGO2 and AMIGO3 can functionally modify the voltage-dependence of activation of Kv2 channels, and AMIGO2 in particular slows Kv2 inactivation [345]. Although the majority of Kv2 channels expressed in heterologous cells are non-conducting and do not contribute to whole-cell ionic currents, there is a large population of conducting channels that reside mostly outside of clusters [288]. Therefore, these electrophysiological results only describe the effect of the AMIGOs on conducting channels, but not the non-conducting channels that form the characteristic micron-sized clusters on the surface

of cells. Thus, the major aim of this chapter was to determine whether AMIGO2 and AMIGO3 co-localize and interact with Kv2 channels in surface clusters.

Given the lack of detailed information regarding the structural basis of the Kv2-AMIGO1 interaction, it is difficult to predict whether AMIGO2 and AMIGO3 will interact with Kv2 channels. Although study of the AMIGO family is still in infancy, several studies support the activity of AMIGO adhesion in regulating neurite outgrowth, axonal regeneration, and cell survival. Existence of AMIGOs in surface clusters of Kv2 channels could create specialized microdomains for cell-cell adhesion driving outgrowth and communication hubs for cell survival. Therefore, the present study aimed to investigate whether AMIGO2 and AMIGO3 also act as auxiliary β-subunits for Kv2.1 and Kv2.2 and to further characterize the effects of interaction on AMIGO localization. The results of this work suggest that all three AMIGOs assemble with both Kv2 channels. The assembly of Kv2 channels with the AMIGOs appears to have isoform-specific effects on AMIGO trafficking but minimal effects on Kv2 trafficking and localization. Together with previous results showing all three AMIGOs modulate Kv2 channel conductance, this work indicates that the three AMIGOs interact with both Kv2.1 and Kv2.2 in and out of Kv2 clusters to alter both channel-conducting functions and the composition of Kv2 surface clusters.

4.3 Materials and Methods

4.3.1 DNA constructs

The original AMIGO1, AMIGO2, and AMIGO3 constructs were obtained from the DNASU plasmid repository (plasmid IDs HsCD0029615, HsCD00513136, and HsCD00512989, respectively). Fluorescent protein fusion constructs were generated by PCR-based addition of restriction sites to the ends of each AMIGO family insert (Appendix B). Fluores-

cent protein vectors were cut with the same enzymes and each insert was ligated into the recipient vector, such that the fluorescent protein (GFP-N1 or Ruby2-N1) was fused to the C-terminus of AMIGO. Full length, codon-optimized Kv2.2 (accession number NM-054000) was synthesized by GeneWiz and inserted into a pEGFP-C1 expression vector (Clontech) via EcoRI and SalI restriction sites. GFP-Kv2.1 and Kv2.1-loopBAD (Kv2.1-LB) have been described previously [346, 347]. hBirA was a gift from Alice Ting [348]. For additional details, see Appendix B.

4.3.2 Cell culture and Transfection

HEK-293 cells (ATCC CRL-1573, Manassas, VA) were maintained in 10 cm dishes (CellTreat 229620, Pepperell, MA) at 37 C under 5% CO2 in DMEM (Corning 10-013-CV, Corning, NY) supplemented with 10% FBS. For transfections, cells were trypsinized and electroporated (BioRad GenePulse Xcell, Berkeley, CA) with either Kv2 α-subunits (500 ng per dish), AMIGO subunits (300 ng per dish), or a combination of both. In some experiments, a GFP-tagged pleckstrin-homology (PH) domain construct was used as a marker to facilitate measurements of fluorescence associated with the PM.

For details about neuronal cultures, see Section 2.3.2.

At DIV5, neurons were transfected using DNA, Lipofectamine 2000 (Invitrogen, Life Technologies, Grand Island, NY), and OptiMEM for experiments in 48 hours. Neurons were transfected with either GFP-Kv2 α-subunits (500 ng per dish) and one of the three Ruby2-AMIGO subunits (300 ng per dish). After 48 hours, neurons were transferred to an imaging saline composed of 126 mM NaCl, 4.7 mM KCl, 2.5 $CaCl_2$, 0.6 mM $MgSO_4$, 0.15 mM NaH_2PO_4, 0.1 mM ascorbic acid, 8 mM glucose, and 20 mM Hepes, pH 7.4, 300 mOsm.

4.3.3 Microscopy

Spinning disk confocal microscopy was used for all imaging experiments where electrophysiology was not conducted. HEK-293 cells were electroporated as described above and plated at a low density on glass-bottom dishes (MatTek P35G-1.5-14-C, Boston, MA) coated with Matrigel (BD Biosciences 354230, Franklin Lakes, NJ) in a maintenance medium for 18-24 hours. Cells were briefly removed from incubation for medium exchange to HEK-293 Imaging Saline (HIS), which contains the following: 146 mM NaCl, 4.7 mM KCl, 2.5 mM $CaCl_2$, 0.6 mM $MgSO_4$, 1.6 mM NaHCO3, 0.15 mM NaH_2PO_4, 0.1 mM ascorbic acid, 8 mM glucose, and 20 mM 4-(2-hydroxyethyl)-1-piperazineethanesulfonic acid (Hepes), pH 7.4. After the medium exchange, cells were immediately placed on the heated microscope stage and allowed to equilibrate for 10 minutes before imaging.

For information about the spinning-disk confocal microscope, see Section 3.3.4.

4.3.4 Co-Immunoprecipitation

HEK-293 cells were transfected with either Kv2.1LB or Kv2.2 alone, or one of the Kv2 α-subunits along with either AMIGO1-GFP, AMIGO2-GFP, or AMIGO3-GFP. After 16-24 hours, cells were washed 1x with cold PBS then scraped in 1 mL Lysis buffer (50 mM Tris Base, 150 mM NaCl, 1 mM EDTA, and 1% Triton X-100, pH 7.2) + Pierce Protease Inhibitor Cocktail (A32955, ThermoFisher; Waltham, MA). After 20 minutes, the lysate was spun at 2000 g for 10 minutes to remove membranes and the supernatant was pre-cleared with Protein G Sepharose Beads (6511, BioVision; Milpitas, CA) for 1 hr. Beads were removed by centrifugation and the pre-cleared lysate split into two aliquots for positive and negative IP. The positive IP samples were incubated with 1 μL of IP antibody (Neuromab mouse anti-Kv2.1 or mouse anti-Kv2.2, clones K89/34 and K37/89, respectively; Davis, CA) for 16 hours at 4°C before adding 50 μL Protein G Sepharose

Beads. An equivalent volume of beads was added to the negative IP samples at the same time and all samples were incubated for 4 hours at 4°C. The beads were pelleted by centrifugation at 1000g for 3 minutes and the supernatant was collected. The beads were washed 3x with 100 μL Lysis Buffer + Protease Inhibitor before resuspending directly in 2X sample buffer (1610737, BioRad; Hercules, CA) + β-Mercaptoethanol and boiling for 10 minutes. Starting material and supernatant fractions were diluted in Lysis buffer and Sample Buffer + β-Mercaptoethanol and boiled for 10 minutes, after which proteins from all samples were separated on SDS-polyacrylamide gels (5671034, Biorad; Hercules, CA) and transferred to nitrocellulose. Membranes were stained briefly with Ponceau S-Stain (P7170-1L, MilliporeSigma; Burlington, MA) before blocking in PBS-Tween + 5% w/v powdered milk, followed by incubation in primary antibodies (1:1000) for 1 hour. The following primary antibodies were used for detection on nitrocellulose membranes: mouse anti-Kv2.1 (K89/34, Neuromab; Davis, CA), mouse anti-Kv2.2 (K37/89, Neuromab; Davis, CA), mouse anti-AMIGO1 (L86A/37, Neuromab; Davis, CA), and rabbit anti-GFP (TP-401, Torrey-Pines; Secaucus, NJ). Blots were washed 3x with PBS-Tween then incubated in appropriate mouse or rabbit secondary antibodies conjugated to horseradish peroxidase at 1:10,000 in PBS-Tween+5% Goat Serum for 45 minutes. After washing, secondary antibodies were visualized with SuperSignal Substrate (34095, ThermoFisher; Waltham, MA) for up to 5 minutes.

4.3.5 Analysis and Statistics

Images were processed and analyzed using ImageJ (v1.52p). All images are single z-planes unless otherwise noted.

Images in Fig 1 which assess subunit assembly were from the basal cell surface. line-scans were drawn such that multiple clusters would be included. Fluorescent values from the line-scans were standardized to the maximum measured fluorescence, in order

to be comparable between image channels. To measure colocalization between Kv2s and AMIGOs, a z-plane at the basal surface of HEK cells or neurons was assessed using the Coloc 2 plugin for Image J. Spearman's ranked correlation coefficients were measured for each cell and were then compiled for one-sample t-tests against a test mean of zero.

Surface trafficking (Figure 2) was measured from single z-planes at the center of each cell. A region of interest (ROI) was hand-drawn around each cell and total fluorescence was measured for each channel. Using cells expressing PH-GFP to mark the membrane, the average width of the membrane was measured to be seven pixels. Seven pixels were then subtracted from the perimeter of the cell ROI to measure total fluorescence which was not on the PM. By subtracting the internal fluorescence from the total fluorescence, the fluorescence on the surface was determined. In the case of AMIGO3, where little fluorescence was on the surface, PH-GFP was co-expressed to determine the location of the plasma membrane. These measurements were performed in ImageJ.

Fluorescence density in arbitrary units per square micron ($AU/\mu m^2$) was calculated by dividing the sum of fluorescence in each ROI by the area of that ROI in square microns. By using a ratio of densities, we eliminate the bias of differences in protein expression between cells. A surface trafficking index was determined by dividing the surface fluorescence density by total fluorescence density. This measure indicates the preference of a protein for surface expression (if greater than one) or intracellular expression (if less than one). The surface trafficking index was compared to a test mean of 1 using a one-sample t-test (t) to determine whether the protein significantly preferred to localize to the surface or intracellularly. To determine if co-expression significantly increased surface trafficking index, one-way ANOVAs with post-hoc Tukey tests were used.

4.4 Results

4.4.1 The three AMIGOs colocalize with Kv2 channels in surface clusters

While previous work demonstrated that AMIGO1 is a β-subunit for Kv2s [226,228], it is unknown whether other members of the AMIGO family can act as β-subunits. To determine whether AMIGO2 and AMIGO3 might also interact with Kv2s, we co-expressed GFP-Kv2.1 or GFP-Kv2.2 and one of the three Ruby2-tagged AMIGOs in HEK-293 cells to assess colocalization between the proteins. When AMIGOs were expressed alone, surface localization was uniform across the plasma membrane surface, as shown by the images and line-scans of the basal cell surface in Figure 4.1A. However, when AMIGOs were co-expressed with Kv2.1, surface localization of all 3 AMIGOs redistributed to micron-sized clusters formed by Kv2.1 (Figure 4.1B). Line-scans below the images show a nearly perfect overlap of fluorescence peaks between each AMIGO (magenta) and Kv2.1 (green), which is vastly different from the uniform distribution seen in Figure 4.1A. Likewise, when AMIGOs were co-expressed with Kv2.2, all 3 AMIGOs redistributed to micron-sized clusters on the surface (Figure 4.1C). When line-scans across clusters were plotted, peaks of AMIGO and Kv2.2 fluorescence also overlapped. When Kv2.1 or Kv2.2 were expressed alone (Figure 4.1B or 1C, bottom right), the surface localization was not qualitatively different from co-expression with AMIGOs. These data indicate that the surface localization of all 3 AMIGOs was altered by the presence of both Kv2s. Co-expression with the Kv2s caused the three AMIGOs to redistribute to clusters that overlapped with Kv2 clusters, suggesting an interaction with Kv2 channels causes the redistribution. To determine whether AMIGOs were colocalized in surface clusters, we measured the Spearman's rank correlation coefficient for each cell. This coefficient scales from negative one to one, which indicates negative correlation and positive correlation, respectively. Indeed, as suggested by the images, all three AMIGOs were significantly positively correlated with both Kv2.1 and Kv2.2 ($p < 0.0001$; Figure 4.1D).

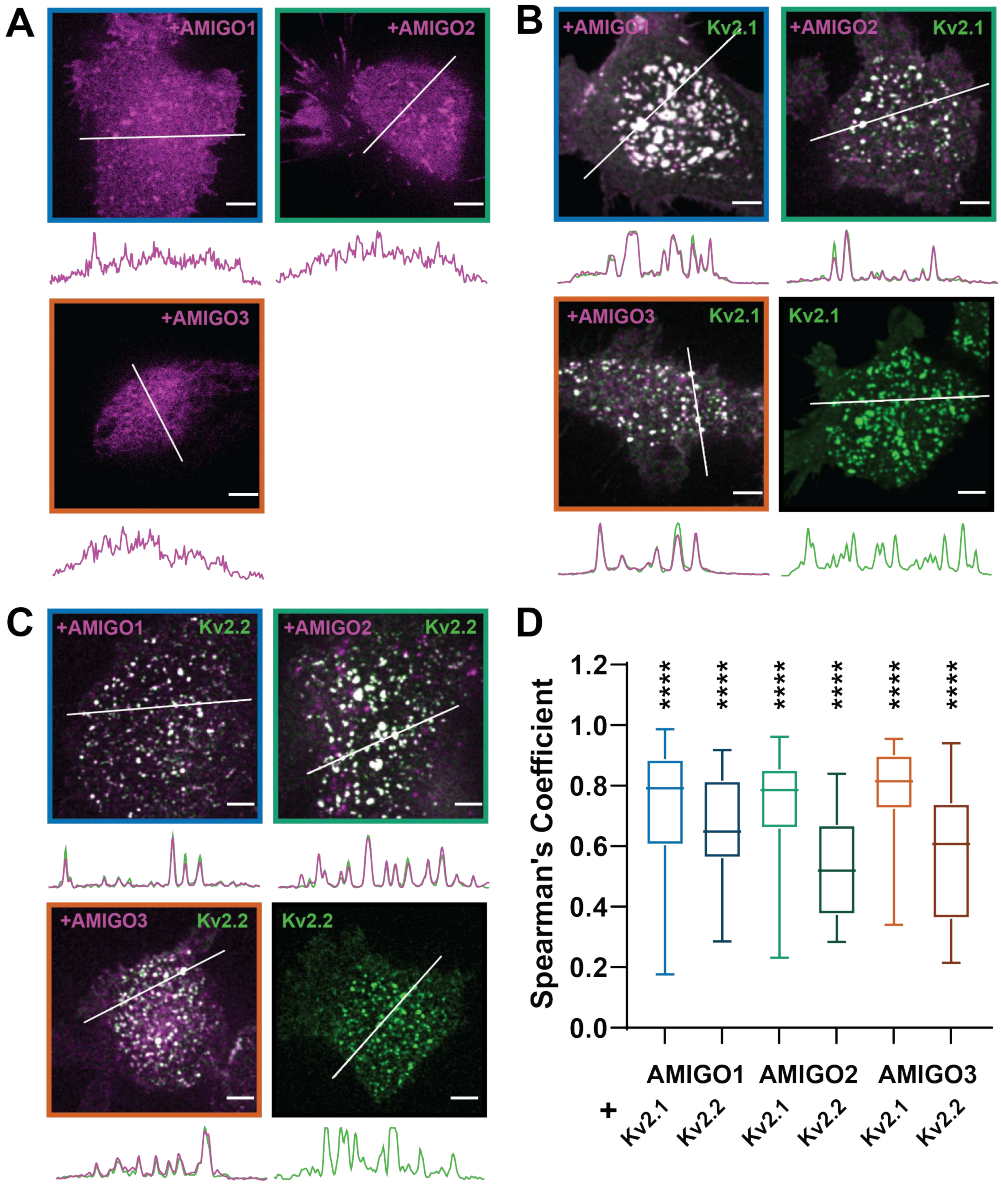

Figure 4.1: AMIGOs colocalize with Kv2.1 and Kv2.2 in clusters. (**A)** Representative images of the basal surface of HEK cells expressing AMIGO1 (left, blue box), AMIGO2 (right, green box), or AMIGO3 (bottom, orange box). line-scans through the center of the basal surface are indicated by the white line on the image and plotted below. Representative images of the basal surface of HEK cells expressing Kv2.1 (**B)** or Kv2.2 (**C)** (green in images and line-scans) and each of the 3 AMIGOs (magenta in images and line-scans) show redistribution of AMIGOs to Kv2 clusters when co-expressed, while the localization of Kv2s remains unchanged (right images). Overlapping fluorescence between the 2 proteins is indicated by white pixels. **D)** Spearman's ranked correlation coefficient was calculated from basal surface clusters of HEK cells. Box plots depict median, interquartile range, and the minimum and maximum values for each dataset. All datasets were significantly higher than 0, indicating that AMIGOs are positively correlated with Kv2s ($p < 0.0001$). Medians are 0.7916, 0.6489, 0.7853, 0.5194, 0.8148, and 0.6070, respectively. Datasets containing 29, 23, 24, 29, 35, and 18 cells respectively. Scale bars are 5 μm.

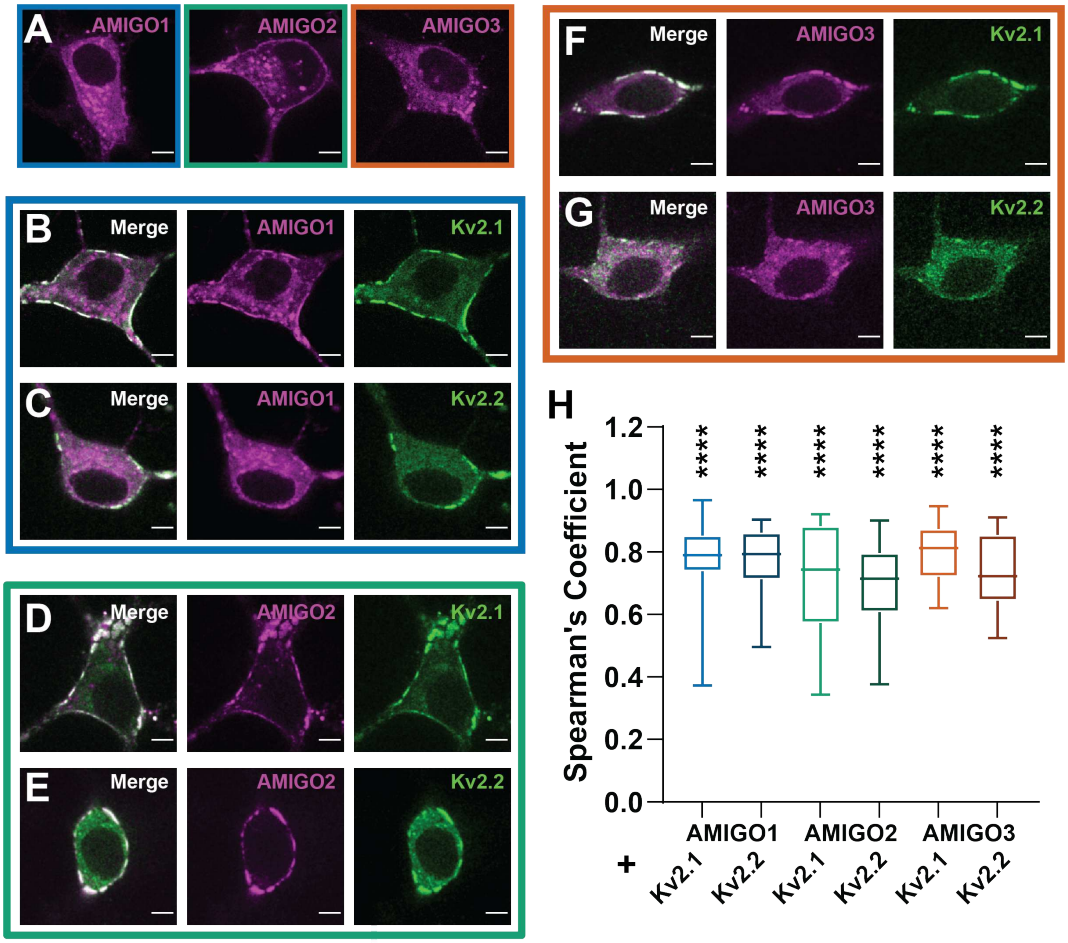

Figure 4.2: AMIGOs colocalize with Kv2 channels on the surface of rat hippocampal neurons. (**A)** Representative images of center z-planes of DIV7 neurons expressing AMIGO1 (left, blue box), AMIGO2 (middle, green box) or AMIGO3 (right, orange box). These data show all 3 AMIGOs have large intracellular expression in the ER and vesicles. AMIGO2 shows the most expression on the plasma membrane, indicated by the ring of fluorescence on the edge of the cell. Representative images of a center z-plane of neurons expressing Kv2.1 (**B)** or Kv2.2 (**C)** (green) and AMIGO1 (magenta) show colocalization of AMIGO1 and Kv2 clusters on the plasma membrane when co-expressed. Notably, AMIGO1 surface trafficking does not appear to improve as much as observed in HEK cells (Figure 2). Co-expression of AMIGO2 and Kv2.1 (**D)** or Kv2.2 (E) also shows colocalization in surface clusters. AMIGO2 surface expression seemed to improve with both Kv2s. Co-expression of AMIGO3 and Kv2.1 (F) or Kv2.2 (G) also shows colocalization in surface clusters. AMIGO3 surface expression seemed to improve with Kv2.1, but not Kv2.2. Overlapping fluorescence between the 2 proteins is indicated by white pixels. H) Spearman's ranked correlation coefficient was calculated from basal surface clusters of neurons. Box plots depict median, interquartile range, and the min and max values for each dataset. All datasets were significantly higher than 0, indicating that AMIGOs are positively correlated with Kv2s ($p < 0.0001$). Medians are 0.7891, 0.7931, 0.7439, 0.7142, 0.8126,and 0.7221, respectively. Medians and t-tests were performed on datasets containing 20, 17, 22, 16, 8, and 8 cells respectively. Scale bars are 5 μm.

Since Kv2 channels are important regulators of neuron excitability, we assessed whether we could observe similar colocalization patterns between Kv2s and AMIGOs in rat hippocampal neurons. As expected, we observed similar colocalization in clusters on the plasma membrane of neurons (Figure 4.2). Altogether, these data indicate that the surface localization of all 3 AMIGOs was altered by the presence of both Kv2s in both HEK cells and rat hippocampal neurons. Co-expression with the Kv2s caused the three AMIGOs to redistribute to clusters that overlapped with Kv2 clusters, suggesting an interaction with Kv2 channels causes the redistribution. Previous studies showed that Kv2 clusters are always associated with the ER [183,210,218,295,349], which is retained even with co-expression of AMIGO1 [228]. Therefore, we believe each of the clusters presented in Figure 4.1 and Figure 4.2 likely represent an ER/PM junction.

4.4.2 Kv2s increase the surface expression of AMIGO isoforms

While Kv2s altered the surface localization of AMIGOs, we also wanted to address the influence of co-expression on the surface trafficking of each AMIGO. When AMIGO1 and AMIGO2 were expressed alone, some surface localization was observed as seen in the optical slices in Figure 4.3 A and B (left images). However, internal vesicles containing each AMIGO were prominent, as indicated by the punctate fluorescence in the middle of these cells and the large peaks in the corresponding line-scans. In contrast, when expressed alone, very little AMIGO3 was expressed on the cell surface. As seen in the left image of Figure 4.3C and its corresponding line-scan, the majority of AMIGO3 fluorescence is internal and little fluorescence overlaps with the membrane marker, PH-GFP. Intracellular AMIGO3 was widespread, with very few bright puncta, likely indicating that the majority of intracellular AMIGO3 was localized within the ER membrane (Figure 4.3C, left image).

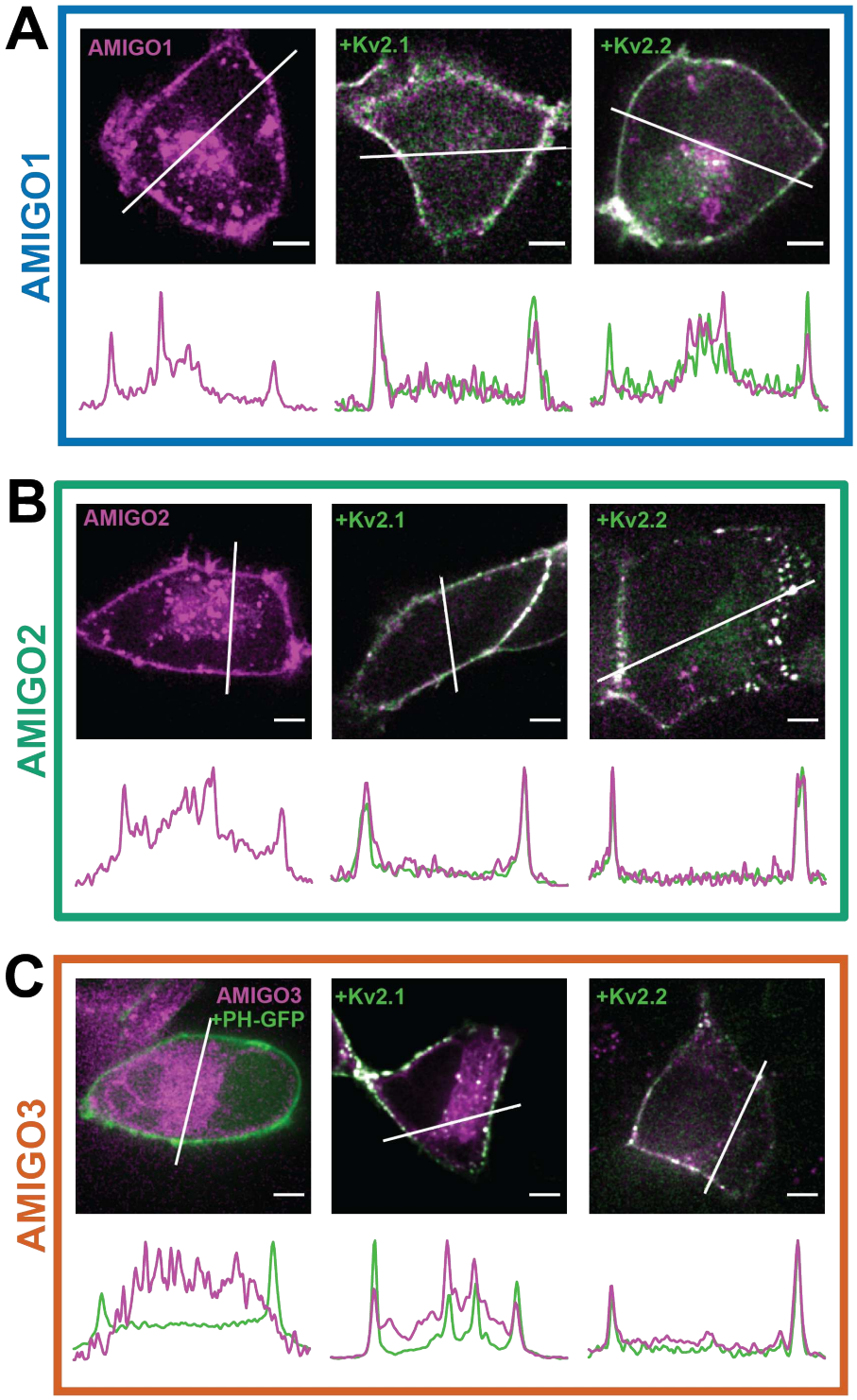

Figure 4.3: Kv2s improve surface trafficking of AMIGOs. Representative images of AMIGO1 (**A**), AMIGO2 (**B**), or AMIGO3 (**C**) alone (left image), with Kv2.1 (middle image), and with Kv2.2 (right image). line-scans through the center of the cells are indicated by the white lines on the images and plotted below. AMIGOs more efficiently traffic to the surface when co-expressed with Kv2s. Images are single z-planes at the middle of the cell. Scale bars are 5 μm.

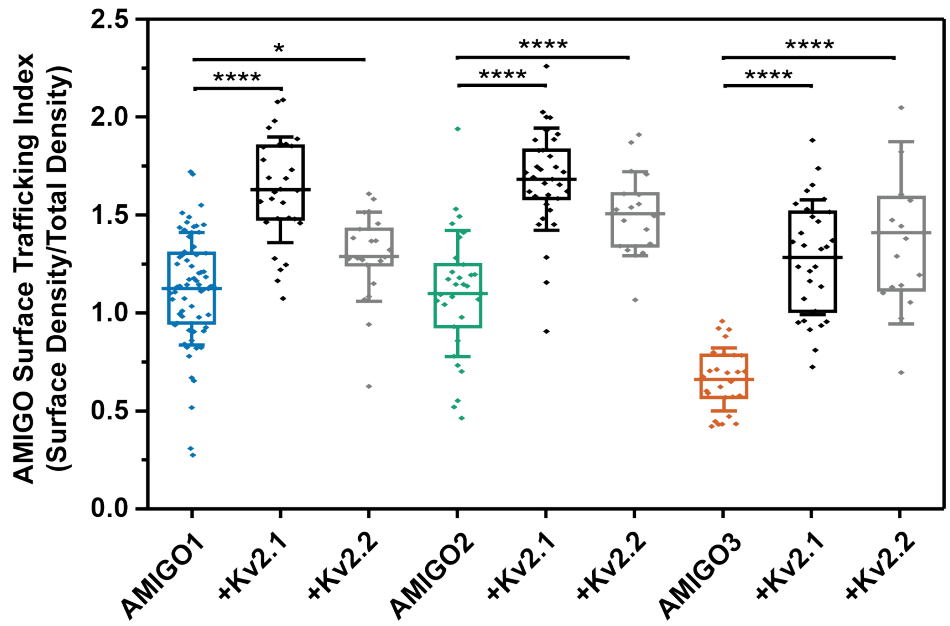

Figure 4.4: Kv2s significantly increase AMIGO surface trafficking. AMIGO surface trafficking was quantified using surface density/total density, where a ratio greater than 1 indicates a preference for surface trafficking, shown with the t-tests below. AMIGO1 surface trafficking was significantly increased with co-expression of Kv2.1 (mean = 1.63 $\pm$ 0.05, N = 29, t = 12.56, $p < 0.0005$) and Kv2.2 (mean = 1.29 $\pm$ 0.05, N = 21, t = 5.82, $p < 0.0005$) compared to AMIGO1 alone (mean = 1.12 $\pm$ 0.04, N = 65 cells, t = 3.54, $p < 0.0005$, One-way ANOVA F = 34.37, $p < 0.0005$, Kv2.1 q = 11.72 $p < 0.0005$, Kv2.2 q = 3.38 $p < 0.05$). AMIGO2 surface trafficking was significantly increased with co-expression of Kv2.1 (mean = 1.69 $\pm$ 0.05, N = 33 cells, t = 15.07, $p < 0.0005$) and Kv2.2 (mean = 1.51 $\pm$ 0.05, N = 18 cells, t = 10.08, $p < 0.0005$) compared to AMIGO2 alone (mean = 1.10 $\pm$ 0.06, N = 30 cells, t = 1.71, $p = 0.096$, One-way ANOVA F = 35.99, $p < 0.0005$, Kv2.1 t = 15.07, $p < 0.0005$, Kv2.2 t = 10.08, $p < 0.0005$). AMIGO3 surface trafficking was significantly increased with co-expression of Kv2.1 (mean = 1.29 $\pm$ 0.05, N = 30 cells, t = 5.32, $p < 0.0005$) and Kv2.2 (mean = 1.41 $\pm$ 0.05, N = 16 cells, t = 3.53, $p < 0.005$) compared to AMIGO3 alone (mean = 0.66 $\pm$ 0.03, N = 27 cells, t = -10.92, $p < 0.0005$, One-way ANOVA F = 35.99, $p < 0.0005$, Kv2.1 q = 10.97, $p < 0.0005$, Kv2.2 q = 11.09, $p < 0.005$), which was largely internal. Error bars are mean $\pm$ S.D. Boxes represent 25-75% of the data. Lines through the center of boxes represent the mean. Scale bars are 5 μm.

Co-expression with Kv2.1 increased the surface trafficking of all 3 AMIGOs (Figure 4.3, middle images) as indicated by overlapping peaks in fluorescence at the edge of the line-scans. While the effect on surface trafficking of AMIGO1 and AMIGO2 was robust, quite a lot of AMIGO3 was still retained within the cell, suggesting the affinity of Kv2.1 for AMIGO3 may be lower. Likewise, co-expression with Kv2.2 appeared to

increase the surface trafficking of all 3 AMIGOs (Figure 4.3A-C, right images), although to perhaps a lesser degree than Kv2.1 in the case of AMIGO1 and AMIGO2.

By taking a ratio of surface density over total density for each AMIGO, we quantified the observed changes in AMIGO localization, while controlling for differences in protein expression between cells. In this measurement, ratios greater than one indicate preferential surface expression, and ratios less than one indicate preferential internal expression (Figure 4.4). Using t-tests against a test mean of one, we determined the preference of each AMIGO for surface or internal localization. When expressed alone, AMIGO1 showed a significant preference for surface localization (Figure 4.4, blue box, $p<0.0005$). This preference was maintained when AMIGO1 was co-expressed with either Kv2.1 ($p<0.0005$) or Kv2.2 ($p<0.0005$), and represented a significant increase in surface trafficking from AMIGO1 expression alone (Kv2.1 $p<0.0005$, Kv2.2 $p<0.05$). Expressed alone, AMIGO2 showed a slight, but not significant preference for surface localization (Figure 4.4, green box, $p=0.096$). However, AMIGO2 showed a significant preference for surface localization when co-expressed with either Kv2.1 ($p<0.0005$) or Kv2.2 ($p<0.0005$), which was a significant improvement from expression alone ($p<0.0005$). In contrast, AMIGO3 alone showed a significant preference for internal localization (Figure 4.4, orange box, $p<0.0005$). With Kv2 co-expression, AMIGO3 surface localization was preferred with Kv2.1 ($p<0.0005$) and Kv2.2 ($p<0.005$), which was significantly different from AMIGO3 alone ($p<0.0005$). These data further indicate that all 3 AMIGOs are capable of interaction with Kv2s since the surface trafficking of each AMIGO was increased by co-expression with a Kv2.

Although Kv2 co-expression significantly increased the surface trafficking of AMIGOs, the AMIGO family did not appear to alter the surface trafficking of Kv2s (Figure 4.5). Kv2.1 alone strongly preferred to be localized on the cell surface, as seen by the two large peaks in the line-scan corresponding to the plasma membrane and a traf-

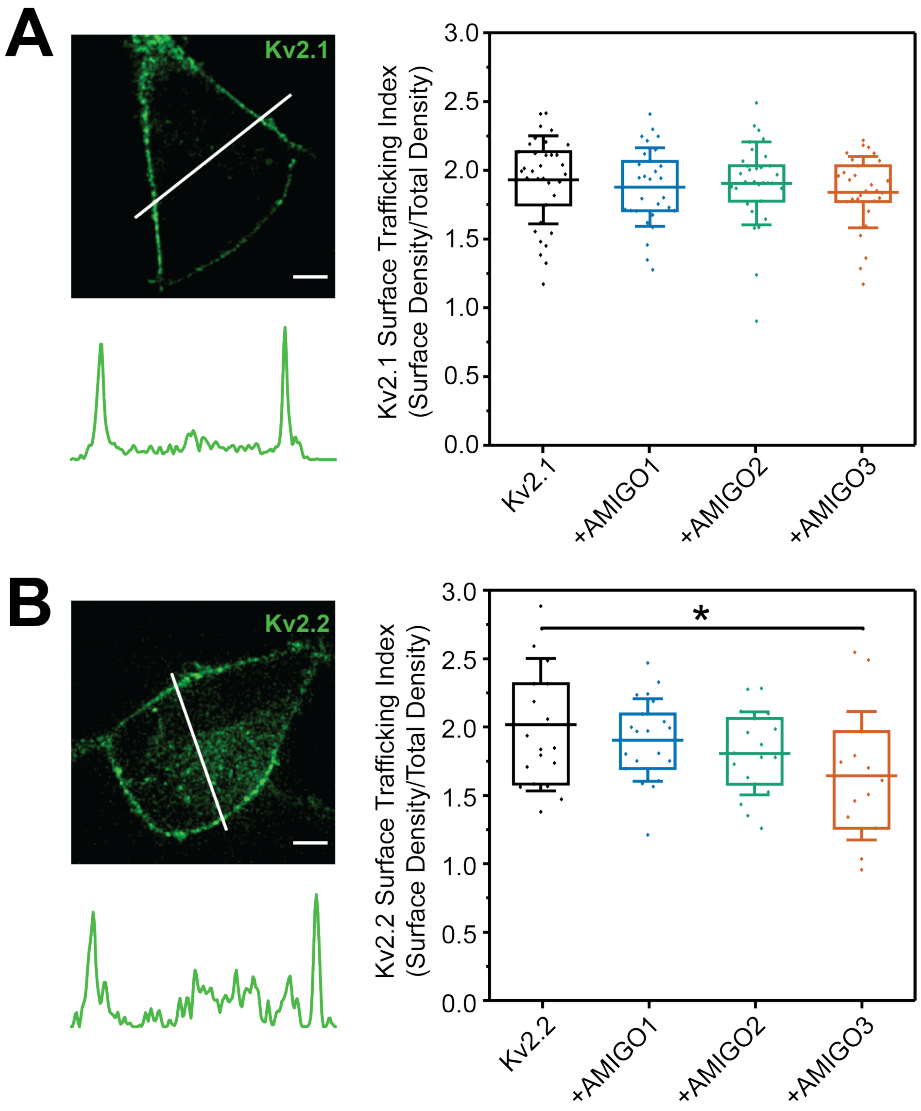

Figure 4.5: AMIGOs do not affect Kv2 surface trafficking. **A)** Representative image of a cell expressing Kv2.1 alone (left). Representative images of cells expressing both Kv2.1 and AMIGOs are shown in panels A, B, and C of Figure 4.3, center images. Co-expression with AMIGOs did not alter Kv2.1 preference for surface expression (right). Kv2.1 alone (N = 34 cells, mean ± SD = 1.92 ± 0.05, t = 16.9, p < 0.0005), Kv2.1+AMIGO1 (N = 29 cells, mean ± SD = 1.87 ± 0.05, t = 16.5, p < 0.0005), Kv2.1+AMIGO2 (N = 33, mean ± SD = 1.90 ± 0.05, t = 17.2, p < 0.0005) and Kv2.1+AMIGO3 (N = 30 cells, mean ± SD = 1.84 ± 0.05, t = 17.6, p < 0.0005). **B)** Representative image of a cell expressing Kv2.2 alone (left). Representative images of cells expressing both Kv2.2 and AMIGOs are shown in panels A, B and C of Figure 4.3, right images. Co-expression with AMIGO1 and AMIGO2 did not alter Kv2.2 preference for surface expression, however, AMIGO3 did significantly decrease Kv2.2 preference for surface trafficking (F = 2.72, p = 0.05, q = 3.88, p < 0.05). Kv2.2 alone (N = 19 cells, mean ± SD = 2.02 ± 0.1, t = 9.13, p < 0.0005), Kv2.2+AMIGO1 (N = 21 cells, mean ± SD = 1.91 ± 0.07, t = 13.7, p < 0.0005), Kv2.2+AMIGO2 (N = 18, mean ± SD = 1.81 ± 0.04, t = 11.2, p < 0.0005) and Kv2.2+AMIGO3 (N = 15 cells, mean ± SD = 1.65 ± 0.12, t = 5.29, p < 0.0005). Error bars are mean ± S.D. Boxes represent 25-75% of the data. Lines through the center of boxes represent the mean. Scale bars are 5 μm.

ficking index near 2 (Figure 4.5A, $p < 0.0005$). Co-expression with AMIGO1, AMIGO2, or AMIGO3 did not significantly change Kv2.1 surface expression compared to Kv2.1 alone ($p = 0.66$, Figure 4.5A graph). Similarly, Kv2.2 showed a strong preference for surface expression (Figure 4.5B, $p < 0.0005$), which was unchanged by co-expression with either AMIGO1 or AMIGO2. However, co-expression with AMIGO3 did significantly decrease the preference of Kv2.2 for surface expression ($p < 0.05$, Figure 4.5B graph), perhaps indicating that at least some Kv2.2 could be prevented from forward trafficking by interaction with AMIGO3. Overall, Kv2s increased the trafficking of AMIGOs to the surface, while AMIGOs had little effect on Kv2 surface trafficking.

4.4.3 All three AMIGOs co-immunoprecipitate with both Kv2 isoforms

The colocalization and trafficking effects we observed above are consistent with the hypothesis that all three AMIGO isoforms act as auxiliary subunits for the Kv2 channels. To confirm an interaction between the AMIGOs and Kv2s, we performed co-immunoprecipitation experiments on HEK-293 cells transfected with Kv2 α-subunits alone or in the presence of AMIGO1-GFP, AMIGO2-GFP, or AMIGO3-GFP. In each of the co-expression conditions, an antibody against the Kv2 α-subunit co-immunoprecipitated an $\sim$80 kDa protein that was detected by a GFP antibody via western blot (Figure 4.6A and B, asterisks). Importantly, no bands were detected by the same GFP antibody when Kv2.1 or Kv2.2 was expressed alone (Figure 4.6C and D). The AMIGO1-GFP bands detected by the GFP antibody were also detected by a monoclonal antibody against AMIGO1 itself, supporting the idea that the GFP antibody successfully detected our transfected AMIGO constructs (data not shown).

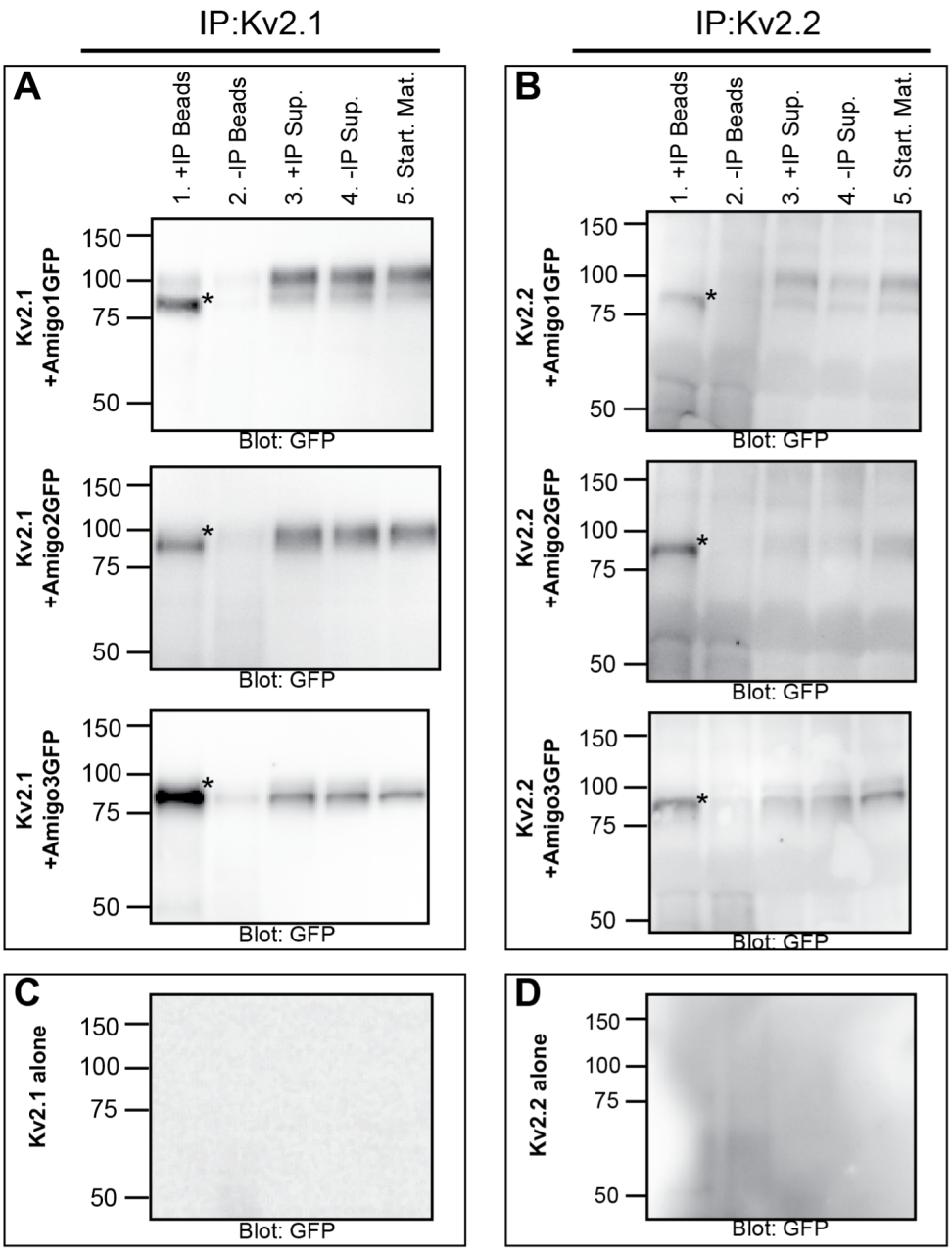

Figure 4.6: All three AMIGOs interact directly with both Kv2.1 and Kv2.2. A) Kv2.1 antibody co-immunoprecipitated AMIGO1-GFP (top), AMIGO2-GFP (middle) and AMIGO3-GFP (bottom) when co-expressed in HEK-293 cells (asterisks). +IP Beads = material pulled down by Kv2.1 antibody; -IP Beads = material pulled down in absence of IP antibody; +IP Sup. = material remaining in supernatant after pull-down with IP antibody; -IP Sup. = material remaining in supernatant after pull-down in absence of IP antibody; Start. Mat. = material in pre-cleared lysate before IP. **B)** Kv2.2 antibody co-immunoprecipitated the same AMIGO1-GFP (top), AMIGO2-GFP (middle), and AMIGO3-GFP (bottom) bands from co-transfected HEK-293 cells (asterisks). Lane titles are the same as in A, except the IP antibody was specific for Kv2.2. C-**D)** The anti-GFP antibody detected nothing in cells transfected with either Kv2.1 (**C)** or Kv2.2 (**D)** alone. These experiments were performed by Emily Maverick, PhD.

4.5 Discussion

Kv β-subunits are well-known for their modulatory effects on channel function and localization. While the effects of assembly on auxiliary subunit trafficking is often overlooked, we demonstrate that both Kv2s confer increased trafficking and a clustered localization to all three AMIGOs. Given the AMIGO family's widespread physiological functions, such as neurite growth and cell survival [227, 231, 235], assembly with Kv2 channels likely modulates some of these functions as well. Therefore, the interaction between Kv2 channels and each AMIGO represents a co-regulatory mechanism for both electrical and non-electrical cell properties.

In addition to AMIGO-dependent changes in Kv2 electrical function [350], we identified Kv2-dependent changes in AMIGO localization and trafficking. Expressed alone in HEK-293 cells, surface AMIGO proteins were distributed evenly across the cell surface. When co-expressed with Kv2 channels, each of the three AMIGOs was trafficked more efficiently to the plasma membrane and underwent re-localization to ER/PM junctions, as was previously observed with AMIGO1 and Kv2 channels [228]. Redistribution of AMIGOs to Kv2 clusters on the cell surface likely demonstrates a direct interaction between the two proteins as has been previously shown for AMIGO1 and Kv2.1 [226]. This interaction was proposed to occur via the transmembrane (TM) domain of AMIGO1 and an unidentified TM domain of Kv2.1. Since the TM domains of the 3 AMIGOs are fairly homologous (48% identical, 81% similar, Uniprot), the interaction between each AMIGO and Kv2 likely occurs via a similar mechanism, although the specific residues involved in interaction have yet to be determined.

In our co-IP experiments, both the GFP-tagged and endogenous AMIGO1 appeared as doublets (Figure 4.6). The lower of the two GFP-AMIGO1 bands was preferentially co-purified with both Kv2.1 and Kv2.2 antibodies, suggesting that the chan-

nels interact more favorably with one AMIGO1 form over the other. Early work with AMIGO1 suggests the two molecular weights represent different glycosylation states of the protein, as AMIGO1 has five predicted N-linked glycosylation sites [229]. Perhaps the lower molecular weight version that assembles with Kv2 channels is not fully glycosylated. Whether assembly with Kv2.1 alters AMIGO1 glycosylation or once assembled the complex no longer traffics through the classic Golgi pathway, as has been suggested [317], remains an open question.

Each of the AMIGO isoforms showed variable levels of surface expression and of the AMIGOs, AMIGO3 showed the lowest surface expression, with much of the internal AMIGO3 appearing to reside in the ER. Although an ER-retention motif has not yet been identified in any of the AMIGOs, interestingly, AMIGO3 has an additional 6 amino acids in the proximal C-terminus. These 6 amino acids (RCRRWP) contain a di-arginine motif, which is a sequence involved in general ER retention [351]. Internal AMIGO1 and AMIGO2 appeared to be localized in trafficking vesicles, which may represent a forward trafficking or recycling pool. Future studies may wish to determine in which pool these vesicles belong, and whether assembly with Kv2 channels prolongs their lifetime at the plasma membrane.

The effect of Kv2 channels on AMIGO surface expression represents a gain-of-function phenotype that likely has downstream effects due to AMIGO functions at the cell surface. For example, AMIGO2 localization to the PM may upregulate lipid-dependent phosphorylation of Akt, leading to increased growth and survivability [239]. Likewise, since all 3 AMIGOs are thought to act as cell adhesion molecules [227], the increased surface expression could increase the size, number, or location of cell-cell adhesions. Indeed, EM micrographs of Kv2.1 clusters in the rat hippocampus have been identified as sites of astrocyte adhesion [183], and more recently, it was reported that microglia often contact neurons at Kv2.1 clusters [186]. Although neither of these

neuron-glia adhesions has been attributed to AMIGO family interactions, it is tempting to speculate that AMIGOs residing in Kv2 clusters play a role in adhesion.

The effects of the AMIGOs on voltage-dependent activation observed in our lab agree with previously published data with AMIGO1 [226]. Namely, each AMIGO conferred a hyperpolarizing shift to the Kv2 channel activation midpoint [350]. The effects of the AMIGOs on Kv2 function are particularly interesting in terms of the brain. As mentioned in the introduction, Kv2 channels are not recruited for single AP repolarization but are thought to be important for maintaining polarized membrane potentials during high-frequency firing. Faster Kv2 activation and slower inactivation, as seen in [350], would result in more outward K^+ current at a given firing frequency. This hyperpolarizing current could enhance the recovery of sodium channels from inactivation during the interspike interval, leading to an overall increase in firing frequency. Indeed, this hypothesis is in line with the observed requirement for Kv2 in preventing depolarization block during high-frequency firing in cervical ganglion neurons, CA1 pyramidal neurons, and cortical neurons [206, 207]. Alternatively, the increased hyperpolarizing current contributed by Kv2s associated with AMIGOs could halt firing by preventing sufficient depolarization for AP initiation. The overall result of AMIGO assembly with Kv2s on neuronal firing properties will likely vary on a cell-by-cell basis and will be determined by the cell's full complement of ion channels and the neuronal inputs it receives.

Of the three isoforms, AMIGO2 had the most dramatic effects on Kv2.1 and Kv2.2 channel function [350]. In the hippocampus, Kv2 channels and AMIGO2 have somewhat reciprocal expression patterns, with Kv2.1 and Kv2.2 more highly expressed in CA1 and CA3 [344], and AMIGO2 highly expressed in CA2 [352,353]. These observations suggest that AMIGO2 may not regulate Kv2 channel electrical function extensively in the hippocampus. An AMIGO2 knockout mouse has been characterized as having perturbed

neuronal morphology in the retina and associated vision impairments (Jackson Labs Amigo2^{emDke}/Amigo2^{emDke}). Whether these effects can be attributed to AMIGO2's regulatory effects on Kv2 currents is unknown, but Kv2.1 is also highly expressed in the retina [354]. According to the Human Protein Atlas, AMIGO2 is also found in peripheral tissues that express Kv2 channels, such as endocrine and muscle cells. Whether AMIGO2's dramatic effects on Kv2 electrical properties regulate the functions of Kv2-containing cells in these tissues will be interesting to investigate.

Until recently, the Kv2 literature and AMIGO literature have been largely distinct bodies of work. The 2011 finding that AMIGO1 is a Kv2.1 auxiliary subunit marks the merging of the two fields. In combination with other work out of our lab, we further intertwine the AMIGO and Kv2 fields by showing functional interactions between all members of both families [350]. This result will inevitably lead to new and renewed interest in various aspects of each family's physiological function. For example, could AMIGOs reduce or exacerbate the effects of the known pathogenic *de novo* Kv2.1 mutations [355–357]? Are Kv2 channels somehow involved in the activity-dependence of AMIGO expression [235]? What are the consequences of concentrating each of the three AMIGOs at the extracellular surface of Kv2-induced ER/PM junctions? These and other questions await future investigation.

Chapter 5

Conclusions

The work presented in this dissertation further identifies the molecular players at Kv2.1-induced neuron-astrocyte contact sites. In Chapter 2, we found Glt1 glutamate transporters are statically localized in nanoclusters overlying the cortical actin cytoskeleton. In Chapter 3, we found that the Glt1-actin interaction is likely responsible for the net-like localization of Glt1 around neuronal Kv2.1/AMIGO clusters in neurons. Finally, in Chapter 4, we delved into the relationship of Kv2 channels and AMIGO family β-subunits, finding that all three members of the AMIGO family of cell adhesion molecules can interact with and alter the function of Kv2 channels.

5.1 Positioning Glt1 for optimal control over glutamate concentration

To adequately buffer extracellular glutamate and terminate synaptic communication, astrocytic glutamate transporters, like Glt1, must be located near areas where glutamate concentrations are high. Despite a vast literature exploring the function of Glt1 and other glutamate transporters, few have focused on the mechanisms regulating Glt1 localization until recently [108, 140, 143, 279, 358]. The work presented in Chapter 2 demonstrates a novel interaction between Glt1a transporters and cortical actin filaments. To our knowledge, these are the first data to suggest surface Glt1a localization relies on an interaction with a component of the actin cytoskeleton. We found that this interaction can be disrupted by over-expression of a cytosolic Glt1a C-terminal fragment, thus implying the C-terminus is an important mediator of localization to actin filaments. Since the Glt1 isoforms, Glt1a and Glt1b, differ only in the final 11-22 amino acids of the C-terminus, and we did not observe similar localization of Glt1b with the actin cytoskeleton, we concluded the last 22 amino acids in Glt1a must bear some responsibility in actin interaction.

These data are the first to ascribe a particular function to the different amino acids in Glt1a.

Although we may have identified the amino acids necessary for interaction in Glt1a, we have not identified any potential candidates that mediate the Glt1a-actin interaction. Since we observed nanoclusters adjacent to actin filaments, we believe this interaction is not direct. However, now that we know the motif required in Glt1a and that expression of this motif can interrupt Glt1a-actin interaction, the final 22 amino acids of the C-terminus could be used as bait to discover this intermediary protein.

Studies of protein localization tend to view location as static, rather than dynamic. This view is likely due in part to fixation and immunodetection being widely available methods. However, by failing to consider the dynamic nature of protein localization, we possibly miss out on important regulated functions. For instance, recent studies discovered that lateral diffusion of Glt1 in the astrocyte membrane was crucial to adequately buffer glutamate at the synaptic cleft [140]. Intriguingly, they found glutamate binding increased the rate of lateral diffusion, a finding we replicated and presented in Chapter 2. We postulated that Glt1 release from static nanoclusters may cause the observed increase in total diffusion. However, we did not detect any differences in the intensity or location of Glt1 nanoclusters following glutamate application, and thus, the mechanism of increased diffusion by glutamate remains a mystery.

5.2 AMIGO and Kv2.1 at the nexus of neuron-astrocyte contacts

Perhaps more importantly, we present evidence in Chapter 3 that shows this Glt1a-actin interaction is likely involved in positioning astrocyte Glt1 near insult-sensitive Kv2.1 clusters in neurons. A previous publication reported astrocyte processes lie directly apposed to more than 90% of Kv2.1 clusters in the intact hippocampus [183]. Other

published data suggests Glt1 membrane localization is regulated by neuronal Kv2.1 clusters [184], a finding we replicated *in vitro* and presented in Chapter 3. Significantly, we found Glt1 and astrocyte actin filaments colocalized around neuronal Kv2.1 clusters. Combined with data showing Glt1 diffusion is not decreased directly across from neuronal Kv2.1 clusters, we propose this neuron-astrocyte adhesion is capable of regulating astrocyte actin filaments, although we do not yet know the mechanism. Is this adhesion mediated by AMIGO family interactions? If so, how do AMIGO family proteins alter the position of the astrocyte actin cytoskeleton?

Astrocyte Glt1 transporters are also localized adjacent to synapses [156]. While we were not able to see if actin and Glt1 colocalize near synapses, one study has shown actin cytoskeleton interacting proteins are localized to peri-synaptic astrocyte processes (PAPs) and that cytoskeletal rearrangement was induced by glutamate [152]. These data suggest the Glt1a-actin interaction may also be important in PAPs, although this awaits future investigation. If so, modifying the actin cytoskeleton would be an elegant way to simultaneously stimulate PAP structural plasticity and modify the localization and/or concentration of Glt1 at the synapse.

Since somatic Kv2.1 clusters and synapses are the only known locations that astrocyte Glt1 shows a specific localization pattern, we wanted to know whether these two neuron-astrocyte contacts may display similarities in composition. To this end, we performed studies of Kv2.1 and AMIGO1 localization near synapses. Interestingly, we found Kv2.1 and AMIGO1 localized to pre- and post-synaptic elements of mature synapses. These data presented in the latter half of Chapter 3 suggest Kv2.1 and AMIGO1 play some sort of role at synapses, which could be functional and/or structural. Unpublished evidence out of the Hoppa lab at Dartmouth suggests that Kv2.1 is important for pre-synaptic function, as knockdown of Kv2.1 by shRNA substantially decreased evoked vesicle fusion by $\sim$50% [communication with Mike Hoppa]. Addi-

tionally, given that EM studies showed Kv2.1 clusters are nearly always associated with an astrocyte process [183], it may be that Kv2.1/AMIGO clusters also mediate astrocyte adhesion at synapses via AMIGO CAM activity. Do Kv2.1 and AMIGO localize to synapses *in vivo*? If so, how does knockdown of Kv2.1 or AMIGO1 affect *in vivo* synaptic communication? Do regional differences in astrocyte synaptic coverage correlate with the presence of Kv2.1 and AMIGO at synapses?

5.3 Different AMIGOs confer different functions

In Chapter 4, we presented data to support the idea that all three members of the AMIGO family act as β-subunits of Kv2 channels. In addition to each of the AMIGOs altering voltage-dependent properties of Kv2s [350], we found that Kv2s both increased the surface trafficking of AMIGOs and redistributed surface AMIGOs to micron-sized clusters. This gain-of-function phenotype is likely to have downstream effects due to AMIGO localization to the surface. Since all three AMIGOs are thought to act as cell adhesion molecules [227], the increased surface expression could increase the size, number, or alter the location of cell-cell adhesions, and could contribute to the formation of neuron-astrocyte contacts in the brain.

All three AMIGOs are expressed throughout the body, with AMIGO1 having the highest expression in the brain, while AMIGO2 and AMIGO3 are more widespread in tissue distribution [227]. The literature describing functions of AMIGO2 is perhaps the most interesting of the three. AMIGO2 has been implicated in enhanced growth and survival in a variety of cells including cerebellar granule neurons [235], vascular endothelial cells [236], gastric adenocarcinoma cells [237], melanoma cells [238], liver endothelial cells [240], and ovarian metastatic cancer cells [241]. The combination of enhanced cell survival and adhesion effects makes AMIGO2 a particularly dangerous molecule for metastatic cancer cells, which has made it a proposed cancer target in re-

cent years. This increase in cell viability may be due to an interaction between AMIGO2 and PDK1, a kinase that activates Akt in cell survival pathways [239]. While AMIGO1 and AMIGO3 have not yet been implicated in cell survival, the AMIGO family shares ∼73% similarity in the region of the C-terminus in AMIGO2 identified in PDK1 interaction. Intriguingly, cerebellar granule neuron activity correlated with AMIGO2 gene expression, such that higher activity resulted in more AMIGO2 protein [235]. Could this be a mechanism to simultaneously increase cell survival via the Akt pathway and limit neuronal hyper-excitability by prolonging the open state of Kv2 channels?

In the central nervous system, AMIGO2 expression has been observed in fairly specific locations, among them the CA2 region of the hippocampus [352], cerebellar granule neurons [235], starburst amacrine cells, and rod bipolar cells of the retina [233]. In contrast, AMIGO1 expression is abundant throughout the brain [228]. Perhaps tighter control over AMIGO2 expression is required to prevent under-excitation of neurons, which would occur due to decreased inactivation of abundant delayed-rectifier Kv2 channels. Now that we know all three AMIGOs can act as Kv2 β-subunits, it will be interesting to discover which AMIGOs associate with Kv2s in different tissues across development and how this interaction might regulate regional differences in neuronal firing properties and neuron-glia adhesion.

5.4 Implications for disease

Since the original description of neuron-astrocyte contacts at Kv2.1 clusters, only two other groups have examined communication at these neuron-astrocyte contacts. Both groups described the need for functional uptake of glutamate by transporters, as inhibition of transport increased extracellular glutamate, activated extrasynaptic NMDA receptors, led to an influx of Ca^{2+}, and led to subsequent dephosphorylation of Kv2.1 by calcineurin [184,185]. Dephosphorylation of the Kv2.1 C-terminus FFAT motif disal-

lows interaction with ER VAP proteins, and thus, leads to a dispersal of Kv2.1 clusters. Positioning Glt1 near Kv2.1 clusters may decrease the local extracellular concentration of glutamate, thereby decreasing the probability of Kv2.1-induced ER/PM junction disintegration, except in the direst situations.

As discussed at length in Section 1.7.2, Kv2.1 channels are involved in both the early neuroprotective response and the late apoptotic response to ischemic insult. In the early phase, both channel conductance and cluster dispersal are thought to contribute to neuroprotection. Dephosphorylation of serine residues in Kv2.1 shifts the voltage-dependence of activation, such that the channels activate earlier, thus decreasing neuronal excitability. While the contribution of channel conductance to dampen neuronal excitability is rather straightforward, we do not yet know why cluster dispersal is neuroprotective. Microglia also contact neurons at Kv2.1 clusters [186]. Interestingly, following ischemic stroke by artery occlusion, the microglia contact area increased. Blocking the increase in contact area following stroke resulted in increased infarct volume and neuronal Ca^{2+} load. Together this suggests that glial contact increases following insult, which is neuroprotective. Could the same be true for the neuron-astrocyte contact area? Does this rely on AMIGO adhesion? If so, perhaps the neuroprotection provided by Kv2.1 cluster dispersal is due to spreading of AMIGO cell-adhesion molecules, and thus an increase in the glial contact area.

Unsurprisingly, several *de novo* mutations in the coding sequence of Kv2.1 are associated with developmental and epileptic encephalopathy (for review: [359]). Many of these mutations are located in the voltage-sensor, pore-forming domain, or K^+ selectivity filter. These mutations most likely directly affect channel function by altering the coupling of the S4 domain [360] or changing the K^+ selectivity of the channel [357,361]. Since the first identification of a disease-causing Kv2.1 variant, 64 patients have been described to date [359]. Of these patients, three have mutations in the S1 transmem-

brane domain of Kv2.1. In a study of one of these variants, Calhoun and colleagues found a I199F mutation caused a depolarizing shift in the voltage-dependence of activation of Kv2.1 expressed in CHO cells [362]. Given the effect of AMIGOs on Kv2.1 activation [350], and the hypothesis that AMIGOs interact with Kv2s via transmembrane domains [226], could this mutation disrupt the assembly of Kv2.1 with AMIGO β-subunits?

While the AMIGO family is a relatively new field of study, AMIGO family mutations are implicated in the development of autism spectrum disorder and schizophrenia [363–366]. A single nucleotide variation (SNV) in the gene encoding AMIGO1 leads to a missense mutation in the C-terminus [367], and this patient displays seizure activity, autism, and developmental delay. This is the only known SNV for AMIGO1, however, other patients who are missing the AMIGO1, AMIGO2, or AMIGO3 genes display similar intellectual disabilities and developmental delays [367]. Given the striking similarities in phenotypes of patients having Kv2.1 or AMIGO family mutations or deletions, it is tempting to speculate that at least some of these genetic variants affect Kv2/AMIGO assembly.

5.5 More to learn

The work presented in this dissertation adds to the under-developed field of neuron-astrocyte contacts at Kv2.1 clusters. An updated working model of this contact is presented in Figure 5.1. While we have now identified actin filaments (magenta, Chapters 2 & 3), AMIGO2 & AMIGO3 (cyan, Chapter 4), and VAP (dark green, Appendix A) as probable constituents of this neuron-astrocyte contact, there is still much to learn. What is the identity of the astrocyte-expressed cell adhesion molecule (CAM, orange)? How does this CAM modify the location of the astrocyte actin cytoskeleton? What is the mechanism of Glt1a localization to actin filaments? How does the presence of different

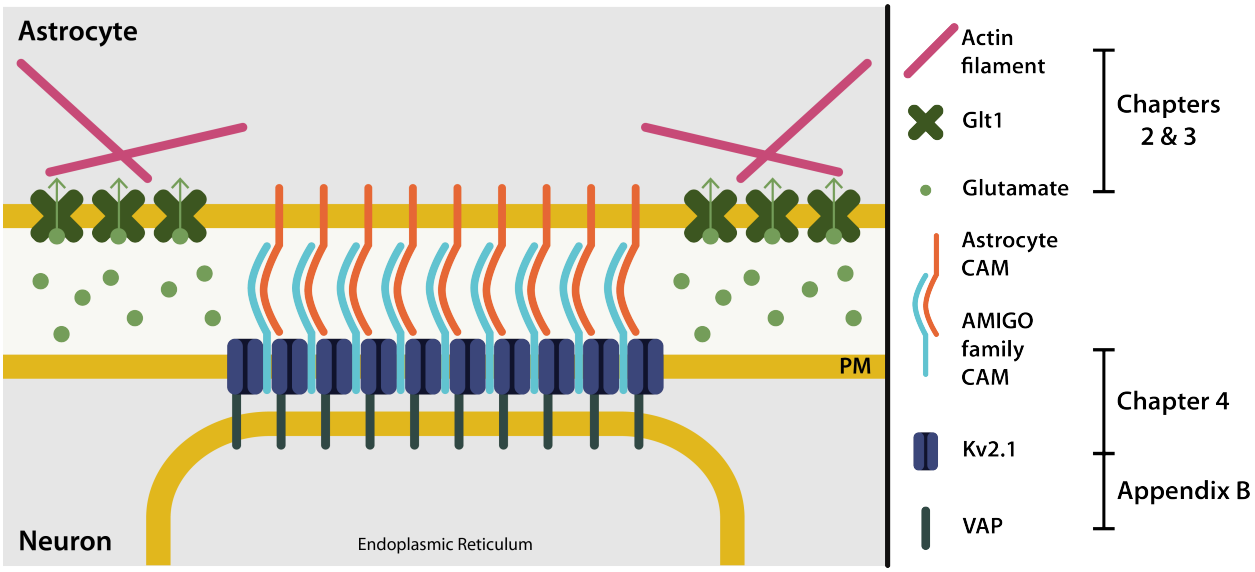

Figure 5.1: A Current working model of the neuron-astrocyte contact at somatic Kv2.1 clusters.

AMIGO family members at the Kv2.1-induced ER/PM junction change the function of this cell-cell contact? How is this cell-cell contact altered under conditions of excitotoxicity and disease? Time will tell.

5.6 Looking backward and forward

Over a century ago, Cajal could only imagine cells as living and dynamic, but we can see it now. We can watch in real-time as cells react to our interventions. Using tools Cajal could scarcely conceive of, we can watch the path of a single-particle, approximate the true location of proteins in intricate detail, and delve deeper into the ever-growing list of things our cells can do.

Cell biology is endlessly fascinating. I feel lucky to have studied and contributed to this field for so many years. The journey of discovery is never over —answers only beget more questions, more unknowns, and more experiments. Truly, the more we know, the more we know what we don't know, and if you're a scientist, the more you want to know. I look forward to following the journeys of the next students who take up this

mantle. Hopefully, it will not take another few decades, as I truly believe this contact between neurons and astrocytes will prove its significance time and time again.

Bibliography

[1] Constantino Sotelo. The History of the Synapse. *The Anatomical Record*, 303(5):1252–1279, 2020.

[2] Marta Navarrete and Alfonso Araque. The Cajal school and the physiological role of astrocytes: a way of thinking. *Frontiers in Neuroanatomy*, 8:33, 2014.

[3] Vladimir Parpura and Alexei Verkhratsky. The astrocyte excitability brief: From receptors to gliotransmission. *Neurochemistry International*, 61(4):610–621, 2012.

[4] Christopher S. Bartheld, Jami Bahney, and Suzana HerculanoHouzel. The search for true numbers of neurons and glial cells in the human brain: A review of 150 years of cell counting. *Journal of Comparative Neurology*, 524(18):3865–3895, 2016.

[5] Wei Sun, Adam Cornwell, Jiashu Li, Sisi Peng, M Joana Osorio, Nadia Aalling, Su Wang, Abdellatif Benraiss, Nanhong Lou, Steven A Goldman, and Maiken Nedergaard. SOX9 Is an Astrocyte-Specific Nuclear Marker in the Adult Brain Outside the Neurogenic Regions. *The Journal of Neuroscience*, 37(17):4493–4507, 2017.

[6] Alexei Verkhratsky and Maiken Nedergaard. Physiology of Astroglia. *Physiological Reviews*, 98(1):239–389, 2018.

[7] I. Lundgaard, M.J. Osório, B.T. Kress, S. Sanggaard, and M. Nedergaard. White matter astrocytes in health and disease. *Neuroscience*, 276:161–173, 2014.

[8] EA Bushong, ME Martone, and YZ Jones. Protoplasmic astrocytes in CA1 stratum radiatum occupy separate anatomical domains. *The Journal of Neuroscience*, 2002.

[9] Eiji Shigetomi, Eric A. Bushong, Martin D. Haustein, Xiaoping Tong, Olan Jackson-Weaver, Sebastian Kracun, Ji Xu, Michael V. Sofroniew, Mark H. Ellisman, and

Baljit S. Khakh. Imaging calcium microdomains within entire astrocyte territories and endfeet with GCaMPs expressed using adeno-associated virusesImaging calcium signals in entire astrocytes. *The Journal of General Physiology*, 141(5):633–647, 2013.

[10] Michael M. Halassa and Philip G. Haydon. Integrated Brain Circuits: Astrocytic Networks Modulate Neuronal Activity and Behavior. *Annual Review of Physiology*, 72(1):335–355, 2010.

[11] Nancy Ann Oberheim, Steven A. Goldman, and Maiken Nedergaard. Astrocytes, Methods and Protocols. *Methods in Molecular Biology*, 814:23–45, 2011.

[12] Michael M. Halassa, Tommaso Fellin, Hajime Takano, Jing-Hui Dong, and Philip G. Haydon. Synaptic Islands Defined by the Territory of a Single Astrocyte. *The Journal of Neuroscience*, 27(24):6473–6477, 2007.

[13] Jean Livet, Tamily A. Weissman, Hyuno Kang, Ryan W. Draft, Ju Lu, Robyn A. Bennis, Joshua R. Sanes, and Jeff W. Lichtman. Transgenic strategies for combinatorial expression of fluorescent proteins in the nervous system. *Nature*, 450(7166):56–62, 2007.

[14] Ulrika Wilhelmsson, Eric A. Bushong, Diana L. Price, Benjamin L. Smarr, Van Phung, Masako Terada, Mark H. Ellisman, and Milos Pekny. Redefining the concept of reactive astrocytes as cells that remain within their unique domains upon reaction to injury. *Proceedings of the National Academy of Sciences*, 103(46):17513–17518, 2006.

[15] Wolfgang Walz. Role of astrocytes in the clearance of excess extracellular potassium. *Neurochemistry International*, 36(4-5):291–300, 2000.

[16] Baljit S Khakh and Michael V Sofroniew. Diversity of astrocyte functions and phenotypes in neural circuits. *Nature Neuroscience*, 18(7):942–952, 2015.

[17] Anna Yu-Szu Huang, Junsung Woo, Debosmita Sardar, Brittney Lozzi, Navish A. Bosquez Huerta, Chia-Ching John Lin, Daniela Felice, Antrix Jain, Adriana Paulucci-Holthauzen, and Benjamin Deneen. Region-Specific Transcriptional Control of Astrocyte Function Oversees Local Circuit Activities. *Neuron*, 106(6):992–1008.e9, 2020.

[18] Sara Mederos, Candela González-Arias, and Gertrudis Perea. AstrocyteNeuron Networks: A Multilane Highway of Signaling for Homeostatic Brain Function. *Frontiers in Synaptic Neuroscience*, 10:45, 2018.

[19] N. Joan Abbott, Lars Rönnbäck, and Elisabeth Hansson. Astrocyteendothelial interactions at the bloodbrain barrier. *Nature Reviews Neuroscience*, 7(1):41–53, 2006.

[20] Thomas Misje Mathiisen, Knut Petter Lehre, Niels Christian Danbolt, and Ole Petter Ottersen. The perivascular astroglial sheath provides a complete covering of the brain microvessels: An electron microscopic 3D reconstruction. *Glia*, 58(9):1094–1103, 2010.

[21] M. Nedergaard and S. A. Goldman. Carrier-mediated transport of lactic acid in cultured neurons and astrocytes. *American Journal of Physiology-Regulatory, Integrative and Comparative Physiology*, 265(2):R282–R289, 1993.

[22] Raymond C. Koehler, Richard J. Roman, and David R. Harder. Astrocytes and the regulation of cerebral blood flow. *Trends in Neurosciences*, 32(3):160–169, 2009.

[23] Costantino Iadecola. The Neurovascular Unit Coming of Age: A Journey through Neurovascular Coupling in Health and Disease. *Neuron*, 96(1):17–42, 2017.

[24] Brian A. MacVicar and Roger J. Thompson. Non-junction functions of pannexin-1 channels. *Trends in Neurosciences*, 33(2):93–102, 2010.

[25] Angus M. Brown and Bruce R. Ransom. Astrocyte glycogen and brain energy metabolism. *Glia*, 55(12):1263–1271, 2007.

[26] Michael Taynnan Barros, Walisson Silva, and Carlos Danilo Miranda Regis. The Multi-Scale Impact of the Alzheimers Disease on the Topology Diversity of Astrocytes Molecular Communications Nanonetworks. *IEEE Access*, 6:78904–78917, 2018.

[27] Leif Hertz and Ye Chen. Importance of astrocytes for potassium ion (K+) homeostasis in brain and glial effects of K+ and its transporters on learning. *Neuroscience & Biobehavioral Reviews*, 71:484–505, 2016.

[28] Nephtali Marina, Egor Turovsky, Isabel N Christie, Patrick S Hosford, Anna Hadjihambi, Alla Korsak, Richard Ang, Svetlana Mastitskaya, Shahriar Sheikhbahaei, Shefeeq M Theparambil, and Alexander V Gourine. Brain metabolic sensing and metabolic signaling at the level of an astrocyte. *Glia*, 66(6):1185–1199, 2018.

[29] J. Marc Simard, Kevin N. Sheth, W. Taylor Kimberly, Barney J. Stern, Gregory J. del Zoppo, Sven Jacobson, and Volodymyr Gerzanich. Glibenclamide in Cerebral Ischemia and Stroke. *Neurocritical Care*, 20(2):319–333, 2014.

[30] Michelle L. Olsen, Baljit S. Khakh, Serguei N. Skatchkov, Min Zhou, C. Justin Lee, and Nathalie Rouach. New Insights on Astrocyte Ion Channels: Critical for Homeostasis and Neuron-Glia Signaling. *The Journal of Neuroscience*, 35(41):13827–13835, 2015.

[31] Ciaran MurphyRoyal, Julien Dupuis, Laurent Groc, and Stéphane H. R. Oliet. Astroglial glutamate transporters in the brain: Regulating neurotransmitter homeostasis and synaptic transmission. *Journal of Neuroscience Research*, 95(11):2140–2151, 2017.

[32] Susan L. Campbell, John J. Hablitz, and Michelle L. Olsen. Functional changes in glutamate transporters and astrocyte biophysical properties in a rodent model of focal cortical dysplasia. *Frontiers in Cellular Neuroscience*, 8:425, 2014.

[33] G Seifert and C Steinhäuser. Neuronastrocyte signaling and epilepsy. *Experimental Neurology*, 2013.

[34] Taizen Nakase, Shinji Fushiki, Goran Söhl, Martin Theis, Klaus Willecke, and Christian C. G. Naus. Neuroprotective Role of Astrocytic Gap Junctions in Ischemic Stroke. *Cell Communication & Adhesion*, 10(4-6):413–417, 2009.

[35] Anke Wallraff, Rüdiger Köhling, Uwe Heinemann, Martin Theis, Klaus Willecke, and Christian Steinhäuser. The Impact of Astrocytic Gap Junctional Coupling on Potassium Buffering in the Hippocampus. *The Journal of Neuroscience*, 26(20):5438–5447, 2006.

[36] Alfonso Araque, Giorgio Carmignoto, PhilipăG. Haydon, StéphaneăH.R. Oliet, Richard Robitaille, and Andrea Volterra. Gliotransmitters Travel in Time and Space. *Neuron*, 81(4):728–739, 2014.

[37] Mirko Santello, Nicolas Toni, and Andrea Volterra. Astrocyte function from information processing to cognition and cognitive impairment. *Nature Neuroscience*, 22(2):154–166, 2019.

[38] Dmitri A. Rusakov. Disentangling calcium-driven astrocyte physiology. *Nature Reviews Neuroscience*, 16(4):226–233, 2015.

[39] Narges Bazargani and David Attwell. Astrocyte calcium signaling: the third wave. *Nature Neuroscience*, 19(2):182–189, 2016.

[40] Vladimir Parpura, Trent A. Basarsky, Fang Liu, Ksenija Jeftinija, Srdija Jeftinija, and Philip G. Haydon. Glutamate-mediated astrocyteneuron signalling. *Nature*, 369(6483):744–747, 1994.

[41] M Nedergaard. Direct signaling from astrocytes to neurons in cultures of mammalian brain cells. *Science*, 263(5154):1768–1771, 1994.

[42] Gertrudis Perea, Marta Navarrete, and Alfonso Araque. Tripartite synapses: astrocytes process and control synaptic information. *Trends in Neurosciences*, 32(8):421–431, 2009.

[43] H. Rheinallt Parri, Timothy M. Gould, and Vincenzo Crunelli. Spontaneous astrocytic Ca2+ oscillations in situ drive NMDAR-mediated neuronal excitation. *Nature Neuroscience*, 4(8):803–812, 2001.

[44] Tommaso Fellin and Giorgio Carmignoto. Neuronetoastrocyte signalling in the brain represents a distinct multifunctional unit. *The Journal of Physiology*, 559(1):3–15, 2004.

[45] María Cecilia Angulo, Andreï S. Kozlov, Serge Charpak, and Etienne Audinat. Glutamate Released from Glial Cells Synchronizes Neuronal Activity in the Hippocampus. *The Journal of Neuroscience*, 24(31):6920–6927, 2004.

[46] Marcello D'Ascenzo, Tommaso Fellin, Miho Terunuma, Raquel Revilla-Sanchez, David F. Meaney, Yves P. Auberson, Stephen J. Moss, and Philip G. Haydon. mGluR5 stimulates gliotransmission in the nucleus accumbens. *Proceedings of the National Academy of Sciences*, 104(6):1995–2000, 2007.

[47] Gertrudis Perea and Alfonso Araque. Glial calcium signaling and neuronglia communication. *Cell Calcium*, 38(3-4):375–382, 2005.

[48] Alfonso Araque, Vladimir Parpura, Rita P. Sanzgiri, and Philip G. Haydon. Glutamatedependent astrocyte modulation of synaptic transmission between cultured hippocampal neurons. *European Journal of Neuroscience*, 10(6):2129–2142, 1998.

[49] Pascal Jourdain, Linda H Bergersen, Khaleel Bhaukaurally, Paola Bezzi, Mirko Santello, Maria Domercq, Carlos Matute, Fiorella Tonello, Vidar Gundersen, and Andrea Volterra. Glutamate exocytosis from astrocytes controls synaptic strength. *Nature Neuroscience*, 10(3):331–339, 2007.

[50] Gertrudis Perea and Alfonso Araque. Astrocytes Potentiate Transmitter Release at Single Hippocampal Synapses. *Science*, 317(5841):1083–1086, 2007.

[51] Jian Kang, Li Jiang, Steven A. Goldman, and Maiken Nedergaard. Astrocyte-mediated potentiation of inhibitory synaptic transmission. *Nature Neuroscience*, 1(8):683–692, 1998.

[52] My Andersson, Fredrik Blomstrand, and Eric Hanse. Astrocytes play a critical role in transient heterosynaptic depression in the rat hippocampal CA1 region. *The Journal of Physiology*, 585(3):843–852, 2007.

[53] Todd A. Fiacco and Ken D. McCarthy. Intracellular Astrocyte Calcium Waves In Situ Increase the Frequency of Spontaneous AMPA Receptor Currents in CA1 Pyramidal Neurons. *The Journal of Neuroscience*, 24(3):722–732, 2004.

[54] Denisa Belov Kirdajova, Jan Kriska, Jana Tureckova, and Miroslava Anderova. Ischemia-Triggered Glutamate Excitotoxicity From the Perspective of Glial Cells. *Frontiers in Cellular Neuroscience*, 14:51, 2020.

[55] Pauline Cavelier, Martine Hamann, David Rossi, Peter Mobbs, and David Attwell. Tonic excitation and inhibition of neurons: ambient transmitter sources and computational consequences. *Progress in Biophysics and Molecular Biology*, 87(1):3–16, 2005.

[56] Melissa A. Herman and Craig E. Jahr. Extracellular Glutamate Concentration in Hippocampal Slice. *The Journal of Neuroscience*, 27(36):9736–9741, 2007.

[57] Richard J. Bridges and C. Sean Esslinger. The excitatory amino acid transporters: Pharmacological insights on substrate and inhibitor specificity of the EAAT subtypes. *Pharmacology & Therapeutics*, 107(3):271–285, 2005.

[58] David Nicholls and David Attwell. The release and uptake of excitatory amino acids. *Trends in Pharmacological Sciences*, 11(11):462–468, 1990.

[59] Noa Zerangue and Michael P. Kavanaugh. Flux coupling in a neuronal glutamate transporter. *Nature*, 383(6601):634–637, 1996.

[60] Line M. Levy, Orpheus Warr, and David Attwell. Stoichiometry of the Glial Glutamate Transporter GLT-1 Expressed Inducibly in a Chinese Hamster Ovary Cell Line Selected for Low Endogenous Na+-Dependent Glutamate Uptake. *Journal of Neuroscience*, 18(23):9620–9628, 1998.

[61] L Pellerin and P J Magistretti. Glutamate uptake into astrocytes stimulates aerobic glycolysis: a mechanism coupling neuronal activity to glucose utilization. *Proceedings of the National Academy of Sciences*, 91(22):10625–10629, 1994.

[62] JeanYves Chatton, Pierre Marquet, and Pierre J. Magistretti. A quantitative analysis of lglutamateregulated Na+ dynamics in mouse cortical astrocytes: implications for cellular bioenergetics. *European Journal of Neuroscience*, 12(11):3843–3853, 2000.

[63] Mary C. McKenna. Glutamate Pays Its Own Way in Astrocytes. *Frontiers in Endocrinology*, 4:191, 2013.

[64] Tara Deemyad, Joel Lüthi, and Nelson Spruston. Astrocytes integrate and drive action potential firing in inhibitory subnetworks. *Nature Communications*, 9(1):4336, 2018.

[65] C R Rose and B R Ransom. Intracellular sodium homeostasis in rat hippocampal astrocytes. *The Journal of Physiology*, 491(2):291–305, 1996.

[66] I.A Silver, J Deas, and M Ereciska. Ion homeostasis in brain cells: differences in intracellular ion responses to energy limitation between cultured neurons and glial cells. *Neuroscience*, 78(2):589–601, 1997.

[67] Christine R. Rose, Stephen G. Waxman, and Bruce R. Ransom. Effects of Glucose Deprivation, Chemical Hypoxia, and Simulated Ischemia on Na+ Homeostasis in Rat Spinal Cord Astrocytes. *Journal of Neuroscience*, 18(10):3554–3562, 1998.

[68] M.C. Longuemare, C.R. Rose, K. Farrell, B.R. Ransom, S.G. Waxman, and R.A. Swanson. K+-induced reversal of astrocyte glutamate uptake is limited by compensatory changes in intracellular Na+. *Neuroscience*, 93(1):285–292, 1999.

[69] Pratap Karki, Eunsook Lee, and Michael Aschner. Manganese Neurotoxicity: a Focus on Glutamate Transporters. *Annals of Occupational and Environmental Medicine*, 25(1):4, 2013.

[70] Georgi Gegelashvili, Niels Christian Danbolt, and Arne Schousboe. Neuronal Soluble Factors Differentially Regulate the Expression of the GLT1 and GLAST Glutamate Transporters in Cultured Astroglia. *Journal of Neurochemistry*, 69(6):2612–2615, 1997.

[71] Jeffrey D. Rothstein, Lee Martin, Allan I. Levey, Margaret Dykes-Hoberg, Lin Jin, David Wu, Norman Nash, and Ralph W. Kuncl. Localization of neuronal and glial glutamate transporters. *Neuron*, 13(3):713–725, 1994.

[72] KP Lehre, LM Levy, OP Ottersen, J Storm-Mathisen, and NC Danbolt. Differential expression of two glial glutamate transporters in the rat brain: quantitative and immunocytochemical observations. *Journal of Neuroscience*, 15(3):1835–1853, 1995.

[73] Farrukh A. Chaudhry, Knut P. Lehre, Menno van Lookeren Campagne, Ole P. Ottersen, Niels C. Danbolt, and Jon Storm-Mathisen. Glutamate transporters in glial plasma membranes: Highly differentiated localizations revealed by quantitative ultrastructural immunocytochemistry. *Neuron*, 15(3):711–720, 1995.

[74] Angelika Schmitt, Esther Asan, Bernd Püschel, and Peter Kugler. Cellular and Regional Distribution of the Glutamate Transporter GLAST in the CNS of Rats: Nonradioactive In SituHybridization and Comparative Immunocytochemistry. *Journal of Neuroscience*, 17(1):1–10, 1997.

[75] Akiko Furuta, Jeffrey D. Rothstein, and Lee J. Martin. Glutamate Transporter Protein Subtypes Are Expressed Differentially during Rat CNS Development. *Journal of Neuroscience*, 17(21):8363–8375, 1997.

[76] F Conti, S DeBiasi, A Minelli, J D Rothstein, and M Melone. EAAC1, a high-affinity glutamate tranporter, is localized to astrocytes and gabaergic neurons besides pyramidal cells in the rat cerebral cortex. *Cerebral Cortex*, 8(2):108–116, 1998.

[77] Peter Kugler and Angelika Schmitt. Glutamate transporter EAAC1 is expressed in neurons and glial cells in the rat nervous system. *Glia*, 27(2):129–142, 1999.

[78] Yoshikatsu Kanai and Matthias A. Hediger. Primary structure and functional characterization of a high-affinity glutamate transporter. *Nature*, 360(6403):467–471, 1992.

[79] Silvia Holmseth, Yvette Dehnes, Yanhua H. Huang, Virginie V. Follin-Arbelet, Nina J. Grutle, Maria N. Mylonakou, Celine Plachez, Yun Zhou, David N. Furness, Dwight E. Bergles, Knut P. Lehre, and Niels C. Danbolt. The Density of EAAC1 (EAAT3) Glutamate Transporters Expressed by Neurons in the Mammalian CNS. *The Journal of Neuroscience*, 32(17):6000–6013, 2012.

[80] W. A. Fairman, R. J. Vandenberg, J. L. Arriza, M. P. Kavanaught, and S. G. Amara. An excitatory amino-acid transporter with properties of a ligand-gated chloride channel. *Nature*, 375(6532):599–603, 1995.

[81] Yvette Dehnes, Farrukh A. Chaudhry, Kyrre Ullensvang, Knut P. Lehre, Jon Storm-Mathisen, and Niels C. Danbolt. The Glutamate Transporter EAAT4 in Rat Cerebellar Purkinje Cells: A Glutamate-Gated Chloride Channel Concentrated near the Synapse in Parts of the Dendritic Membrane Facing Astroglia. *Journal of Neuroscience*, 18(10):3606–3619, 1998.

[82] Ann Massie, Frans Vandesande, and Lutgarde Arckens. Expression of the high-affinity glutamate transporter EAAT4 in mammalian cerebral cortex. *Neuroreport*, 12(2):393–397, 2001.

[83] Ann Massie, Lieselotte Cnops, Ilse Smolders, Robert McCullumsmith, Ron Kooijman, Shin Kwak, Lutgarde Arckens, and Yvette Michotte. Highaffinity Na+/K+dependent glutamate transporter EAAT4 is expressed throughout the rat fore and midbrain. *Journal of Comparative Neurology*, 511(2):155–172, 2008.

[84] S Nagao, S Kwak, and I Kanazawa. Correspondence. *Neuroscience*, 78(4):929–933, 1997.

[85] Kohichi Tanaka, Kei Watase, Toshiya Manabe, Keiko Yamada, Masahiko Watanabe, Katsunobu Takahashi, Hisayuki Iwama, Toru Nishikawa, Nobutsune Ichihara, Tateki Kikuchi, Shigeru Okuyama, Naoya Kawashima, Seiji Hori, Misato Takimoto, and Keiji Wada. Epilepsy and Exacerbation of Brain Injury in Mice Lacking the Glutamate Transporter GLT-1. *Science*, 276(5319):1699–1702, 1997.

[86] Jeffrey L. Arriza, Scott Eliasof, Michael P. Kavanaugh, and Susan G. Amara. Excitatory amino acid transporter 5, a retinal glutamate transporter coupled to a chlorideconductance. *Proceedings of the National Academy of Sciences*, 94(8):4155–4160, 1997.

[87] David V. Pow and Nigel L. Barnett. Developmental expression of excitatory amino acid transporter 5: a photoreceptor and bipolar cell glutamate transporter in rat retina. *Neuroscience Letters*, 280(1):21–24, 2000.

[88] Nicole Schneider, Sönke Cordeiro, Jan-Philipp Machtens, Simona Braams, Thomas Rauen, and Christoph Fahlke. Functional Properties of the Retinal Glutamate Transporters GLT-1c and EAAT5* * These studies were supported by the Deutsche

Forschungs-gemeinschaft FA301/9 (to Ch. F.). *Journal of Biological Chemistry*, 289(3):1815–1824, 2014.

[89] Eric Wersinger, Yannick Schwab, JoséAlain Sahel, Alvaro Rendon, David V. Pow, Serge Picaud, and Michel J. Roux. The glutamate transporter EAAT5 works as a presynaptic receptor in mouse rod bipolar cells. *The Journal of Physiology*, 577(1):221–234, 2006.

[90] Carsten Mim, Poonam Balani, Thomas Rauen, and Christof Grewer. The Glutamate Transporter Subtypes EAAT4 and EAATs 1-3 Transport Glutamate with Dramatically Different Kinetics and Voltage Dependence but Share a Common Uptake Mechanism. *The Journal of General Physiology*, 126(6):571–589, 2005.

[91] Margaret Lin Veruki, Svein Harald Mørkve, and Espen Hartveit. Activation of a presynaptic glutamate transporter regulates synaptic transmission through electrical signaling. *Nature Neuroscience*, 9(11):1388–1396, 2006.

[92] Armanda Gameiro, Simona Braams, Thomas Rauen, and Christof Grewer. The Discovery of Slowness: Low-Capacity Transport and Slow Anion Channel Gating by the Glutamate Transporter EAAT5. *Biophysical Journal*, 100(11):2623–2632, 2011.

[93] Gregory P. Leary, Emily F. Stone, David C. Holley, and Michael P. Kavanaugh. The Glutamate and Chloride Permeation Pathways Are Colocalized in Individual Neuronal Glutamate Transporter Subunits. *The Journal of Neuroscience*, 27(11):2938–2942, 2007.

[94] JD Clements, RA Lester, G Tong, CE Jahr, and GL Westbrook. The time course of glutamate in the synaptic cleft. *Science*, 258(5087):1498–1501, 1992.

[95] Douglas L. Rothman, Henk M. De Feyter, Robin A. Graaf, Graeme F. Mason, and Kevin L. Behar. 13C MRS studies of neuroenergetics and neurotransmitter cycling in humans. *NMR in Biomedicine*, 24(8):943–957, 2011.

[96] Michael D. Norenberg and Antonio Martinez-Hernandez. Fine structural localization of glutamine synthetase in astrocytes of rat brain. *Brain Research*, 161(2):303–310, 1979.

[97] David J. Rossi, Takeo Oshima, and David Attwell. Glutamate release in severe brain ischaemia is mainly by reversed uptake. *Nature*, 403(6767):316–321, 2000.

[98] Albert C. Yu, Arne Schousboec, and Leif Hertz. Metabolic Fate of 14CLabeled Glutamate in Astrocytes in Primary Cultures. *Journal of Neurochemistry*, 39(4):954–960, 1982.

[99] Stephen E. Farinelli and William J. Nicklas. Glutamate Metabolism in Rat Cortical Astrocyte Cultures. *Journal of Neurochemistry*, 58(5):1905–1915, 1992.

[100] Mary C. McKenna, Ursula Sonnewald, Xueli Huang, Joseph Stevenson, and H. Ronald Zielke. Exogenous Glutamate Concentration Regulates the Metabolic Fate of Glutamate in Astrocytes. *Journal of Neurochemistry*, 66(1):386–393, 1996.

[101] Ursula Sonnewald, Niels Westergaard, and Arne Schousboe. Glutamate transport and metabolism in astrocytes. *Glia*, 21(1):56–63, 1997.

[102] Leif Hertz, Ralf Dringen, Arne Schousboe, and Stephen R. Robinson. Astrocytes: Glutamate producers for neurons. *Journal of Neuroscience Research*, 57(4):417–428, 1999.

[103] Dwight E Bergles, Jeffrey S Diamond, and Craig E Jahr. Clearance of glutamate inside the synapse and beyond. *Current Opinion in Neurobiology*, 9(3):293–298, 1999.

[104] Yosra Trabelsi, Mohamed Amri, Hélène Becq, Florence Molinari, and Laurent Aniksztejn. The conversion of glutamate by glutamine synthase in neocortical astrocytes from juvenile rat is important to limit glutamate spillover and peri/extrasynaptic activation of NMDA receptors. *Glia*, 65(2):401–415, 2017.

[105] Arne Schousboe, Lasse K. Bak, and Helle S. Waagepetersen. Astrocytic Control of Biosynthesis and Turnover of the Neurotransmitters Glutamate and GABA. *Frontiers in Endocrinology*, 4:102, 2013.

[106] Alison C. Todd, MariCarmen Marx, Sarah R. Hulme, Stefan Bröer, and Brian Billups. SNAT3mediated glutamine transport in perisynaptic astrocytes in situ is regulated by intracellular sodium. *Glia*, 65(6):900–916, 2017.

[107] Nneka M. Uwechue, MariCarmen Marx, Quentin Chevy, and Brian Billups. Activation of glutamate transport evokes rapid glutamine release from perisynaptic astrocytes. *The Journal of Physiology*, 590(10):2317–2331, 2012.

[108] Elizabeth N. Genda, Joshua G. Jackson, Amanda L. Sheldon, Susannah F. Locke, Todd M. Greco, John C. O'Donnell, Lynn A. Spruce, Rui Xiao, Wensheng Guo, Mary Putt, Steven Seeholzer, Harry Ischiropoulos, and Michael B. Robinson. Co-compartmentalization of the Astroglial Glutamate Transporter, GLT-1, with Glycolytic Enzymes and Mitochondria. *The Journal of Neuroscience*, 31(50):18275–18288, 2011.

[109] Joshua G. Jackson, John C. O'Donnell, Hajime Takano, Douglas A. Coulter, and Michael B. Robinson. Neuronal Activity and Glutamate Uptake Decrease Mitochondrial Mobility in Astrocytes and Position Mitochondria Near Glutamate Transporters. *The Journal of Neuroscience*, 34(5):1613–1624, 2014.

[110] Niels C Danbolt. Glutamate uptake. *Progress in Neurobiology*, 65(1):1–105, 2001.

[111] Knut P. Lehre and Niels C. Danbolt. The Number of Glutamate Transporter Subtype Molecules at Glutamatergic Synapses: Chemical and Stereological Quantification in Young Adult Rat Brain. *Journal of Neuroscience*, 18(21):8751–8757, 1998.

[112] A Mitani and K Tanaka. Functional changes of glial glutamate transporter GLT-1 during ischemia: an in vivo study in the hippocampal CA1 of normal mice and mutant mice lacking GLT-1. *Journal of Neuroscience*, 23(18):7176 7182, 2003.

[113] Chihiro Takasaki, Rieko Okada, Akira Mitani, Masahiro Fukaya, Miwako Yamasaki, Yuri Fujihara, Tetsuo Shirakawa, Kohichi Tanaka, and Masahiko Watanabe. Glutamate Transporters Regulate Lesion-Induced Plasticity in the Developing Somatosensory Cortex. *The Journal of Neuroscience*, 28(19):4995–5006, 2008.

[114] Julie V. Selkirk, Lisa M. Nottebaum, Alicia M. Vana, Gail M. Verge, Kenneth B. Mackay, Theodore H. Stiefel, Greg S. Naeve, Jordan E. Pomeroy, Robert E. Petroski, John Moyer, John Dunlop, and Alan C. Foster. Role of the GLT1 subtype of glutamate transporter in glutamate homeostasis: the GLT1preferring inhibitor WAY855 produces marginal neurotoxicity in the rat hippocampus. *European Journal of Neuroscience*, 21(12):3217–3228, 2005.

[115] Hiroyuki Katagiri, Kohichi Tanaka, and Toshiya Manabe. Requirement of appropriate glutamate concentrations in the synaptic cleft for hippocampal LTP induction. *European Journal of Neuroscience*, 14(3):547–553, 2001.

[116] Azar Omrani, Marcello Melone, Michele Bellesi, Victoria Safiulina, Tomomi Aida, Kohishi Tanaka, Enrico Cherubini, and Fiorenzo Conti. Upregulation of GLT1 severely impairs LTD at mossy fibreCA3 synapses. *The Journal of Physiology*, 587(19):4575–4588, 2009.

[117] Geraldine T. Petr, Yan Sun, Natalie M. Frederick, Yun Zhou, Sameer C. Dhamne, Mustafa Q. Hameed, Clive Miranda, Edward A. Bedoya, Kathryn D. Fischer, Wencke Armsen, Jianlin Wang, Niels C. Danbolt, Alexander Rotenberg, Chiye J. Aoki, and Paul A. Rosenberg. Conditional Deletion of the Glutamate Transporter GLT-1 Reveals That Astrocytic GLT-1 Protects against Fatal Epilepsy While Neu-

ronal GLT-1 Contributes Significantly to Glutamate Uptake into Synaptosomes. *The Journal of Neuroscience*, 35(13):5187–5201, 2015.

[118] Kei Watase, Kouichi Hashimoto, Masanobu Kano, Keiko Yamada, Masahiko Watanabe, Yoshiro Inoue, Shigeru Okuyama, Takashi Sakagawa, Shinichi Ogawa, Naoya Kawashima, Seiji Hori, Misato Takimoto, Keiji Wada, and Kohichi Tanaka. Motor discoordination and increased susceptibility to cerebellar injury in GLAST mutant mice. *European Journal of Neuroscience*, 10(3):976–988, 1998.

[119] Rose-Marie Karlsson, Kohichi Tanaka, Markus Heilig, and Andrew Holmes. Loss of Glial Glutamate and Aspartate Transporter (Excitatory Amino Acid Transporter 1) Causes Locomotor Hyperactivity and Exaggerated Responses to Psychotomimetics: Rescue by Haloperidol and Metabotropic Glutamate 2/3 Agonist. *Biological Psychiatry*, 64(9):810–814, 2008.

[120] S. Holmseth, H.A. Scott, K. Real, K.P. Lehre, T.B. Leergaard, J.G. Bjaalie, and N.C. Danbolt. The concentrations and distributions of three C-terminal variants of the GLT1 (EAAT2; slc1a2) glutamate transporter protein in rat brain tissue suggest differential regulation. *Neuroscience*, 162(4):1055–1071, 2009.

[121] Florian M. Gebhardt, Ann D. Mitrovic, Daniel F. Gilbert, Robert J. Vandenberg, Joseph W. Lynch, and Peter R. Dodd. Exon-skipping Splice Variants of Excitatory Amino Acid Transporter-2 (EAAT2) Form Heteromeric Complexes with Full-length EAAT2*. *Journal of Biological Chemistry*, 285(41):31313–31324, 2010.

[122] Inmaculada M. GonzálezGonzález, Noemí GarcíaTardón, Cecilio Giménez, and Francisco Zafra. Splice variants of the glutamate transporter GLT1 form hetero oligomers that interact with PSD95 and NMDA receptors. *Journal of Neurochemistry*, 110(1):264–274, 2009.

[123] Inmaculada M. GonzálezGonzález, Noemí GarcíaTardón, Beatriz Cubelos, Cecilio Giménez, and Francisco Zafra. The glutamate transporter GLT1b interacts with the scaffold protein PSD95. *Journal of Neurochemistry*, 105(5):1834–1848, 2008.

[124] Merav Bassan, Hongguang Liu, Kenneth L. Madsen, Wencke Armsen, Jiayi Zhou, Tara DeSilva, Weizhi Chen, Allison Paradise, Michael A. Brasch, Jeff Staudinger, Ulrik Gether, Nina Irwin, and Paul A. Rosenberg. Interaction between the glutamate transporter GLT1b and the synaptic PDZ domain protein PICK1. *European Journal of Neuroscience*, 27(1):66–82, 2008.

[125] Suzanne M. Underhill, David S. Wheeler, and Susan G. Amara. Differential Regulation of Two Isoforms of the Glial Glutamate Transporter EAAT2 by DLG1 and CaMKII. *The Journal of Neuroscience*, 35(13):5260–5270, 2015.

[126] T. Rauen, J. D. Rothstein, and H. Wässle. Differential expression of three glutamate transporter subtypes in the rat retina. *Cell and Tissue Research*, 286(3):325–336, 1996.

[127] Weizhi Chen, Veeravan Mahadomrongkul, Urs V. Berger, Merav Bassan, Tara DeSilva, Kohichi Tanaka, Nina Irwin, Chiye Aoki, and Paul A. Rosenberg. The Glutamate Transporter GLT1a Is Expressed in Excitatory Axon Terminals of Mature Hippocampal Neurons. *The Journal of Neuroscience*, 24(5):1136–1148, 2004.

[128] Urs V. Berger, Tara M. DeSilva, Weizhi Chen, and Paul A. Rosenberg. Cellular and subcellular mRNA localization of glutamate transporter isoforms GLT1a and GLT1b in rat brain by in situ hybridization. *Journal of Comparative Neurology*, 492(1):78–89, 2005.

[129] D.N. Furness, Y. Dehnes, A.Q. Akhtar, D.J. Rossi, M. Hamann, N.J. Grutle, V. Gundersen, S. Holmseth, K.P. Lehre, K. Ullensvang, M. Wojewodzic, Y. Zhou, D. Attwell, and N.C. Danbolt. A quantitative assessment of glutamate uptake into hip-

pocampal synaptic terminals and astrocytes: New insights into a neuronal role for excitatory amino acid transporter 2 (EAAT2). *Neuroscience*, 157(1):80–94, 2008.

[130] Adrienne M. Benediktsson, Glen S. Marrs, Jian Cheng Tu, Paul F. Worley, Jeffrey D. Rothstein, Dwight E. Bergles, and Michael E. Dailey. Neuronal activity regulates glutamate transporter dynamics in developing astrocytes. *Glia*, 60(2):175–188, 2012.

[131] Raymond A. Swanson, Jialing Liu, Johann W. Miller, Jeffrey D. Rothstein, Kevin Farrell, Becky A. Stein, and Maria C. Longuemare. Neuronal Regulation of Glutamate Transporter Subtype Expression in Astrocytes. *Journal of Neuroscience*, 17(3):932–940, 1997.

[132] Christel Genoud, Charles Quairiaux, Pascal Steiner, Harald Hirling, Egbert Welker, and Graham W Knott. Plasticity of Astrocytic Coverage and Glutamate Transporter Expression in Adult Mouse Cortex. *PLoS Biology*, 4(11):e343, 2006.

[133] Mausam Ghosh, Yongjie Yang, Jeffrey D. Rothstein, and Michael B. Robinson. Nuclear Factor-B Contributes to Neuron-Dependent Induction of Glutamate Transporter-1 Expression in Astrocytes. *The Journal of Neuroscience*, 31(25):9159–9169, 2011.

[134] Carol L. PoitryYamate, Laszlo Vutskits, and Thomas Rauen. Neuronalinduced and glutamatedependent activation of glial glutamate transporter function. *Journal of Neurochemistry*, 82(4):987–997, 2002.

[135] Edward Pajarillo, Asha Rizor, Jayden Lee, Michael Aschner, and Eunsook Lee. The role of astrocytic glutamate transporters GLT-1 and GLAST in neurological disorders: potential targets for neurotherapeutics. *Neuropharmacology*, 161:107559, 2019.

[136] Yoo Sung Kim, Juwon Choi, and Bo-Eun Yoon. Neuron-Glia Interactions in Neurodevelopmental Disorders. *Cells*, 9(10):2176, 2020.

[137] Annamaria Lanzillotta, Vanessa Porrini, Arianna Bellucci, Marina Benarese, Caterina Branca, Edoardo Parrella, Pier Franco Spano, and Marina Pizzi. NF-B in Innate Neuroprotection and Age-Related Neurodegenerative Diseases. *Frontiers in Neurology*, 6:98, 2015.

[138] Stefan Raunser, Winfried Haase, Cornelia Franke, Gunter P. Eckert, Walter E. Müller, and Werner Kühlbrandt. Heterologously Expressed GLT-1 Associates in 200-nm Protein-Lipid Islands. *Biophysical Journal*, 91(10):3718–3726, 2006.

[139] Jianzheng Zhou and Margaret L. Sutherland. Glutamate Transporter Cluster Formation in Astrocytic Processes Regulates Glutamate Uptake Activity. *The Journal of Neuroscience*, 24(28):6301–6306, 2004.

[140] Ciaran Murphy-Royal, Julien P Dupuis, Juan A Varela, Aude Panatier, Benoît Pinson, Jérôme Baufreton, Laurent Groc, and Stéphane H R Oliet. Surface diffusion of astrocytic glutamate transporters shapes synaptic transmission. *Nature Neuroscience*, 18(2):219–226, 2015.

[141] Matthew E.R. Butchbach, Guilian Tian, Hong Guo, and Chien-liang Glenn Lin. Association of Excitatory Amino Acid Transporters, Especially EAAT2, with Cholesterol-rich Lipid Raft Microdomains IMPORTANCE FOR EXCITATORY AMINO ACID TRANSPORTER LOCALIZATION AND FUNCTION*. *Journal of Biological Chemistry*, 279(33):34388–34396, 2004.

[142] Robert Sullivan, Thomas Rauen, Frauke Fischer, Michael WieSSner, Christof Grewer, Ana Bicho, and David V. Pow. Cloning, transport properties, and differential localization of two splice variants of GLT1 in the rat CNS: Implications for CNS glutamate homeostasis. *Glia*, 45(2):155–169, 2004.

[143] Sana Al Awabdh, Swati GuptaAgarwal, David F. Sheehan, James Muir, Rosalind Norkett, Alison E. Twelvetrees, Lewis D. Griffin, and Josef T. Kittler. Neuronal

activity mediated regulation of glutamate transporter GLT1 surface diffusion in rat astrocytes in dissociated and slice cultures. *Glia*, 64(7):1252–1264, 2016.

[144] Nancy Ann Oberheim, Takahiro Takano, Xiaoning Han, Wei He, Jane H. C. Lin, Fushun Wang, Qiwu Xu, Jeffrey D. Wyatt, Webster Pilcher, Jeffrey G. Ojemann, Bruce R. Ransom, Steven A. Goldman, and Maiken Nedergaard. Uniquely Hominid Features of Adult Human Astrocytes. *The Journal of Neuroscience*, 29(10):3276–3287, 2009.

[145] Nikolai Medvedev, Victor Popov, Christian Henneberger, Igor Kraev, Dmitri A. Rusakov, and Michael G. Stewart. Glia selectively approach synapses on thin dendritic spines. *Philosophical Transactions of the Royal Society B: Biological Sciences*, 369(1654):20140047, 2014.

[146] Yann Bernardinelli, Jerome Randall, Elia Janett, Irina Nikonenko, Stéphane König, EmmaăVictoria Jones, CarmenăE. Flores, KeithăK. Murai, ChristianăG. Bochet, Anthony Holtmaat, and Dominique Muller. Activity-Dependent Structural Plasticity of Perisynaptic Astrocytic Domains Promotes Excitatory Synapse Stability. *Current Biology*, 24(15):1679–1688, 2014.

[147] Andreas Reichenbach, Amin Derouiche, and Frank Kirchhoff. Morphology and dynamics of perisynaptic glia. *Brain Research Reviews*, 63(1-2):11–25, 2010.

[148] Amin Derouiche and Michael Frotscher. Peripheral astrocyte processes: Monitoring by selective immunostaining for the actinbinding ERM proteins. *Glia*, 36(3):330–341, 2001.

[149] Dmitry Molotkov, Svetlana Zobova, Jose Miguel Arcas, and Leonard Khiroug. Calcium-induced outgrowth of astrocytic peripheral processes requires actin binding by Profilin-1. *Cell Calcium*, 53(5-6):338–348, 2013.

[150] Sam SafaviAbbasi, Joachim R. Wolff, and Markus Missler. Rapid morphological changes in astrocytes are accompanied by redistribution but not by quantitative changes of cytoskeletal proteins. *Glia*, 36(1):102–115, 2001.

[151] Bert Seidel, Werner Zuschratter, Heike Wex, Craig C. Garner, and Eckart D. Gundelfinger. Spatial and sub-cellular localization of the membrane cytoskeleton-associated protein -adducin in the rat brain. *Brain Research*, 700(1-2):13–24, 1995.

[152] Monique Lavialle, Georg Aumann, Enrico Anlauf, Felicitas Pröls, Monique Arpin, and Amin Derouiche. Structural plasticity of perisynaptic astrocyte processes involves ezrin and metabotropic glutamate receptors. *Proceedings of the National Academy of Sciences*, 108(31):12915–12919, 2011.

[153] Dionysia T. Theodosis. Oxytocin-Secreting Neurons: A Physiological Model of Morphological Neuronal and Glial Plasticity in the Adult Hypothalamus. *Frontiers in Neuroendocrinology*, 23(1):101–135, 2002.

[154] Øyvind Haugeto, Kyrre Ullensvang, Line M. Levy, Farrukh A. Chaudhry, Tage Honoré, Mogens Nielsen, Knut P. Lehre, and Niels C. Danbolt. Brain Glutamate Transporter Proteins Form Homomultimers*. *Journal of Biological Chemistry*, 271(44):27715–27722, 1996.

[155] Mark R. Witcher, Sergei A. Kirov, and Kristen M. Harris. Plasticity of perisynaptic astroglia during synaptogenesis in the mature rat hippocampus. *Glia*, 55(1):13–23, 2007.

[156] Rachel Ventura and Kristen M. Harris. Three-Dimensional Relationships between Hippocampal Synapses and Astrocytes. *Journal of Neuroscience*, 19(16):6897–6906, 1999.

[157] Knut Petter Lehre and Dmitri A. Rusakov. Asymmetry of Glia near Central Synapses Favors Presynaptically Directed Glutamate Escape. *Biophysical Journal*, 83(1):125–134, 2002.

[158] Astrid Rollenhagen, Kurt Sätzler, E. Patricia Rodríguez, Peter Jonas, Michael Frotscher, and Joachim H. R. Lübke. Structural Determinants of Transmission at Large Hippocampal Mossy Fiber Synapses. *The Journal of Neuroscience*, 27(39):10434–10444, 2007.

[159] Mark R. Witcher, Yong D. Park, Mark R. Lee, Suash Sharma, Kristen M. Harris, and Sergei A. Kirov. Threedimensional relationships between perisynaptic astroglia and human hippocampal synapses. *Glia*, 58(5):572–587, 2010.

[160] Irina Lushnikova, Galina Skibo, Dominique Muller, and Irina Nikonenko. Synaptic potentiation induces increased glial coverage of excitatory synapses in CA1 hippocampus. *Hippocampus*, 19(8):753–762, 2009.

[161] Garrick Salois and Jeffrey S. Smith. Housing Complexity Alters GFAP-Immunoreactive Astrocyte Morphology in the Rat Dentate Gyrus. *Neural Plasticity*, 2016:1–11, 2016.

[162] Lisiani Saur, Pedro Porto Alegre Baptista, Priscylla Nunes de Senna, Mariana Fontoura Paim, Patricia do Nascimento, Jocemar Ilha, Pamela Brambilla Bagatini, Matilde Achaval, and Léder Leal Xavier. Physical exercise increases GFAP expression and induces morphological changes in hippocampal astrocytes. *Brain Structure and Function*, 219(1):293–302, 2014.

[163] P. Sampedro-Piquero, Paola De Bartolo, Laura Petrosini, C. Zancada-Menendez, J.L. Arias, and A. Begega. Astrocytic plasticity as a possible mediator of the cognitive improvements after environmental enrichment in aged rats. *Neurobiology of Learning and Memory*, 114:16–25, 2014.

[164] Alexander Popov, Pavel Denisov, Maxim Bychkov, Alexey Brazhe, Ekaterina Lyukmanova, Zakhar Shenkarev, Natalia Lazareva, Alexei Verkhratsky, and Alexey Semyanov. Caloric restriction triggers morphofunctional remodeling of astrocytes and enhances synaptic plasticity in the mouse hippocampus. *Cell Death & Disease*, 11(3):208, 2020.

[165] AH Cornell-Bell, SM Finkbeiner, MS Cooper, and SJ Smith. Glutamate induces calcium waves in cultured astrocytes: long-range glial signaling. *Science*, 247(4941):470–473, 1990.

[166] Mika Tanaka, Pei-Yu Shih, Hiroshi Gomi, Takamasa Yoshida, Junichi Nakai, Reiko Ando, Teiichi Furuichi, Katsuhiko Mikoshiba, Alexey Semyanov, and Shigeyoshi Itohara. Astrocytic Ca2+ signals are required for the functional integrity of tripartite synapses. *Molecular Brain*, 6(1):6, 2013.

[167] Alberto Perez-Alvarez, Marta Navarrete, Ana Covelo, Eduardo D. Martin, and Alfonso Araque. Structural and Functional Plasticity of Astrocyte Processes and Dendritic Spine Interactions. *The Journal of Neuroscience*, 34(38):12738–12744, 2014.

[168] Michel K. Herde, Kirsten Bohmbach, Cátia Domingos, Natascha Vana, Joanna A. Komorowska-Müller, Stefan Passlick, Inna Schwarz, Colin J. Jackson, Dirk Dietrich, Martin K. Schwarz, and Christian Henneberger. Local Efficacy of Glutamate Uptake Decreases with Synapse Size. *Cell Reports*, 32(12):108182, 2020.

[169] Arne Schousboe, Susanna Scafidi, Lasse K. Bak, Helle S. Waagepetersen, and Mary C. McKenna. Glutamate and ATP at the Interface of Metabolism and Signaling in the Brain. *Advances in Neurobiology*, 11:13–30, 2014.

[170] Jeffrey D Rothstein, Margaret Dykes-Hoberg, Carlos A Pardo, Lynn A Bristol, Lin Jin, Ralph W Kuncl, Yoshikatsu Kanai, Matthias A Hediger, Yanfeng Wang, Jerry P Schielke, and Devin F Welty. Knockout of Glutamate Transporters Reveals a Major

Role for Astroglial Transport in Excitotoxicity and Clearance of Glutamate. *Neuron*, 16(3):675–686, 1996.

[171] A Minelli, P Barbaresi, R.J Reimer, R.H Edwards, and F Conti. The glial glutamate transporter GLT-1 is localized both in the vicinity of and at distance from axon terminals in the rat cerebral cortex. *Neuroscience*, 108(1):51–59, 2001.

[172] Takayuki Nakagawa, Yasuto Otsubo, Yumi Yatani, Hisashi Shirakawa, and Shuji Kaneko. Mechanisms of substrate transportinduced clustering of a glial glutamate transporter GLT1 in astroglialneuronal cultures. *European Journal of Neuroscience*, 28(9):1719–1730, 2008.

[173] Jeffrey S. Diamond. Deriving the Glutamate Clearance Time Course from Transporter Currents in CA1 Hippocampal Astrocytes: Transmitter Uptake Gets Faster during Development. *The Journal of Neuroscience*, 25(11):2906–2916, 2005.

[174] Steven Mennerick and Charles F. Zorumski. Glial contributions to excitatory neurotransmission in cultured hippocampal cells. *Nature*, 368(6466):59–62, 1994.

[175] Jeffrey S. Diamond and Craig E. Jahr. Transporters Buffer Synaptically Released Glutamate on a Submillisecond Time Scale. *Journal of Neuroscience*, 17(12):4672–4687, 1997.

[176] Boris Barbour, Bernhard U. Keller, Isabel Llano, and Alain Marty. Prolonged presence of glutamate during excitatory synaptic transmission to cerebellar Purkinje cells. *Neuron*, 12(6):1331–1343, 1994.

[177] Gang Tong and Craig E. Jahr. Block of glutamate transporters potentiates postsynaptic excitation. *Neuron*, 13(5):1195–1203, 1994.

[178] Linda S. Overstreet, Gregory A. Kinney, Ying-Bing Liu, Daniela Billups, and N. Traverse Slater. Glutamate Transporters Contribute to the Time Course of Synaptic

Transmission in Cerebellar Granule Cells. *Journal of Neuroscience*, 19(21):9663–9673, 1999.

[179] Jeffrey S. Diamond and Craig E. Jahr. Synaptically Released Glutamate Does Not Overwhelm Transporters on Hippocampal Astrocytes During High-Frequency Stimulation. *Journal of Neurophysiology*, 83(5):2835–2843, 2000.

[180] Thomas S. Otis and Craig E. Jahr. Anion Currents and Predicted Glutamate Flux through a Neuronal Glutamate Transporter. *Journal of Neuroscience*, 18(18):7099–7110, 1998.

[181] Jacques I Wadiche, Jeffrey L Arriza, Susan G Amara, and Michael P Kavanaugh. Kinetics of a human glutamate transporter. *Neuron*, 14(5):1019–1027, 1995.

[182] Dwight E. Bergles, Jeffrey A. Dzubay, and Craig E. Jahr. Glutamate transporter currents in Bergmann glial cells follow the time course of extrasynapticglutamate. *Proceedings of the National Academy of Sciences*, 94(26):14821–14825, 1997.

[183] J Du, J.-H Tao-Cheng, P Zerfas, and C.J McBain. The K+ channel, Kv2.1, is apposed to astrocytic processes and is associated with inhibitory postsynaptic membranes in hippocampal and cortical principal neurons and inhibitory interneurons. *Neuroscience*, 84(1):37–48, 1998.

[184] Hiroaki Misonou, Scott M. Thompson, and Xiang Cai. Dynamic Regulation of the Kv2.1 Voltage-Gated Potassium Channel during Brain Ischemia through Neuroglial Interaction. *The Journal of Neuroscience*, 28(34):8529–8538, 2008.

[185] Patrick J. Mulholland, Ezekiel P. Carpenter-Hyland, Matthew C. Hearing, Howard C. Becker, John J. Woodward, and L. Judson Chandler. Glutamate Transporters Regulate Extrasynaptic NMDA Receptor Modulation of Kv2.1 Potassium Channels. *The Journal of Neuroscience*, 28(35):8801–8809, 2008.

[186] Csaba Cserép, Balázs Pósfai, Nikolett Lénárt, Rebeka Fekete, Zsófia I. László, Zsolt Lele, Barbara Orsolits, Gábor Molnár, Steffanie Heindl, Anett D. Schwarcz, Katinka Ujvári, Zsuzsanna Környei, Krisztina Tóth, Eszter Szabadits, Beáta Sperlágh, Mária Baranyi, László Csiba, Tibor Hortobágyi, Zsófia Maglóczky, Bernadett Martinecz, Gábor Szabó, Ferenc Erdélyi, Róbert Szipcs, Michael M. Tamkun, Benno Gesierich, Marco Duering, István Katona, Arthur Liesz, Gábor Tamás, and Ádám Dénes. Microglia monitor and protect neuronal function through specialized somatic purinergic junctions. *Science*, 367(6477):528–537, 2020.

[187] Paul M. Hwang, Charles E. Glatt, David S. Bredt, Gary Yellen, and Solomon H. Snyder. A novel K+ channel with unique localizations in mammalian brain: Molecular cloning and characterization. *Neuron*, 8(3):473–481, 1992.

[188] Elizabeth A. L. Muennich and R. E. W. Fyffe. Focal aggregation of voltagegated, Kv2.1 subunitcontaining, potassium channels at synaptic sites in rat spinal motoneurones. *The Journal of Physiology*, 554(3):673–685, 2004.

[189] Hannah I. Bishop, Dongxu Guan, Elke Bocksteins, Laxmi Kumar Parajuli, Karl D. Murray, Melanie M. Cobb, Hiroaki Misonou, Karen Zito, Robert C. Foehring, and James S. Trimmer. Distinct Cell- and Layer-Specific Expression Patterns and Independent Regulation of Kv2 Channel Subtypes in Cortical Pyramidal Neurons. *The Journal of Neuroscience*, 35(44):14922–14942, 2015.

[190] PM Hwang, M Fotuhi, DS Bredt, AM Cunningham, and SH Snyder. Contrasting immunohistochemical localizations in rat brain of two novel K+ channels of the Shab subfamily. *Journal of Neuroscience*, 13(4):1569–1576, 1993.

[191] P.M. Hwang, A.M. Cunningham, Y.W. Peng, and S.H. Snyder. CDRK and DRK1 K+ channels have contrasting localizations in sensory systems. *Neuroscience*, 55(3):613–620, 1993.

[192] Stephen Yazulla and Keith M. Studholme. Differential distribution of Shakerlike and Shablike K+channel subunits in goldfish retina and retinal bipolar cells. *Journal of Comparative Neurology*, 396(1):131–140, 1998.

[193] Kristen M. S. O'Connell, Jennifer D. Whitesell, and Michael M. Tamkun. Localization and mobility of the delayed-rectifer K+ channel Kv2.1 in adult cardiomyocytes. *American Journal of Physiology-Heart and Circulatory Physiology*, 294(1):H229–H237, 2008.

[194] Gregory C. Amberg and Luis F. Santana. Kv2 channels oppose myogenic constriction of rat cerebral arteries. *American Journal of Physiology-Cell Physiology*, 291(2):C348–C356, 2006.

[195] Samantha C. ODwyer, Stephanie Palacio, Collin Matsumoto, Laura Guarina, Nicholas R. Klug, Sendoa Tajada, Barbara Rosati, David McKinnon, James S. Trimmer, and L. Fernando Santana. Kv2.1 channels play opposing roles in regulating membrane potential, Ca2+ channel function, and myogenic tone in arterial smooth muscle. *Proceedings of the National Academy of Sciences*, 117(7):3858–3866, 2020.

[196] Jianyang Fu, Xiaoqing Dai, Gregory Plummer, Kunimasa Suzuki, Mette Jensen, Dafna Greitzer-Antes, Jocelyn E. Manning Fox, Herbert Y. Gaisano, Christopher B. Newgard, and Patrick E. Macdonald. 33 Kv2.1 Clustering Contributes to Exocytosis Hotspots and Rescues Human -Cell Dysfunction. *Canadian Journal of Diabetes*, 41(5):S11–S12, 2017.

[197] Jianyang Fu, Xiaoqing Dai, Gregory Plummer, Kunimasa Suzuki, Austin Bautista, John M Githaka, Laura Senior, Mette Jensen, Dafna Greitzer-Antes, Jocelyn E Manning Fox, Herbert Y Gaisano, Christopher B Newgard, Nicolas Touret, and Patrick E MacDonald. Kv2.1 Clustering Contributes to Insulin Exocytosis and Rescues Human -Cell Dysfunction. *Diabetes*, 66(7):1890–1900, 2017.

[198] Dafna Greitzer-Antes, Li Xie, Tairan Qin, Huanli Xie, Dan Zhu, Subhankar Dolai, Tao Liang, Fei Kang, Alexandre B. Hardy, Yan He, Youhou Kang, and Herbert Y. Gaisano. Kv2.1 clusters on -cell plasma membrane act as reservoirs that replenish pools of newcomer insulin granule through their interaction with syntaxin-3. *Journal of Biological Chemistry*, 293(18):6893–6904, 2018.

[199] Patrick E. MacDonald. Signal integration at the level of ion channel and exocytotic function in pancreatic -cells. *American Journal of Physiology-Endocrinology and Metabolism*, 301(6):E1065–E1069, 2011.

[200] Masashi Yoshida, Masanori Nakata, Shiho Yamato, Katsuya Dezaki, Hitoshi Sugawara, San-e Ishikawa, Masanobu Kawakami, Toshihiko Yada, and Masafumi Kakei. Voltage-dependent metabolic regulation of Kv2.1 channels in pancreatic -cells. *Biochemical and Biophysical Research Communications*, 396(2):304–309, 2010.

[201] A. Scholle, S. Dugarmaa, T. Zimmer, M. Leonhardt, R. Koopmann, B. Engeland, O. Pongs, and K. Benndorf. Rate-limiting Reactions Determining Different Activation Kinetics of Kv1.2and Kv2.1 Channels. *The Journal of Membrane Biology*, 198(2):103–112, 2004.

[202] Hideyuki Murakoshi and James S. Trimmer. Identification of the Kv2.1 K+ Channel as a Major Component of the Delayed Rectifier K+ Current in Rat Hippocampal Neurons. *Journal of Neuroscience*, 19(5):1728–1735, 1999.

[203] Haodong Xu, Dianne M. Barry, Huilin Li, Sylvain Brunet, Weinong Guo, and Jeanne M. Nerbonne. Attenuation of the Slow Component of Delayed Rectification, Action Potential Prolongation, and Triggered Activity in Mice Expressing a Dominant-Negative Kv2 Subunit. *Circulation Research*, 85(7):623–633, 1999.

[204] Jing Du, Laurel L. Haak, Emily PhillipsTansey, James T. Russell, and Chris J. McBain. Frequencydependent regulation of rat hippocampal somatodendritic ex-

citability by the K+ channel subunit Kv2.1. *The Journal of Physiology*, 522(1):19–31, 2000.

[205] Sacha A. Malin and Jeanne M. Nerbonne. Delayed Rectifier K+ Currents,IK, Are Encoded by Kv2 -Subunits and Regulate Tonic Firing in Mammalian Sympathetic Neurons. *Journal of Neuroscience*, 22(23):10094–10105, 2002.

[206] Dongxu Guan, William E. Armstrong, and Robert C. Foehring. Kv2 channels regulate firing rate in pyramidal neurons from rat sensorimotor cortex. *The Journal of Physiology*, 591(19):4807–4825, 2013.

[207] Xinying Liu, Yingmei Fu, Huan Yang, Timur Mavlyutov, Jun Li, Christopher R. McCurdy, Lian-Wang Guo, and Bikash R. Pattnaik. Potential independent action of sigma receptor ligands through inhibition of the Kv2.1 channel. *Oncotarget*, 5(0):59345–59358, 2014.

[208] Shannon H. Romer, Adam S. Deardorff, and Robert E. W. Fyffe. A molecular rheostat: Kv2.1 currents maintain or suppress repetitive firing in motoneurons. *The Journal of Physiology*, 597(14):3769–3786, 2019.

[209] Kristen M. S. O'Connell, Robert Loftus, and Michael M. Tamkun. Localization-dependent activity of the Kv2.1 delayed-rectifier K+ channel. *Proceedings of the National Academy of Sciences*, 107(27):12351–12356, 2010.

[210] Philip D. Fox, Christopher J. Haberkorn, Elizabeth J. Akin, Peter J. Seel, Diego Krapf, and Michael M. Tamkun. Induction of stable ERplasma-membrane junctions by Kv2.1 potassium channels. *J Cell Sci*, 128(11):2096–2105, 2015.

[211] J S Trimmer. Immunological identification and characterization of a delayed rectifier K+ channel polypeptide in rat brain. *Proceedings of the National Academy of Sciences*, 88(23):10764–10768, 1991.

[212] R H Scannevin, H Murakoshi, K J Rhodes, and J S Trimmer. Identification of a cytoplasmic domain important in the polarized expression and clustering of the Kv2.1 K+ channel. *The Journal of Cell Biology*, 135(6):1619–1632, 1996.

[213] Yoshitaka Kihira, Tracey O. Hermanstyne, and Hiroaki Misonou. Formation of Heteromeric Kv2 Channels in Mammalian Brain Neurons*. *Journal of Biological Chemistry*, 285(20):15048–15055, 2010.

[214] Patrick D Sarmiere, Cecile M Weigle, and Michael M Tamkun. The Kv2.1 K+ channel targets to the axon initial segment of hippocampal and cortical neurons in culture and in situ. *BMC Neuroscience*, 9(1):112, 2008.

[215] Emily Deutsch, Aubrey V. Weigel, Elizabeth J. Akin, Phil Fox, Gentry Hansen, Christopher J. Haberkorn, Rob Loftus, Diego Krapf, and Michael M. Tamkun. Kv2.1 cell surface clusters are insertion platforms for ion channel delivery to the plasma membrane. *Molecular Biology of the Cell*, 23(15):2917–2929, 2012.

[216] Hideyuki Murakoshi, Gongyi Shi, Robert H. Scannevin, and James S. Trimmer. Phosphorylation of the Kv2.1 K+ Channel Alters Voltage-Dependent Activation. *Molecular Pharmacology*, 52(5):821–828, 1997.

[217] Seung T Lim, Dana E Antonucci, Robert H Scannevin, and James S Trimmer. A Novel Targeting Signal for Proximal Clustering of the Kv2.1 K+ Channel in Hippocampal Neurons. *Neuron*, 25(2):385–397, 2000.

[218] Benjamin T. Johnson, Ashley Leek, Michael Kirmiz, Emily Maverick, and James Trimmer. The Kv2.1 Potassium Channel Forms Endoplasmic Reticulum/Plasma Membrane Junctions via Interaction with VAP-A and VAP-B. *Biophysical Journal*, 114(3):295a, 2018.

[219] D.E. Antonucci, S.T. Lim, S. Vassanelli, and J.S. Trimmer. Dynamic localization and clustering of dendritic Kv2.1 voltage-dependent potassium channels in developing hippocampal neurons. *Neuroscience*, 108(1):69–81, 2001.

[220] Philip D. Fox, Christopher J. Haberkorn, Aubrey V. Weigel, Jenny L. Higgins, Elizabeth J. Akin, Matthew J. Kennedy, Diego Krapf, and Michael M. Tamkun. Plasma membrane domains enriched in cortical endoplasmic reticulum function as membrane protein trafficking hubs. *Molecular Biology of the Cell*, 24(17):2703–2713, 2013.

[221] Yumei Wu, Christina Whiteus, C. Shan Xu, Kenneth J. Hayworth, Richard J. Weinberg, Harald F. Hess, and Pietro De Camilli. Contacts between the endoplasmic reticulum and other membranes in neurons. *Proceedings of the National Academy of Sciences*, 114(24):E4859–E4867, 2017.

[222] Chenlu Li, Tiantian Qian, Ruyue He, Chun Wan, Yinghui Liu, and Haijia Yu. Endoplasmic ReticulumPlasma Membrane Contact Sites: Regulators, Mechanisms, and Physiological Functions. *Frontiers in Cell and Developmental Biology*, 9:627700, 2021.

[223] Yasunori Saheki and Pietro De Camilli. Endoplasmic ReticulumPlasma Membrane Contact Sites. *Annual Review of Biochemistry*, 86(1):1–26, 2016.

[224] Lori Feinshreiber, Dafna SingerLahat, Uri Ashery, and Ilana Lotan. Voltagegated Potassium Channel as a Facilitator of Exocytosis. *Annals of the New York Academy of Sciences*, 1152(1):87–92, 2009.

[225] Lori Feinshreiber, Dafna Singer-Lahat, Reut Friedrich, Ulf Matti, Anton Sheinin, Ofer Yizhar, Rachel Nachman, Dodo Chikvashvili, Jens Rettig, Uri Ashery, and Ilana Lotan. Non-conducting function of the Kv2.1 channel enables it to recruit vesicles for release in neuroendocrine and nerve cells. *Journal of Cell Science*, 123(11):1940–1947, 2010.

[226] Marjaana A Peltola, Juha KujaPanula, Sari E Lauri, Tomi Taira, and Heikki Rauvala. AMIGO is an auxiliary subunit of the Kv2.1 potassium channel. *EMBO reports*, 12(12):1293–1299, 2011.

[227] Juha Kuja-Panula, Marjaana Kiiltomäki, Takashi Yamashiro, Ari Rouhiainen, and Heikki Rauvala. AMIGO, a transmembrane protein implicated in axon tract development, defines a novel protein family with leucine-rich repeats. *The Journal of Cell Biology*, 160(6):963–973, 2003.

[228] Hannah I. Bishop, Melanie M. Cobb, Michael Kirmiz, Laxmi K. Parajuli, Danielle Mandikian, Ashleigh M. Philp, Mikhail Melnik, Juha Kuja-Panula, Heikki Rauvala, Ryuichi Shigemoto, Karl D. Murray, and James S. Trimmer. Kv2 Ion Channels Determine the Expression and Localization of the Associated AMIGO-1 Cell Adhesion Molecule in Adult Brain Neurons. *Frontiers in Molecular Neuroscience*, 11(7):1, 2018.

[229] Tommi Kajander, Juha Kuja-Panula, Heikki Rauvala, and Adrian Goldman. Crystal Structure and Role of Glycans and Dimerization in Folding of Neuronal Leucine-Rich Repeat Protein AMIGO-1. *Journal of Molecular Biology*, 413(5):1001–1015, 2011.

[230] Yanan Chen, Selina Aulia, Lingzhi Li, and Bor Luen Tang. AMIGO and friends: An emerging family of brain-enriched, neuronal growth modulating, type I transmembrane proteins with leucine-rich repeats (LRR) and cell adhesion molecule motifs. *Brain Research Reviews*, 51(2):265–274, 2006.

[231] Yanan Chen, Hong Huan Hor, and Bor Luen Tang. AMIGO is expressed in multiple brain cell types and may regulate dendritic growth and neuronal survival. *Journal of Cellular Physiology*, 227(5):2217–2229, 2012.

[232] Zubair Ahmed, Michael R. Douglas, Gabrielle John, Martin Berry, and Ann Logan. AMIGO3 Is an NgR1/p75 Co-Receptor Signalling Axon Growth Inhibition in the Acute Phase of Adult Central Nervous System Injury. *PLoS ONE*, 8(4):e61878, 2013.

[233] Florentina Soto, Nai-Wen Tien, Anurag Goel, Lei Zhao, Philip A. Ruzycki, and Daniel Kerschensteiner. AMIGO2 Scales Dendrite Arbors in the Retina. *Cell Reports*, 29(6):1568–1578.e4, 2019.

[234] Xiang Zhao, Juha Kuja-Panula, Maria Sundvik, Yu-Chia Chen, Vilma Aho, Marjaana A. Peltola, Tarja Porkka-Heiskanen, Pertti Panula, and Heikki Rauvala. Amigo Adhesion Protein Regulates Development of Neural Circuits in Zebrafish Brain*. *Journal of Biological Chemistry*, 289(29):19958–19975, 2014.

[235] Tomio Ono, Naoko Sekino-Suzuki, Yoshiaki Kikkawa, Hiromichi Yonekawa, and Seiichi Kawashima. Alivin 1, a Novel Neuronal Activity-Dependent Gene, Inhibits Apoptosis and Promotes Survival of Cerebellar Granule Neurons. *Journal of Neuroscience*, 23(13):5887–5896, 2003.

[236] Sharmin Hossain, Minhaz Uddin Ahmed, Shamiul Alam, Akuo Watanabe, Ai Harashima, Hideto Yonekura, and Hiroshi Yamamoto. Expression and Roles of AMIGO Gene Family in Vascular Endothelial Cells. *International Journal of Molecular Medicine and Advance Sciences*, 7(2):5–11, 2011.

[237] Karen E Rabenau, Jennifer M O'Toole, Rajiv Bassi, Helen Kotanides, Larry Witte, Dale L Ludwig, and Daniel S Pereira. DEGA/AMIGO-2, a leucine-rich repeat family member, differentially expressed in human gastric adenocarcinoma: effects on ploidy, chromosomal stability, cell adhesion/migration and tumorigenicity. *Oncogene*, 23(29):5056–5067, 2004.

[238] Barbara Fontanals-Cirera, Dan Hasson, Chiara Vardabasso, Raffaella Di Micco, Praveen Agrawal, Asif Chowdhury, Madeleine Gantz, Ana de Pablos-Aragoneses,

Ari Morgenstern, Pamela Wu, Dan Filipescu, David Valle-Garcia, Farbod Darvishian, Jae-Seok Roe, Michael A. Davies, Christopher R. Vakoc, Eva Hernando, and Emily Bernstein. Harnessing BET Inhibitor Sensitivity Reveals AMIGO2 as a Melanoma Survival Gene. *Molecular Cell*, 68(4):731–744.e9, 2017.

[239] Hyojin Park, Sungwoon Lee, Pravesh Shrestha, Jihye Kim, Jeong Ae Park, Yeongrim Ko, Young Ho Ban, Dae-Young Park, Sang-Jun Ha, Gou Young Koh, Victor Sukbong Hong, Naoki Mochizuki, Young-Myeong Kim, Weontae Lee, and Young-Guen Kwon. AMIGO2, a novel membrane anchor of PDK1, controls cell survival and angiogenesis via Akt activationAMIGO2 regulates PDK1Akt signaling. *The Journal of Cell Biology*, 211(3):619–637, 2015.

[240] Yusuke Kanda, Mitsuhiko Osaki, Kunishige Onuma, Ayana Sonoda, Masanobu Kobayashi, Junichi Hamada, Garth L. Nicolson, Takahiro Ochiya, and Futoshi Okada. Amigo2-upregulation in Tumour Cells Facilitates Their Attachment to Liver Endothelial Cells Resulting in Liver Metastases. *Scientific Reports*, 7(1):43567, 2017.

[241] Yueying Liu, Jing Yang, Zonggao Shi, Xuejuan Tan, Norman Jin, Catlin O'Brien, Connor Ott, Anna Grisoli, Eric Lee, Kelly Volk, Meghan Conroy, Emily Franz, Annamarie Bryant, Leigh Campbell, Brian Crowley, Stephen Grisoli, Aris T. Alexandrou, Chunyan Li, Elizabeth I. Harper, Marwa Asem, Jeff Johnson, Annemarie Leonard, Katie Santanello, Ashley Klein, Qingfei Wang, Siyuan Zhang, Tyvette S. Hilliard, and M. Sharon Stack. In vivo selection of highly metastatic human ovarian cancer sublines reveals role for AMIGO2 in intra-peritoneal metastatic regulation. *Cancer Letters*, 503:163–173, 2021.

[242] David J Rossi, James D Brady, and Claudia Mohr. Astrocyte metabolism and signaling during brain ischemia. *Nature Neuroscience*, 10(11):1377–1386, 2007.

[243] Christine R. Rose, Lisa Felix, Andre Zeug, Dirk Dietrich, Andreas Reiner, and Christian Henneberger. Astroglial Glutamate Signaling and Uptake in the Hippocampus. *Frontiers in Molecular Neuroscience*, 10:451, 2018.

[244] Li-Nan Zhang, Liang Hao, Yu-Song Guo, Hai-Yan Wang, Lin-lin Li, Li-Zhe Liu, and Wen-Bin Li. Are glutamate transporters neuroprotective or neurodegenerative during cerebral ischemia? *Journal of Molecular Medicine*, 97(3):281–289, 2019.

[245] Stefan Passlick, Christine R. Rose, Gabor C. Petzold, and Christian Henneberger. Disruption of Glutamate Transport and Homeostasis by Acute Metabolic Stress. *Frontiers in Cellular Neuroscience*, 15:637784, 2021.

[246] Kaiyu Zheng, Annalisa Scimemi, and Dmitri A. Rusakov. Receptor Actions of Synaptically Released Glutamate: The Role of Transporters on the Scale from Nanometers to Microns. *Biophysical Journal*, 95(10):4584–4596, 2008.

[247] Takayuki Yamashita, Takeshi Kanda, Kohgaku Eguchi, and Tomoyuki Takahashi. Vesicular glutamate filling and AMPA receptor occupancy at the calyx of Held synapse of immature rats. *The Journal of Physiology*, 587(10):2327–2339, 2009.

[248] Amaia M. Arranz, Miroslav Gottlieb, Fernando Pérez-Cerdá, and Carlos Matute. Increased expression of glutamate transporters in subcortical white matter after transient focal cerebral ischemia. *Neurobiology of Disease*, 37(1):156–165, 2010.

[249] YiXian Liu, Min Zhang, LiZhe Liu, Xin Cui, YuYan Hu, and WenBin Li. The role of glutamate transporter1a in the induction of brain ischemic tolerance in rats. *Glia*, 60(1):112–124, 2012.

[250] Catrinel Girbovan and Hélène Plamondon. Resveratrol downregulates type-1 glutamate transporter expression and microglia activation in the hippocampus following cerebral ischemia reperfusion in rats. *Brain Research*, 1608:203–214, 2015.

[251] Cristina Romera, Olivia Hurtado, Judith Mallolas, Marta P Pereira, Jesús R Morales, Alejandro Romera, Joaquín Serena, José Vivancos, Florentino Nombela, Pedro Lorenzo, Ignacio Lizasoain, and Maria A Moro. Ischemic Preconditioning Reveals that GLT1/EAAT2 Glutamate Transporter is a Novel PPAR Target Gene Involved in Neuroprotection. *Journal of Cerebral Blood Flow & Metabolism*, 27(7):1327–1338, 2006.

[252] Jeffrey D. Rothstein, Sarjubhai Patel, Melissa R. Regan, Christine Haenggeli, Yanhua H. Huang, Dwight E. Bergles, Lin Jin, Margaret Dykes Hoberg, Svetlana Vidensky, Dorothy S. Chung, Shuy Vang Toan, Lucie I. Bruijn, Zao-zhong Su, Pankaj Gupta, and Paul B. Fisher. -Lactam antibiotics offer neuroprotection by increasing glutamate transporter expression. *Nature*, 433(7021):73–77, 2005.

[253] Min Zhang, Wen-Bin Li, Jin-Xia Geng, Qing-Jun Li, Xiao-Cai Sun, Xiao-Hui Xian, Jie Qi, and Shu-Qin Li. The Upregulation of Glial Glutamate Transporter-1 Participates in the Induction of Brain Ischemic Tolerance in Rats. *Journal of Cerebral Blood Flow & Metabolism*, 27(7):1352–1368, 2006.

[254] Christof Grewer, Armanda Gameiro, Zhou Zhang, Zhen Tao, Simona Braams, and Thomas Rauen. Glutamate forward and reverse transport: From molecular mechanism to transportermediated release after ischemia. *IUBMB Life*, 60(9):609–619, 2008.

[255] Niklas J Gerkau, Cordula Rakers, Simone Durry, Gabor C Petzold, and Christine R Rose. Reverse NCX Attenuates Cellular Sodium Loading in Metabolically Compromised Cortex. *Cerebral Cortex*, 28(12):4264–4280, 2017.

[256] Vladimir Parpura, Vladimir Grubii, and Alexei Verkhratsky. Ca2+ sources for the exocytotic release of glutamate from astrocytes. *Biochimica et Biophysica Acta (BBA) - Molecular Cell Research*, 1813(5):984–991, 2011.

[257] Hiroaki Misonou, Durga P. Mohapatra, Milena Menegola, and James S. Trimmer. Calcium- and Metabolic State-Dependent Modulation of the Voltage-Dependent Kv2.1 Channel Regulates Neuronal Excitability in Response to Ischemia. *The Journal of Neuroscience*, 25(48):11184–11193, 2005.

[258] Shannon H. Romer, Kathleen M. Dominguez, Marc W. Gelpi, Adam S. Deardorff, Robert C. Tracy, and Robert. E.W. Fyffe. Redistribution of Kv2.1 ion channels on spinal motoneurons following peripheral nerve injury. *Brain Research*, 1547(Ann. N. Y. Acad. Sci. 1198 2010):1–15, 2014.

[259] Niyathi Hegde Shah and Elias Aizenman. Voltage-Gated Potassium Channels at the Crossroads of Neuronal Function, Ischemic Tolerance, and Neurodegeneration. *Translational Stroke Research*, 5(1):38–58, 2014.

[260] Shannon H. Romer, Adam S. Deardorff, and Robert E. W. Fyffe. Activitydependent redistribution of Kv2.1 ion channels on rat spinal motoneurons. *Physiological Reports*, 4(22):e13039, 2016.

[261] Hiroaki Misonou, Durga P Mohapatra, Eunice W Park, Victor Leung, Dongkai Zhen, Kaori Misonou, Anne E Anderson, and James S Trimmer. Regulation of ion channel localization and phosphorylation by neuronal activity. *Nature Neuroscience*, 7(7):711–718, 2004.

[262] Kang-Sik Park, Durga P. Mohapatra, Hiroaki Misonou, and James S. Trimmer. Graded Regulation of the Kv2.1 Potassium Channel by Variable Phosphorylation. *Science*, 313(5789):976–979, 2006.

[263] Anthony J. Schulien, Chung-Yang Yeh, Bailey N. Orange, Olivia J. Pav, Madelynn P. Hopkins, Aubin Moutal, Rajesh Khanna, Dandan Sun, Jason A. Justice, and Elias Aizenman. Targeted disruption of Kv2.1-VAPA association provides neuropro-

tection against ischemic stroke in mice by declustering Kv2.1 channels. *Science Advances*, 6(27):eaaz8110, 2020.

[264] Ling Wei, Shan Ping Yu, Frank Gottron, B. Joy Snider, Gregory J. Zipfel, and Dennis W. Choi. Potassium Channel Blockers Attenuate Hypoxia- and Ischemia-Induced Neuronal Death In Vitro and In Vivo. *Stroke*, 34(5):1281–1286, 2003.

[265] Sumon Pal, Karen A. Hartnett, Jeanne M. Nerbonne, Edwin S. Levitan, and Elias Aizenman. Mediation of Neuronal Apoptosis by Kv2.1-Encoded Potassium Channels. *Journal of Neuroscience*, 23(12):4798–4802, 2003.

[266] S K Pal, K Takimoto, E Aizenman, and E S Levitan. Apoptotic surface delivery of K+ channels. *Cell Death & Differentiation*, 13(4):661–667, 2006.

[267] Meghan C. McCord, Paul H. Kullmann, Kai He, Karen A. Hartnett, John P. Horn, Ilana Lotan, and Elias Aizenman. Syntaxinbinding domain of Kv2.1 is essential for the expression of apoptotic K+ currents. *The Journal of Physiology*, 592(16):3511–3521, 2014.

[268] Paramita Mookherjee, Pattie S. Green, G. Stennis Watson, Marcos A. Marques, Kohichi Tanaka, Kole D. Meeker, James S. Meabon, Ning Li, Ping Zhu, Valerie G. Olson, and David G. Cook. GLT-1 Loss Accelerates Cognitive Deficit Onset in an Alzheimer's Disease Animal Model. *Journal of Alzheimer's Disease*, 26(3):447–455, 2011.

[269] Dwight E Bergles and Craig E Jahr. Synaptic Activation of Glutamate Transporters in Hippocampal Astrocytes. *Neuron*, 19(6):1297–1308, 1997.

[270] Fredrik Asztely, Gül Erdemli, and Dimitri M. Kullmann. Extrasynaptic Glutamate Spillover in the Hippocampus: Dependence on Temperature and the Role of Active Glutamate Uptake. *Neuron*, 18(2):281–293, 1997.

[271] Elizabeth J. Akin, Laura Solé, Sulayman D. Dib-Hajj, Stephen G. Waxman, and Michael M. Tamkun. Preferential Targeting of Nav1.6 Voltage-Gated Na+ Channels to the Axon Initial Segment during Development. *PLOS ONE*, 10(4):e0124397, 2015.

[272] Diego Krapf. Compartmentalization of the plasma membrane. *Current Opinion in Cell Biology*, 53:15–21, 2018.

[273] Aubrey V. Weigel, Blair Simon, Michael M. Tamkun, and Diego Krapf. Ergodic and nonergodic processes coexist in the plasma membrane as observed by single-molecule tracking. *Proceedings of the National Academy of Sciences*, 108(16):6438–6443, 2011.

[274] Sanaz Sadegh, Jenny L. Higgins, Patrick C. Mannion, Michael M. Tamkun, and Diego Krapf. Plasma Membrane is Compartmentalized by a Self-Similar Cortical Actin Meshwork. *Physical Review X*, 7(1):011031, 2017.

[275] Gilia Pines, Niels C. Danbolt, Magnar Bjørås, Yumin Zhang, Annie Bendahan, Lars Eide, Hermann Koepsell, Jon Storm-Mathisen, Erling Seeberg, and Baruch I. Kanner. Cloning and expression of a rat brain L-glutamate transporter. *Nature*, 360(6403):464–467, 1992.

[276] Weizhi Chen, Chiye Aoki, Veeravan Mahadomrongkul, Christian E. Gruber, Guang Jian Wang, Rachel Blitzblau, Nina Irwin, and Paul A. Rosenberg. Expression of a Variant Form of the Glutamate Transporter GLT1 in Neuronal Cultures and in Neurons and Astrocytes in the Rat Brain. *Journal of Neuroscience*, 22(6):2142–2152, 2002.

[277] Thomas Rauen, Michael WieSSner, Robert Sullivan, Aven Lee, and David V. Pow. A new GLT1 splice variant: cloning and immunolocalization of GLT1c in the mammalian retina and brain. *Neurochemistry International*, 45(7):1095–1106, 2004.

[278] Hélène Marie, Daniela Billups, Fiona K. Bedford, Andrea Dumoulin, Rakesh K. Goyal, Gregory D. Longmore, Stephen J. Moss, and David Attwell. The Amino Terminus of the Glial Glutamate Transporter GLT-1 Interacts with the LIM Protein Ajuba. *Molecular and Cellular Neuroscience*, 19(2):152–164, 2002.

[279] Dolores Piniella, Elena MartínezBlanco, Ignacio Ibáñez, David BartoloméMartín, Eva Porlan, Javier DíezGuerra, Cecilio Giménez, and Francisco Zafra. Identification of novel regulatory partners of the glutamate transporter GLT1. *Glia*, 66(12):2737–2755, 2018.

[280] Shengwei Zou, Juan D. PitaAlmenar, and Arnold Eskin. Regulation of glutamate transporter GLT1 by MAGI1. *Journal of Neurochemistry*, 117(5):833–840, 2011.

[281] WP Bartlett and GA Banker. An electron microscopic study of the development of axons and dendrites by hippocampal neurons in culture. I. Cells which develop without intercellular contacts. *Journal of Neuroscience*, 4(8):1944–1953, 1984.

[282] G. J. Brewer, J. R. Torricelli, E. K. Evege, and P. J. Price. Optimized survival of hippocampal neurons in B27supplemented neurobasal, a new serumfree medium combination. *Journal of Neuroscience Research*, 35(5):567–576, 1993.

[283] Nils Gustafsson, Siân Culley, George Ashdown, Dylan M. Owen, Pedro Matos Pereira, and Ricardo Henriques. Fast live-cell conventional fluorophore nanoscopy with ImageJ through super-resolution radial fluctuations. *Nature Communications*, 7(1):12471, 2016.

[284] Romain F Laine, Kalina L Tosheva, Nils Gustafsson, Robert D M Gray, Pedro Almada, David Albrecht, Gabriel T Risa, Fredrik Hurtig, Ann-Christin Linds, Buzz Baum, Jason Mercer, Christophe Leterrier, Pedro M Pereira, Sin Culley, and Ricardo Henriques. NanoJ: a high-performance open-source super-resolution microscopy toolbox. *Journal of Physics D: Applied Physics*, 52(16):163001, 2019.

[285] Khuloud Jaqaman, Dinah Loerke, Marcel Mettlen, Hirotaka Kuwata, Sergio Grinstein, Sandra L Schmid, and Gaudenz Danuser. Robust single-particle tracking in live-cell time-lapse sequences. *Nature Methods*, 5(8):695–702, 2008.

[286] Diego Krapf and Ralf Metzler. Strange interfacial molecular dynamics. *Physics Today*, 72(9):48–54, 2019.

[287] Diego Krapf. Chapter Five Mechanisms Underlying Anomalous Diffusion in the Plasma Membrane. *Current Topics in Membranes*, 75:167–207, 2015.

[288] Philip D. Fox, Rob J. Loftus, and Michael M. Tamkun. Regulation of Kv2.1 K+ Conductance by Cell Surface Channel Density. *The Journal of Neuroscience*, 33(3):1259–1270, 2013.

[289] Maximilian H Ulbrich and Ehud Y Isacoff. Subunit counting in membrane-bound proteins. *Nature Methods*, 4(4):319–321, 2007.

[290] Ignacio Ibáñez, David Bartolomé-Martín, Dolores Piniella, Cecilio Giménez, and Francisco Zafra. Activity dependent internalization of the glutamate transporter GLT-1 requires calcium entry through the NCX sodium/calcium exchanger. *Neurochemistry International*, 123:125–132, 2019.

[291] Alexandra E. Schreiner, Eric Berlinger, Julia Langer, Karl W. Kafitz, and Christine R. Rose. Lesion-Induced Alterations in Astrocyte Glutamate Transporter Expression and Function in the Hippocampus. *ISRN Neurology*, 2013:1–16, 2013.

[292] Alexandra E. Schreiner, Simone Durry, Tomomi Aida, Martin C. Stock, Ulrich Rüther, Kohichi Tanaka, Christine R. Rose, and Karl W. Kafitz. Laminar and subcellular heterogeneity of GLAST and GLT1 immunoreactivity in the developing postnatal mouse hippocampus. *Journal of Comparative Neurology*, 522(1):204–224, 2014.

[293] Angus S. Harding and John F. Hancock. Using plasma membrane nanoclusters to build better signaling circuits. *Trends in Cell Biology*, 18(8):364–371, 2008.

[294] Ruth Nussinov, Hyunbum Jang, and ChungJung Tsai. Oligomerization and nanocluster organization render specificity. *Biological Reviews*, 90(2):587–598, 2015.

[295] Michael Kirmiz, Nicholas C. Vierra, Stephanie Palacio, and James S. Trimmer. Identification of VAPA and VAPB as Kv2 channel-interacting proteins defining endoplasmic reticulum-plasma membrane junctions in mammalian brain neurons. *Journal of Neuroscience*, 38(35):0893–18, 2018.

[296] Sjoerd van Deventer, Abbey B. Arp, and Annemiek B. van Spriel. Dynamic Plasma Membrane Organization: A Complex Symphony. *Trends in Cell Biology*, 31(2):119–129, 2020.

[297] Maria F. Garcia-Parajo, Alessandra Cambi, Juan A. Torreno-Pina, Nancy Thompson, and Ken Jacobson. Nanoclustering as a dominant feature of plasma membrane organization. *Journal of Cell Science*, 127(23):4995–5005, 2014.

[298] Joseph Mathew Kalappurakkal, Parijat Sil, and Satyajit Mayor. Toward a new picture of the living plasma membrane. *Protein Science*, 29(6):1355–1365, 2020.

[299] Mariko Kato Hayashi and Masato Yasui. The transmembrane transporter domain of glutamate transporters is a process tip localizer. *Scientific Reports*, 5(1):9032, 2015.

[300] Nawrin F Pinky, Crystal M Wilkie, Jocelyn R Barnes, and Matthew P Parsons. Region- and Activity-Dependent Regulation of Extracellular Glutamate. *The Journal of Neuroscience*, 38(23):5351–5366, 2018.

[301] H.-R. Weng, J.H. Chen, Z.Z. Pan, and H. Nie. Glial glutamate transporter 1 regulates the spatial and temporal coding of glutamatergic synaptic transmission in spinal lamina II neurons. *Neuroscience*, 149(4):898–907, 2007.

[302] S. J. Singer and Garth L. Nicolson. The Fluid Mosaic Model of the Structure of Cell Membranes. *Science*, 175(4023):720–731, 1972.

[303] Félix M. Goñi. The basic structure and dynamics of cell membranes: An update of the SingerNicolson model. *Biochimica et Biophysica Acta (BBA) - Biomembranes*, 1838(6):1467–1476, 2014.

[304] Akihiro Kusumi, Kenichi G.N. Suzuki, Rinshi S. Kasai, Ken Ritchie, and Takahiro K. Fujiwara. Hierarchical mesoscale domain organization of the plasma membrane. *Trends in Biochemical Sciences*, 36(11):604–615, 2011.

[305] Frederick R Maxfield. Plasma membrane microdomains. *Current Opinion in Cell Biology*, 14(4):483–487, 2002.

[306] Garth Nicolson. Update of the 1972 Singer-Nicolson Fluid-Mosaic Model of Membrane Structure. *Discoveries*, 1(1):e3, 2013.

[307] Darius V Köster and Satyajit Mayor. Cortical actin and the plasma membrane: inextricably intertwined. *Current Opinion in Cell Biology*, 38:81–89, 2016.

[308] Kripa Gowrishankar, Subhasri Ghosh, Suvrajit Saha, Rumamol C., Satyajit Mayor, and Madan Rao. Active Remodeling of Cortical Actin Regulates Spatiotemporal Organization of Cell Surface Molecules. *Cell*, 149(6):1353–1367, 2012.

[309] Parijat Sil, Nicolas Mateos, Sangeeta Nath, Sonja Buschow, Carlo Manzo, Kenichi G N Suzuki, Takahiro Fujiwara, Akihiro Kusumi, Maria F Garcia-Parajo, and Satyajit Mayor. Dynamic actin-mediated nano-scale clustering of CD44 regulates its meso-scale organization at the plasma membrane. *Molecular Biology of the Cell*, 31(7):561–579, 2020.

[310] Nagatoki Kinoshita, Kazushi Kimura, Naoya Matsumoto, Masahiko Watanabe, Masahiro Fukaya, and Chizuka Ide. Mammalian septin Sept2 modulates the ac-

tivity of GLAST, a glutamate transporter in astrocytes. *Genes to Cells*, 9(1):1–14, 2004.

[311] Natsumi Ageta-Ishihara, Maya Yamazaki, Kohtarou Konno, Hisako Nakayama, Manabu Abe, Kenji Hashimoto, Tomoki Nishioka, Kozo Kaibuchi, Satoko Hattori, Tsuyoshi Miyakawa, Kohichi Tanaka, Fathul Huda, Hirokazu Hirai, Kouichi Hashimoto, Masahiko Watanabe, Kenji Sakimura, and Makoto Kinoshita. A CDC42EP4/septin-based perisynaptic glial scaffold facilitates glutamate clearance. *Nature Communications*, 6(1):10090, 2015.

[312] Elias T. Spiliotis. Spatial effectssite-specific regulation of actin and microtubule organization by septin GTPases. *J Cell Sci*, 131(1):jcs207555, 2018.

[313] R.M. Guasch, M. Tomas, R. Miñambres, S. Valles, J. RenauPiqueras, and C. Guerri. RhoA and lysophosphatidic acid are involved in the actin cytoskeleton reorganization of astrocytes exposed to ethanol. *Journal of Neuroscience Research*, 72(4):487–502, 2003.

[314] Ignacio Ibáñez, F. Javier Díez-Guerra, Cecilio Giménez, and Francisco Zafra. Activity dependent internalization of the glutamate transporter GLT-1 mediated by -arrestin 1 and ubiquitination. *Neuropharmacology*, 107:376–386, 2016.

[315] Anders E Carlsson. Membrane bending by actin polymerization. *Current Opinion in Cell Biology*, 50:1–7, 2018.

[316] Yixing Du, Wei Wang, Anthony D. Lutton, Conrad M. Kiyoshi, Baofeng Ma, Anne T. Taylor, John W. Olesik, Dana M. McTigue, Candice C. Askwith, and Min Zhou. Dissipation of transmembrane potassium gradient is the main cause of cerebral ischemia-induced depolarization in astrocytes and neurons. *Experimental Neurology*, 303:1–11, 2018.

[317] Camilla Stampe Jensen, Shoji Watanabe, Jeroen Ingrid Stas, Jessica Klaphaak, Ayaka Yamane, Nicole Schmitt, Søren-Peter Olesen, James S. Trimmer, Hanne Borger Rasmussen, and Hiroaki Misonou. Trafficking of Kv2.1 Channels to the Axon Initial Segment by a Novel Nonconventional Secretory Pathway. *Journal of Neuroscience*, 37(48):11523–11536, 2017.

[318] Anna N. King, Colleen F. Manning, and James S. Trimmer. A unique ion channel clustering domain on the axon initial segment of mammalian neurons. *Journal of Comparative Neurology*, 522(11):2594–2608, 2014.

[319] Alessandra Gallo, Christian Vannier, and Thierry Galli. Endoplasmic Reticulum-Plasma Membrane Associations: Structures and Functions. *Annual Review of Cell and Developmental Biology*, 32(1):1–23, 2015.

[320] Nicholas C Vierra, Michael Kirmiz, Deborah van der List, L Fernando Santana, and James S Trimmer. Kv2.1 mediates spatial and functional coupling of L-type calcium channels and ryanodine receptors in mammalian neurons. *eLife*, 8:e49953, 2019.

[321] Michael Kirmiz, Taryn E. Gillies, Eamonn J. Dickson, and James S. Trimmer. Neuronal ERplasma membrane junctions organized by Kv2VAP pairing recruit Nir proteins and affect phosphoinositide homeostasis. *Journal of Biological Chemistry*, 294(47):17735–17757, 2019.

[322] Hiroaki Misonou, Milena Menegola, Durga P. Mohapatra, Lauren K. Guy, Kang-Sik Park, and James S. Trimmer. Bidirectional Activity-Dependent Regulation of Neuronal Ion Channel Phosphorylation. *The Journal of Neuroscience*, 26(52):13505–13514, 2006.

[323] Durga P. Mohapatra, Helene Vacher, and James S. Trimmer. The Surprising Catch of a Voltage-Gated Potassium Channel in a Neuronal SNARE. *Sci. STKE*, 2007(393):pe37–pe37, 2007.

[324] ElizabethăJ. Akin, Laura Solé, Ben Johnson, Mohamedăel Beheiry, Jean-Baptiste Masson, Diego Krapf, and MichaelăM. Tamkun. Single-Molecule Imaging of Nav1.6 on the Surface of Hippocampal Neurons Reveals Somatic Nanoclusters. *Biophysical Journal*, 111(6):1235–1247, 2016.

[325] Aubrey V. Weigel, Michael M. Tamkun, and Diego Krapf. Kv2.1 Cell Surface Clusters Promote Maturation of Clathrin-Coated Pits. *Biophysical Journal*, 104(2):619a, 2013.

[326] Aleksander Weron, Krzysztof Burnecki, Elizabeth J. Akin, Laura Solé, Micha Balcerek, Michael M. Tamkun, and Diego Krapf. Ergodicity breaking on the neuronal surface emerges from random switching between diffusive states. *Scientific Reports*, 7(1):5404, 2017.

[327] G J Brewer, M D Boehler, R A Pearson, A A DeMaris, A N Ide, and B C Wheeler. Neuron network activity scales exponentially with synapse density. *Journal of Neural Engineering*, 6(1):014001, 2009.

[328] Ye Zhang, Kenian Chen, Steven A. Sloan, Mariko L. Bennett, Anja R. Scholze, Sean O'Keeffe, Hemali P. Phatnani, Paolo Guarnieri, Christine Caneda, Nadine Ruderisch, Shuyun Deng, Shane A. Liddelow, Chaolin Zhang, Richard Daneman, Tom Maniatis, Ben A. Barres, and Jia Qian Wu. An rna-sequencing transcriptome and splicing database of glia, neurons, and vascular cells of the cerebral cortex. *Journal of Neuroscience*, 34(36):11929–11947, 2014.

[329] Anne E.J. Hillen, J.Peter H. Burbach, and Elly M. Hol. Cell adhesion and matricellular support by astrocytes of the tripartite synapse. *Progress in Neurobiology*, 165-167(PLoS One 8 2013):66–86, 2018.

[330] Vivian W. Tang and William M. Brieher. FSGS3/CD2AP is a barbed-end capping protein that stabilizes actin and strengthens adherens junctionsCD2AP regulates junctional actin at the adherens junction. *The Journal of Cell Biology*, 203(5):815–833, 2013.

[331] Daisuke Yamazaki, Tsukasa Oikawa, and Tadaomi Takenawa. Rac-WAVE-mediated actin reorganization is required for organization and maintenance of cell-cell adhesion. *Journal of Cell Science*, 120(1):86–100, 2007.

[332] In Ha Cho, Lauren C. Panzera, Morven Chin, Scott A. Alpizar, Genaro E. Olveda, Robert A. Hill, and Michael B. Hoppa. The potassium channel subunit Kv1 serves as a major control point for synaptic facilitation. *Proceedings of the National Academy of Sciences*, 117(47):29937–29947, 2020.

[333] Christopher J Stefan, Andrew G Manford, and Scott D Emr. ERPM connections: sites of information transfer and inter-organelle communication. *Current Opinion in Cell Biology*, 25(4):434–442, 2013.

[334] Zahid Padamsey, William J. Foster, and Nigel J. Emptage. Intracellular Ca2+ Release and Synaptic Plasticity: A Tale of Many Stores. *The Neuroscientist*, 25(3):208–226, 2019.

[335] Håvard Ringsevjen, Heidi Marie Umbach Hansen, Suleman Hussain, Øyvind Hvalby, Vidar Jensen, S. Ivar Walaas, and Svend Davanger. Presynaptic increase in IP3 receptor type 1 concentration in the early phase of hippocampal synaptic plasticity. *Brain Research*, 1706:125–134, 2019.

[336] Nishant Singh, Thomas Bartol, Herbert Levine, Terrence Sejnowski, and Suhita Nadkarni. Presynaptic endoplasmic reticulum regulates short-term plasticity in hippocampal synapses. *Communications Biology*, 4(1):241, 2021.

[337] Yan Li, Sung Yon Um, and Thomas V. Mcdonald. Voltage-Gated Potassium Channels: Regulation by Accessory Subunits. *The Neuroscientist*, 12(3):199–210, 2006.

[338] Olaf Pongs and Jürgen R. Schwarz. Ancillary Subunits Associated With Voltage-Dependent K+ Channels. *Physiological Reviews*, 90(2):755–796, 2010.

[339] Xiaohui Sun, Mark A. Zaydman, and Jianmin Cui. Regulation of Voltage-Activated K+ Channel Gating by Transmembrane Subunits. *Frontiers in Pharmacology*, 3:63, 2012.

[340] S K England, V N Uebele, H Shear, J Kodali, P B Bennett, and M M Tamkun. Characterization of a voltage-gated K+ channel beta subunit expressed in human heart. *Proceedings of the National Academy of Sciences*, 92(14):6309–6313, 1995.

[341] T Leicher, J Roeper, K Weber, X Wang, and O Pongs. Structural and Functional Characterization of Human Potassium Channel Subunit 1 (KCNA1B). *Neuropharmacology*, 35(7):787–795, 1996.

[342] Ben Johnson, Ashley N. Leek, and Michael M. Tamkun. Kv2 channels create endoplasmic reticulum / plasma membrane junctions: a brief history of Kv2 channel subcellular localization. *Channels*, 13(1):88–101, 2019.

[343] Yan Fu, Peter W. Winter, Raul Rojas, Victor Wang, Matthew McAuliffe, and George H. Patterson. Axial superresolution via multiangle TIRF microscopy with sequential imaging and photobleaching. *Proceedings of the National Academy of Sciences*, 113(16):4368–4373, 2016.

[344] Stephanie Palacio, Vivien Chevaleyre, David H. Brann, Karl D. Murray, Rebecca A. Piskorowski, and James S. Trimmer. Heterogeneity in Kv2 Channel Expression

Shapes Action Potential Characteristics and Firing Patterns in CA1 versus CA2 Hippocampal Pyramidal Neurons. *eNeuro*, 4(4):ENEURO.0267–17.2017, 2017.

[345] Emily E Maverick, Ashley N Leek, and Michael M Tamkun. Kv2 channel/amigo β-subunit assembly modulates both channel function and cell adhesion molecule surface trafficking. *Journal of Cell Science*, 2021.

[346] Kristen M. S. O'Connell and Michael M. Tamkun. Targeting of voltage-gated potassium channel isoforms to distinct cell surface microdomains. *Journal of Cell Science*, 118(10):2155–2166, 2005.

[347] Michael M. Tamkun, Kristen M. S. O'Connell, and Annah S. Rolig. A cytoskeletal-based perimeter fence selectively corrals a sub-population of cell surface Kv2.1 channels. *Journal of Cell Science*, 120(14):2413–2423, 2007.

[348] Irwin Chen, Mark Howarth, Weiying Lin, and Alice Y Ting. Site-specific labeling of cell surface proteins with biophysical probes using biotin ligase. *Nature Methods*, 2(2):99–104, 2005.

[349] Danielle Mandikian, Elke Bocksteins, Laxmi Kumar Parajuli, Hannah I. Bishop, Oscar Cerda, Ryuichi Shigemoto, and James S. Trimmer. Cell typespecific spatial and functional coupling between mammalian brain Kv2.1 K+ channels and ryanodine receptors. *Journal of Comparative Neurology*, 522(15):3555–3574, 2014.

[350] Emily E. Maverick. *Electrophysiological analysis of Kv2 channel regulation by non-canonical and canonical mechanisms*. PhD thesis, Colorado State University, 2020.

[351] Parveen Sharma, Vladimir Ignatchenko, Kevin Grace, Claudia Ursprung, Thomas Kislinger, and Anthony O. Gramolini. Endoplasmic Reticulum Protein Targeting of Phospholamban: A Common Role for an N-Terminal Di-Arginine Motif in ER Retention? *PLoS ONE*, 5(7):e11496, 2010.

[352] Annelies Laeremans, Julie Nys, Walter Luyten, Rudi DHooge, Melissa Paulussen, and Lut Arckens. AMIGO2 mRNA expression in hippocampal CA2 and CA3a. *Brain Structure and Function*, 218(1):123–130, 2013.

[353] Ed S. Lein, Michael J. Hawrylycz, Nancy Ao, Mikael Ayres, Amy Bensinger, Amy Bernard, Andrew F. Boe, Mark S. Boguski, Kevin S. Brockway, Emi J. Byrnes, Lin Chen, Li Chen, Tsuey-Ming Chen, Mei Chi Chin, Jimmy Chong, Brian E. Crook, Aneta Czaplinska, Chinh N. Dang, Suvro Datta, Nick R. Dee, Aimee L. Desaki, Tsega Desta, Ellen Diep, Tim A. Dolbeare, Matthew J. Donelan, Hong-Wei Dong, Jennifer G. Dougherty, Ben J. Duncan, Amanda J. Ebbert, Gregor Eichele, Lili K. Estin, Casey Faber, Benjamin A. Facer, Rick Fields, Shanna R. Fischer, Tim P. Fliss, Cliff Frensley, Sabrina N. Gates, Katie J. Glattfelder, Kevin R. Halverson, Matthew R. Hart, John G. Hohmann, Maureen P. Howell, Darren P. Jeung, Rebecca A. Johnson, Patrick T. Karr, Reena Kawal, Jolene M. Kidney, Rachel H. Knapik, Chihchau L. Kuan, James H. Lake, Annabel R. Laramee, Kirk D. Larsen, Christopher Lau, Tracy A. Lemon, Agnes J. Liang, Ying Liu, Lon T. Luong, Jesse Michaels, Judith J. Morgan, Rebecca J. Morgan, Marty T. Mortrud, Nerick F. Mosqueda, Lydia L. Ng, Randy Ng, Geralyn J. Orta, Caroline C. Overly, Tu H. Pak, Sheana E. Parry, Sayan D. Pathak, Owen C. Pearson, Ralph B. Puchalski, Zackery L. Riley, Hannah R. Rockett, Stephen A. Rowland, Joshua J. Royall, Marcos J. Ruiz, Nadia R. Sarno, Katherine Schaffnit, Nadiya V. Shapovalova, Taz Sivisay, Clifford R. Slaughterbeck, Simon C. Smith, Kimberly A. Smith, Bryan I. Smith, Andy J. Sodt, Nick N. Stewart, Kenda-Ruth Stumpf, Susan M. Sunkin, Madhavi Sutram, Angelene Tam, Carey D. Teemer, Christina Thaller, Carol L. Thompson, Lee R. Varnam, Axel Visel, Ray M. Whitlock, Paul E. Wohnoutka, Crissa K. Wolkey, Victoria Y. Wong, Matthew Wood, Murat B. Yaylaoglu, Rob C. Young, Brian L. Youngstrom, Xu Feng Yuan, Bin Zhang, Theresa A. Zwingman, and Allan R.

Jones. Genome-wide atlas of gene expression in the adult mouse brain. *Nature*, 445(7124):168–176, 2007.

[354] Jacqueline Gayet-Primo, Daniel B. Yaeger, Roupen A. Khanjian, and Teresa Puthussery. Heteromeric KV2/KV8.2 Channels Mediate Delayed Rectifier Potassium Currents in Primate Photoreceptors. *Journal of Neuroscience*, 38(14):3414–3427, 2018.

[355] Seok Kyu Kang, Carlos G. Vanoye, Sunita N. Misra, Dennis M. Echevarria, Jeffrey D. Calhoun, John B. O'Connor, Katarina L. Fabre, Dianalee McKnight, Laurie Demmer, Paula Goldenberg, Lauren E. Grote, Isabelle Thiffault, Carol Saunders, Kevin A. Strauss, Ali Torkamani, Jasper der Smagt, Koen Gassen, Robert P. Carson, Jullianne Diaz, Eyby Leon, Joseph E. Jacher, Mark C. Hannibal, Jessica Litwin, Neil R. Friedman, Allison Schreiber, Bryan Lynch, Annapurna Poduri, Eric D. Marsh, Ethan M. Goldberg, John J. Millichap, Alfred L. George, and Jennifer A. Kearney. Spectrum of KV2.1 Dysfunction in KCNB1Associated Neurodevelopmental Disorders. *Annals of Neurology*, 86(6):899–912, 2019.

[356] Carolien G. F. de Kovel, Steffen Syrbe, Eva H. Brilstra, Nienke Verbeek, Bronwyn Kerr, Holly Dubbs, Allan Bayat, Sonal Desai, Sakkubai Naidu, Siddharth Srivastava, Hande Cagaylan, Uluc Yis, Carol Saunders, Martin Rook, Susanna Plugge, Hiltrud Muhle, Zaid Afawi, Karl-Martin Klein, Vijayakumar Jayaraman, Ramakrishnan Rajagopalan, Ethan Goldberg, Eric Marsh, Sudha Kessler, Christina Bergqvist, Laura K. Conlin, Bryan L. Krok, Isabelle Thiffault, Manuela Pendziwiat, Ingo Helbig, Tilman Polster, Ingo Borggraefe, Johannes R. Lemke, Marie-José van den Boogaardt, Rikke S. Møller, and Bobby P. C. Koeleman. Neurodevelopmental Disorders Caused by De Novo Variants in KCNB1 Genotypes and Phenotypes. *JAMA Neurology*, 74(10):1228, 2017.

[357] Isabelle Thiffault, David J. Speca, Daniel C. Austin, Melanie M. Cobb, Kenneth S. Eum, Nicole P. Safina, Lauren Grote, Emily G. Farrow, Neil Miller, Sarah Soden, Stephen F. Kingsmore, James S. Trimmer, Carol J. Saunders, and Jon T. Sack. A novel epileptic encephalopathy mutation in KCNB1 disrupts Kv2.1 ion selectivity, expression, and localizationEpileptic encephalopathy Kv2.1 mutant. *The Journal of General Physiology*, 146(5):399–410, 2015.

[358] Joshua G. Jackson, John C. O'Donnell, Elizabeth Krizman, and Michael B. Robinson. Displacing hexokinase from mitochondrial voltagedependent anion channel impairs GLT1mediated glutamate uptake but does not disrupt interactions between GLT1 and mitochondrial proteins. *Journal of Neuroscience Research*, 93(7):999–1008, 2015.

[359] Claire Bar, Giulia Barcia, Mélanie Jennesson, Gwenaël Le Guyader, Amy Schneider, Cyril Mignot, Gaetan Lesca, Delphine Breuillard, Martino Montomoli, Boris Keren, Diane Doummar, Thierry Billette de Villemeur, Alexandra Afenjar, Isabelle Marey, Marion Gerard, Hervé Isnard, Alice Poisson, Sophie Dupont, Patrick Berquin, Pierre Meyer, David Genevieve, Anne De Saint Martin, Salima El Chehadeh, Jamel Chelly, Agnès Guët, Emmanuel Scalais, Nathalie Dorison, Candace T. Myers, Heather C. Mefford, Katherine B. Howell, Carla Marini, Jeremy L. Freeman, Anca Nica, Gaetano Terrone, Tayeb Sekhara, AnneSophie Lebre, Sylvie Odent, Lynette G. Sadleir, Arnold Munnich, Renzo Guerrini, Ingrid E. Scheffer, Edor Kabashi, and Rima Nabbout. Expanding the genetic and phenotypic relevance of KCNB1 variants in developmental and epileptic encephalopathies: 27 new patients and overview of the literature. *Human Mutation*, 41(1):69–80, 2020.

[360] Hirotomo Saitsu, Tenpei Akita, Jun Tohyama, Hadassa Goldberg-Stern, Yu Kobayashi, Roni Cohen, Mitsuhiro Kato, Chihiro Ohba, Satoko Miyatake, Yoshinori Tsurusaki, Mitsuko Nakashima, Noriko Miyake, Atsuo Fukuda, and

Naomichi Matsumoto. De novo KCNB1 mutations in infantile epilepsy inhibit repetitive neuronal firing. *Scientific Reports*, 5(1):15199, 2015.

[361] Ali Torkamani, Kevin Bersell, Benjamin S. Jorge, Robert L. Bjork, Jennifer R. Friedman, Cinnamon S. Bloss, Julie Cohen, Siddharth Gupta, Sakkubai Naidu, Carlos G. Vanoye, Alfred L. George, and Jennifer A. Kearney. De novo KCNB1 mutations in epileptic encephalopathy. *Annals of Neurology*, 76(4):529–540, 2014.

[362] Jeffrey D. Calhoun, Carlos G. Vanoye, Fernando Kok, Alfred L. George, and Jennifer A. Kearney. Characterization of a KCNB1 variant associated with autism, intellectual disability, and epilepsy. *Neurology: Genetics*, 3(6):&NA;, 2017.

[363] Marjaana A. Peltola, Juha Kuja-Panula, Johanna Liuhanen, Vootele Võikar, Petteri Piepponen, Tero Hiekkalinna, Tomi Taira, Sari E. Lauri, Jaana Suvisaari, Natalia Kulesskaya, Tiina Paunio, and Heikki Rauvala. AMIGO-Kv2.1 Potassium Channel Complex Is Associated With Schizophrenia-Related Phenotypes. *Schizophrenia Bulletin*, 42(1):191–201, 2016.

[364] Anthony J. Griswold, Nicole D. Dueker, Derek Van Booven, Joseph A. Rantus, James M. Jaworski, Susan H. Slifer, Michael A. Schmidt, William Hulme, Ioanna Konidari, Patrice L. Whitehead, Michael L. Cuccaro, Eden R. Martin, Jonathan L. Haines, John R. Gilbert, John P. Hussman, and Margaret A. Pericak-Vance. Targeted massively parallel sequencing of autism spectrum disorder-associated genes in a case control cohort reveals rare loss-of-function risk variants. *Molecular Autism*, 6(1):43, 2015.

[365] Merlin G. Butler, Syed K. Rafi, Waheeda Hossain, Dietrich A. Stephan, and Ann M. Manzardo. Whole Exome Sequencing in Females with Autism Implicates Novel and Candidate Genes. *International Journal of Molecular Sciences*, 16(1):1312–1335, 2015.

[366] Namshin Kim, Kyoung Hyoun Kim, Won-Jun Lim, Jiwoong Kim, Soon Ae Kim, and Hee Jeong Yoo. Whole Exome Sequencing Identifies Novel De Novo Variants Interacting with Six Gene Networks in Autism Spectrum Disorder. *Genes*, 12(1):1, 2020.

[367] Helen V. Firth, Shola M. Richards, A. Paul Bevan, Stephen Clayton, Manuel Corpas, Diana Rajan, Steven Van Vooren, Yves Moreau, Roger M. Pettett, and Nigel P. Carter. DECIPHER: Database of Chromosomal Imbalance and Phenotype in Humans Using Ensembl Resources. *The American Journal of Human Genetics*, 84(4):524–533, 2009.

[368] D James Surmeier and Robert Foehring. A mechanism for homeostatic plasticity. *Nature Neuroscience*, 7(7):691–692, 2004.

[369] S.B. Baver and K.M.S. OConnell. The C-terminus of neuronal Kv2.1 channels is required for channel localization and targeting but not for NMDA-receptor-mediated regulation of channel function. *Neuroscience*, 217:56–66, 2012.

[370] Tomohiko Irie and Laurence O. Trussell. Double-Nanodomain Coupling of Calcium Channels, Ryanodine Receptors, and BK Channels Controls the Generation of Burst Firing. *Neuron*, 96(4):856–870.e4, 2017.

[371] EamonnăJ Dickson, JillăB Jensen, and Bertil Hille. Regulation of calcium and phosphoinositides at endoplasmic reticulummembrane junctions. *Biochemical Society Transactions*, 44(2):467–473, 2016.

[372] P.A. Skehel, B.A. Armitage, D. Bartsch, Yinghe Hu, Bong-Kiun Kaang, S.A. Siegelbaum, E.R. Kandel, and K.C. Martin. Proteins functioning in synaptic transmission at the sensory to motor synapse of Aplysia. *Neuropharmacology*, 34(11):1379–1385, 1995.

[373] Edward L. Huttlin, Lily Ting, Raphael J. Bruckner, Fana Gebreab, Melanie P. Gygi, John Szpyt, Stanley Tam, Gabriela Zarraga, Greg Colby, Kurt Baltier, Rui Dong, Virginia Guarani, Laura Pontano Vaites, Alban Ordureau, Ramin Rad, Brian K. Erickson, Martin Wühr, Joel Chick, Bo Zhai, Deepak Kolippakkam, Julian Mintseris, Robert A. Obar, Tim Harris, Spyros Artavanis-Tsakonas, Mathew E. Sowa, Pietro De Camilli, Joao A. Paulo, J. Wade Harper, and Steven P. Gygi. The BioPlex Network: A Systematic Exploration of the Human Interactome. *Cell*, 162(2):425–440, 2015.

[374] Sarah E. Murphy and Tim P. Levine. VAP, a Versatile Access Point for the Endoplasmic Reticulum: Review and analysis of FFAT-like motifs in the VAPome. *Biochimica et Biophysica Acta (BBA) - Molecular and Cell Biology of Lipids*, 1861(8):952–961, 2016.

[375] Dhrubajyoti Chattopadhyay and Soma Sengupta. First evidence of pathogenicity of V234I mutation of hVAPB found in Amyotrophic Lateral Sclerosis. *Biochemical and Biophysical Research Communications*, 448(1):108–113, 2014.

[376] Edor Kabashi, Hajer El Oussini, Valérie Bercier, François Gros-Louis, Paul N. Valdmanis, Jonathan McDearmid, Inge A. Mejier, Patrick A. Dion, Nicolas Dupre, David Hollinger, Jérome Sinniger, Sylvie Dirrig-Grosch, William Camu, Vincent Meininger, Jean-Philippe Loeffler, Frédérique René, Pierre Drapeau, Guy A. Rouleau, and Luc Dupuis. Investigating the contribution of VAPB/ALS8 loss of function in amyotrophic lateral sclerosis. *Human Molecular Genetics*, 22(12):2350–2360, 2013.

[377] Zongping Xia and Yuechueng Liu. Reliable and Global Measurement of Fluorescence Resonance Energy Transfer Using Fluorescence Microscopes. *Biophysical Journal*, 81(4):2395–2402, 2001.

[378] Adam Hoppe, Kenneth Christensen, and Joel A. Swanson. Fluorescence Resonance Energy Transfer-Based Stoichiometry in Living Cells. *Biophysical Journal*, 83(6):3652–3664, 2002.

[379] Stephen E. Kaiser, Jason H. Brickner, Amy R. Reilein, Tim D. Fenn, Peter Walter, and Axel T. Brunger. Structural Basis of FFAT Motif-Mediated ER Targeting. *Structure*, 13(7):1035–1045, 2005.

[380] SoHui Kim, Sónia S. Leal, Daniel Ben Halevy, Cláudio M. Gomes, and Sima Lev. Structural Requirements for VAP-B Oligomerization and Their Implication in Amyotrophic Lateral Sclerosis-associated VAP-B(P56S) Neurotoxicity*. *Journal of Biological Chemistry*, 285(18):13839–13849, 2010.

[381] Eva Teuling, Suaad Ahmed, Elize Haasdijk, Jeroen Demmers, Michel O. Steinmetz, Anna Akhmanova, Dick Jaarsma, and Casper C. Hoogenraad. Motor Neuron Disease-Associated Mutant Vesicle-Associated Membrane Protein-Associated Protein (VAP) B Recruits Wild-Type VAPs into Endoplasmic Reticulum-Derived Tubular Aggregates. *The Journal of Neuroscience*, 27(36):9801–9815, 2007.

[382] Bryce T. Bajar, Emily S. Wang, Shu Zhang, Michael Z. Lin, and Jun Chu. A Guide to Fluorescent Protein FRET Pairs. *Sensors*, 16(9):1488, 2016.

[383] Sima Lev, Daniel Ben Halevy, Diego Peretti, and Nili Dahan. The VAP protein family: from cellular functions to motor neuron disease. *Trends in Cell Biology*, 18(6):282–290, 2008.

[384] Oscar Cerda and James S. Trimmer. Activity-dependent Phosphorylation of Neuronal Kv2.1 Potassium Channels by CDK5*. *Journal of Biological Chemistry*, 286(33):28738–28748, 2011.

[385] Patrick T. Redman, Karen A. Hartnett, Mandar A. Aras, Edwin S. Levitan, and Elias Aizenman. Regulation of apoptotic potassium currents by coordinated zincdependent signalling. *The Journal of Physiology*, 587(18):4393–4404, 2009.

[386] Patrick T. Redman, Kai He, Karen A. Hartnett, Bahiyya S. Jefferson, Linda Hu, Paul A. Rosenberg, Edwin S. Levitan, and Elias Aizenman. Apoptotic surge of potassium currents is mediated by p38 phosphorylation of Kv2.1. *Proceedings of the National Academy of Sciences*, 104(9):3568–3573, 2007.

[387] Dafna Singer-Lahat, Anton Sheinin, Dodo Chikvashvili, Sharon Tsuk, Dafna Greitzer, Reut Friedrich, Lori Feinshreiber, Uri Ashery, Morris Benveniste, Edwin S. Levitan, and Ilana Lotan. K+ Channel Facilitation of Exocytosis by Dynamic Interaction with Syntaxin. *The Journal of Neuroscience*, 27(7):1651–1658, 2007.

Appendix A

Kv2 potassium channels form endoplasmic reticulum/ plasma membrane junctions via interaction with VAPA and VAPB

This appendix is excerpted from the published paper entitled "Kv2 potassium channels form endoplasmic reticulum/ plasma membrane junctions via interaction with VAPA and VAPB" in the journal Proceedings of the National Academy of Sciences (PNAS) [218]. In accordance with PNAS copyright, I am including this in my dissertation as an author on the manuscript. In this appendix, I only present the experiment that I performed. Interested readers are directed to the original manuscript for additional information.

Introduction. Kv2.1 and Kv2.2 are abundant voltage-gated K+ channels in the mammalian brain. Kv2.1 is the predominant channel in the hippocampus while both channels are differentially expressed in the cortex [189]. Both channels localize to micrometer-sized clusters on the neuronal surface of the soma, proximal dendrites, and axon initial segment (AIS) *in vivo* and *in vitro* [214]. Clustered Kv2.1 channels disperse in response to ischemic or hypoxic conditions, neuronal activity, and glutamate-induced excitotoxicity via calcineurin-dependent dephosphorylation of the channel C terminus [260, 261]. While Kv2.1 clustering was first proposed to regulate channel voltage dependence [368], several studies indicate little connection between channel clustering and regulation of conductance [209, 288, 369]. Our evidence suggests that the freely diffusive channel population provides the voltage-dependent K+ conductance that regulates neuronal electrical activity while clustered channels are nonconducting and have other functions. We previously reported that the clusters represent trafficking hubs where membrane protein insertion and retrieval at the cell surface are localized [215]. These findings agree with re-

sults from Lotan and coworkers [225] that indicate one nonconducting function of Kv2.1 is to enhance dense-core vesicle release from neuroendocrine cells. Recent studies also indicate Kv2.1 clusters regulate insulin exocytosis from pancreatic beta cells [196, 198]. Taken together these studies strongly suggest that Kv2.1 clustering plays a structural role related to the cell biology of the neuronal surface. Indeed, we recently determined that the clustered localization pattern is due to Kv2.1 interacting with the cortical endoplasmic reticulum (ER) and inducing stable ER/plasma membrane (ER/ PM) contact sites [210]. In rat hippocampal neurons this cortical ER remodeling is regulated by activity, for glutamate treatment induces Kv2.1 declustering that is shortly followed by cortical ER retraction from the cell surface [210]. While ER/PM contacts are best understood for their role in store-operated calcium entry and nonvesicular lipid transfer from the ER to the cell surface [223], additional research indicates these microdomains regulate neuronal burst firing [370] and plasma membrane PIP2 levels [371]. In addition, a recent study from Hess and coworkers [221] reveals that neuronal ER/PM contact sites represent 12% of the somatic surface *in vivo*. Given the abundance and functional significance of neuronal ER/PM contacts, and that Kv2.1-ER interaction likely influences processes within these domains, it is paramount to understand the mechanisms underlying the activity-dependent interaction between Kv2 channels and the cortical ER.

Significance of published work. This work demonstrates that Kv2 channels interact with VAMP-associated proteins (VAPs) embedded in the ER membrane. VAPs were first discovered in *Aplysia* where they are required for fast neurotransmitter release [372]. VAPs are now known to be ubiquitous ER scaffolding proteins with a large and growing list of interactors, including AKAPs, protein kinases, Rabs, and lipid transfer proteins [373, 374]. Interestingly, single amino acid substitutions in VAP-B cause late-onset spinal muscular atrophy and amyotrophic lateral sclerosis (ALS)-type 8 [375, 376], which is intriguing given that Kv2.1 clustering over the cortical ER also exists in α-motoneurons [188]. Both the clustering of the Kv2 channels and induction of ER/PM

junctions occur via a noncanonical VAP-binding motif contained within the Kv2 channel C terminus. This binding motif contains phosphorylation sites that are known to regulate Kv2 clustering and cortical ER remodeling. The balance of phosphorylation and dephosphorylation at these sites likely governs affinity for VAPs, thus explaining the phosphorylation dependence of the Kv2-ER interaction. Since Kv2 channels concentrate VAPs at the ER/PM contact site, the Kv2-VAP interaction summarized in the present work is likely to have a major influence on neuronal physiology.

The remainder of this appendix will focus on the Förster resonance energy transfer (FRET) experiment, originally presented in Figure 3. Although this experiment only represents one figure in the published manuscript, a lot of effort was expended in the acquisition and analysis of this data.

FRET Concept. To determine whether Kv2.1 interacts directly with VAP proteins in the ER, we used sensitized-emission Förster resonance energy transfer (FRET) to measure direct contact. Fluorescence relies upon the absorption of photons by a fluorophore at a wavelength that causes a transition of an electron to an excited state. As this electron relaxes, a photon is emitted at lower energy. The difference between the energy required for excitation and the energy released in emission is called the Stokes shift, usually in the range of tens to hundreds of nanometers. The most useful fluorophores for fluorescent microscopy have large Stokes shifts, as this allows for separation of the excitation light and the fluorophore emitted light. Due to diffraction limits in resolution, colocalization of two different fluorophores is not enough to determine whether they are in direct contact. Therefore, we use FRET to determine whether two proteins are in direct contact.

In principle, FRET relies on the electronic relaxation energy transferred from one fluorescent molecule (donor) to excite an adjacent fluorescent molecule (acceptor) in extremely close contact (<10 nm). Therefore, FRET experiments require pairs of fluorescent

proteins. Because the relaxation energy from the donor fluorophore is lower than the excitation energy, the acceptor fluorophore must be excited at a lower energy wavelength. With well-suited FRET pairs, the donor will not emit light upon electronic relaxation, but instead, that relaxation energy will be directly transferred to the acceptor fluorophore. Experimentally, we can measure protein interaction by exciting with the optimal donor wavelength, while collecting emitted fluorescence from the acceptor fluorophore. In our case, we decided to use the FRET pair, Clover (donor) and mRuby2 (acceptor), which have the excitation and emission spectra shown in Figure A.1.

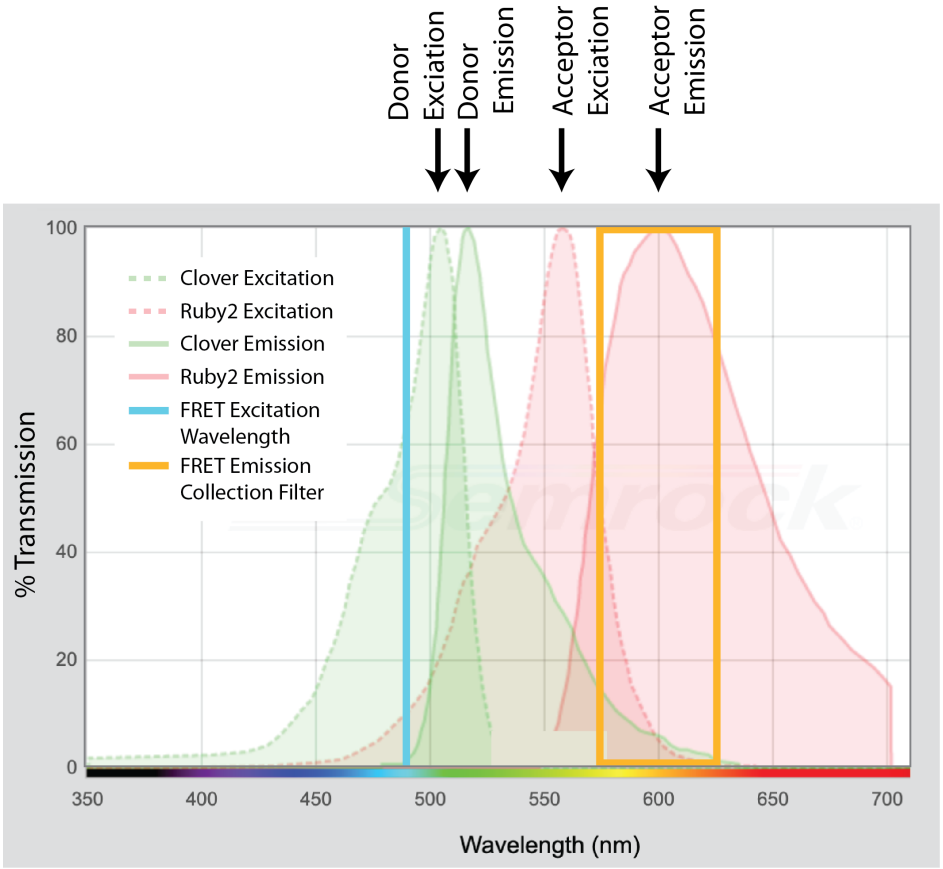

Figure A.1: Excitation and emission spectra of the FRET pair, Clover and Ruby2. Representative images of donor, acceptor, and FRET efficiency between the indicated constructs. FRET is illustrated by the representative heat maps. Scale bars are 5 μm.

Materials and Methods. Sensitized-emission FRET imaged in living cells employed Clover-Ruby2 pairs analyzed as previously described [377]. HEK-293 cells were transfected using Lipofectamine 2000 (2μL; Invitrogen) and 100μL OptiMEM (LifeTechnologies) per dish, using the following DNAs: 1μg Clover-Kv2.1, 1μg Ruby2-Kv2.1, 200 ng pcDNA3.1-Clover-Ruby2 (tandem), 200 ng mClover-C1,200 ng mRuby2-C1, 600 ng Ruby2-VAPA, 600 ng Ruby2-VAPAmut, and 600 ng Ruby2-VAPB. FRET images were obtained on the Olympus/Andor spinning-disk confocal microscope. For each cell, four images were collected: (i) excitation with 488 nm paired with a 500/25 bandpass filter (Donor image), (ii) excitation with 488 nm paired with a 600/50 bandpass filter (FRET image), (iii) excitation with 561 nm paired with a 600/50 bandpass filter (Acceptor image), and (iv) a DIC image. Using ImageJ, 15 3-pixel by 3-pixel regions of interest (ROIs) were placed on Kv2.1 clusters (or randomly in the case of tandem and soluble conditions) and the fluorescence intensity of each channel was measured. Cells expressing only the donor (Clover) or acceptor (Ruby2) constructs alone were imaged to calculate bleed-through coefficients for the FRET efficiency calculations. Bleed-through coefficients (BT_{Clover} or BT_{Ruby2}) were calculated as the average intensity of the FRET channel (I_{FRET}) divided by the average intensity of the donor or acceptor (I_{Clover} or I_{Ruby2}). For our experimental conditions, BT_{Clover}=11% and BT_{Ruby2}=4.3%. Although there are many options for the calculation of FRET, we decided to use N_{FRET}, due to its correction for expression levels of donor and acceptor and its utility in the study of intermolecular protein interactions [378]. To calculate FRET (N_{FRET}), the following relationship was used as previously described [377]:

$$N_{FRET} = \frac{I_{FRET} - BT_{Clover} \times I_{Clover} - BT_{Ruby2} \times I_{Ruby2}}{\sqrt{I_{Clover} \times I_{Ruby2}}} \tag{A.1}$$

FRET efficiency images were created using the image calculator in ImageJ and applying mathematical transformations to FRET, donor and acceptor images as described in the equation above.

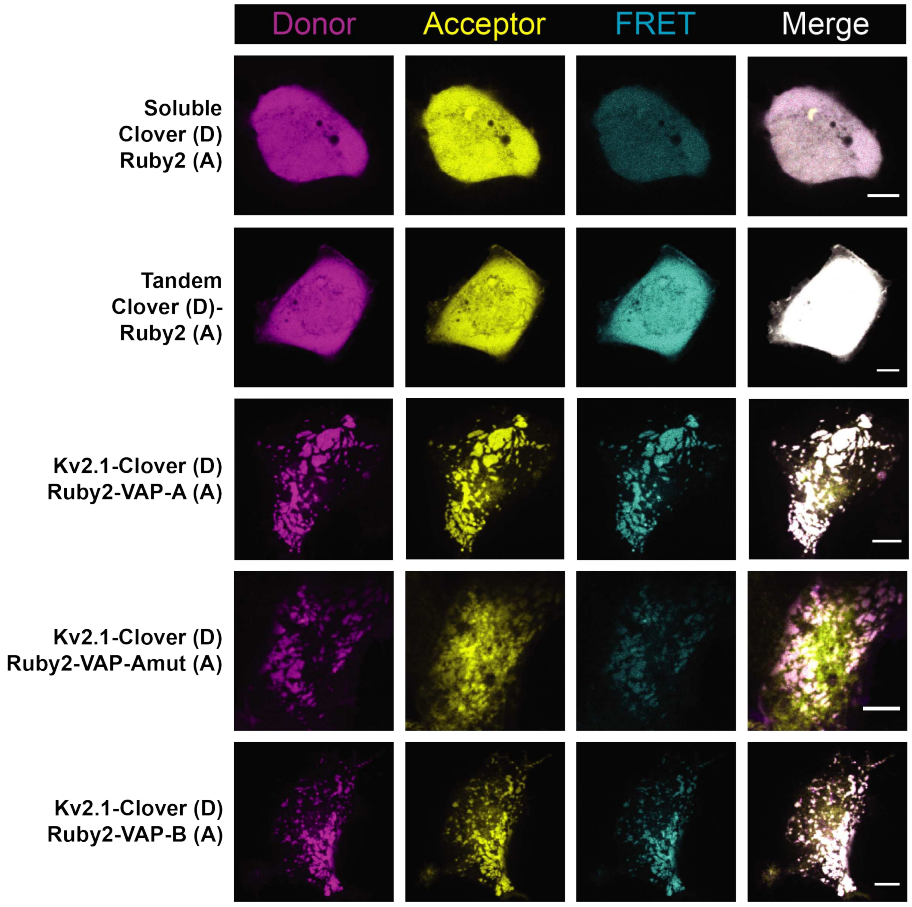

Figure A.2: FRET between Kv2.1 and both VAPs in transfected HEK cells. Representative images of donor, acceptor, and FRET efficiency between the indicated constructs. FRET is illustrated by the representative heat maps. Scale bars are 5 μm.

Results. We attached the FRET acceptor (mRuby2) and donor (Clover) to the VAP cytoplasmic domains and the N termini of Kv2.1, respectively. A Clover-mRuby2 linked tandem construct was used as a positive control while co-expression of soluble unlinked mRuby2 and Clover served as a negative control. The FRET signals obtained from these two controls, and the FRET observed between Kv2.1 and VAPA, are shown in Figure A.2, cyan images. The FRET signals observed in all experiments are summarized in Figure A.3. We observed significant FRET efficiency between Kv2.1 and both VAPA and VAPB (75% of linked control and 63% of linked control, $P \leq 0.000001$ and $P \leq 0.000001$ compared with unlinked control, respectively), indicative of protein-protein interaction. By contrast, unlinked Clover and mRuby2 displayed FRET efficiency val-

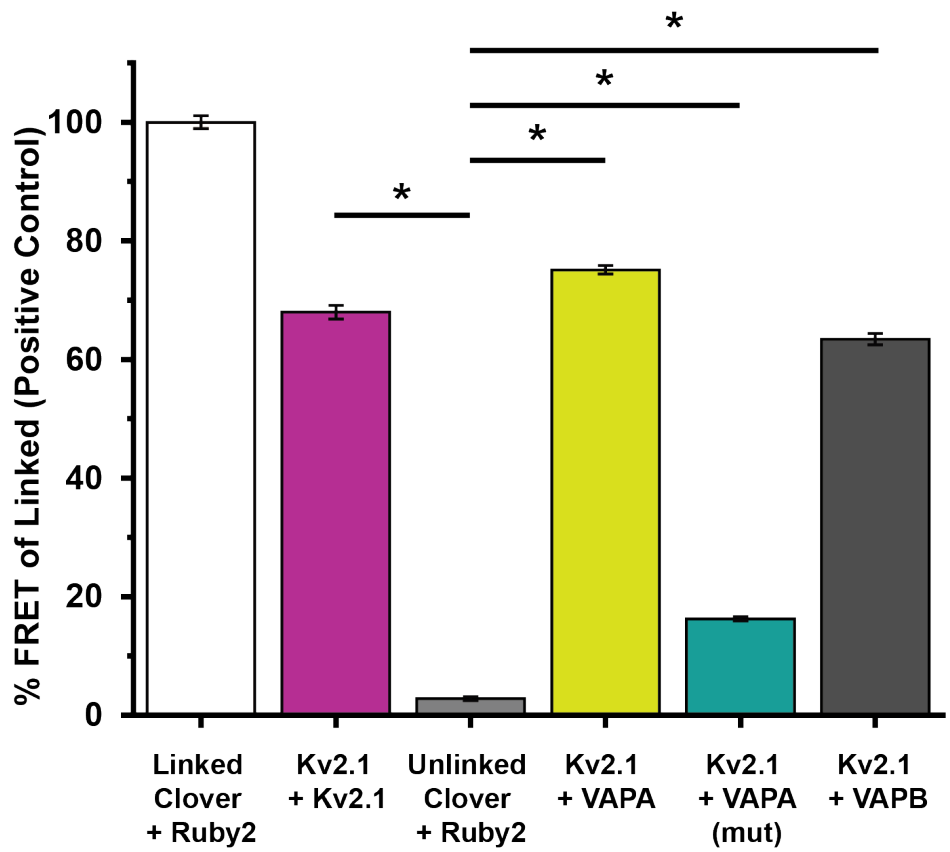

Figure A.3: Quantified FRET efficiency between Kv2.1 and both VAPs in transfected HEK cells. Here the FRET signals were standardized to that obtained with the linked Clover-Ruby2 positive control. Positive controls are indicated by the black bars, negative controls are in light gray, and the Kv2.1/VAP interactions are in darker gray. A one-way ANOVA was performed, F(5, 481) = 195.7, p = 1.81x10133 with post hoc Tukey's tests to examine significance. *p < 0.000001, significant difference relative to the unlinked negative control. Error bars represent SEM. n = 109 linked, 104 VAPA, 76 VAPA (mutant), 48 VAPB, 75 Kv2.1, and 58 unlinked cells. Each cell had 15 ROIs examined. Scale bars are 5 μm.

ues that were only 3% of the linked control. An additional positive control examined the FRET efficiency existing between Kv2.1 subunits within a heteromeric channel, i.e., mRuby2- and Clover-Kv2.1 subunits (68% of linked control). The decreased FRET between Kv2.1 subunits, relative to the linked Clover-mRuby2 positive control, is likely due to the random assembly of the channel tetramer. Interestingly, a second negative control, the VAPA(K87D/M89D) mutant, which is incapable of binding FFAT motifs [379], displayed a diminished, but still significant (16% of linked control, P $\leq$ 0.000001 compared with unlinked control) FRET efficiency. This signal could be due to oligomer-

ization with endogenous VAPs via the transmembrane domain as has been previously described [380]. In essence, the VAPA(K87D/M89D) mutant which is incapable of binding Kv2.1 is oligomerizing with endogenous VAPs that are bound to the channel. Such a mechanism would allow for the of VAPs with available FFAT motif-binding domains within the Kv2.1-induced ER/PM contacts.

Summary of published data. Our data demonstrate that a Kv2 channel-VAP interaction links the PM to cortical ER. The formation of this membrane contact site gives rise to Kv2 channel clusters on the neuronal surface. VAPA and VAPB are abundantly expressed in hippocampal, cortical, and motor neurons based on both Western blot and immunostaining approaches and these neuronal types display prominent Kv2.1 clusters on the somatic surface [381]. However, no concentration of VAPs into plasma membrane-associated clusters has been previously reported, perhaps because the available antibodies target VAP domains associated with FFAT motif binding, thus preventing immune labeling of VAPs within an assembled complex. While we previously proposed that individual Kv2 channels within these microdomains must be corralled behind a cytoskeletal fence due to their high lateral mobility within the PM [347], both the mobility and clustering are now best explained by the binding to freely diffusing VAPs within the ER. The FRET experiments presented here indicate Kv2.1 and VAPs reside within 1-10 nm of each other [382], suggesting they are in direct contact.

Discussion. The data presented in Figure A.3 also suggest the VAPA(K87D/M89D) mutant, which is unable to bind FFAT motifs, still localizes to Kv2 channel-induced ER/PM junctions, although to a reduced extent relative to WT VAPA. Since VAPs can form homomeric and heteromeric oligomers, possibly through a transmembrane GxxxG motif [380], the mutant GFP-tagged VAPA may be assembling into oligomers with endogenous WT VAPs that are bound to Kv2 channels at junctions. Such a mechanism would allow for the localization of VAPs to these microdomains which possess FFAT-

binding motifs available to interact with additional partners apart from Kv2 channels. VAPs have a growing list of interactors, including AKAPs, protein kinases, kinase regulators, transcription factors, Rabs, and lipid transfer proteins [373, 374, 383], and any concentration of these proteins to ER/PM contact sites should be physiologically significant. Given that the Kv2-VAP interaction is likely directly regulated by phosphorylation within, and adjacent to, the Kv2 C-terminal FFAT motif, it is possible that the kinases and phosphatases involved are VAP tethered. However, to the best of our knowledge, known Kv2.1-modifying kinases (CDK5, p38 MAPK, src) [384–386] and phosphatases (calcineurin) [257,261] have not been confirmed to be part of the VAP interactome [373]. However, FFAT motif-containing proteins are involved in the nonvesicular transfer of ceramide, cholesterol, and phosphotidylinositols between the ER and late secretory organelles, including TGN and PM. Kv2 channels may establish an ER/PM junction where the concentrated VAPs function as a scaffolding hub, making these membrane contact sites not only functionally distinct from ER/ PM contacts such as those induced by STIM1 or the extended synaptotagmins [223], but also regulated by neuronal activity and sensitive to insult. In addition, it is possible that the converse is true, where the VAP-mediated concentration of Kv2 channels imparts specific functions onto the ER/PM junction due to domains contained within the channel itself. Kv2.1 contains a syntaxinbinding region [225,387], an ion pore, and a voltage-sensing domain that, even in the nonconducting channel, responds to membrane potential [209]. In addition to localized SNARE protein binding or K+ conductance, perhaps Kv2.1 communicates neuronal electrical activity to functions occurring at the ER/ PM contacts.

As with many ion channels, mutations in Kv2.1 that alter conductance are linked to human disease, with mutations that alter ion selectivity and voltage sensing being associated with epilepsy and developmental delay [357, 361]. However, three recently described Kv2.1 mutations result in premature stop codons that are predicted to not alter Kv2.1 conductance [356]. These mutations occur downstream of the conserved

channel domains, falling between the last transmembrane domain and the noncanonical FFAT motif identified in the present work. One of these mutations truncates Kv2.1 at the arginine residue immediately upstream from the FFAT motif flanker region (R571). All three mutations result in developmental delay and all three are expected to abolish the ER/PM junctions formed by Kv2.1. Thus, mutations that specifically interfere with Kv2.1- VAP binding are likely to be involved in human disease.

Appendix B

DNA plasmids created for use in this dissertation

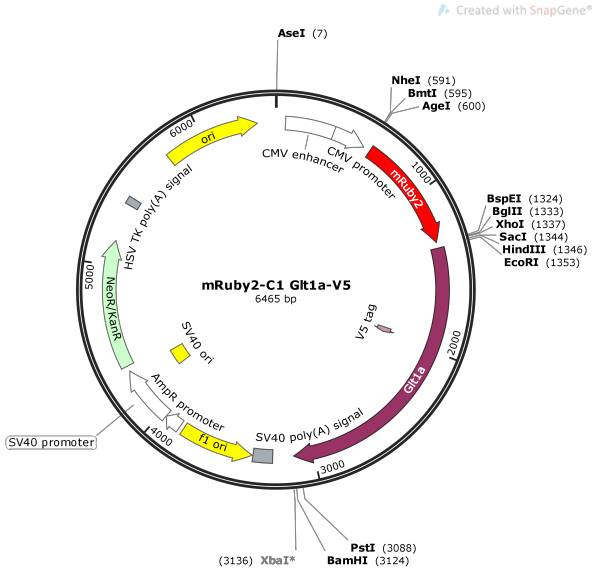

(a) Map of CMV>mRuby2-Glt1a-V5.

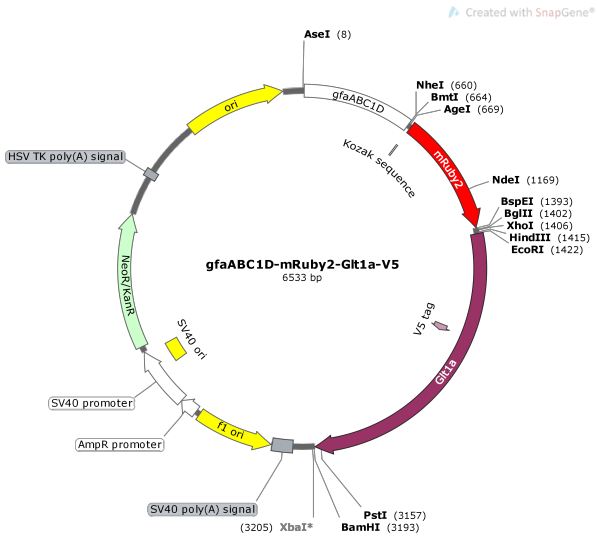

(b) Map of gfaABC1D>mRuby2-Glt1a-V5.

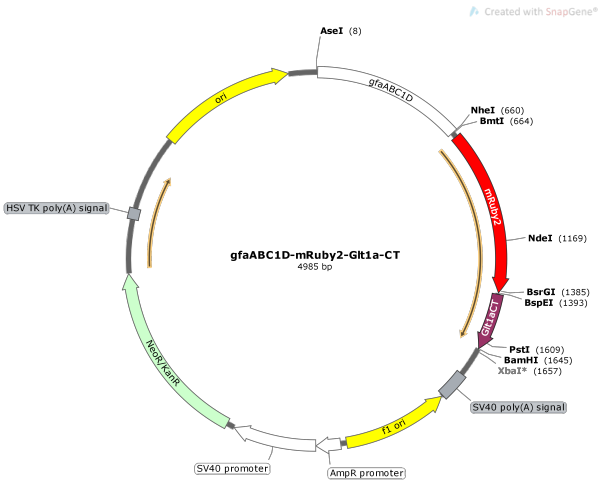

(c) Map of gfaABC1D>mRuby2-Glt1a-CT.

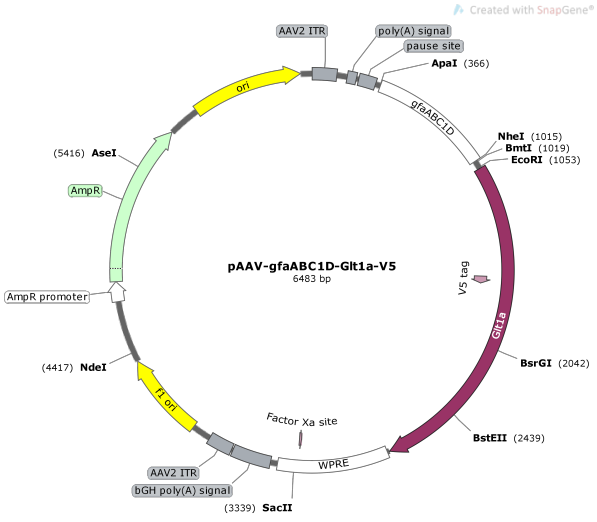

(d) Map of pAAV-gfaABC1D-Glt1a-V5.

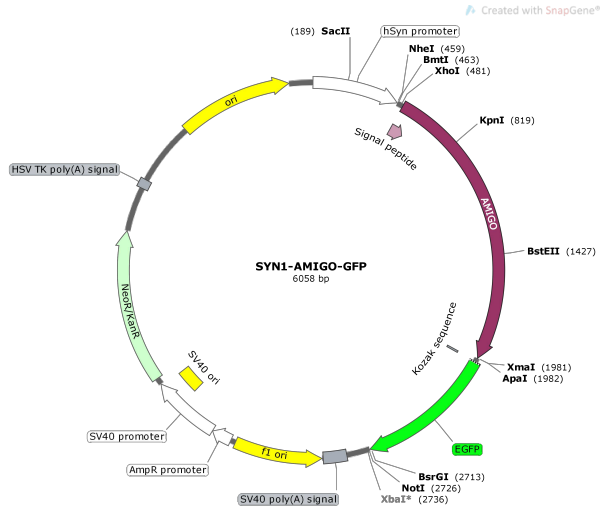

(e) Map of SYN1>AMIGO-GFP.

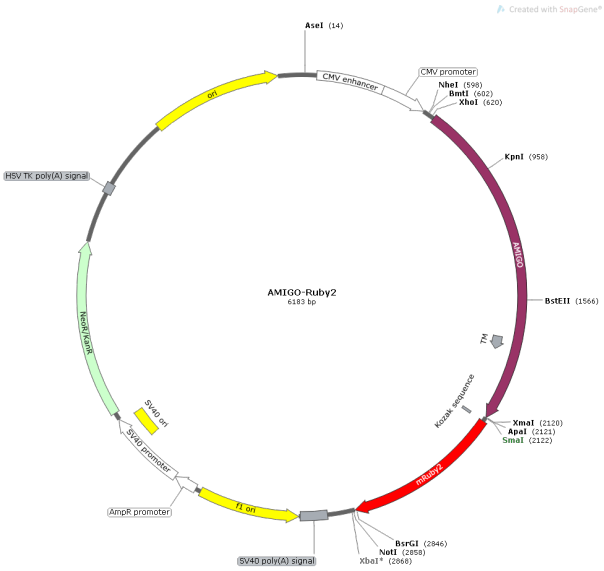

(f) Map of CMV>AMIGO1-mRuby2.

(g) Map of CMV>AMIGO2-mRuby2.

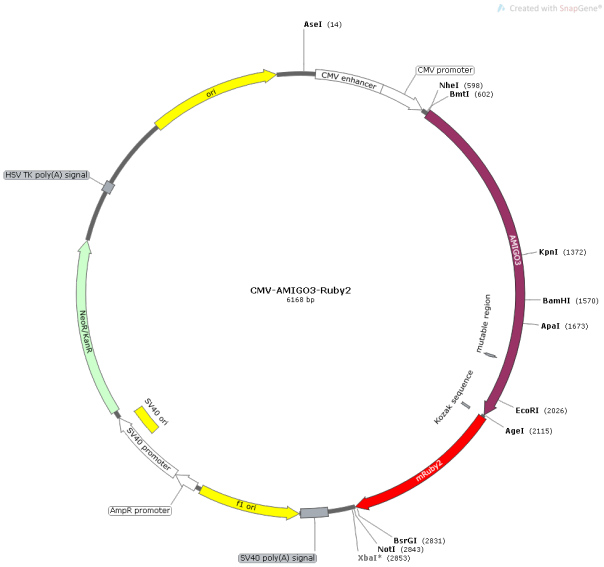

(h) Map of CMV>AMIGO3-mRuby2.

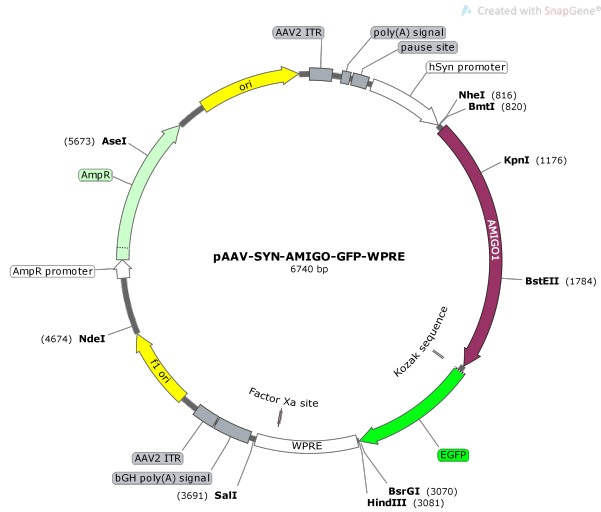

(i) Map of AAV:SYN>AMIGO-GFP.

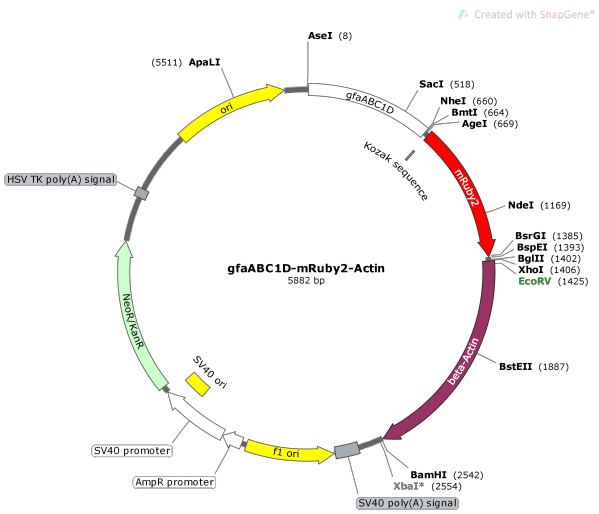

(j) Map of gfaABC1D>mRuby2-Actin.

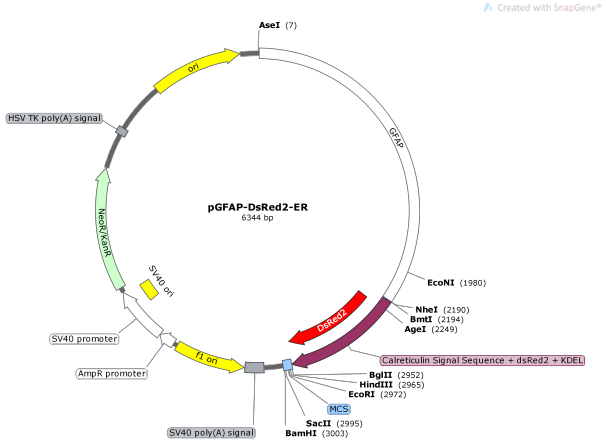

(k) Map of GFAP>dsRed-ER.

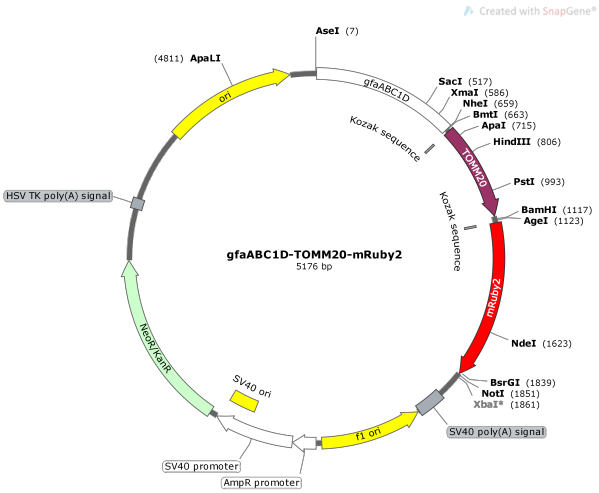

(l) Map of gfaABC1D>TOMM20-mRuby2.

(m) Map of CMV>Clover-Ruby2 Tandem.

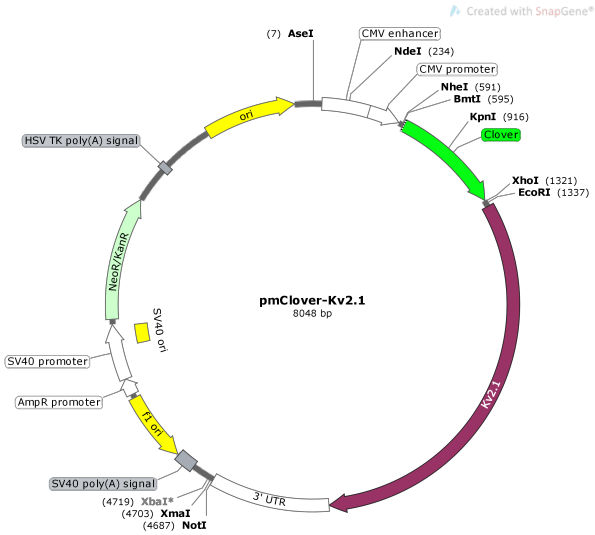

(n) Map of CMV>Clover-Kv2.1.

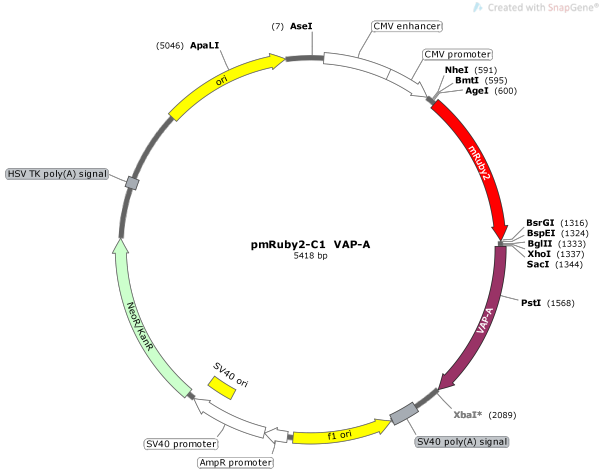

(o) Map of CMV>mRuby2-VAPA.